LARGE-SCALE EFFECTS INDUCED BY SALT MARSH AND SEAGRASS LOSS IN SHALLOW TIDAL LAGOONS

CARMINE DONATELLI

Department of Geography and Planning

Faculty of Science and Engineering, University of Liverpool

Doctor of Philosophy

July 2020

Supervisor: Dr. Nicoletta Leonardi, Co-Supervisor: Prof. Andy Plater

External collaborator: Prof. Sergio Fagherazzi, Boston University

External collaborator: Dr. Neil Ganju, USGS

Internal examiner: Prof. Janet Hooke

External examiner: Dr. Mark Schuerch, University of Lincoln

Abstract

Global environmental change is currently threatening many estuaries and tidal lagoons worldwide with significant ecological and socio-economical losses for our coastal communities. Several studies have emphasized the coastal protection functions of intertidal and subtidal vegetated surfaces, but their influence on the resilience of tidal back-barrier basins is understudied. Understanding the non-linear feedbacks and the large-scale effects induced by the disappearence of salt marshes and seagrass beds on sediment dynamics and hydrodynamic circulation is a critical step to predicting future impacts of sea-level rise on coastal areas and is highly topical given the current interest in wetland restoration around the world. Here, I have first explored the effects associated with salt marsh removal on sediment transport processes and tidal dynamics in shallow estuaries, employing a meta-analysis of high-resolution numerical modeling results in six lagoon-type estuaries spanning the entire Northeastern shore of the USA. In the second part of this work, I have unraveled the fate of salt marsh-derived sediments generated by wave-induced edge erosion in a small estuary located in New York City using the numerical framework COAWST. Finally, I have explored how changes in bottom friction associated with seagrass disappearance affect the sediment budget of coastal bays through local and regional changes in hydrodynamics.

The main results from this dissertation highlighted that: I) salt marsh loss reduces the ability of shallow estuaries to retain sediment inputs through changes in the regional scale

hydrodynamics; II) a fascinating non-linear relationship exists between salt marsh sediment trapping capacity and salt marsh size, which strongly affects the adaptive capacity of these coastal ecosystems to sea-level rise; III) only a small fraction of the sediment generated by salt marsh lateral erosion is trapped by vegetated marsh platforms; IV) reductions in seagrass coverage destabilize estuarine systems, increasing the flood phase in areas affected by seagrass disappearance and increasing bed-shear stress values across the entire back-barrier basin; V) seagrass beds reduce the wave thrust acting along salt marsh boundaries; VI) the location of the seagrass patch, in addition to its areal extent, plays an important role in attenuating wave energy along the shoreline; and VI) seagrass presence decreases the suspended sediment concentrations in the water column and consequently the sediment stock on salt marsh platforms.

To my family

Acknowledgments

Table of Contents

List of Tables

(d); 1968 seagrass distribution with a uniform plant density of 900 shoots/m^2 (e).

List of Figures

deposited on the vegetated marsh (c), as a function of percentage increament in marsh loss and after 30 simulated days.

Considerate la vostra semenza:
fatti non foste a viver come bruti,
ma per seguir virtute e canoscenza..

Li miei compagni fec'io sì aguti,
con questa orazion picciola, al cammino,
che a pena poscia li avrei ritenuti;

e volta nostra poppa nel mattino,
de'remi facemmo ali al folle volo,
sempre acquistando dal lato mancino.

Tutte le stelle già de l'altro polo
vedea la notte e'l nostro tanto basso,
che non surgea fuor del marin suolo.

Cinque volte racceso e tante casso
lo lume era di sotto da la luna,
poi che' ntrati eravam ne l'alto passo,

quando n'apparve una montagna, bruna
per la distanza, e parvemi alta tanto
quanto veduta non avea alcuna.

Noi ci allegrammo, e tosto tornò il pianto,
chè de la nova terra un turbo nacque,
e percosse del legno il primo canto.

Tre volte il fè girar con tutte l'acque;
a la quarta levar la poppa in suso
e la prora ire in giù, com'altrui piacque,

infin che'l mar fu sovra noi richiuso.

(*Canto XXVI*, Divina Commedia)

Chapter 1.

1.1 Goals of the study

The present dissertation applies high-resolution numerical models to investigate the response of shallow estuaries to salt marsh and seagrass disappearance. We first aim to improve the knowledge of the influence of salt marsh areal extent on the sediment dynamics in Barnegat Bay-Little Egg Harbor estuary, a large coastal embayment located in New Jersey. We compare different scenarios with progressively larger amounts of salt marsh loss, analyzing how the sediment stock on marshes, tidal flats and channels varies with salt marsh deterioration. Successively, we apply the same methodology to other five shallow bays characterized by different morphological features located along the North-Eastern shore of the United States. The goal is to explore how salt marsh removal affects tidal-propagation characteristics and the trapping efficiency of intertidal areas in estuarine systems. Subsequently, we focus our analysis on the fate of marsh-derived sediments generated by wave-induced lateral erosion in Jamaica Bay, a small coastal lagoon located in New York City. We aim to understand how this amount of sediments is distributed between vegetated platforms, tidal flats and open water. Finally, we study the large-scale effects induced by seagrass decline in back-barrier basins, investigating the benefits provided by this aquatic ecosystem on the stability of coastal bays. The numerical simulations carried out in this manuscript employ the numerical frameworks COAWST and Delft3D.

The present work is divided into a brief introduction and six chapters. Each chapter is organized as a research paper, whose content is summarized below.

Chapter 2: This chapter has been published in *Journal of Geophysical Research: Earth Surface* (doi: 10.1029/2018JF004617). It illustrates the effect of salt marsh erosion on sediment dynamics and hydrodynamic circulation in shallow bays using the numerical model COAWST. A positive feedback between morphological changes associated with salt marsh loss and suspended sediment deposition is demonstrated, using Barnegat Bay-Little Egg Harbor estuary (USA) as test case. Starting from the present-day salt marsh distribution, different salt marsh loss scenarios are tested using an exploratory model approach [Murray, 2007]. The erosion of salt marshes was simulated by removing vegetation from the eroded marsh cells, and by matching the corresponding bathymetry values with the elevation of the surrounding tidal flats. The algorithm was repeated sufficient times to reach a reduction of 25%, 50%, 75% and 100% in the current salt marsh area.

Chapter 3: This chapter has been published in the Journal *Geology*. This chapter describes the influence of salt marsh loss on the regional scale hydrodynamics and on the capacity of shallow estuaries to store sediment inputs on salt marshes, channels and tidal flats. In this numerical investigation, a new and generalized understanding on the response of lagoon-type estuaries to salt marsh deterioration is provided. In Chapter 2, I have studied the influence of salt marsh deterioration on the sediment dynamics in Barnegat Bay-Little Egg Harbor estuary, showing an exponential decrease in the sediment deposition over

vegetated surfaces with marsh decline. This chapter demonstrates systematic sediment-budget variations related to salt marsh erosion in six coastal bays, ascribing this reduction to changing tidal-propagation characteristics. In support of this, the existence of a unique relationship between salt marsh extent and salt marsh sediment trapping capacity is presented, which is independent of the specific setting of the back-barrier estuary and rather depends on the extent of the salt marsh area with respect to the basin size. This investigation uses COAWST and Delft3D as numerical frameworks, and Plum Island Sound, Jamaica Bay, Great South Bay, Barnegat Bay-Little Egg Harbor estuary, Chincoteague Bay and Virginia Coast Reserve as test cases. The final goal of this research is to add more bays in the near future by inviting more scientists to collaborate within this framework.

Chapter 4: This chapter is currently under review in *Journal of Geophysical Research: Earth Surface.* This chapter investigates the fate of marsh-derived sediments within a coastal embayment using a fully coupled hydrodynamic and morphological model. Recently, Ganju et al. [2015] and Hopkinson et al. [2017] demonstrated that salt marshes benefit from lateral erosion to increase their resilience to sea-level rise. However, how the eroded sediment is redistributed between vegetated platforms, tidal flats and open water is still unknown and can be only assessed through the use of high resolution numerical models. For this purpose, a new routine recently implemented in COAWST is employed to compute salt marsh lateral erosion based on wave thrust values [Beudin et al., 2017] and to investigate the redistribution of eroded sediments. Furthermore, this study estimates the net sediment import in the bay and shows how the sediment coming from offshore is redistributed within the back-barrier basin. The setup and the calibration of water levels

and suspended sediment concentrations is presented in the supplementary material (Appendix 4).

Chapter 5: This chapter has been published in *Advances in Water Resources* (doi: 10.1016/j.advwatres.2019.04.017) and the supporting material is available in a data article published on *Data in Brief* (doi: 10.1016/j.dib.2019.104197).

This chapter deals with a numerical study demonstrating how reductions in seagrass coverage affects the hydrodynamics and the morphological evolution of tidal systems. Six historical maps of Barnegat Bay and the modelling framework COAWST are employed to demonstrate how seagrass disappearance enhances salt marsh edge erosion, increasing wave thrust values along marsh boundaries, altering the capacity of tidal basins to retain sediments inputs from in-land and coastal ocean through changes in the regional scale hydrodynamics. As showed in recent studies [Bologna et al., 2000], seagrass coverage has decreased by 62% over the last several decades in Barnegat Bay, with a total loss is estimated as 2000–3000 ha in 30 years (from 1960 to 1990). The goal of this research is to evaluate how seagrass beds protect coastal lagoons, showing the multiple benefits provided by submerged aquatic vegetation in estuarine systems.

Chapter 6: This chapter has been published in *Geophysical Research Letters* (doi:10.1029/2018GL078056).

The main focus of this chapter is to show how seagrass decline alters the sediment dynamics in shallow bays. Six historical maps of Barnegat Bay and the modelling framework COAWST are used to explore the effects of seagrass loss on suspended

sediment concentrations and sediment deposition over intertidal areas using an exploratory model approach [Murray, 2007]. A new routine recently implemented by Beudin [2017] is used to model seagrass canopies. This chapter documents the importance of seagrass beds for the retention of sediments within bay systems, showing how seagrass presence reduces the sediment lost in the ocean, which is relevant for the long-term survival of coastal wetlands as an abundance of sediments generally corresponds to more resilient wetlands [Ganju et al., 2017]. The results presented in this section highlight the importance of seagrasses and are relevant for coastal communities and coastal managers worldwide as they could aid the design of coastal protection schemes.

Chapter 7 summarizes the main outcomes and implications of this thesis.

1.3 Shallow estuaries and tidal lagoons

Shallow estuaries are common features along the U.S. Atlantic Coast [Aretxabaleta et al., 2017]. According to Ketchum [1951], estuaries are transitional ecosystems between the land and the ocean where fluvial water meets salt water [Miranda et al., 2017]:

'Estuary is a region where river water mixes with, and measurably dilutes, sea water.'

However, the Latin word *aestuarium* has a deeper meaning and can be translated as 'rough waters', indicating a highly dynamic coastal environment. Estuaries or coastal bays may be divided from the open ocean by barrier islands, which offer protection to the back-barrier basin. Another type of coastal bays is lagoons, which is an elongated body of water characterized by a small tidal prism and little fresh water input [Davis and FitzGerald, 2004]. Water exchange between the estuary and the ocean occurs through the channels separating two barrier islands, known as tidal inlets [Van de Kreeke and Brouwer, 2017]. Figure 1.1 shows different type of coastal systems [Davis and FitzGerald, 2004].

Figure 1.1 Bay/estuary (a), coastal lagoon (b), basin with marshes, tidal flats and tidal channels (from Van de Kreek and Brouwer [2017]).

Coastal embayments must trap sediments in order to keep pace with sea-level rise [Fagherazzi et al., 2014]. The conceptual model of estuarine response to sea-level rise proposed by Pethick [1994] suggests that the resultant increase in hydraulic depth associated with sea-level rise enhances the flood dominance of estuaries. With sufficient

sediment supply the intertidal areas can raise, reducing the hydraulic depth and making the system move towards ebb dominance [Dronkers, 1986; Townend and Pethick, 2002]. Sea-level rise may lead to the disappearance of intertidal areas and barrier island fragmentation when the sediment supply from rivers and coastal ocean is insufficient to offset the increased in water depth. Fitzgerald et al. [2008] present the fate of a back-barrier bay under a regime of accelerated sea-level rise (Figure 1.2). Their conceptual model shows that salt marsh conversion into open water increases tidal prism values, enlarging inlet sizes and flood/ebb tidal delta volumes. The existence of a consistent relationship between ebb delta volume and tidal prism values was corroborated through observations and regression analysis [e.g, Walton and Adams, 1976]. On the contrary, FietzGerald [1996] demonstrates a weak correlation between flood delta volumes and tidal prism, suggesting that flood delta volume size depends on the amount of water space in the back-barrier basin [Van de Kreeke and Brouwer, 2017]. These processes lead to a progressive deterioration of barrier islands with catastrophic consequences on the entire estuarine ecosystem.
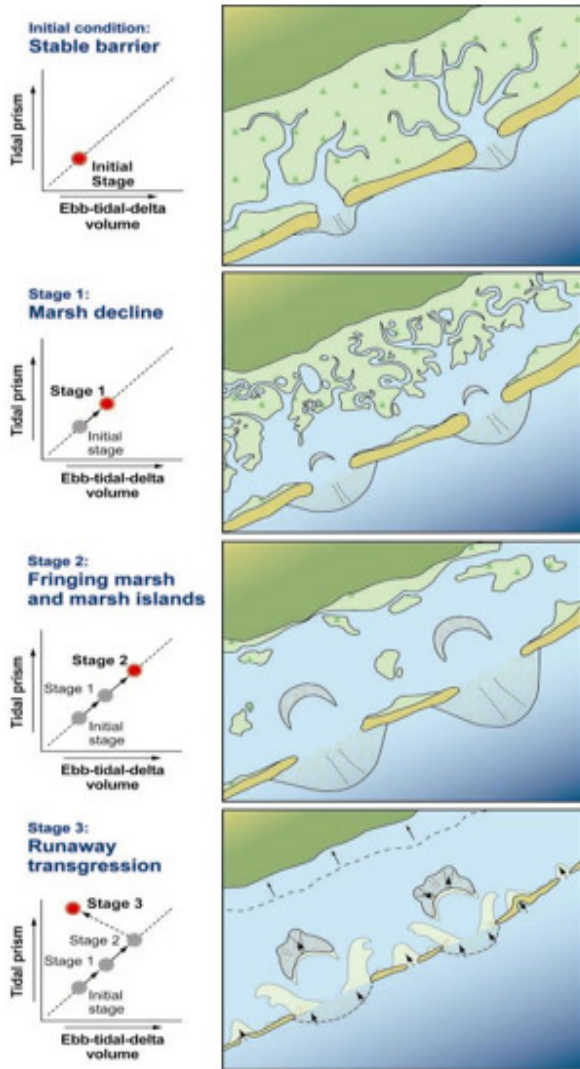
Figure 1.2 Back-barrier lagoon evolution under sea-level rise with no sufficient sediment supply (from Fitzgerald et al., [2008]).

1.3.1 Tidal propagation in shallow estuaries and tidal lagoons

This paragraph highlights the main mechanisms governing tidal propagation in lagoon-type estuaries. An analytical solution can be derived for water levels in a back-barrier basin connected with the ocean through a single inlet, showing how the attenuation of the ocean wave within the basin depends on specific geometric characteristics of the embayment and on the frequency of the action. This section supports the understanding of the hydrodynamic processes presented in the next chapters. More details can be found in the book 'Tidal hydrodynamics' of Parker [1991].

A tidal inlet causes a phase shift between the ocean and the lagoon tidal wave, decreasing tidal amplitude in the system. Keulegan [1967] derived an analytical solution for shallow inlets neglecting the inertial term in the along-channel depth-averaged momentum equation. More recently, Aretxabaleta et al. [2017] presented an analytical solution for interconnected inlet-bay systems by expanding the formulation proposed by Chuang and Swenson [1981] for a single inlet connecting to a bay.

Herein, I have schematized a coastal lagoon with a back-barrier basin of uniform depth connected to the ocean through a single prismatic channel [e.g., Parker, 1991; Talke and Jay, 2020]. The conservation of mass and momentum can be expressed using the following expression:

$$U = \frac{d\eta_B}{dt} \cdot \frac{\Omega}{A} \tag{1.1}$$

$$\frac{dU}{dt} = -g \cdot \frac{\partial \eta}{\partial x} + \frac{1}{\rho}\frac{\partial \tau}{\partial z} \tag{1.2}$$

where U is the cross-sectional averaged velocity, Ω is the bay planform area, L is the inlet length, A is the mean inlet cross sectional area, g is gravity acceleration, ρ is the water density, $\partial\tau/\partial z$ is the stress term, η_o is the ocean wave ($\eta_0 = \overline{\eta_0}\cos(\omega t)$), η_b is the basin wave ($\eta_B = \overline{\eta_B}\cos(\omega t + \varphi)$), and ω and φ represent the frequency and the phase lag.
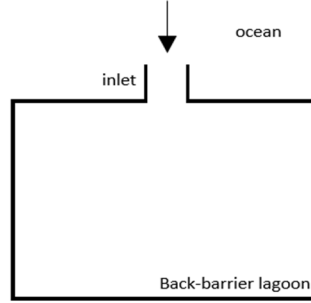
Figure 1.3 Schematic setting of a back-barrier basin connected to the ocean through a prismatic channel.

Integrating equation (1.2) over depth, the following is obtained:

$$h\frac{dU}{dt} = -gh \cdot \frac{\partial\eta}{\partial x} + \frac{1}{\rho}(\tau_\eta - \tau_{bottom}) \tag{1.3}$$

Using a linearized bottom stress formulation ($\tau_{bottom} = \rho f U$) and no wind conditions ($\tau_\eta = 0$), equation (1.3) can be written as:

$$h\frac{dU}{dt} = -gh \cdot \frac{\partial\eta}{\partial x} - fU \tag{1.4}$$

Integrating equation (1.4) along the channel:

$$Lh\frac{dU}{dt} = -gh \cdot (\eta_B - \eta_0) - fUL \tag{1.5}$$

and using equation (1.1), the resulting expression is:

22

$$\frac{d^2\eta_B}{dt^2} + \frac{f}{h}\frac{d\eta_B}{dt} + \frac{A}{\Omega}\frac{g}{L}\eta_B = \frac{A}{\Omega}\frac{g}{L}\eta_0 \tag{1.6}$$

Equation (1.6) can be seen as the equation describing a forced mass-spring-dashpot system, where the external force is reduced by a geometric factor:

$$m\ddot{x} + c\dot{x} + kx = F(t) \tag{1.7}$$
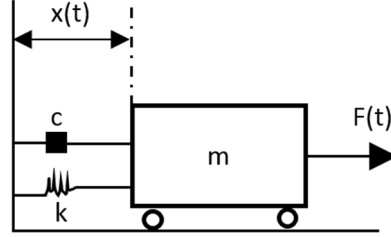
Figure 1.4 The response of a mass-spring-dashpot system and a shallow tidal lagoon to external forces can be described by the same equation.

where m is the mass, c is the damping constant, k is the spring constant and F is the external force.

The analytical solution of equation (1.7) is well-known in vibration mechanics. The ocean wave is attenuated in the back-barrier basin by a function q, which depends on the bay geometry, frequency of the action and friction in the channel:

$$\eta_B = \frac{\frac{A}{\Omega}\frac{g}{L}\overline{\eta_0}}{\sqrt{(\frac{A}{\Omega}\frac{g}{L} - \omega_o^2)^2 + (\frac{f}{h})^2\omega_o^2}}\cos(\omega t + \varphi) \tag{1.8}$$

$$q = \frac{\frac{A}{\Omega}\frac{g}{L}}{\sqrt{(\frac{A}{\Omega}\frac{g}{L} - \omega_o^2)^2 + (\frac{f}{h})^2\omega_o^2}} \tag{1.9}$$

The phase shift between the ocean and the lagoon wave can be written as:

$$\varphi = -tg^{-1}\left(\frac{\frac{f}{h}\omega_o}{\frac{Ag}{\Omega L}-\omega_o{}^2}\right)$$

<div align="right">(1.10)</div>

As an example, a system with the following geometry can be considered: channel length 2 km, channel width 1 km, channel depth 9 m, basin area 50 km^2 and a linear drag coefficient of 0.01 m/s. The natural frequency of the system (=0.0009 1/s) can be calculated as:

$$\omega_N = \sqrt{\frac{k}{m}} \text{ (mass-spring system)} \qquad \omega_N = \sqrt{\frac{A}{\Omega}\frac{g}{L}} \text{ (coastal bay)} \qquad (1.11)$$

Using the expressions (1.9) and (1.10), the frequency-response of an inlet/bay system is obtained for different Ω/A ratios and water depths:
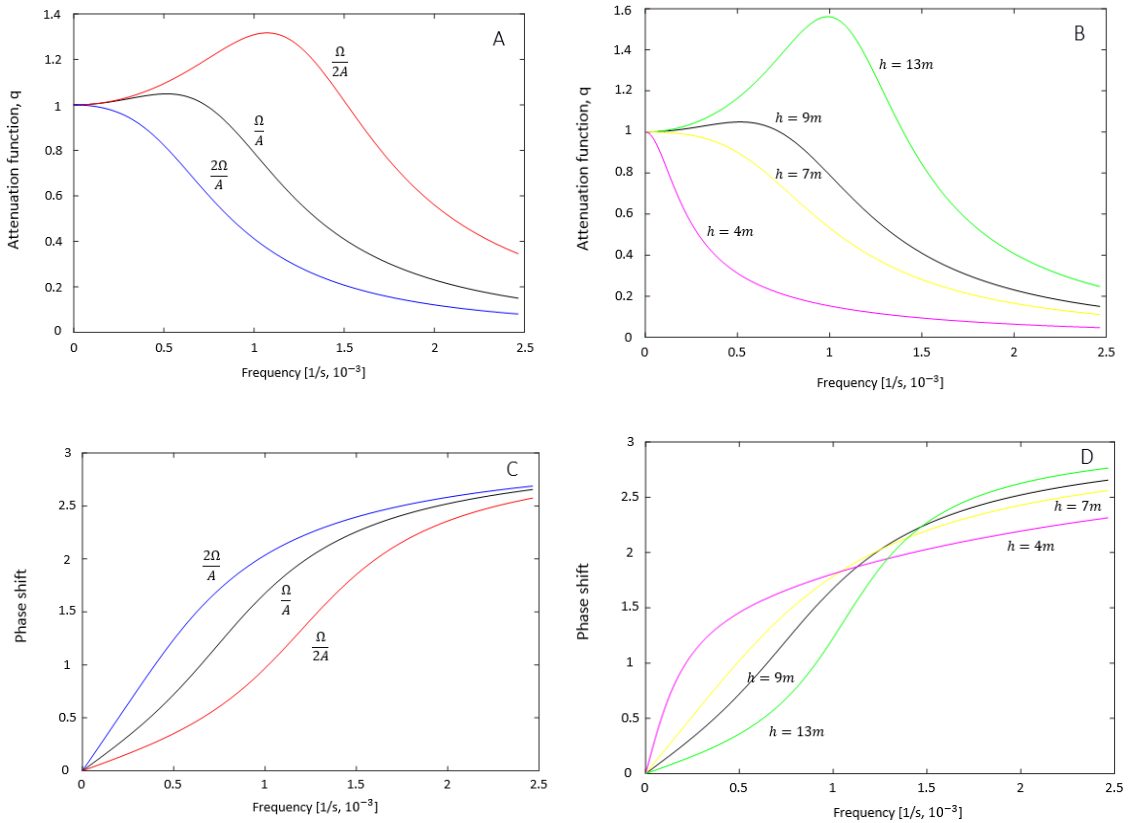
Figure 1.5 Attenuation function (a,b) and phase lag (c,d) as a function of the frequency for different basin area/inlet area ratios ($\frac{0.5A}{\Omega}, \frac{A}{\Omega}, \frac{2A}{\Omega}$) and water depths (h = 4m, 7m, 9m, 13m).

1.3.2 Tidal asymmetry in shallow estuaries and tidal lagoons

Tidal asymmetry is a well-known driver of sediment transport pathways in estuarine systems [Postma, 1967]. In the next chapters, the asymmetry between the flood and ebb phase is analysed by extracting the M_4 constituent from tidal harmonic analysis, and noting changes between the M_2 and M_4 constituents [Friedrichs and Aubrey, 1988]. In this paragraph, this procedure is briefly described. The paper 'Non-linear tidal distortion in shallow well-mixed estuaries: a synthesis' of Friedrichs and Aubrey [1988] provides a nicely written guide to interpreting these patterns. Tidal asymmetry in estuaries depends on the intertidal storage volume of the system and on the shallowness of the basin. The intertidal storage volume is calculated as the tidal prism minus the estuary tidal range multiplied by the channel area at low tide [Friedrichs and Aubrey, 1988]. Thus, the resulting asymmetry is a compromise between two effects:

i) the relative amount of water stored in intertidal areas (Vs) compared to the volume of water transported in the main channel (Vc); this contribution slows down the propagation of high water; and

ii) the interaction of the tidal wave with the channel bottom; this contribution slows down tidal currents during the ebb phase.

Along the U.S. Atlantic Coast, the semi-diurnal lunar tide (M_2) is the largest constituent. Hence, the M_4 is the largest overtide formed within the estuary or lagoon. The water levels in the back-barrier basin (z) can be expressed as the sum of two harmonics:

$$z = z_{M_2} \cos(\omega t - \theta_{M_2}) + z_{M_4} \cos(2\omega t - \theta_{M_4}) \tag{1.12}$$

where ω is the frequency, t is the time, θ_{M_2} (or θ_{M_4}) is the phase and z_{M_2} (or z_{M_4}) is the amplitude of the M_2 (or M_4) harmonic.
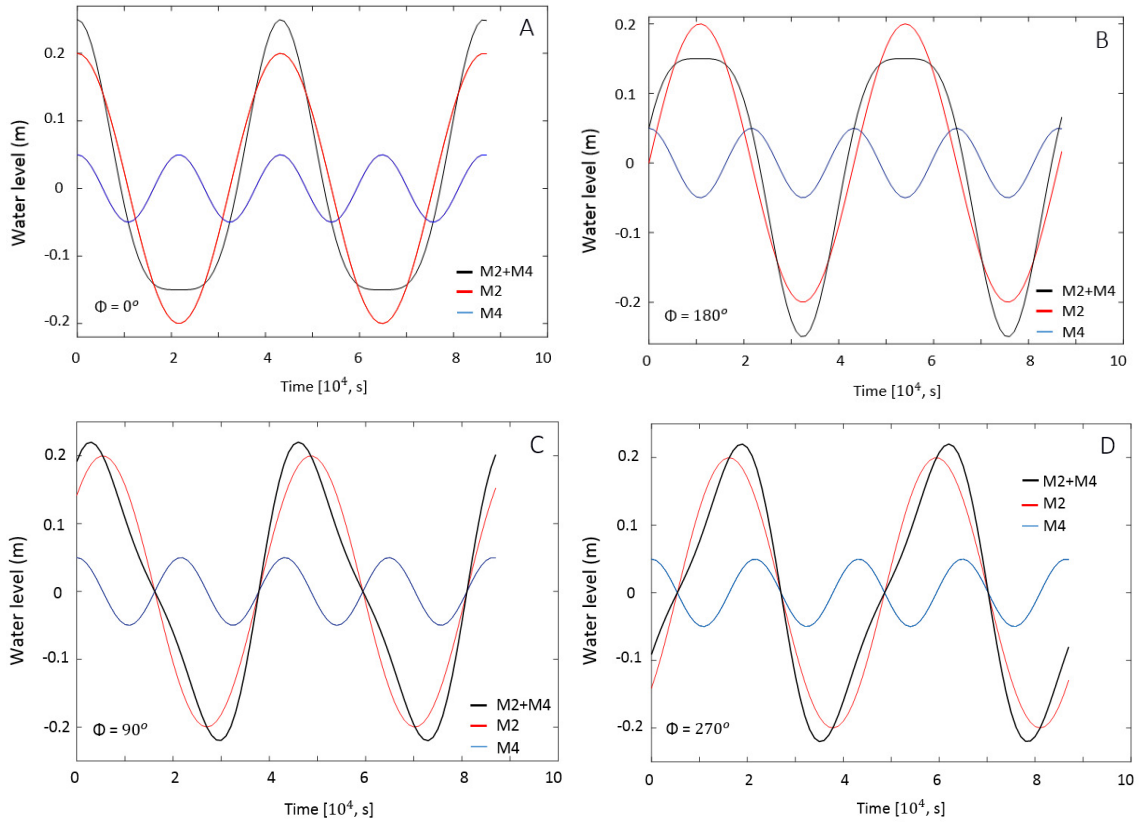
Figure 1.6 Symmetric tidal wave (a, b), shorter flood period (c, flood dominant) and shorter ebb period (ebb dominant).

Two parameters are needed to apply the Friedrichs and Aubrey formulation [1988]: the sea-surface amplitude ratio, which is a measure of tidal distortion (1.13), and the sea-surface phase, which gives the sense of the asymmetry (1.14):

$$\frac{M_4}{M_2} = \frac{z_{M_4}}{z_{M_2}} \tag{1.13}$$

$$\varphi = 2M_2 - M_4 = 2\theta_{M_2} - \theta_{M_4} \tag{1.14}$$

Considering a sea-surface amplitude ratio of 0.2, the tidal wave can be distorted in different ways by changing the relative phase between the two harmonics. For a sea-surface phase

of $0°$ or $180°$, the tidal wave is symmetric and the flood and ebb phases have same period (Figure 1.6 a, b); for a sea-surface phase between $0°$ and $180°$, the tidal wave has a shorter flood phase (Figure 1.6 c); for a sea-surface phase between $180°$ and $360°$, the tidal wave has a shorter ebb period (Figure 1.6 d). These results are summarized in the following figure:
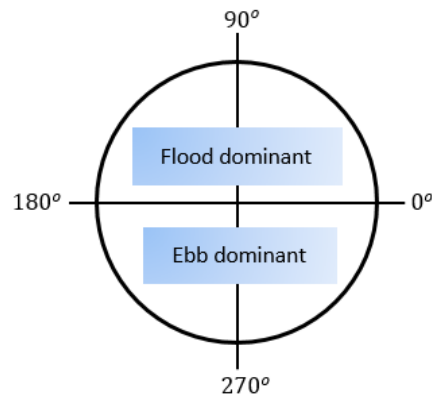
Figure 1.7 Relative phase between $0°$ and $180°$ indicate a shorter flood phase (flood dominance); relative phase between $180°$ and $270°$ indicate a shorter ebb phase (ebb dominance). The tidal wave is symmetric if the relative phase is $0°$ or $180°$.

1.3.3 Major assumptions of the modelling

The major assumptions of the modelling are listed below:

- Morphology does not adjust dynamically and changes in geometry are imposed at the beginning of the simulations. I followed an exploratory model approach in the sense proposed by Murray [2007], as the main goal of my thesis is to unravel a specific mechanism: the influence of marsh extent on the sediment trapping capacity of back-barrier basins (Chapters 2 and 3).

- The geometry of channels does not change in response to variations in tidal prism values associated with marsh loss (Chapters 2 and 3).

- The sediment released by marsh lateral erosion is removed from the system (Chapters 2 and 3). In reality, the sediment generated by marsh deterioration could contribute to salt marsh survival, or might be distributed in the basin further modifying the hydrodynamic field.

- The sediment injected in each system to evaluate the sediment budget after 30 days represents a fictitious input, and therefore I neglect that sediments released in the basin by rivers might be trapped with a different efficiency with respect to sediments coming from offshore. I used only one class of sediments for all the systems, because my goal is to compare the sediment stock under different marsh/basin area ratios in six shallow tidal lagoons (Chapters 2 and 3).

- I used the same morphology in Chapters 5 and 6, because I want to reveal the sole effect of seagrass beds on hydrodynamics and sediment transport in shallow tidal lagoons.

1.3.4 Salt marshes, tidal flats, channels and seabed in tidal lagoons

In this thesis, I defined as salt marshes the area of the lagoon located between mean sea level and high water (at spring tide). Green areas are locations where salt marshes are present. The area of the system located between low water (at spring tide) and mean sea level is defined as tidal flats. The area of the system below low water (at spring tide) is defined as seabed. Figure 1.8 depicts these zones, using Plum Island Sound (USA) as an example.
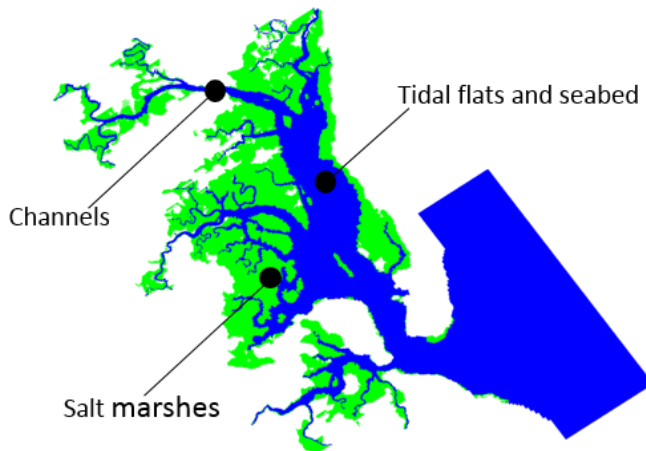
Figure 1.8 Locations of salt marshes, tidal flats, channels and seabed in Plum Island Sound, USA. Green areas are locations where salt marshes are present.

References

Aretxabaleta, A.L., Butman, B., and Ganju, N.K., (2014). Water level response in back-barrier bays unchanged following Hurricane Sandy, Geophys. Res. Lett., 41, 3163–3171, doi:10.1002/2014GL059957.

Bologna, P., Lathrop, R., Bowers, P., and Able, K., (2000). Assessment of submerged aquatic vegetation in Little Egg Harbor, New Jersey. Technical Report 2000-11, Institute of Marine and Coastal Sciences, Rutgers University, New Brunswick, New Jersey, USA.

Chuang, W.S., and Swenson, E.M., (1981). Subtidal Water level variations in Lake Pontchartrain, Louisiana, J. Geophys. Res., 86(C5), 4198–4204, doi:10.1029/JC086iC05p04198.

Davis, R.A., and FitzGerald, D.M., (2004). Beaches and Coasts. Blackweel Publishing Ltd., 419 pp.

de Miranda, L.B., Andutta, F.P., Kjerfve, B., Castro Filho, B.M., (2017). Fundamentals of Estuarine Physical Oceanography. Springer.

Donatelli, C., Ganju, N.K., Fagherazzi, S., and Leonardi, N., (2018a). Seagrass impact on sediment exchange between tidal flats and salt marsh, and the sediment budget of shallow bays, Geophysical Research Letters, doi:10.1029/2018GL078056.

Donatelli, C., Ganju, N.K., Zhang, X., Fagherazzi, S., and Leonardi, N., (2018b). Salt marsh loss affects tides and the sediment budget of shallow bays, Journal of Geophysical Research: Earth Surface, doi: 10.1029/2018JF004617.

Donatelli, C., Ganju, N. K., Kalra, T., Fagherazzi, S., Leonardi, N., Changes in hydrodynamics and wave energy as a result of seagrass decline along the shoreline of a microtidal back-barrier estuary, Advances in Water Resources (2019a), doi: 10.1016/j.advwatres.2019.04.017

Donatelli, C., Ganju, N. K., Kalra, T., Fagherazzi, S., Leonardi, N., (2019b). Numerical modelling results of wave thrust acting on salt marsh boundaries with different seagrass coverages in a shallow back-barrier estuary, *Data in Brief*, doi: 10.1016/j.dib.2019.104197

Dronkers, J., (1986), Tidal asymmetry and estuarine morphology. Netherlands Journal of Sea Research, 20 (2/3), 117-131.

Fagherazzi, S., (2014). Coastal processes: Storm-proofing with marshes. Nat Geosci 7(10): 701–702.

FitzGerald, D.M., (1996). Geomorphic variability and morphologic and sedimentologic controls on tidal inlets. *Journal of Coastal Research*, pp.47-71.

FitzGerald, D.M., Kulp, M., Penland, P., Flocks, J., Kindinger, J., (2004). Morphologic and stratigraphic evolution of ebb-tidal deltas along a subsiding coast: Barataria Bay, Mississippi River Delta. Sedimentology 15:1125–48.

Friedrichs, C.T., and Aubrey, D.G., (1988). Non-linear tidal distortion in shallow well-mixed estuaries: a synthesis. Estuarine Coastal and Shelf Science, 27(5), 521-545.

Ganju, N.K., Defne, Z., Kirwan, M.L., Fagherazzi, S., D'Alpaos, A. and Carniello, L., (2017). Spatially integrative metrics reveal hidden vulnerability of microtidal salt marshes. Nature communications, 8, p.ncomms14156.

Keulegan, G.H., (1967). Tidal Flow in Entrances, U.S. Army Corps of Engineers, Committee on Tidal Hydraulics, Tech. Bull. 14, Vicksburg.

Ketchum, B.H., (1951). The flashing of tidal estuaries Sewage and Industrial Wastes, 23, pp. 198-209.

Murray, A.B., (2007). Reducing model complexity for explanation and prediction. Geomorphology, 90 (3-4), 178-191.

Parker, B.B., (1991). Tidal Hydrodynamics, John Wiley, New York.

Pethick, J.S., (1994). Estuaries and wetlands: function and form., Falconer R A and Goodwin P(eds), Wetland Management, pp. 75-87, Thomas Telford.

Postma, H., (1967). Sediment transport and sedimentation in the marine environment. G.H. Lauff (Ed.), Estuaries, American Association for the Advancement of Science Publ. 83, pp. 158-179, Washington, DC.

Talke, S., and Jay, D.A., (2020). Changing tides: The role of natural and anthropogenic factors. Annual Review of Marine Science. doi:10.1146/annurev-marine-010419-010727

Townend, I.H., and Pethick, J., (2002), Estuarine flooding and managed retreat. Phil.Trans.R.Soc.Lond.A, 360 (1796), 1477-1495.

van de Kreeke, J., and Brouwer, R.L., (2017). Tidal Inlets: Hydrodynamics and Morphodynamics. Cambridge University Press.

Walton, T.L., and Adams, W.D., (1976). Capacity of inlet outer bars to store sand. In Proceedings of the 15th International Conference on Coastal Engineering. Vol. 1. ASCE, pp. 1919-1937.

Salt marsh loss affects tides and the sediment budget in shallow bays

Carmine Donatelli [1*], Neil Kamal Ganju [2], Xiaohe Zhang [3], Sergio Fagherazzi [3], Nicoletta Leonardi [1]

*corresponding Author: Carmine@liverpool.ac.uk

(1)   Department of Geography and Planning, School of Environmental Sciences, Faculty of Science and Engineering, University of Liverpool, Roxby Building, Chatham St., Liverpool L69 7ZT, UK

(2)   U.S. Geological Survey, Woods Hole Coastal and Marine Science Center, MA 02543, USA

(3)   Department of Earth Sciences, Boston University, 675 Commonwealth Avenue, Boston, MA 02215, USA

Supplementary material can be found in Appendix 3

C.D. performed COAWST simulations and carried out the analysis; C.D. wrote the manuscript assisted by N.L., S.F., N.K.G.; C.D. designed part of the study (changes in tides associated with salt marsh loss).

Abstract

The current paradigm is that salt marshes and their important ecosystem services are threatened by global climate change; indeed, large marsh losses have been documented worldwide. Morphological changes associated with salt marsh erosion are expected to influence the hydrodynamics and sediment dynamics of coastal systems. Here, the influence of salt marsh erosion on the tidal hydrodynamics and sediment storage capability of shallow bays is investigated. Hydrodynamics, sediment transport, and vegetation dynamics are simulated using the numerical framework COAWST in the Barnegat Bay-Little Egg Harbor system, USA. We show that salt marsh erosion influences the propagation of tides into back-barrier basins, reducing the periodic inundation and sediment delivery to marsh platforms. As salt marshes erode, the sediment trapping potential of marsh platforms decreases exponentially. In this test case, up to 50% of the sediment mass trapped by vegetation is lost once a quarter of the marsh area is eroded. Similarly, without salt marshes the sediment budget of the entire bay significantly declines. Therefore, a positive feedback might be triggered such that as the salt marsh retreats the sediment storage capacity of the system declines which could in turn further exacerbate marsh degradation.

Keywords: salt marsh erosion, tidal propagation, sediment trapping, COAWST, vegetation

2.1 Introduction

Salt marshes are coastal ecosystems generally located in low energy environments, regularly flooded by tides and storm surges, and relying on vegetation for stabilization in response to wave attack and sea-level rise [e.g. Allen and Pye, 1992; Boorman, 1995; Fagherazzi et al., 2012]. Salt marshes provide several important ecosystem services; for instance, they filter pollutants, act as buffers against coastal storms, serve as nurseries for commercial fisheries, and store significant amounts of carbon and sediment on a geological time scale [e.g. Costanza et al.1997]. In recent years salt marshes have been the focus of many restoration plans built on the concept of 'nature-based solutions' for flood defenses [e.g. Temmerman et al., 2013] which aim to use vegetated surfaces to reduce the impact of storms on coastlines. The storm protection function of these ecosystems has been estimated up to 5 million USD per km^2 in the United States [Costanza et al., 2008], and 786 million GBP per year for the UK marshes [UK National Ecosystem assessment, 2011; Foster et al., 2013; Li et al., 2018; Goodwin et al., 2018]. Salt marshes are thought to be relatively stable along the vertical direction, because inorganic matter accumulation and organic mass production allow the marsh to keep pace with sea level; however, salt marshes are seldom in equilibrium along the horizontal direction, and continuously expand or contract in response to external forcing such as wind-waves and sediment inputs [e.g. Schwimmer and Pizzuto, 2000; Schwimmer, 2001; Carniello et al., 2011; Marani et al., 2011; Fagherazzi et al., 2013; Leonardi et al., 2014, 2016a]. For instance, Schwimmer [2001] first suggested the existence of a relationship between wave energy and marsh erosion, and then Marani et al. [2011] demonstrated the existence of a linear relation between wave power density and marsh retreat, using a non-dimensional analysis and observations; subsequent studies

further corroborated the dependence of marsh erosion and wave power for several locations worldwide [e.g. Leonardi et al., 2016].

Many studies have investigated the feedbacks between vegetation biomass production and marsh elevation [e.g. Morris et al., 2002; Marani et al., 2007; Marani et al., 2010; D'Alpaos et al., 2012]. Morris et al. [2002] showed that up to a limit, increasing submergence levels aids the productivity of the salt marsh macrophyte *Spartina alterniflora*. Marani et al. [2007] introduced a 0D model coupling physical and biological processes and able to reproduce the different elevations of tidal landforms regularly inundated by the tide and characterized by the presence of different vegetation species; for the different vegetation types, the relationship between biomass change and submergence level was varied depending on the physiological character of the plants. Marani et al., [2010] provided a comprehensive theory to describe stable states and equilibrium shifts in tidal bio-morphodynamics and demonstrated that the organic sediment production associated with halophytic vegetation represents a major component of the deposition flux.

Ultimately, the maintenance of salt marsh areal extent has been linked to the sediment budget of the marsh complex as a whole, including not only the vegetated surfaces, but surrounding tidal flats, sea bed, and tidal channels [Ganju et al., 2013, 2017]. Indeed, Ganju et al. [2017] synthesized sediment budgets of eight micro tidal salt marsh complexes, and demonstrated the existence of a relationship between sediment budget and the unvegetated-vegetated marsh ratio, indicating that sediment deficits are linked to conversion of vegetated marsh portions to open water.

The regular flooding of marsh surfaces during high tides is one of the most important factors contributing to the delivery of sediments and maintenance of marsh

elevation. Among other factors, the frequency and extent of flooding depends on the elevation of the marsh, local tidal range, and dissipative properties of vegetation. Large flooded areas and frequent inundation allow for greater sediment trapping on the marsh platform. Specifically, vegetation stems largely contribute to the accumulation of suspended sediments through two main mechanisms: reduction of flow speed due to increased drag, and trapping of sediments within the stems [Knutson et al., 1982; Yang, 1998; Möller et al., 1999; Leonard and Reed, 2002; Mudd et al., 2010]. The direct particle capture by stems is strongly dependent on flow velocities and in typical marshes (flow velocity <0.1 m/s), this contribution makes up less than 10% of the sediment delivered from flood waters [Mudd et al., 2010].

There have been extensive studies on both vertical and horizontal salt marsh dynamics, and on the response of these ecosystems to changes in hydrodynamics and sediment inputs. However, there is not a specific knowledge about the reverse problem, i.e., the impact of marsh loss on tides and sediment budget in coastal embayments [Friedrichs and Aubrey, 1988; Friedrichs and Madsen, 1992; Fortunato and Oliveira, 2005]. In this paper we investigate how geomorphic modifications caused by marsh lateral erosion can alter tides and transport dynamics across the whole back-barrier basin, and this can in turn affect the survival of marsh ecosystems. Our findings can be applied to a wide range of coastal bays where salt marshes are located landward and are extremely relevant for coastal communities given that marsh erosion is a common issue. For instance, changes in tidal levels can influence marsh flooding and changes in the sediment budget can alter the resilience of the marsh and of the surrounding coastlines as well. The Barnegat Bay-Little Egg Harbor system (USA) is used as test case, and a coupled hydrodynamic-sediment

transport model is applied. Starting from the current distribution and extent of vegetated marsh areas, different simulations are created which represent incremental salt marsh loss scenarios. Different erosion scenarios are implemented to quantify changes in hydrodynamics and sediment transport of the whole bay system. We then highlight the influence of salt marsh erosion on the sediment budget of the whole system and discuss the implications in terms of wetland resilience and survival under future sea-level rise scenarios.

2.2 Study site

The Barnegat Bay-Little Egg Harbor Estuary (BBLEH) is a shallow lagoon type estuary located along the east coast of New Jersey, USA, between 39º41' N and 39º56' N latitude and 74º04' W and 74º12' W longitude. The system is composed of three shallow bays: Barnegat Bay, Manahawkin Bay, and Little Egg Harbor, which are separated from the Atlantic Ocean by ~ 70 km of barrier islands. In the bay the average water depth is 1.5 m, with a maximum of 5 m. The basin has a total surface area of 279 km^2 and it ranges from 2.0 to 6.5 km in width [Hunchak-Kariouk et al., 1999]. The estuary connects with the ocean through Little Egg Inlet, having a width of approximately 2 km with an average water depth of 10 m, and Barnegat Inlet, which is approximately 400 m wide with an average water depth of 15 m.

Tides are primarily semidiurnal, with the M_2 tide being the dominant constituent. The tidal range in the ocean is over 1 m, while within the lagoon the tidal range is significantly attenuated, especially in the north where it reduces to less than 20 cm [Aretxabaleta et al., 2014]. As reported by Lathrop and Bognar [2001], natural and human drivers, such as land use change and dredging operations, have drastically reduced salt marsh area from around 14,850 ha to 9940 ha over the last century. For the majority of the system, salt marsh erosion rates have been relatively constant since the 1930s. Around half of the interior shoreline is eroding less than 0.5 m/yr, or is not eroding at all; the other half is eroding at around 0.5-2 m/yr and only 2% of the marsh has erosion rates exceeding 2 m/yr [Leonardi et al., 2016a, b]. The highest erosion rates are found in the marshes surrounding Great Bay [Leonardi et al., 2016b]. *Spartina alterniflora* and *Spartina patens* are the dominant species

in tidal wetlands of the estuary [Kennish, 2001]. The bathymetry of the study area and the

distribution of salt marshes are illustrated in Figure 2.1 and Figure 2.2a.
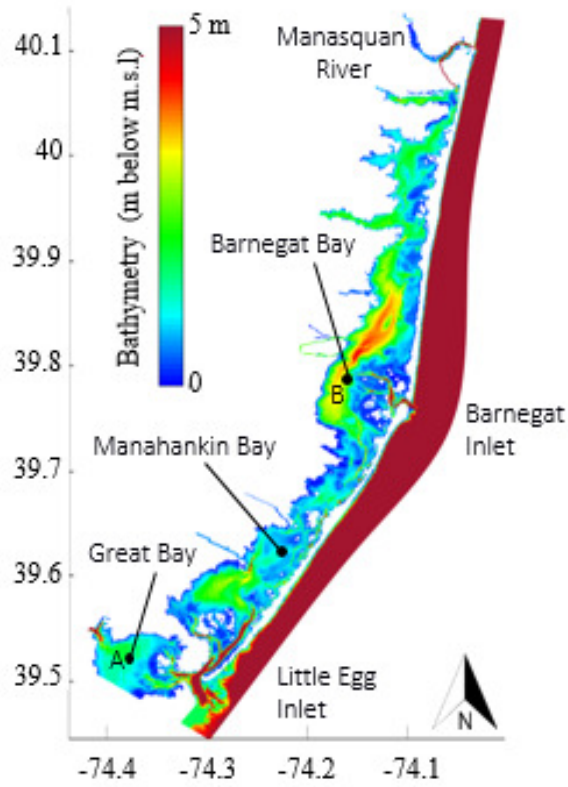
Figure 2.1 Bathymetry of the Barnegat Bay-Little Egg Harbor system.

2.3 Methods

The COAWST modeling framework [Warner et al., 2010] was used to simulate the hydrodynamics and sediment transport processes in the Barnegat Bay-Little Egg harbor system. The ocean model used in COAWST is ROMS (Regional Ocean Modeling System), which currently incorporates a sediment transport module based on CSTMS (the Community Sediment Transport Modeling System) [Shchepetkin and McWilliams, 2005; Warner et al., 2008]. The wave field is simulated by SWAN [Booij et al., 1999]. ROMS and SWAN are fully coupled and data exchange occurs every 600 sec in this application. The model computes the hydrodynamic flow field, sediment transport, and wind-waves on the same computational grid. ROMS solves the finite-difference approximations of the Reynolds-averaged Navier-Stokes (RANS) equations using the hydrostatic and Boussinesq assumptions (Chassignet et al., 2000; Haidvogel et al., 2000) with a split-explicit time stepping algorithm (Shchepetkin and McWilliams, 2005; Haidvogel et al., 2007). The ROMS barotropic and baroclinic time steps are respectively 0.1 s and 1 s. Morphology does not adjust dynamically and changes in estuary geometry are imposed at the beginning of the simulations.

The domain is defined by a numerical grid of dimension 160x800 cells with 7 layers equally spaced in the vertical. The grid, with cell sizes ranging from 40 m to 200 m, was refined around elements with complex geometry and around the inlets. The model is forced at the boundaries of the domain with tides, defined using ADCIRC tidal constituents database for the North Atlantic Ocean [Mukai et al., 2002]. The calibration of the model was done by changing the bottom roughness coefficient in order to obtain the best accordance with measurements from seven water level stations and three tidal discharge

stations within the Barnegat Bay-Little Egg Harbor estuary and for a period comprising the first two weeks of March 2012. A quadratic drag formulation with a drag coefficient of 0.0015 was used to define the bottom roughness for the whole domain. The modeling framework has been implemented and calibrated by Defne and Ganju [2014]. The Brier-Skill-Score [Murphy and Epstein, 1989] was used to evaluate the model performance, and as reported by Defne and Ganju [2014] skill assessment of the model varies from very good to excellent.

The suspended sediment in the water column is transported by solving the advection-diffusion equation, and by accounting for source/sink terms induced by downward settling or upward flux of eroded material. Sediment sources from the bed are computed following Arulanandan [1978] as $c_{source} = \varepsilon_s (1 - n) (\tau_w / \tau_c - 1)$ for $\tau_w > \tau_c$, where ε_s is the bed erodibility (0.0005 kg m^{-2}s^{-1}), n is the porosity of the bed (0.5), τ_w is the shear stress applied on the bed and τ_c is the critical erosion shear stress of the sediment (0.05 Pa). In our test cases, we only used one class of sediments, having a mass density of 2650 kg/m^3 and a settling velocity of 0.5 mm/sec. Values were chosen based on sediment characteristics typical of a coastal embayment [Fagherazzi et al., 2013]. Sink terms are calculated as: $c_{sink} = \partial w_s c / \partial s$, where w_s is the vertical-settling velocity and the 's' coordinate is the vertical sigma coordinate. The friction exerted on the flow by the bed is calculated using the Sherwood-Signell-Warner bottom boundary layer formulation [Warner et al., 2008]. The bottom boundary layer roughness is increased by the presence of waves that produce enhanced drag on the mean flow [Madsen, 1994; Styles and Glenn, 2000; Ganju and Sherwood, 2010]. In numerical models, the simplest method to simulate the influence of vegetation on the mean flow is to increase the bottom roughness coefficient [Ree, 1949;

Morin et al., 2000]. However, this approximation cannot properly represent the three-dimensional influence of vegetation on the mean and turbulent flow [e.g. Lapetina and Sheng, 2014; Marioribanks et al., 2014]. In this paper, a recently implemented vegetation module is used [Beudin, et al., 2016]. The vegetation module affects the flow field through the plant posture-dependent three dimensional drag, in-canopy wave-induced streaming, and production of turbulent kinetic energy [Beudin, et al., 2016]. The spatially averaged vegetation drag force is approximated using a quadratic drag law (Eq. 2.1, 2.2) and the effect of plant flexibility on drag is computed using the approach of Luhar and Nepf [2011] (Eq. 2.3):

$$F_{d,veg,u} = \frac{1}{2} C_D b_v n_v u \sqrt{u^2 + v^2} \tag{2.1}$$

$$F_{d,veg,v} = \frac{1}{2} C_D b_v n_v v \sqrt{u^2 + v^2} \tag{2.2}$$

$$\frac{l_{ve}}{l_v} = 1 - \frac{1 - 0.9 Ca^{-1/3}}{1 + Ca^{-3/2}(8 + B^{3/2})} \tag{2.3}$$

where C_D is the plant drag coefficient, b_v is the width of individual plants, n_v is the number of plants per unit area, (u,v) are the horizontal velocity components at each vertical layer, Ca is the Cauchy number, B is the buoyancy parameter and l_{ve} is the length of a rigid vertical blade that generates the same drag on the mean flow as a flexible cylinder of length l_v. Apart from the mean flow velocity, vegetation also significantly impacts turbulence intensity and mixing. The selected turbulence model is the k–ε scheme [Rodi, 1984] which accounts for extra dissipation and turbulence kinetic energy production due to vegetation [Uittenbogaard, 2003]. Turbulence influences settling velocities of particles, and a reduction in turbulent energy can lead to enhanced particle settling in salt marshes [e.g., Leonard and Luther, 1995; Nepf, 1999; Christiansen et al., 2000; Leonard and Croft, 2006].

In this work, we used uniform values of canopy structure and density; however these parameters can vary widely in tidal marshes. In the model, plant stems are 50 cm high, 0.1 cm wide, with 1 mm thickness and the stem density is defined as 250 stems/m^2 [U.S. Department of Agriculture, 2008]. The mass density and elastic modulus are equal to 700 kg/m^3 and 1 kN/mm^2 respectively [Feagin, et al., 2011], the drag coefficient is set to 1. The marsh coverage data came from the CRSSA's (Center for Remote Sensing and Spatial Analysis) geographic information systems (GIS) data base.

Different salt marsh loss scenarios are tested, which represent a uniform erosion of the marsh areas (Figure 2.2); these are simplified cases as some marshes within the bay eroded faster than others [Leonardi et al., 2016a, b]. Loss percentage ranges from 25% to 100% (when all vegetated areas are removed). Results are presented in terms of marsh loss percentages. The erosion of salt marshes was simulated by removing vegetation from the eroded marsh cells, and by matching the corresponding bathymetry values with the elevation of the surrounding tidal flats. For each vegetated pixels was checked whether one of the bordering elements was water. If one of the bordering element was water, the marsh pixel was transformed into water by assigning as bathymetry value the average of the elevations of the nearby water pixels. The algorithm was repeated sufficient times to reach a reduction of 25%, 50%, 75% and 100%. As marsh erosion is associated with an increase in tidal prism the size of the inlets has been updated following the O'Brien-Jarrett-Marchi law [O'Brien 1931, 1969; Jarrett 1976; List et al. 1994, 1997; FitzGerald, 1996; FitzGerald et al. 2004; FitzGerald et al. 2008; D'Alpaos et al., 2010], (Figure 2.2). Specifically we calculated the slope coefficient of the O'Brien-Jarrett-Marchi law with an exponent equals

to 6/7 for the existing configuration and we modified the cross sectional area by increasing

only the width of the inlets.
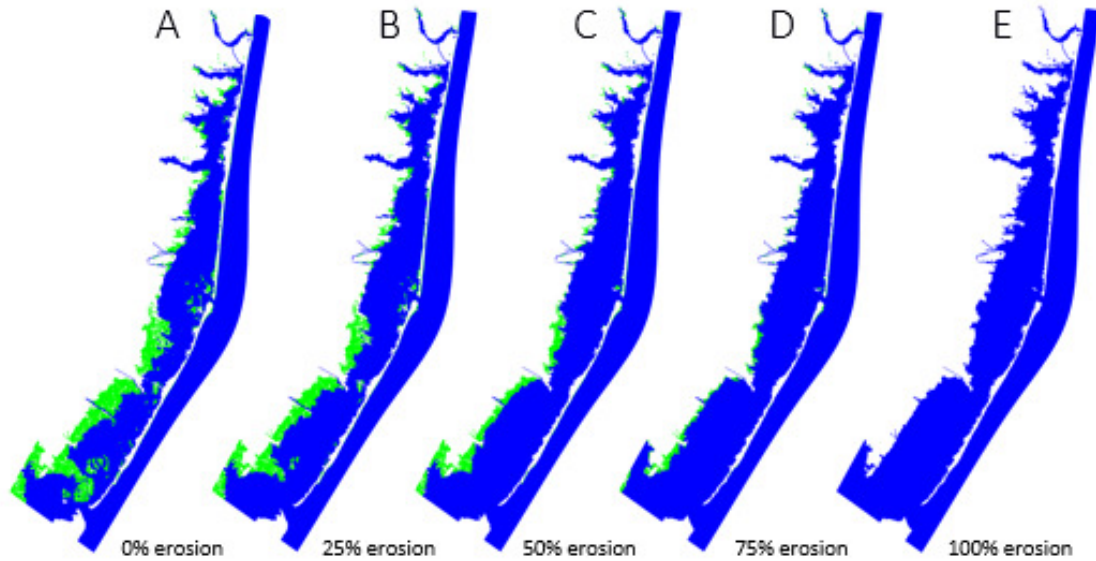
Figure 2.2 Model domains (a-e) under different salt marsh erosion scenarios, i.e. BBLEH, BBLEH-25, BBLEH-50, BBLEH-75 and BBLEH-100. Green areas are locations where salt marshes are present.

For those simulations used to investigate the transport of sediments, a spatially uniform

concentration value is imposed at the starting time in areas inside the bay system.

Specifically, the sediment injection occurs at mean sea level, and during the first flood

period. During the simulation there are no other external sediments inputs. Morphological

updates, as well as depositional and erosional fluxes only account for those sediments

which are placed in suspension at the simulation start time. Several scenarios are simulated

to evaluate the effects of marsh erosion on the hydrodynamics and sediment budget of the

system, where BBLEH stands for Barnegat Bay-Little Egg Harbor estuary: (1) BBLEH:

current salt marsh distribution (no erosion); (2) BBLEH-25: 25% of salt marshes are

eroded; (3) BBLEH-50: 50% of salt marshes are eroded; (4) BBLEH-75: 75% of salt

marshes are eroded; (5) BBLEH-100: salt marshes are completely eroded; (6) vegetation die-off: vegetation is completely removed but there are no morphological changes with respect to the 0% erosion case. All the simulations are forced at the open boundaries by tidal forcing, defined using nine constituents: K_1, O_1, Q_1, M_2, S_2, N_2, K_2., M_4 and M_6. In addition, we test the effects of locally generated waves for the scenario with the current salt marsh distribution (BBLEH) and the scenario with the removal of the entire marsh surface (BBLEH-100). For these test cases a constant southwest wind of 10 m/s is assumed. Barnegat Bay is mostly influenced by locally generated waves and given the orientation of the bay, the South-West direction is the one corresponding to the highest fetch values (Figure S5a).

Throughout the manuscript we will show that changes in marsh areal extent modify tidal amplitudes. To unravel whether the associated changes in sediment balance are mainly impacted by the sole reduction of marsh areal extent or by the sole changes in tidal amplitude, a set of idealized simulations are conducted. Five simulations are forced by the main tidal component (M_2) for different marsh erosion scenarios (0%, 25%, 50%, 75% and 100%). Five additional simulations have a constant marsh area (0% erosion case), but are forced at the boundary through an M_2 harmonic reduced by 0%, 5%, 10%, 15% and 20% with respect to existing values.

2.4 Results

The first two sections (paragraphs 2.4.1 and 2.4.2) deal with hydrodynamic results with a special focus on changes in tidal prism and tidal amplitude as a consequence of salt marsh loss. In the third part (paragraph 2.4.3) we investigate the influence of salt marsh loss on the sediment trapping potential and sediment budget of the bay.

2.4.1 Influence of salt marsh loss on tidal prism

The tidal prism value, P, was assessed at spring tide as the volume entering the bay between high and low tide. The tidal prism increases as a consequence of salt marsh loss (Figure 2.3). The percentage increase in tidal prism correlates well with the increment in basin area ($R^2 = 0.99$) and a polynomial fit was used to highlight the non-linear behaviour of the system.
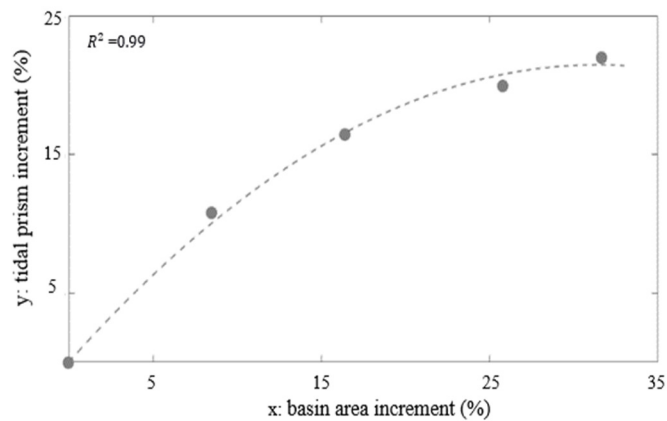
Figure 2.3 Relationship between percent increment in tidal prism and percentage increment in basin area with salt marsh loss.

The fact that the relationship presented in Figure 2.3 differs from a straight line with a unit slope suggests that variations in tidal prism associated with an increase in basin area are also accompanied by changes in tidal amplitude. Indeed, the tidal amplitude within the

bay considerably decreases once the marsh is eroded as shown by a comparison of the time-series of water levels for two points located in the centre of Great Bay and Barnegat Bay (points A and B, Figure 2.1a, Figure 2.4c, 2.4d); coloured lines are water levels for the 0% marsh erosion case, and black lines are the difference in water level before and after the removal of the marsh. The water levels at the inlet sections are presented in Figure 2.4a, b.
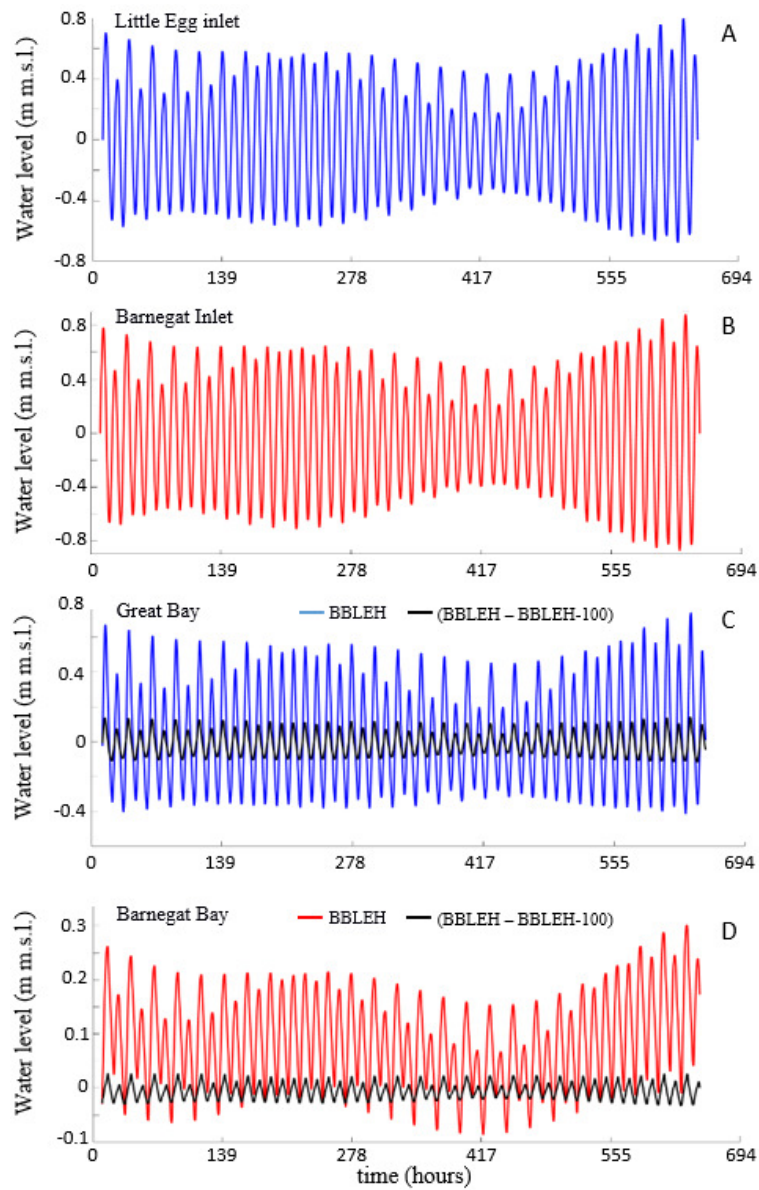
Figure 2.4 Time series of water levels at Little Egg Inlet (a) and Barnegat Inlet (b); time series of water levels for one point in Great Bay (point A, Figure 2.1a) and in Barnegat Bay (point B, Figure 2.1a). Colored lines represent water level fluctuations for the scenario with the current salt marsh configuration while black lines represent differences in water level fluctuations between the 0% and 100% erosion scenarios.

2.4.2 Influence of salt marsh loss on tidal propagation

For a shallow bay characterized by a complex geometry, significant variations in the tidal signal are expected across different portions of the domain, as well as between spring and neap tides. We computed the spatial distribution of the amplitude and phase lag of the M_2 constituent using T_Tide [Pawlowicz et al., 2002]; this harmonic has most of the tidal energy and can be considered representative of the tidal signal of the system.

The tidal signal within the bay is strongly damped with respect to the ocean boundary, which is in agreement with previous investigations [e.g. Aretxabaleta et al., 2014]. The smallest tidal amplitude is observed in Barnegat Bay, due to the smaller cross section of Barnegat Inlet with respect to Little Egg Inlet (Figure 2.5a). The tidal signal in the bay is also delayed with respect to the tide in the ocean. (Figure 2.5d). The phase shift is maximum in Barnegat Bay whose far end has a delay of 110° (3.5 hours). Little phase shift is noticeable in Great Bay and in the Manasquan River. A comparison between amplitude and phase lag values for the current salt marsh configuration, and after the complete erosion of the marsh (Figure 2.5b, 2.5e) reveals that the entire domain experiences a decrease in amplitude and an increase in phase lag once the marsh is completely eliminated from the system (Figure 2.5c, 2.5f). Changes in M_2 amplitude vary from 0 to 9 cm, with the highest reduction occurring in Great Bay whose geometry changes the most after removal of vegetated areas (Figure 2.1, Figure 2.2).
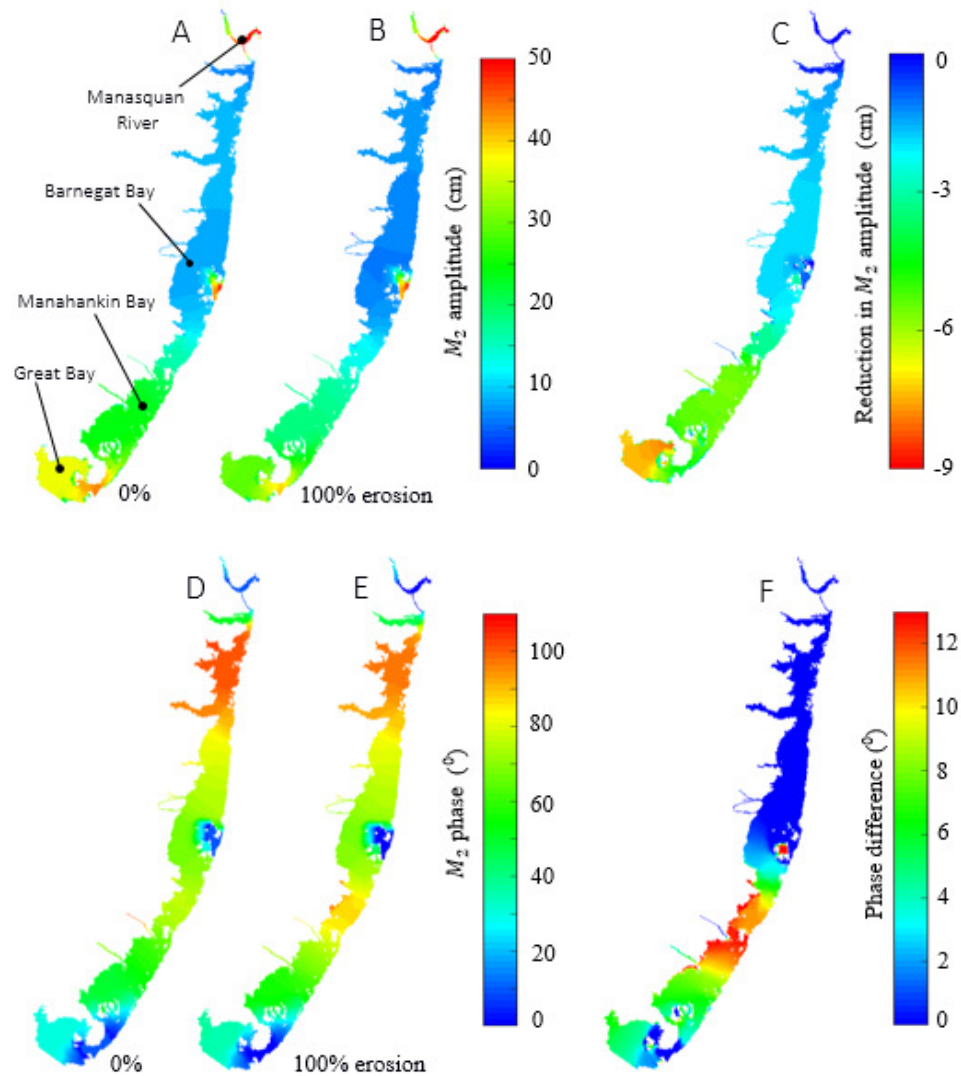
Figure 2.5 M_2 amplitude (cm), for the 0% erosion case (a); M_2 amplitude (cm) after removal of the entire marsh surface, 100% erosion scenario (b); difference in M_2 amplitude (cm) between the case with salt marshes completely eroded and the case with the current salt marsh extent (c); M_2 phase lag in BBLEH (d); M_2 phase lag after removal of the entire marsh surface (e); difference in phase lag between the case with salt marshes completely eroded and the case with the current salt marsh extent (f).

In terms of phase lag, Great Bay and Manahankin Bay are the areas experiencing the largest changes, getting a maximum increment of the phase lag of 13° (about 27 minutes). This outcome is confirmed when considering changes in spring (Figure 2.6) and neap tide

(Figure 2.7) as consequence of salt marsh removal; the spatial distribution of differences in tidal amplitude is similar to the one of the M₂ component.
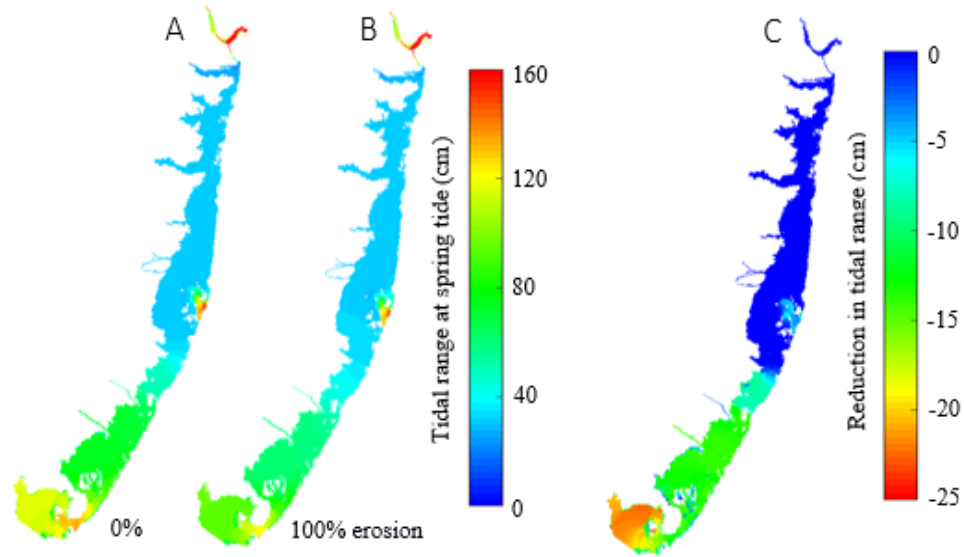
Figure 2.6 Tidal range (cm) in spring tide conditions: for the current salt marsh extent (a); after removal of the entire marsh surface (b); difference in tidal range between the case with salt marsh completely eroded and the case with the current salt marsh distribution (c).
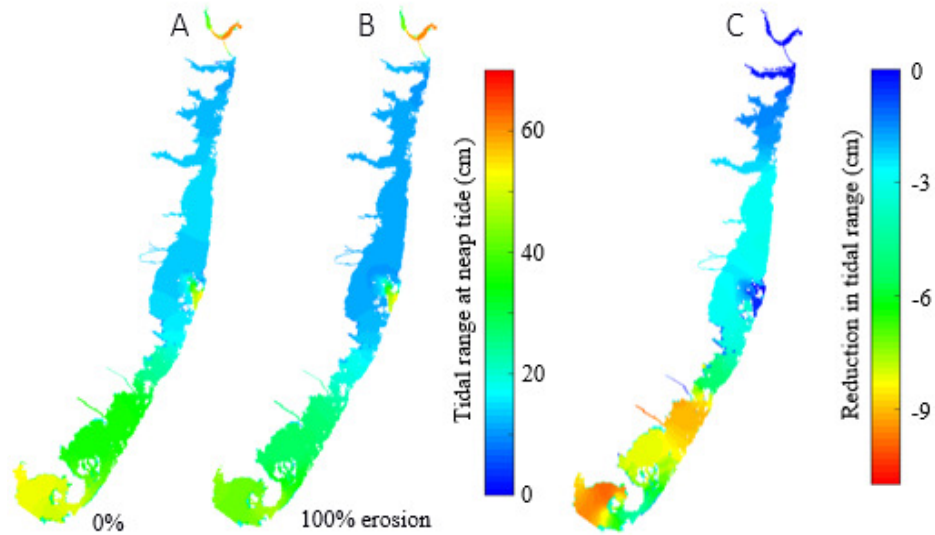
Figure 2.7. Tidal range (cm) in neap tide conditions: for the current sal marsh distribution (a); after the removal of the entire marsh surface (b); difference in tidal range between the case with salt marsh completely eroded and the case with the current salt marsh distribution (c).

The erosion of the marsh changes the morphology of the bay which, in turn, causes interrelated variations of phase lag and tidal amplitude. Indeed, as the phase lag between the ocean and the lagoon wave increases, leading to a reduction in the magnitude of the signal within the system. Figure 2.8 illustrates an idealized time history of tides in the ocean and in the bay. As the water level in the ocean is higher than the bay level, a flow is generated at the inlet which fills and raises the water level within the bay. When the high tide is reached in the ocean, the water level in the bay keeps rising due to existing phase lag values, and the bay continues to fill until the water level in the ocean and the one in the bay are the same. When the marsh is eroded a slower increase in water levels within the bay caused by an increase in the intertidal storage volume delays the tidal wave and increases the phase lag. An increment in phase lag causes maximum water level values within the bay to decrease as the peak of the tidal wave occurs later in the falling limb of the ocean wave [Keulegan, 1967]. For the Barnegat Bay-Little Egg Harbor estuary the hydrodynamics of the problem is significantly more complicated with respect to the idealized diagram in Figure 2.8, as rather than having a single-inlet system, there are two inlets and therefore two overlapping waves entering the bay. As the amplitude and phase of the main tidal constituent change with the increase of the intertidal storage volume, tidal asymmetry should also be affected by marsh lateral erosion.
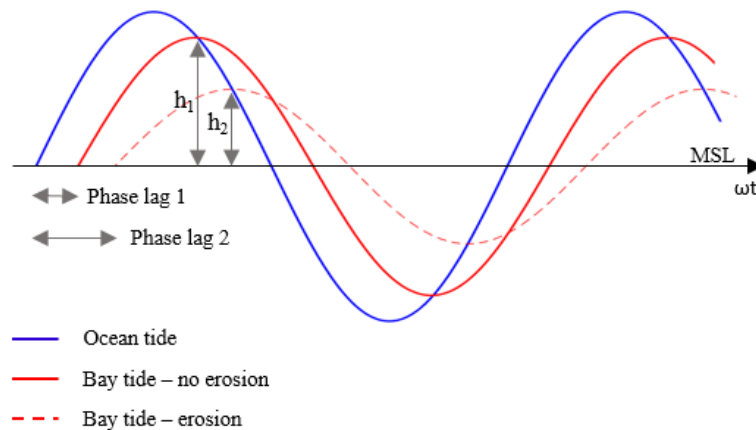
Figure 2.8 Time histories of idealized ocean and bay tides under the present-day salt marsh distribution and salt marshes eroded.

Changes in the M_4 to M_2 sea-surface amplitude ratio and the sea-surface phase M_4 relative to M_2 were calculated following Friedrichs and Aubrey [1988]. The amplitude and phase ratios of the system with the current salt marsh distribution and with marshes completely eroded are depicted in Figure 2.9. The magnitude of the non-linear distortion increases (+15% on average) when marshes retreat (Figure 2.9a, b) and although the relative phase moves away from the limit that would provide maximum asymmetry, the estuary remains flood dominant ($0°<\varphi<180°$, Figure 2.9b, d) [Friedrichs and Aubrey, 1988; Araújo et al., 2008; Picado et al., 2010]. The average of the maximum shear stress calculated during a spring tidal cycle increases around 5% during the ebb phase and 7% during the flood phase with mars loss. Extensive vegetation die-off without erosion (i.e. same morphology than Figure 2.2a but no vegetation, Figure S1a) does not significantly impact the tidal propagation within the bay. Vegetation die-off still influences tidal propagation and energy dissipation over the marsh platforms. This result is connected to the fact that fringing marshes are at the boundary with the mainland and different results might be expected for

salt marshes located at the centre of the embayment, or for different vegetated surfaces such as seagrasses [e.g. Donatelli et al., 2018]. A comparison between the amplitude of the main harmonic with and without full vegetation cover of the marsh platform shows that changes in the frictional character of marsh platforms do not impact the tidal propagation into the back-barrier basin (Figure S1b, S1c), but influences the propagation of the tide on marsh platforms by reducing the flooded areas by 15% (Figure S1d).
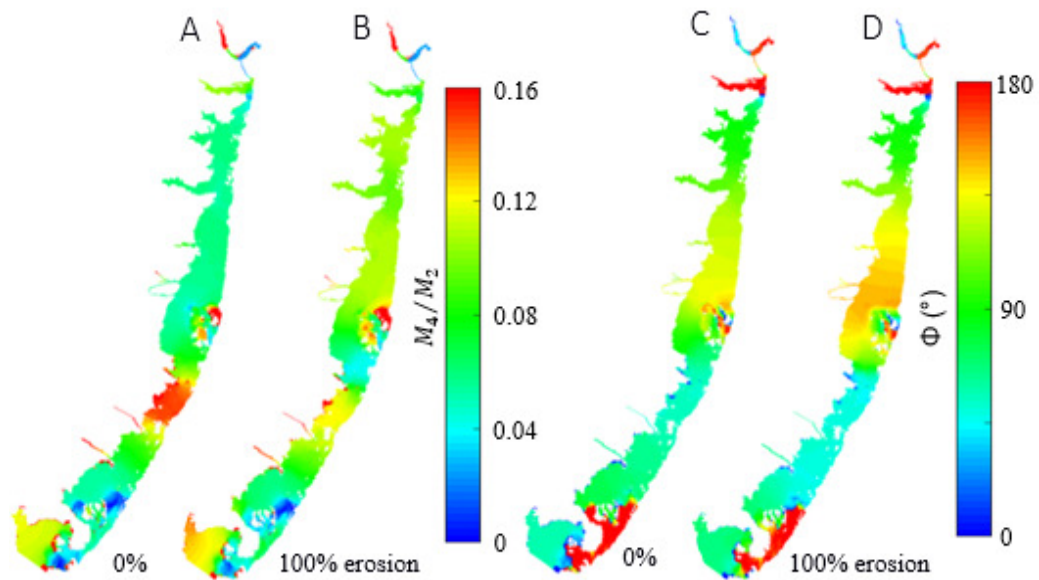
Figure 2.9 Sea-surface amplitude ratio for the current marsh distribution (a) and marsh completely eroded (b); sea-surface phase of M_4 relative to M_2 for the current marsh distribution (c) and marsh completely eroded (d).

2.4.3 Influence of salt marsh loss on the sediment trapping potential of shallow bays

The stability of coastal wetlands and their survival in response to sea level rise and external forcing depends on the sediment budget of the system [e.g. Fagherazzi et al., 2013; Ganju et al., 2013, 2017]. As shown in the previous section, salt marsh erosion increases the tidal prism which could in turn enhances the flushing capacity of the system and distort

the tidal signal causing thus a possible increase in the loss of sediments during a tidal cycle and a reduction in the sediment-trapping capability of the bay. Furthermore, a reduction in tidal amplitude can decrease plant biomass production [Morris et al., 2002].

To test this hypothesis, and to investigate the sediment trapping potential of salt marshes, we conducted a series of experiments focusing on sediment dynamics. For every salt marsh loss scenario, a 30-day simulation was run by superimposing at t=0, and over the initial footprint of the lagoon open-water area, a uniform (100 mg/l) suspended sediment concentration. The sediment injection occurs instantaneously at mean sea level and at the beginning of the simulation, during the first flood phase. The sediment injection occurs only once. The initial suspended sediment mass is equal for each erosion scenario because the footprint where the initial sediment concentration is imposed is the same. A uniformly distributed input sediment concentration represents potential riverine inputs during flood conditions, or large resuspensions events during storms; such conditions represent major contributors of inorganic sediments to salt marshes [e.g. Fagherazzi and Priestas 2010; Falcini et al 2012; Leonardi et al., 2017]. A qualitative assessment about the order of magnitude of suspended sediment concentrations values is presented in Table S1, Figure S2. Sediments can be stored within the estuary in one of the following forms, which are quantified for the different erosion scenarios: i) suspended sediment in the water column; ii) sediment deposited on tidal flats and over the within-bay sea bed iii) sediment deposited within the vegetated areas. The sum of these quantities represents the total mass of sediments within the bay, and it tends to decline in time because some sediments are flushed out of the bay system during ebb (Figure S4). The total mass of sediments stored within the bay exponentially decays and asymptotically approaches equilibrium values.

Specifically, given the existing marsh configuration (0% erosion), equilibrium values are approached after 5 days, while it takes 18 days for the system to reach equilibrium when the marsh is completely removed (100% erosion) (Figure S4). When the salt marsh is removed, the total amount of sediments stored within the lagoon largely decreases (Figure 2.10, Figure S4).
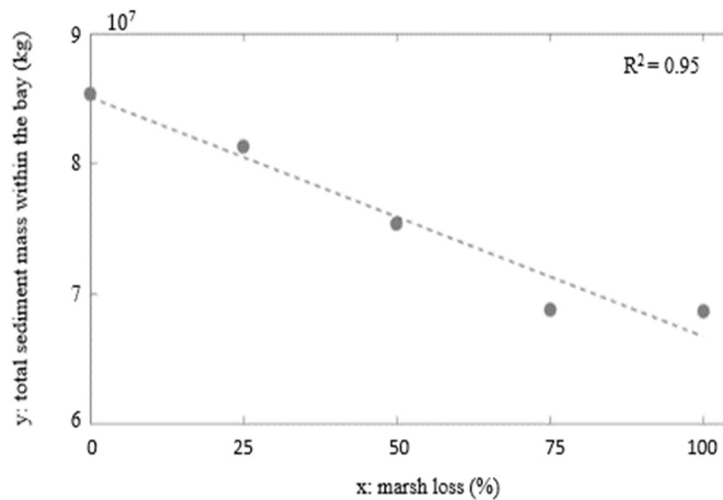
Figure 2.10 Total sediment mass stored in the domain as a function of percentage increament in marsh loss and after 30 simulated days.

Figure 2.11 illustrates how marsh loss alters the eventual destination of deposited sediment mass. The sediment mass deposited on tidal flats and the sea bed (Figure 2.11a) linearly decreases when the marsh is eroded. The suspended sediment mass tends instead to increase with increasing marsh loss (Figure 2.11b). The sediment mass trapped by vegetation (Figure 2.11c), and deposited on vegetated marsh areas exponentially decreases when marsh is lost. This is due to two main mechanisms: i) from a geometrical point of view, the spatial extent covered by vegetation where sediments can be deposited decreases when the salt marsh erodes; and ii) increasing marsh loss reduces tidal amplitudes and the

56

submergence level of the marsh. The exponential decrease indicates that the removal of

25% of the marsh area causes a reduction in the sediment mass trapped by the marsh of

more than 50%, and that a removal of 50% of the marsh has an effect comparable to the

removal of the entire vegetated surface. When waves are added to the model the associated

increase in bottom shear stress causes greater sediment resuspension; this leads to a large

increase in the sediment mass deposited on marsh platforms, and a decrease in tidal flat

deposits. Generally, the presence of waves decreases the total sediment mass stored within

the bay (Figure S5b). Overall trends in sediment storage in response to salt marsh removal

in the presence of waves are the same than for cases without waves (Figure S6).
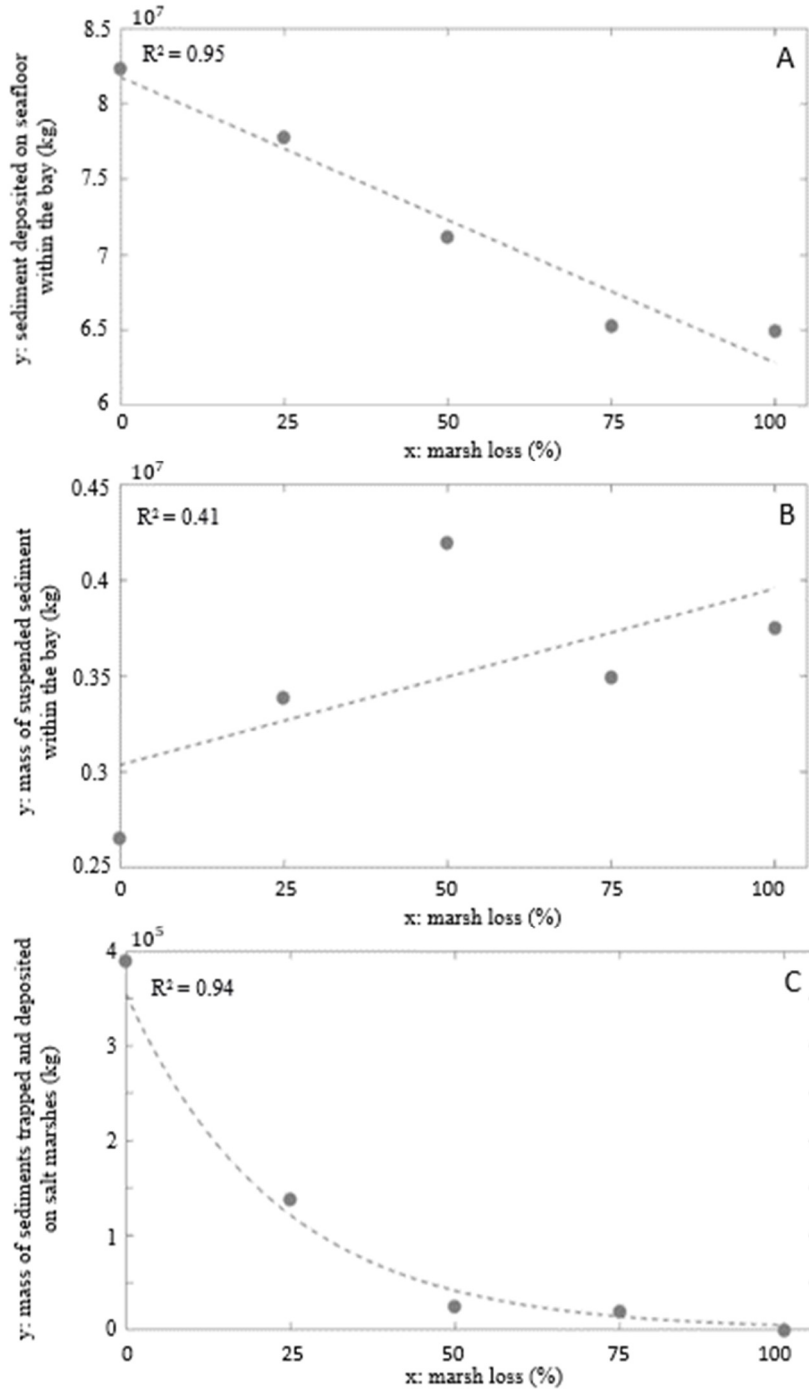
Figure 2.11 Mass of sediments deposited on tidal flats and on the "within-bay" bed (a); mass of sediments in suspension (b); mass of sediments trapped and deposited on the vegetated marsh (c), as a function of percentage increament in marsh loss and after 30 simulated days.

For the sediment storage on marsh platforms, to test the relative importance of the direct impact associated to a reduction of salt marsh areal extent with respect to the indirect impact related to the erosion-induced decrease in tidal amplitude, we conducted a set of idealized simulations. Given the same bay morphology (0% erosion scenario), different scenarios were forced at the ocean boundary by M_2 signals with varying amplitude (Figure S7a). Specifically, tested values for the M_2 component ranged from the existing 0.59m to 0.47m, with the latter being a 20% reduced value in agreement with the average within-bay deacrese in tidal amplitude associated to the 100% erosion case. Different erosion scenarios were then tested which were forced by the sole M_2 component (Figure S7b). We estimate that a 20% reduction in tidal amplitude reduces the sediment trapping on marsh platform by 30%.

2.5 Discussion

Salt marsh losses have been documented worldwide because of land-use change, wave erosion, and sea-level rise. Using the COAWST modelling framework, the impact of salt marsh erosion on the tidal propagation and sediment budget of a shallow lagoon type estuary has been studied. Salt marsh loss causes an increase in tidal prism and a decrease in the sediment trapping capacity of the lagoon system (Figure 2.10). Salt marsh erosion also decreases tidal amplitude values across the entire domain (Figure 2.4-2.7). The areas subject to the highest variations in tidal amplitude are the ones where geometric variations associated to marsh loss are more pronounced. Changes in tidal amplitude are due to the increased filling time of the system and to the consequent increase in phase lag between the ocean and bay-tidal signals. Our results show that an increase in the intertidal storage volume dampens the tidal wave for those systems where the increased filling time is the

main consequence associated to marsh erosion. Specifically, we have shown that when marshes are located landward, marsh lateral erosion can induce changes in tidal dynamics that could lead to a positive feedback which is detrimental for marsh survival (i.e. lower amplitude, less biomass production, lower vertical growth). Our findings are in agreement with studies carried out in the coastal lagoon Ria de Aveiro, Portugal [Picado et al., 2010]. For the coastal lagoon Ria de Aveiro, the authors showed how the enlargement of the lagoon flooded area, due to the collapse of protective walls, decreases tidal amplitude within the system. With respect to Barnegat Bay, Ria de Aveiro has a different number of inlets (number of inlets = 1), different tidal range (2m) and different geometry. The findings have been verified for shallow lagoon type estuaries and marshes fringing the landward side of the estuary; different results might occur when salt marshes are located at the center of the embayment or at seaward side of the embayment, or in case of estuaries with very different morphologies e.g., significantly longer and deeper estuarine channels.

Salt marsh lateral erosion enhances the export of sediments, and reduces the sediment delivery to marsh platforms and the storage of sediments on tidal flats (Figure 2.11). Such changes in the sediment budget could trigger a positive feedback undermining salt marsh survival to climate change: once the marsh is eroded the capability of the system to store sediments declines and sediments are more easily lost in the open ocean; accretion rates are also reduced as the marsh platform receives less sediments during inundation periods. A reduction in the sediment mass available in the estuary affects negatively marsh stability, because without an adequate sediment supply, vegetated areas are more easily converted into open-water [Ganju et al., 2017]. Furthermore, an increase in tidal flat areas increases the erosion hazard connected to locally generated waves which could more easily develop;

60

finally a reduction in salt marsh accretion rates could cause salt marshes to be more susceptible to sea level rise as a consequence of which a further increase in tidal prism and accelerated marsh submergence rates might occur (Figure 2.12). A shortcoming of this modelling framework is related to the usage of only one sediment fraction and to the choice to remove all of the sediments deriving from the progressive reduction in salt marsh area. In reality, the erosion of marsh edges generates a source of sediments, which can be delivered to the marsh trough channels or be directly dropped on submerged marsh platform. This sediment could contribute to salt marsh survival and affect the geomorphological evolution of the bay over long time scales. This approach would cause an overestimation of marsh vulnerability if the morphological evolution of the marsh was explicitly accounted for. However while possibly underestimating the absolute mass of sediments available within the embayment, this approach does not undermine the main outcome concerning the reduction of the potential sediment storage capability of shallow bays as a consequence of salt marsh erosion.
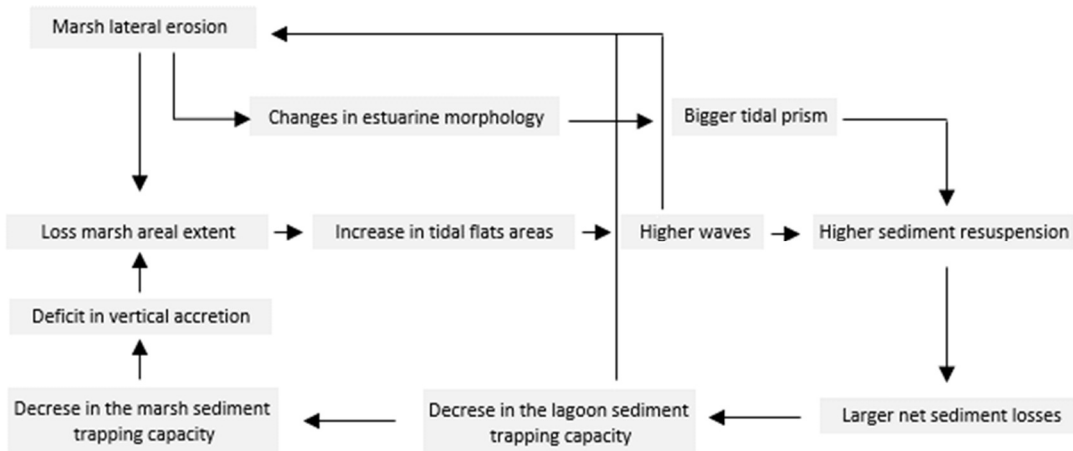
Figure 2.12 Feedbacks between salt marsh lateral erosion and marsh sediment trapping reduction.

2.6 Conclusion

Many studies have focused on the impact of external agents on marsh ecosystems, and much focus has been rightly given to the undertsanding of how climate change might impact salt marshes. However, the reverse problem i.e., how the morphological changes of salt marshes, possibly associated to climate change, are influencing the hydrodynamic and sediment transport of large scale coastal environments is still poorly understood. This contribution focuses on the influence of salt marsh erosion on tidal fluctuations, and sediment trapping potential of shallow bays and associated consequences in terms of system vulnerability. The Barnegat Bay-Little Harbour system, a lagoon type estuary located along the east coast of United States is used as a test case.

Salt marsh erosion influences the sediment budget of bay systems and for our study case salt marsh loss has been found to largely decrease the capability of the bay to retain sediments. The amount of sediment stored within the bay has been classified into three classes: average suspended sediments in the water column, sediments deposited on tidal flats and on the within-bay sea bed, sediments deposited on vegetated surfaces. The amount of sediments trapped on the vegetated surfaces decreases exponentially with the conversion of the system to open water, and in our test case a 50% removal of the marsh surface has an effect comparable to the complete removal of the marsh (Figure 2.9c). This decline is connected to two mechanisms: i) a direct impact associated to the decrease in the spatial extent of vegetated areas were deposition is possible; and ii) an indirect impact connected to the decrease in tidal amplitude, and associated reduced delivery to marsh platforms; the latter has been found to be less important in marsh sediment trapping. The amount of sediment deposited on tidal flats shows a linear decrease with salt marsh lateral erosion.

Generally, as the marshes erode, the capability of the system to retain sediment decreases; therefore positive feedbacks between marsh erosion and a decrease in the available sediment could be triggered which is detrimental for salt marsh survival, and especially for the maintenance of vertical accretion rates.

References

Allen, J.R.L., and Pye, K., (1992). Saltmarshes: Morphodynamics, Conservation, and Engineering Significance , 196 pp., Cambridge Univ. Press, U. K.

Araújo, I.B., Dias, J.M., and Pugh, D.T., (2008). Model simulations of tidal changes in a coastal lagoon, the Ria de Aveiro (Portugal). Cont. Shelf Res. 28, 1010-1025.

Aretxabaleta, A.L., Butman, B., and Ganju, N.K., (2014). Water level response in back-barrier bays unchanged following Hurricane Sandy, Geophys. Res. Lett., 41, 3163–3171, doi:10.1002/2014GL059957.

Aretxabaleta, A.L., Ganju, N.K., Butman, B., and Signell, R.P., (2017). Observations and a linear model of water level in an interconnected inletbay system, J. Geophys. Res. Oceans, 122, 2760–2780, doi:10.1002/ 2016JC012318.

Ariathurai, C.R., and Arulanandan, K., (1978). Erosion rates of cohesive soils. Journal of Hydraulics Division, 104 (2), pp. 279-282.

Aubrey, D.G., and Speer, P.E., (1985). A study of non-linear tidal propagation in shallow inlet estuarine systems. Part I. Observations. Estuar. Coast. Shelf Sci. 21, 185-205.

Beudin, A., Kalra, T.S., Ganju, N.K., and Warner, J.C., (2016). Development of a coupled wave-flow vegetation interaction model. Computers & Geosciences.

Boorman, L.A., (1995). Sea level rise and the future of the British coast. Coastal Zone Topics: Process, Ecology and Management, 1, 10-13.

Booij, N., Ris, R.C., Holthuijsen, L.H., (1999). A third-generation wave model for coastal regions, Part I, model description and validation**.** J. Geophys. Res. C4, 104, pp. 7649-7666.

Carniello, L., D'Alpaos, A. and Defina, A., (2011). Modeling wind waves and tidal flows in shallow micro-tidal basins. *Estuarine, Coastal and Shelf Science*, *92*(2), pp.263-276.

Cavaleri, L., and Malanotte-Rizzoli, P., (1981). Wind wave prediction in shallow water: Theory and applications, J. Geophys. Res., 86C11, 10,961–10,973.

Chassignet, E.P., Arango, H.G., Dietrich, D., Ezer, T., Ghil, M., Haidvogel, D.B., Ma, C.-C., Mehra, A., Paiva, A.M., Sirkers, Z., (2000). DAMEE-NAB: the base experiments. Dynamics of Atmospheres and Oceans 32, 155-183.

Chuang, W.S., and Swenson, E.M., (1981). Subtidal Water level variations in Lake Pontchartrain, Louisiana, J. Geophys. Res., 86(C5), 4198–4204, doi:10.1029/JC086iC05p04198.

Costanza R., et al., (1997), The value of the world's ecosystem services and natural capital. nature 387.6630: 253-260.

Costanza, R., Perez-Maqueo, O., Martinez, M. L., Sutton, P., Anderson, S. J., and Mulder, K., (2008). The value of coastal wetlands for hurricane protection: Ambio, v. 37, no. 4, p. 241-248.

Christiansen, T., Wiberg, P. L., and Milligan, T.G., (2000). Flow and sediment transport on a tidal salt marsh surface, Estuarine Coastal Shelf Sci., 50, 315–331.

D'Alpaos, A., Lanzoni, S., Marani, M., Rinaldo, A., (2010). On the tidal prism–channel area relations. Journal of Geophysical Research, 115. F01003doi:10.1029/2008JF001243.

Dabees, M. A., and Moore, B. D., (2011). "Evaluation of inlet management practices at navigation inlets in southwest Florida, USA." Coastal Engineering Proceedings 1.32: 89.

Dean, R.G., and Dalrymple, R.A. (2004). Coastal processes with engineering applications. Cambridge University Press.

Defne, Z., and Ganju, N., (2014). Quantifying the residence time and flushing characteristics of a shallow, back-barrier estuary: Application of hydrodynamic and particle tracking models, Estuaries Coasts,1 – 16, doi:10.1007/s12237-014-9885-3.

Dickhudt, P.J., Ganju, N.K., and Montgomery, E.T., (2015). Summary of Oceanographic measurements for characterizing light attenuation and sediment resuspension in the Barnegat Bay- Little Egg Harbor estuary, New Jersey, 2013: U.S. Geological Survey Open File Report 2015-1146 18p. (http://dx.doi.org/10.3133/ofr20151146).

Donatelli Carmine. (2018a-s). bbleh. http://doi.org/10.5281/zenodo.1210164.

Donatelli, C., Ganju, N.K., Fagherazzi, S. and Leonardi, N., (2018). Seagrass Impact on Sediment Exchange Between Tidal Flats and Salt Marsh, and The Sediment Budget of Shallow Bays. Geophysical Research Letters, 45(10), pp.4933-4943.

Dronkers J. (1988). Coastal-offshore ecosystem. Lecture Notes on Coastal and Estuaries Studies, ed Jansson B-O (AGU, Washington, DC), Vol 22, pp 3-39.

Fagherazzi, S., et al. (2006). Critical bifurcation of shallow microtidal landforms in tidal flats and salt Marshes. Proceedings of the National Academy of Sciences 103.22: 8337-8341.

Fagherazzi, S., Priestas, A.M., (2010). Sediments and water fluxes in a muddy coastline: interplay between waves and tidal channel hydrodynamics. Earth Surf Process Landforms 2010, 35(3):284–293. 10.1002/esp.1909.

Fagherazzi, S., et al., (2012), Numerical models of salt marsh evolution: Ecological, geomorphic, and climatic factors. Rev. Geophys.,50, RG1002, doi:10.1029/2011RG000359.

Fagherazzi, S., Wiberg, P.L., Temmerman, S., Struyf, E., Zhao, Y. and Raymond, P.A., (2013). Fluxes of water, sediments, and biogeochemical compounds in salt marshes. Ecological Processes, *2*(1), p.3.

Fagherazzi, S., (2014) Coastal processes: Storm-proofing with marshes. Nat Geosci 7(10): 701–702.

F. Falcini, Khan, N.S., Macelloni, L., Horton, B.P., Lutken, C.B., Mckee, K.L., Santoleri, R., Colella, S., Li, C., Volpe, G., D'emidio, M., Salusti, A., Jerolmack, D.J., (2012). Linking the historic 2011 Mississippi River flood to coastal wetland sedimentation. Nat. Geosci., 5, pp. 803-807.

Feagin, R. A., et al., (2011). Engineering properties of wetland plants with application to wave attenuation. Coastal Engineering 58.3: 251-255.

FitzGerald, D.M., (1996). Geomorphic variability and morphologic and sedimentologic controls on tidal inlets. *Journal of Coastal Research*, pp.47-71.

FitzGerald, D.M., Kulp, M., Penland, P., Flocks, J., Kindinger, J., (2004). Morphologic and stratigraphic evolution of ebb-tidal deltas along a subsiding coast: Barataria Bay, Mississippi River Delta. Sedimentology 15:1125–48.

FitzGerald, D. M., et al., (2008). Coastal impacts due to sea-level rise." Annu. Rev. Earth Planet. Sci. 36: 601-647.

Fortunato, A.B., Oliveira, A., (2005). Influence of intertidal flats on tidal asymmetry. Journal of Coastal Research 21 (5), 1062-1067.

Friedrichs, C.T., and Aubrey, D.G., (1988). Non-linear tidal distortion in shallow well-mixed estuaries: a synthesis. Estuarine Coastal and Shelf Science, 27(5), 521-545.

Friedrichs, C.T., and Madsen, O.S., (1992). Non-linear diffusion of the tidal signal in frictionally dominated embayments. Journal of Geophysical Research, 97 (C4), 5637-5650.

Ganju, N.K, Sherwood, C.R., (2010). Effect of roughness formulation on the performance of a coupled wave, hydrodynamic, and sediment transport model. Ocean Modelling 33(3–4): 299–313.

Ganju, N.K., Defne, Z., Kirwan, M.L., Fagherazzi, S., D'Alpaos, A. and Carniello, L., (2017). Spatially integrative metrics reveal hidden vulnerability of microtidal salt marshes. Nature communications, 8, p.ncomms14156.

Ganju, N.K., Nidzieko, N.J. and Kirwan, M.L., (2013). Inferring tidal wetland stability from channel sediment fluxes: Observations and a conceptual model. Journal of Geophysical Research: Earth Surface, *118*(4), pp.2045-2058.

Goodwin, G.C., Mudd, S.M. and Clubb, F.J., (2018). Unsupervised detection of salt marsh platforms: a topographic method. Earth Surface Dynamics, 6(1), pp.239-255.

D'alpaos, A., Da Lio, C. and Marani, M., (2012). Biogeomorphology of tidal landforms: physical and biological processes shaping the tidal landscape. *Ecohydrology*, *5*(5), pp.550-562.

Haidvogel, D.B., Arango, H.G., Hedstrom, K., Beckmann, A., Malanotte-Rizzoli, P., Shchepetkin, A.F., (2000). Model evaluation experiments in the north Atlantic basin: simulations in nonlinear terrain-following coordinates. Dyn. Atmos. Oceans, 17 (32), pp. 239-281.

Haidvogel, D.B., Arango, H.G., Budgell, W.P., Cornuelle, B.D., Curchitser, E., Di Lorenzo, E., Fennel, K., Geyer, W.R., Hermann, A.J., Lanerolle, L., Levin, J., McWilliams, J.C., Miller, A.J., Moore, A.M., Powell, T.M., Shchepetkin, A.F., Sherwood, C.R., Signell, R.P., Warner, J.C., Wilkin, J., (2007). Regional Ocean forecasting in terrain-following coordinates: model formulation and skill assessment. Journal of Computational Physics.

Haidvogel, D. B., et al. (2008). Ocean forecasting in terrain-following coordinates: Formulation and skill assessment of the Regional Ocean Modeling System. Journal of Computational Physics 227.7: 3595-3624.

Hughes, S. A., and Nicholas, C.K., (2006). Frequently-asked Questions (FAQs) About Coastal Inlets and US Army Corps of Engineers' Coastal Inlets Research Program (CIRP). No. ERDC/CHL-CHETN-IV-67. Engineer Research and Development center Vicksburg MS Coastal and Hydraulics Lab.

Hunchak-Kariouk, K., (1999). Relation of water quality to land use in the drainage basins of four tributaries to the Toms River, New Jersey, 1994--1995. No. PB-99-149098/XAB; USGS/WRI--99-4001. Geological Survey, Water Resources Div., West Trenton, NJ

(United States); New Jersey Dept. of Environmental Protection, Trenton, NJ (United States).

Jarrett, J.T., (1976). Tidal prism-inlet area relationships. GITI Rep. 3, U.S. Army Eng.Waterw. Exp. Stn., Vicksburg, MS.

Keulegan, G.H., (1967). Tidal Flow in Entrances, U.S. Army Corps of Engineers, Committee on Tidal Hydraulics, Tech. Bull. 14, Vicksburg.

Kennish, M.J., (2001). State of the estuary and watershed: an overview. Journal of Coastal Research Special Issue 32:243– 273.

Kirwan, M.L., and Murray, A.B., (2007), A coupled geomorphic and ecological model of tidal marsh evolution, Proc. Natl. Acad. Sci. U. S. A., 104, 6118- 6122.

Kirwan, M.L., et al., (1984). Limits on the adaptability of coastal marshes to rising sea level. Geophysical Research Letters 37.23.

Komen, G. J., Hasselmann, S., Hasselmann, K., (1984). On the existence of a fully developed wind☐sea spectrum, J. Phys. Oceanogr., 14, 1271–1285.

Knutson, P.L., Brochu, R.A., Seelig, W.N., and Inskee, M., (1982). Wave damping in Spartina alterniflora marshes. Wetlands, 2, 87– 104.

Lapentina, A., Sheng, Y.P., (2014). Three-dimensional modeling of storm surge and inundation including the effects of coastal vegetation. Estuar. Coasts 37, 1028-1040.

Lathrop, R. G., Jr., and J. A. Bognar (2001), Habitat loss and alteration in the Barnegat Bay Region, J. Coastal Res., 212–228, doi:10.2307/25736235.

Leonard, L. A., and Croft, A.L., (2006). The effect of standing biomass on flow velocity and turbulence in Spartina alterniflora canopies, Estuarine Coastal Shelf Sci., 69, 325–336.

Leonard, L.A., and Luther, M.E., (1995). Flow hydrodynamics in tidal marsh canopies, Limnol. Oceanogr., 40, 1474–1484.

Leonard, L.A. and Reed, D.J., (2002). Hydrodynamics and sediment transport through tidal marsh canopies. Journal of Coastal Re-search, 36, 459–469.

Leonardi, N. and Fagherazzi, S., (2014). How waves shape salt marshes. *Geology*, *42*(10), pp.887-890.

Leonardi, N., Ganju, N.K., and Fagherazzi, S., (2016°). A linear relationship between wave power and erosion determines salt-marsh resilience to violent storms and hurricanes. *Proceedings of the National Academy of Sciences* 113.1: 64-68.

Leonardi, N., Defne, Z., Ganju, N.K., and Fagherazzi, S., (2016b). Salt marsh erosion rates and boundary features in a shallow Bay. Journal of Geophysical Research: Earth Surface, 121(10), pp.1861-1875.

Leonardi, N., Carnacina, I., Donatelli, C., Ganju, N.K., Plater, A.J., Schuerch, M., and Temmerman, S., (2018). Dynamic interactions between coastal storms and salt marshes: A review. Geomorphology 301: 92–107. https://doi.org/10.1016/j.geomorph.2017.11.001.

Li, X., Plater, A. and Leonardi, N., (2018). Modelling the Transport and Export of Sediments in Macrotidal Estuaries with Eroding Salt Marsh. Estuaries *and Coasts*, pp.1-14.

List, J.H., Jaffe, B.E., Sallenger, A.H. Jr, Hansen, M.E., (1997). Bathymetric comparisons adjacent to the Louisiana barrier islands—processes of large-scale change. *J. Coast. Res.* 13:670–78.

List, J.H., Jaffe, B.E., Sallenger, A.H. Jr, Williams, S.J., McBride, R.A., Penland, S., (1994). Louisiana barrier island erosion study: atlas of seafloor changes from 1878 to 1989. USGS/La. State Univ., Misc. Investig. Ser. I-2150-A, USGS, Reston, VA.

Luhar, M., Nepf, H.M., (2011). Flow-induced reconfiguration of buoyant and flexible aquatic vegetation Limnol. Oceanogr., 56 (6), pp. 2003-2017.

Madsen, O.S., Poon, Y.K., Graber, H.C., (1988). Spectral wave attenuation by bottom friction: Theory, Proceedings of 21th International Conference on Coastal Engineering, 492–504Am. Soc. of Civ. Eng., New York.

Madsen, O.S., (1994). Spectral wave–current bottom boundary layer flows. In: Coastal Engineering 1994. Proceedings of the 24th International Conference on Coastal Engineering Research Council, Kobe, Japan, pp. 384–398.

Marani, M., D'Alpaos, A., Lanzoni, S., Carniello, L. and Rinaldo, A., (2007). Biologically-controlled multiple equilibria of tidal landforms and the fate of the Venice lagoon. *Geophysical Research Letters*, *34*(11).

Marani, M., D'Alpaos, A., Lanzoni, S., Carniello, L., and Rinaldo, A., (2010b), The importance of being coupled: Stable states and catastrophic shifts in tidal biomorphodynamics, J. Geophys. Res., 115, F04004, doi:10.1029/2009JF001600.

Marani, M., D'Alpaos, A., Lanzoni, S., and Santalucia, M., (2011), Understanding and predicting wave erosion of marsh edges, Geophys. Res. Lett., 38, L21401, doi:10.1029/2011GL048995.

Marjoribanks, T.I., Hardy, R.J., Lane, S.N., (2014). The hydraulic description of vegetated river channels: the weaknesses of existing formulations and emerging alternatives. WIREs Water 1, 549-560.

Meyer-Peter, E., Müeller, R., (1948). Formulas for bedload transport. In: Report on the 2nd Meeting International Association Hydraulic Structure Research. Stockholm, Sweden, pp. 39–64.

Moller, I., Spencer, T., French, J.R., Leggett, D.J., and Dixon, M., (1999). Wave transformation over tidalmarshes: a field and numerical modeling study from North Norfolk, Estuarine, Coastal and Shelf Science, 49, 411–426.

Moller, I., et al., (2014). Wave attenuation over coastal salt marshes under storm surge conditions. Nat Geosci 7(10):727–731.

Morin, J., Leclerc, M.M., Secretan, Y., Boudreau, P., (2000). Integrated two-dimensional macrophytes-hydrodynamic modelling. J. Hydraul. Res., 38, pp. 163-172.

Morris, J.T., Sundareshwar, P.V., Nietch, C.T., Kjerfve, B., and Cahoon, D.R., (2002). Responses of coastal wetlands to rising sea level. Ecology, 83, 2869–2877.

Mudd, S.M., D'Alpaos, A., and Morris, J.T., (2010). How does vegetation affect sedimentation on tidal marshes? Investigating particle capture and hydrodynamic controls on biologically mediated sedimentation, J. Geophys. Res., 115, F03029, doi:10.1029/2009J.

Mukai, A.Y., Westerink, J.J., Luettich Jr., R.A., and Mark, D., (2002). Eastcoast 2001: A tidal constituent database for the western North Atlantic, Gulf of Mexico and Caribbean Sea. US Army Engineer Research and Development Center, Coastal and Hydraulics Laboratory, Technical Report, ERDC/CHL TR-02-24.

Murphy, A. H., and Epstein, E.S., (1989). "Skill scores and correlation coefficients in model verification." Monthly Weather Review 117.3 (1989): 572-582.

Nepf, H.M., (1999). Drag, turbulence, and diffusion in flow through emergent vegetation, Water Resour. Res., 35, 479–489, doi:10.1029/1998WR900069.

O'Brien, M.P., (1931). Estuary tidal prisms related to entrance areas. *Civil Eng.* 1:738–39.

O'Brien, M.P., (1969). Equilibrium flow areas of inlets on sandy coasts. J. Waterw. Port Coast. Ocean Eng. 95:43–55.

Pawlowicz, R., Beardsley, B., and Lentz, S., (2002). Classical tidal harmonic analysis including error estimates in MATLAB using T_TIDE, Comput. Geosci., 28, 929–937.

Picado, A., Dias, J.M., Fortunato, A.B. (2010). Tidal changes in estuarine systems induced by local geomorphologic modifications. Continental Shelf Research, 30 (17), pp. 1854-1864, 10.1016/j.csr.2010.08.012.

Ree, W.O., (1949). "Hydraulic characteristics of vegetation for vegetated waterways."Agric. Eng., 30, 184–189.

Rodi, W., (1984). Turbulence models and their application in hydrulicsm a state of the art review. Technical report, International Association of Hydraulics Research, Delft.

Rodríguez, J. F., et al., (2017). Potential increase in coastal wetland vulnerability to sea-level rise suggested by considering hydrodynamic attenuation effects. Nature Communications 8.

Schwimmer, R.A., and Pizzuto, J.E., (2000). A model for the evolution of marsh shorelines. Journal of Sedimentation Research, 70, 1026–1035.

Schwimmer, R. (2001). Rates and processes of marsh shoreline erosion in Rehoboth Bay, Delaware, U.S.A., J. Coastal Res., 17(3), 672-683, doi:10.1016/j.csr.2009.08.018.

Shchepetkin, A. F., and McWilliams, J. C., (2005). The Regional Ocean Modeling System: A split-explicit, free-surface, topography following coordinates ocean model, Ocean Modelling, 9, 347-404.

Shchepetkin, A. F., and McWilliams, J.C., (2009). Correction and Commentary for "Ocean forecasting in terrain-following coordinates: formulation and skill assessment of the Regional Ocean Modeling System" by Haidvogel et al., J. Comp. Phys., 228, 8985-9000.

Soulsby, R.L., Damgaard, J.S., 2005. Bedload sediment transport in coastal waters. Coastal Engineering, 52 (8), pp. 673-689.

Styles, R., Glenn, S.M., (2000). Modeling stratified wave and current bottom boundary layers on the continental shelf, Journal of Geophysical Research, 105 (C10), pp. 24,119-24,139.

Suk, N.S., Guo, Q., and Psuty, N. P., (1999). Suspended solids flux between salt marsh and adjacent bay: A long-term continuous measurement, Estuarine Coastal Shelf Sci., 49(1), 61–81.

Temmerman S, et al., (2013) Ecosystem-based coastal defence in the face of global change. Nature 504(7478):79–83.

Temmerman, S., Moonen, P., Schoelynck, J., Govers, G. and Bouma, T.J., (2012). Impact of vegetation die-off on spatial flow patterns over a tidal marsh. Geophys. Res. Lett. 39, L03406.

U.S. Department of Agriculture, (2008). Plants database. Natural Resources Conservation Service. http://plants.usda.gov/.

Uittenbogaard R., (2003). Modelling turbulence in vegetated aquatic flows. International workshop on Riparian Forest vegetated channels: hydraulic, morphological and ecological aspects, Trento, Italy, 20–22 February 2003.

Walton TL, Adams WD. 1976. Capacity of inlet outer bars to store sand. Proc. Coast.Eng. Conf., 15th, Honolulu, *HI*, pp. 1919–37, New York: ASCE.

Warner, J.C., Sherwood, C.R., Signell, R.P., Harris, C., Arango, H.G., (2008). Development of a three-dimensional, regional, coupled wave, current, and sediment-transport model, Computers and Geosciences, 34, pp. 1284–1306.

Warner, J.C., Armstrong, B., He, R., Zambon, J.B., (2010). Development of a coupled ocean-atmosphere-wave-sediment transport (COAWST) modeling system. Ocean Model., 35 (3), pp. 230-244.

Yang, S.L., (1998). The role of Scirpus marsh in attenuation of hydrodynamics and retention of fine-grained sediment in the Yangtze Estuary. Estuarine, Coastal and Shelf Science, 47, 227–233.Table 1. List of numerical runs.

A non-linear relationship between marsh size and sediment trapping capacity compromises salt marsh resilience to sea-level rise

Carmine Donatelli[1] [(*)], Xiaohe Zhang[2] [(*)], Neil K. Ganju[3], Alfredo L. Aretxabaleta[3], Sergio Fagherazzi[2], Nicoletta Leonardi[1]

*corresponding Author: Carmine@liverpool.ac.uk; zhangbu@bu.edu

(1) Department of Geography and Planning, School of Environmental Sciences, Faculty of Science and Engineering, University of Liverpool, Roxby Building, Chatham St., Liverpool L69 7ZT, UK

(2) Department of Earth Sciences, Boston University, 675 Commonwealth Avenue, Boston, MA 02215, USA

(3) U.S. Geological Survey, Woods Hole Coastal and Marine Science Center, MA 02543, USA

Supplementary material can be found in Appendix 4

C.D. performed COAWST simulations and carried out the analysis; C.D. wrote the manuscript assisted by N.L., S.F. and N.K.G.; C.D. designed part of the study (changes in tides associated with salt marsh loss).

Abstract

Global assessments predict the impact of sea-level rise on salt marshes with present-day levels of sediment supply from rivers and the coastal ocean. However, these assessments do not consider that variations in marsh extent and the related reconfiguration of intertidal area driven by sea-level rise affect local sediment dynamics, ultimately controlling the fate of the marshes themselves. Herein, we conduct a meta-analysis of six bays along the US East Coast to show that a reduction in the current salt marsh area negatively affects the sediment availability in estuarine systems through changes in the regional scale hydrodynamics. This positive feedback between marsh disappearance and the ability of coastal bays to retain sediments, including sediments stored in tidal flats and tidal channels, reduces the trapping capacity of the system and jeopardizes the survival of the remaining marshes. Here we show that on marsh platforms the sediment deposition per unit area decreases exponentially with marsh loss. Marsh erosion elarges tidal prism values and enhances the tendency towards ebb dominance, thus decreasing the overall sediment availability of the system. Our findings highlight that marsh deterioration reduces the sediment stock in back-barrier basins and therefore compromises the resilience of salt marshes.

Keywords: salt marshes, coastal resilience, ecosystem services, COAWST, Delft3D.

3.1 Introduction

Salt marshes provide critical ecosystem services [Costanza et al., 1997]. For instance, in recent years salt marshes have been the focus of many restoration plans built on the concept of 'nature-based solutions' for flood defenses that aim to use vegetated surfaces to protect coastal communities from storms [Temmerman et al., 2013]. The economic value of salt marsh ecosystem services has been estimated to be up to 5 million USD per km^2 in the United States [Costanza et al., 2008], and 786 million GBP per year for all UK marshes [Foster et al., 2013; Leonardi et al., 2017]. Projections of salt marsh response to climate change are variable, with initial studies suggesting a 46% to 59% reduction of the present-day area by 2100 under moderate sea-level rise [Spencer et al., 2016], and more refined studies estimating "coastal squeezing" of up to 30% when accounting for landward migration [Schuerch et al., 2018]. When allowed by the availability of accommodation space, the landward migration of fringing marshes supports the maintenance of marsh extent but lateral erosion remains a serious threat to areal preservation [Schwimmer and Pizzuto, 2000; Schwimmer, 2011].

Apart from hydrodynamics, salt marsh resilience has been linked to the sediment budget of the marsh complex as a whole, including not only the vegetated surfaces but surrounding tidal flats, sea bed, and tidal channels [Ganju et al., 2013; Fagherazzi, 2014]. Ganju et al. [2017] synthesized sediment budgets of eight micro-tidal salt marsh complexes, and demonstrated the existence of a relationship between sediment budget and the unvegetated-vegetated marsh ratio (UVVR), indicating that sediment deficits are linked to conversion of vegetated marsh portions into open water. A positive sediment budget is indeed

necessary to allow marshes and tidal flats to keep pace with sea-level rise [Mariotti and Fagherazzi, 2010; Fagherazzi and Priestas, 2010].

Regional effects are crucial when evaluating coastal interventions under the management of multiple agencies. Though many studies have focused on local marsh dynamics, less attention has been paid to how changes in marsh areal extent might drive large-scale variations of hydrodynamic and sediment transport processes [Donatelli et al., 2018a; Zhang et al., 2018]. Generally, marsh erosion has only concerned adjacent anthropogenic settlements, while less attention has been paid to regional scale impacts of erosion on distal areas. We conduct a meta-analysis of high resolution numerical modeling results for the hydrodynamics and sediment transport of six lagoon-type estuaries along the US Atlantic Coast. The sediment dynamics of these bays were simulated under different scenarios of salt marsh loss obtained by artificially changing the current bathymetries [Donatelli et al., 2018b]. The Coupled-Ocean-Atmosphere-Wave-Sediment Transport (COAWST) modelling system [Warner et al., 2010] and the computational fluid mechanics package Delft3D [Lesser et al., 2004] were used to carry out a set of exploratory models [Murray, 2007]. Our study demonstrates that the same proportion of marsh removal can have different impacts on the trapping capacity of estuaries and we find that marsh vulnerability in lagoon-type settings can be underestimated when not accounting for the effect of marsh loss on potential sediment storage of the entire system. The study sites are listed in Table 3.1, while the present-day salt marsh area is highlighted in Figure 3.1.
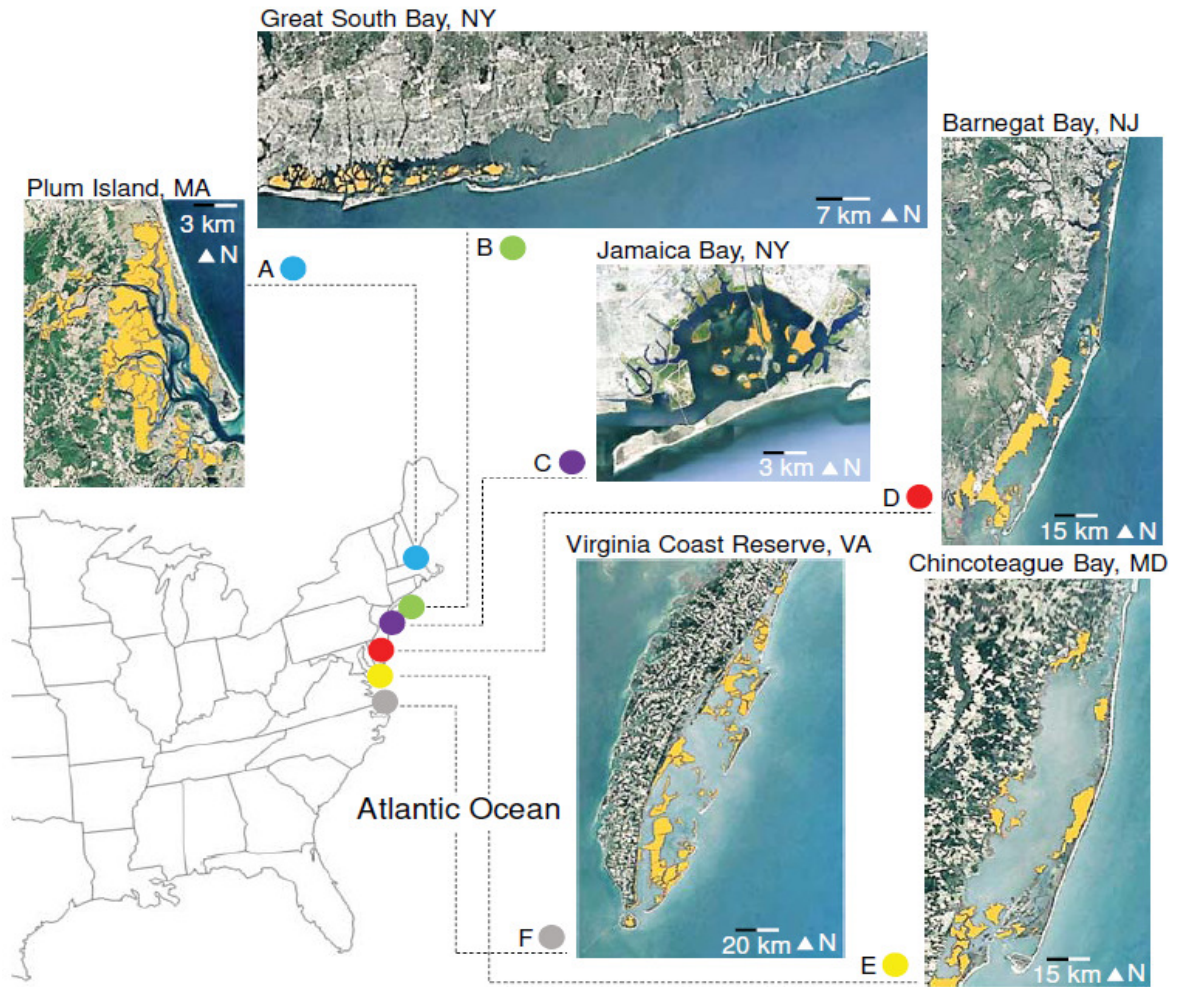
Figure 3.1 Satellite images of the studied bays. All the systems are located along the Atlantic coast of the USA: Plum Island Sound (a), Great South Bay (b), Jamaica Bay (c), Barnegat Bay-Little Egg Harbor (d), Chincoteague Bay (e) and Virginia Coast Reserve (f). The satellite images were acquired from Google Earth.

System	Location	Marsh/basin area	Mean tidal range (m)	Mean water depth (m)	Numerical model
PI	42^{0}45'N, 70^{0}47'W	0.6	3	3	Delft3D
GSB	40^{0}68'N, 73^{0}11'W	0.16	1.2	1.2	COAWST
JB	40^{0}60'N, 73^{0}87'W	0.07	4	4	COAWST
BB-LEH	39^{0}86'N, 74^{0}11'W	0.25	1.5	1.5	COAWST
CB	38^{0}02'N, 75^{0}30'W	0.13	1.4	1.2	COAWST
VCR	37^{0}41'N, 75^{0}68'W	0.32	1.35	1.5	Delft3D

Table 3.1 Location (latitude and longitude), initial marsh/basin area ratio, average water depth (m), mean tidal range (m) and numerical framework used for each estuary.

3.2 Study sites

The selected study areas include six lagoon-type estuaries characterized by different tidal ranges and morphological features, located between the states of Massachusetts and Virginia (Figure 3.1). From north to south the estuarine systems are: Plum Island Sound, Great South Bay, Jamaica Bay, Barnegat Bay-Little Egg Harbor, Chincoteague Bay, and Virginia Coast Reserve (Figure 3.1, A to E). Along the US East Coast tides are mainly semidiurnal, with the M_2 harmonic being the dominant constituent. Table 3.1 summarizes the present-day marsh/basin area ratio, the average water depth and the mean tidal range. Plum Island Sound (PI) is located in northeastern Massachusetts, USA (Figure 3.1, A). The total estuarine area is approximately 59.8 km^2 and it is characterized by extensive salt marshes, which account for 60% of the estuary surface [Buchsbaum et al., 2009]. The average tidal range is 2.6 m and the mean water depth is 3 m.

Great South Bay (GSB) and Jamaica Bay (JB) are shallow lagoon-type estuaries located in the State of New York, USA (Figure 3.1, B and C). GSB [Aretxabaleta et al., 2017] is connected to the ocean through three inlets: East Rockaway Inlet, Jones Inlet and Fire

Island Inlet; the total basin area is 250 km^2 and its width ranges from 2.5 to 8 km. The average water depth is 1.2 m and the mean tidal range is ~0.3 m over most of the bay. Jamaica Bay has an area of 50 km^2 and an average water depth of 4 m and is connected to the ocean through Rockaway Inlet. As documented by the New York City Department of Environmental Protection [2007], over 75% of salt marshes in Jamaica Bay have been lost since the mid-1800s. The mean tidal range is around 1.5 m.

Barnegat Bay-Little Harbor Estuary (BB-LEH) is a narrow and long coastal embayment, approximately 70 km in the north-south direction, located in New Jersey, USA (Figure 3.1D). The lagoon is composed of three shallow bays: Barnegat Bay, Manahawkin Bay and Little Egg Harbor; the main connections with the Atlantic Ocean are through two inlets (Little Egg Inlet and Barnegat Inlet) and the Point Pleasant Canal [Hunchak-Kariouk, 1999]. The average water depth is 1.5 m and the mean tidal range is ~0.4 m. As reported by Lathrop and Bognar [Lathrop and Bognar, 2001], natural and human drivers have drastically reduced salt marsh area from around 148.5 km^2 to 99.4 km^2 over the last century in this system.

The southernmost estuaries are Chincoteague Bay (CB) and Virginia Coast Reserve (VCR), located between the states of Maryland and Virginia (Figure 3.1, E and F). Chincoteague Bay [Beudin et al., 2017] is a shallow (average water depth 1.4 m) and long bay, around 60 km from Ocean City Inlet in the north to Chincoteague Inlet in the south, with a total back-barrier area of 315 km^2, a maximum width of 10 km and a mean tidal range of 0.25 m throughout most of the bay. VCR includes several bays, characterized by shallow tidal flats (about 1 m below MLLW) and deep channels (about 10 m below MSL),

which are connected to the ocean through tidal inlets [Nardin et al., 2018]. The total plan area is 550 km^2, the average water depth 1.3 m and the mean tidal range is 1.2 m. Bathymetries are illustrated in the supplementary material (Appendix 3, Figure A.3.1a, f, A.3.2a, h and A.3.3-4a).

3.3 Methods

The hydrodynamics and sediment transport of the bays were simulated using the COAWST (Coupled-Ocean-Atmosphere-Wave-Sediment Transport Modeling System) modeling framework [Warner et al., 2010] for Great South Bay, Jamaica Bay, Barnegat Bay-Little Egg Harbor and Chincoteague Bay (Table 3.1). The ocean model used in COAWST is ROMS (Regional Ocean Modeling System), which incorporates a sediment transport module based on the Community Sediment Transport Modeling System [Shchepetkin and McWilliams, 2005; Warner et al., 2008]. The computational fluid dynamics package Delft3D [Lesser et al., 2004] was used for Plum Island Sound and Virginia Coast Reserve (Table 3.1). Numerical simulations were conducted to identify the impact of different marsh removal scenarios on tidal propagation and on the amount of sediments potentially being retained in the system given an initial sediment input. The suspended sediment transport was modelled by solving the advection-diffusion equation, and by accounting for source/sink terms induced by downward settling or upward flux of eroded material. The depositional flux is proportional to the bottom concentration and settling velocity values; the erosion flux was calculated following the Ariathurai and Arulanandan formulation [1978] in ROMS and the Partheniades formulation [1965] in Delft3D. In both formulations the erosion flux depends on the exceedance shear stress with respect to the critical shear stress, and on a user-defined erosion parameter. The selected turbulence model was the k–ε scheme [Rodi, 1984].

COAWST explicitly accounts for the influence of flexible cylindrical plant structures on drag and turbulence [Beudin et al., 2017]. The spatially averaged vegetation drag force was approximated using a quadratic drag law and the effect of plant flexibility on drag is

81

computed defining an effective blade length [Luhar and Nepf, 2011]. Apart from the mean flow velocity, vegetation also modifies turbulence intensity and mixing. The extra dissipation and turbulence kinetic energy production due to vegetation was accounted for following Uittenbogaard [2003]. In Delft3D we accounted for vegetation following the Baptist [2005] and Uittenbogaard [2003] formulations for drag and turbulence calculations. The marsh coverage data were retrieved from the CRSSA's (Center for Remote Sensing and Spatial Analysis) geographic information systems (GIS) database (Figure 3.1). For each bay, five simulations were run with different marsh loss percentages: 0% (current salt marsh distribution), 25%, 50%, 75% and 100% (vegetated area completely eroded). The erosion of salt marshes was simulated by removing vegetation from the eroded marsh cells, and by matching the corresponding bathymetry values with the elevation of the surrounding tidal flats. Specifically, when a vegetated 'salt marsh pixel' was adjacent to one or more 'tidal flat pixels', the 'salt marsh pixel' was converted into tidal flat by assigning to it a water depth equivalent to the average of the surrounding 'tidal flat pixels'. The algorithm was repeated enough times to reach a reduction of 25%, 50%, 75% and 100% in the present-day salt marsh area. The sediments eroded from marshes were artificially removed from the bays. As salt marsh removal increases tidal prism values, the mouth of the inlets was updated changing its width through an iterative procedure following the O'Brien-Jarrett-Marchi law [D'Alpaos et al., 2010]. We computed the slope coefficient of the O'Brien-Jarrett-Marchi law [D'Alpaos et al., 2010] with an exponent of $6/7$ for the current estuarine morphology and modified the cross-sectional area by increasing only the width of the inlets. Convergence of the modified system was considered to have been established once the changes in inlet cross-sectional area modified the tidal

prism by less than 1%. For this study, only one class of sediments was defined for all estuaries, with mass density of 2650 kg/m^3, settling velocity of 0.5 mm/s, erodibility and critical shear stress equal to 0.0005 kg m^{-2}s^{-1} and 0.05 N/m^{-2} respectively; these values were chosen based on sediment fraction parameters typical of lagoon-type estuaries [Wiberg et al., 2015]. The seabed was defined as one layer having an initial thickness of zero. The time frame of the analysis was 30 days. As an initial condition, a uniform suspended sediment concentration (100 mg/l) was imposed in the water column inside the estuary; specifically, the sediment injection occurs at mean sea level, during the first flood period. During the simulation there are no other external sediment inputs. The amount of sediment initially released in the system does not impact the results, as the main outcomes are expressed in terms of sediment fraction. As the initial sediment thickness at the bottom was zero, sediment transport, erosive and depositional fluxes are solely related to the concentration imposed at the beginning of the simulation. The models were forced with observed tidal forcings and changes in the tidal signal were investigated following a classic harmonic analysis [Pawlowicz et al., 2002]. Further information of the model set-up can be found in Appendix 1: Model validation.

3.4 Results

For each bay, five simulations were run with different marsh loss percentages: 0% (current salt marsh distribution), 25%, 50%, 75% and 100% (vegetated area completely eroded). Salt marsh disappearance changes the morphology of the back-barrier basin, and consequently alters tidal prism values (Appendix 3, Figure A.3.5). The tidal signal also changes across different portions of the basins. A comparison of tidal amplitude and phase lag values between the pre- and post-erosion salt marsh configurations suggests that changes in tidal amplitude depend on the increased filling time of the back-barrier bay due to post-erosion increases in volume [Keulegan, 1967].

As a consequence of salt marsh removal, the water levels change within the entire back-barrier basin. For those systems where marshes mainly fringe the mainland and barrier island boundary (Plum Island Sound, Jamaica Bay, Barnegat Bay-Little Egg Harbor), the tidal phase lag between the ocean and the lagoon increases, leading to a reduction in tidal amplitude over the entire back-barrier bay. In contrast, in Great South Bay, Chincoteague Bay and Virginia Coast Reserve, large marsh portions are detached from the mainland, and different parts of the domain experience different variations in tidal amplitude. Specifically, when salt marshes are detached from the mainland, the deterioration of the marshes produces an increase in tidal amplitude between the original location of the marsh and the mainland, and a decrease in tidal amplitude between the marsh and the inlets. This suggests that locations near the mainland sheltered by marsh will be more affected by frictional reduction due to marsh disappearance than by the increase in filling time. The spatial distribution of tidal amplitude and phase lag before and after salt marsh removal for

each bay are depicted in Figure 3.2a, b, 3.3a, b and in the supplementary material (Appendix 3, Figure A.3.2-3-4f, g and A.3.2o, p).
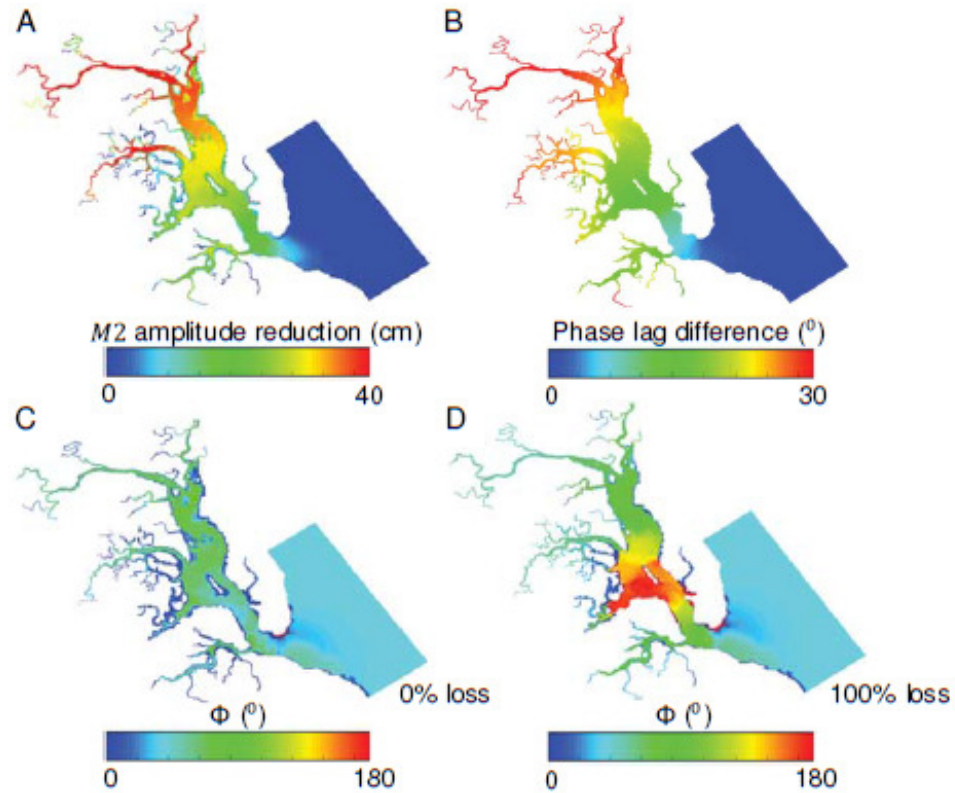
Figure 3.2 Changes in tidal dynamics induced by marsh loss in Plum Island Sound. Reduction in M_2 amplitude (cm) and increase in phase lag (Φ) after the removal of the entire marsh surface (a-b); sea-surface phase of M_4 relative to M_2 for the current marsh distribution (c) and marsh completely eroded (d).
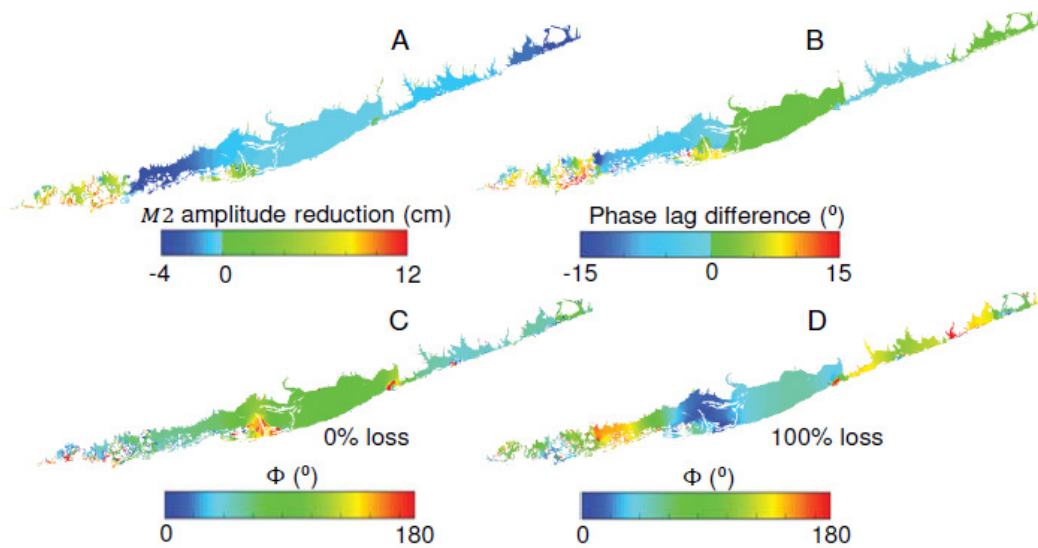
Figure 3.3 Changes in tidal dynamics induced by marsh loss in Great South Bay. Reduction in M_2 amplitude (cm) and increase in phase lag (Φ) after the removal of the entire marsh surface (a-b); sea-surface phase of M_4 relative to M_2 for the current marsh distribution (c) and marsh completely eroded (d).

We isolated the effect of salt marsh location from the effect of tidal wave interaction coming from multiple inlets by artificially transforming the estuaries into systems with a single entrance (Figure A.3.6-8). For coastal bays with multiple inlets, water levels are controlled by overlapping waves propagating from each inlet, and changes in estuary morphology can alter their relative phase and amplitude. Additional simulations were conducted to verify that increases/decreases in tidal amplitude were caused by changes in salt marsh area rather than by the overlap of multiple tidal waves (Appendix 3, Figure A.3.6-8).

Salt marsh erosion also influences tidal asymmetry. Asymmetric tides are important for the transport and deposition of sediment in shallow estuaries [Aubrey and Speer, 1985]. Changes in the M_4 to M_2 water level amplitude ratio and the phase difference between M_4

and M_2 were calculated for each scenario. The relative phase is based on $2\varphi_2 - \varphi_4$, where φ_2 is the M_2 phase and φ_4 is the M_4 phase as per Friedrichs and Aubrey [1988]. For all test cases the estuaries remain flood dominated, even though marsh loss raises the tendency towards ebb dominance in some systems (Figure 3.2c, d, 3.3c, d; Appendix 3, Figure A.3.10-11c, d, g, h); the magnitude of the non-linear distortion increases with marsh removal (Appendix 3, Figure A.3.9 and A.3.10-11a, b, e, f). These results are consistent with previous 1D numerical investigations [Friedrichs and Aubrey, 1988]. Recent 2D numerical studies suggest that these findings might be also dependent on the choice of friction for small ratios of tidal amplitude to mean water depth [Zhou et al., 2018].

To quantitatively evaluate how changes in tidal dynamics impact the sediment budget of the systems, we quantified sediment trapping efficiency before and after the removal of the marsh. Sediment trapping was evaluated by releasing a fixed amount of sediment in the bay, and then computing the fraction stored in the marshes, tidal flats and channels. We stopped the simulations after 30 days because after this period the deposited volume did not significantly change. The sediment deposit was sampled in the last day of simulation. Results are presented as a function of the ratio between marsh extent and basin area (Figure 3.4).
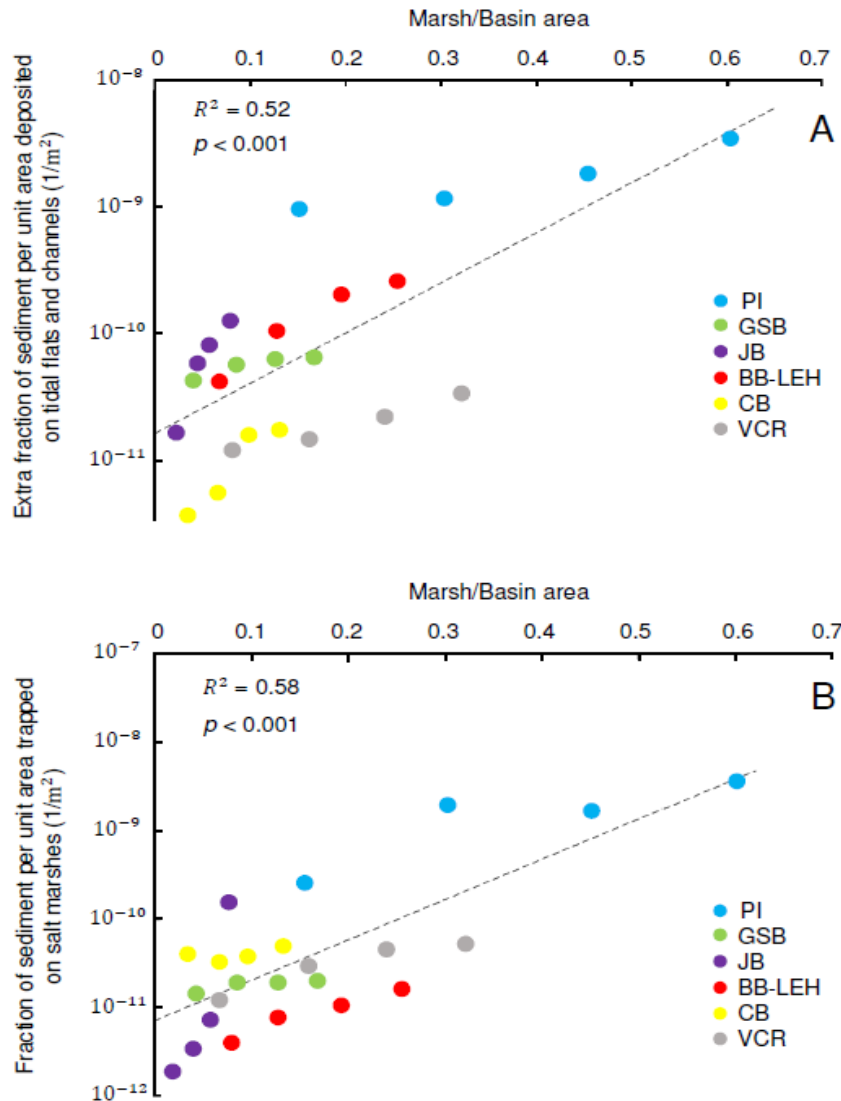
Figure 3.4 Effect of marsh extent on the ability of tidal flats, channels and salt marshes to trap sediment inputs. Fraction of sediment per unit area deposited on tidal flats and channels directly related to marsh presence as a function of normalized marsh area (a); fraction of sediment per unit area trapped on the marshes as a function of normalized marsh area (b). The four values for each location are the four quartiles tested (0, 25, 50 and 75%).

The fraction of sediment potentially stored in channels and tidal flats per unit area decreases non-linearly as the ratio between marsh area becomes smaller (Figure 3.4a); furthermore, the fraction of sediment per unit area trapped by salt marshes drops exponentially (Figure 3.4b). Excluding Jamaica Bay, the exponential decay in sediment trapping as a function of

marsh loss is relatively similar in each bay and close to the overall trend. This finding shows that marsh resilience to sea-level rise might be compromised even by small percentages of marsh lateral erosion, as the relationship between marsh areal extent and marsh sediment trapping capacity is strongly non-linear. Changes in marsh extent due to erosion or restoration projects will cause changes in the amount of sediment trapped within the estuarine system. This might in turn promote further establishment or erosion of salt marshes. A decrease in salt marsh area causes a decrease in sediment trapping of the system, which could in turn promote further marsh deterioration. Given the assumption that the net sediment budget is the driving factor for marsh stability, the non-linear relationship further suggests that any restoration project increasing salt marsh areas will trigger a positive feedback increasing sediment retention, but such changes will depend on the initial marsh extent.

3.5 Discussion

Our findings in relation to the sediment budget are relevant for the long-term resilience of the systems, as the sediment budget is an integrated metric of ecosystem stability [Ganju et al., 2017]. Donatelli et al., [2018b] studied the influence of salt marsh deterioration on the sediment budget in Barnegat Bay-Little Egg Harbor estuary and showed an exponential decrease in the sediment deposition on vegetated surfaces with marsh decline. The results of Donatelli et al., [2018b] are site-specific. Herein, we demonstrate that the effect of marsh loss on the resilience of salt marshes to sea-level rise is independent of the specific setting of the back-barrier estuary and rather depends on the extent of the eroded marsh area with respect to the basin size. More specifically, our model results show a non-linear trend between marsh/basin area ratio and the capacity of coastal bays to store sediments over

marsh platforms and demonstrate that as salt marshes erode they become more sensitive to the deleterious effects of sea-level rise. This finding challenges the common idea that most salt marshes will survive accelerated sea-level rise with current levels of sediment supply from rivers and coastal ocean [Kirwan et al., 2016]. Indeed, global scale-studies based on simplified hydrodynamic conditions do not consider marsh extent and the reconfiguration of intertidal area affecting the ability of estuaries to retain sediment inputs. Marsh loss enlarges the intertidal storage volume, raises the tendency towards ebb dominance and therefore reduces the overall sediment availability of the system, ultimately controlling the fate of the marshes themselves [Ganju et al., 2013; Fagherazzi, 2014]. Under future sea-level rise scenarios, further tidal prism enlargements and additional fragmentation of the barrier islands might be expected and these could potentially compromise the survival of entire lagoon ecosystems [FitzGerald et al., 2006]. Even if increasing hydraulic depth would reinforce existing tidal asymmetries [Pethick, 1994; Friedrichs et al., 1990] and enlarge the mean tidal range of the estuary, with insufficient sediment supply the system will not be able to keep pace with sea-level rise. Bottom shear stresses will be reduced by the increase in the mean water depth and this would enhance deposition on tidal flats rather than resuspension and sediment storage on salt marshes. As a result, marsh stability in the vertical direction will be further compromised by sea-level rise. In the long-term, a reduced sediment trapping capacity might also control the lateral extension of salt marshes. A simple model proposed by Mariotti and Fagherazzi [2013] shows that the ratio between marsh to open water area in a bay is controlled by sediment availability (and sediment concentration). Similarly, the long-term modelling framework of Walters et al. [2014] indicates that marsh extension in back-barrier areas is a function of sediment supply; more

sediment flushing and less trapping would therefore lead to a reduced marsh extension in these models.

Our study highlights the importance of coastal restoration interventions, which should target coastal erosion before the vegetated surface becomes too small compared to the basin area in order to maximize the large-scale efficiency of the interventions. Our findings further show the necessity to account for the nonlinearity of ecosystem response to changes in habitat size. A simplified approach that assumes ecosystem services provided by coastal habitats change linearly with their size would lead to a misrepresentation of the true economic value of salt marshes in terms of coastline resilience [Barbier, 2008].

Acknowledgment

References

Aretxabaleta, A. L., Ganju, N. K., Butman, B., and Signell, R. P., (2017). Observations and a linear model of water level in an interconnected inlet-bay system. J Geophys. Res. Oceans, p. 122, 10.1002/2016JC012318.

Aubrey, D. G., and Speer, P. E., (1985). A study of non-linear tidal propagation in shallow inlet estuarine systems. Part I. Observations. Estuarine, Coastal and Shelf Science, 21(2), 185–205. https://doi.org/10.1016/0272-7714(85)90096-4.

Barbier, E. B., (2008). Ecosystems as natural assets. Foundations and Trends in Microeconomics 4: 611–681.

Beudin, A., Kalra, T. S., Ganju, N. K., and Warner, J. C., (2017). Development of a coupled wave-flow vegetation interaction model. Computers & Geosciences.

Bricker-Urso, S., Nixon, S.W., Cochran, J.K., Hirshberg, D. J., and Hunt, C., (1989). Accretion rates and sediment accumulation in Rhode Island salt marshes. Estuaries 12: 300–317.

Buchsbaum, R. N., Deegan, L. A., Horowitz, J., Garritt, R. H., Giblin, A. E., Ludlam, J. P., and Shull, D. H., (2009). ShullEffects of regular salt marsh haying on marsh plants, algae, invertebrates and birds at Plum Island Sound, Massachusetts. Wetlands Ecology and Management, 17, pp. 469-487.

Costanza, R., d'Arge, R., de Groot, R.S., Farber, S., Grasso, M., Hannon, B., Limburg, K., Naeem, S., O'Neill, R.V., Paruelo, J., Raskin, R.G., Sutton, P., and van den Belt, M., (1997). The value of the world's ecosystem services and natural capital. Nature, 387, pp. 253-260.

Costanza, R., Perez-Maqueo, O., Martinez, M. L., Sutton, P., Anderson, S. J., and Mulder, K., (2008). The value of coastal wetlands for hurricane protection: Ambio, v. 37, no. 4, p. 241-248.

Donatelli, C., Ganju, N. K., Fagherazzi, S., and Leonardi, N., (2018a). Seagrass impact on sediment exchange between tidal flats and salt marsh, and the sediment budget of shallow bays, Geophysical Research Letters, doi:10.1029/2018GL078056.

Donatelli, C., Ganju, N. K., Zhang, X., Fagherazzi, S., and Leonardi, N., (2018b). Salt marsh loss affects tides and the sediment budget of shallow bays, Journal of Geophysical Research: Earth Surface, doi: 10.1029/2018JF004617.

D'Alpaos, A., Lanzoni, S., Marani, M., and Rinaldo, A., (2010). On the tidal prism–channel area relations. Journal of Geophysical Research, 115. F01003doi:10.1029/2008JF001243.

Fagherazzi, S., and Priestas, A.M., (2010). Sediments and water fluxes in a muddy coastline: interplay between waves and tidal channel hydrodynamics. Earth Surf Process Landforms, 35(3):284–293. 10.1002/esp.1909.

Fagherazzi, S., (2014). Coastal processes: Storm-proofing with marshes. Nature Geoscience 7(10): 701–702.

FitzGerald DM, Buynevich IV, Argow BA., 2006. Model of tidal inlet and barrier island dynamics in a regime of accelerated sea-level rise. J. Coast. Res. 39:789–95.

Foster, N. M., Hudson, M. D., Bray, S., and Nicholls, R. J., (2013). Intertidal mudflat and salt marsh conservation and sustainable use in the UK: a review. Journal of Environmental Management, 126, 96–104.

Friedrichs, C. T., and Aubrey, D.G., (1988). Non-linear tidal distortion in shallow well-mixed estuaries: a synthesis. Estuarine Coastal and Shelf Science, 27(5), 521-545.

Friedrichs, C.T., Aubrey, D.G., and Speer, P.E., (1990). Impacts of relative sea-level rise on evolution of shallow estuaries. In: Cheng, R.T. (ed.), Residual Currents and Long-Term Transport. New York: Springer-Verlag, 105-122.

Ganju, N.K., Nidzieko, N.J. and Kirwan, M.L., (2013). Inferring tidal wetland stability from channel sediment fluxes: Observations and a conceptual model. Journal of Geophysical Research: Earth Surface, 118(4), pp.2045-2058.

Ganju, N.K., Defne, Z., Kirwan, M.L., Fagherazzi, S., D'Alpaos, A. and Carniello, L., (2017). Spatially integrative metrics reveal hidden vulnerability of microtidal salt marshes. Nature communications, 8, p.ncomms14156.

Hunchak-Kariouk, K., (1999). Relation of water quality to land use in the drainage basins of four tributaries to the Toms River, New Jersey, 1994--1995. No. PB-99-149098/XAB; USGS/WRI--99-4001. Geological Survey, Water Resources Div., West Trenton, NJ (United States); New Jersey Dept. of Environmental Protection, Trenton, NJ (United States).

Keulegan, G.H., (1967). Tidal flow in entrances: water level fluctuations in basins in communication with seas. Comm. Tidal Hydraul., U.S. Army Corps Eng., Tech. Bull. 14, p. 89, Vicksburg.

Kirwan, M.L., Temmerman, S., Skeehan, E. E., Guntenspergen, G. R., and Fagherazzi, S., (2016). Overestimation of marsh vulnerability to sea level rise. Nature Climate Change, 6(3), 253-260. https://doi.org/10.1038/nclimate2909.

Lathrop, R. G., Jr.*, and* Bognar, J. A., (2001). Habitat loss and alteration in the Barnegat Bay Region*, J. Coastal Res., 212–228, doi:*10.2307/25736235.

Leonardi, N., Carnacina, I., Donatelli, C., Ganju, N. K., Plater, A. J., Schuerch, M., and Temmerman, S., (2017). Dynamic interactions between coastal storms and salt marshes: A review. Geomorphology, 301, 92–107. https://doi.org/10.1016/j.geomorph.2017.11.001.

Luhar, M., and Nepf, H.M., (2011). Flow-induced reconfiguration of buoyant and flexible aquatic vegetation Limnol. Oceanogr., 56 (6), pp. 2003-2017.

Mariotti, G., and Fagherazzi, S., (2010). A numerical model for the coupled long-term evolution of salt marshes and tidal flats. J Geophys Res 115:F01004.

Mariotti, G., and Fagherazzi, S., (2013). Critical width of tidal flats triggers marsh collapse in the absence of sea-level rise. Proceedings of the National Academy of Sciences, 110(14), pp.5353-5356.

Murray A. B., (2007). Reducing model complexity for explanation and prediction. Geomorphology, 90 (3-4), 178-191.

New York City Department of Environmental Protection, (2007). Jamaica Bay Watershed Protection Plan, col. I, New York.

Pethick, J. S., (1994). Estuaries and wetlands: function and form. In Wetland Management, pp. 75-87. London: Thomas Telford.

Pethick, J. S., (1981). Long-term accretion rates on tidal marshes. Journal of Sedimentary Petrology 61: 571–577.

Schuerch, M., Spencer, T., Temmerman, S., Kirwan, M.L., Wolff, C., Lincke, D., McOwen, C.J., Pickering, M.D., Reef, R., Vafeidis, A.T. and Hinkel, J., (2018). Future response of global coastal wetlands to sea-level rise. Nature, 561(7722), p.231.

Schwimmer, R.A. and Pizzuto, J.E., (2000). A model for the evolution of marsh shorelines. Journal of Sedimentation Research, 70, 1026–1035.

Schwimmer, R., (2001). Rates and processes of marsh shoreline erosion in Rehoboth Bay, Delaware, U.S.A., J. Coastal Res., 17(3), 672-683, doi:10.1016/j.csr.2009.08.018.

Spencer, T., Schuerch, M., Nicholls, R.J., Hinkel, J., Lincke, D., Vafeidis, A.T., Reef, R., McFadden, L., and Brown, S., (2016). Global coastal wetland change under sea-level rise and related stresses: the diva wetland change model, Global and Planetary Change, 139, 15-30.

Temmerman, S., Meire, P., Bouma, T.J., Herman, P.M., Ysebaert, T., and De Vriend, H.J., (2013). Ecosystem-based coastal defence in the face of global change. Nature 504 (7478): 79–83. https://doi.org/10. 1038/nature12859.

Walters, D., Moore, L.J., Duran Vinent, O., Fagherazzi, S., and Mariotti, G., 2014. Interactions between barrier islands and backbarrier marshes affect island system response to sea level rise: Insights from a coupled model. Journal of Geophysical Research: Earth Surface, 119(9), pp.2013-2031.

Warner, J.C., Armstrong, B., He, R., and Zambon, J.B., (2010). Development of a coupled ocean-atmosphere-wave-sediment transport (COAWST) modeling system. Ocean Model., 35 (3), pp. 230-244.

Zhang, X., Fagherazzi, S., Leonardi, N., and Li, J., (2018). A positive feedback between sediment deposition and tidal prism may affect the morphodynamic evolution of tidal deltas, Journal of Geophysical Research: Earth Surface, doi: 10.1029/2018JF004639.

Zhou, Z., Chen, L.Y., Townend, I., Coco, G., Friedrichs, C. T., and Zhang, C.K., (2018). Revisiting the relationship between tidal asymmetry and basin morphology: A comparison between 1D and 2D models. Journal of Coastal Research, SI 85 (Special Issue for International Coastal Symposium 2018), 117-121.

Marsh-derived sediments influence the resilience of intertidal areas to sea-level rise

Carmine Donatelli[1] [(*)], Tarandeep Kalra[3], Xiaohe Zhang[4], Sergio Fagherazzi[4], Nicoletta Leonardi[1]

*corresponding Author: Carmine@liverpool.ac.uk

(1) Department of Geography and Planning, School of Environmental Sciences, Faculty of Science and Engineering, University of Liverpool, Roxby Building, Chatham St., Liverpool L69 7ZT, UK

(2) U.S. Geological Survey, Woods Hole Coastal and Marine Science Center, MA 02543, USA

(3) Integrated Statistics, Contracted to the U.S. Geological Survey, Woods Hole Coastal and Marine Science Center, MA 02543, USA

(4) Department of Earth Sciences, Boston University, 675 Commonwealth Avenue, Boston, MA 02215, USA

Supplementary material can be found in Appendix 5

Abstract

Salt marshes are valuable ecosystems that must trap sediments and accrete in order to offset the deleterious effect of sea-level rise. Previous studies have shown that the capacity of marshes to build-up vertically depends on both autogenous and exogenous processes including eco-geomorphic feedbacks and sediment supply from in-land and coastal ocean. Currently, there are several uncertainties in relation to the quantification of the interplay between marsh vertical accretion and marsh lateral erosion, with the latter possibly serving as an autogenous source of sediments in support of accretion. Furthermore, the majority of existing studies investigating the interplay between lateral and vertical dynamics frequently use simplified modelling approaches neglecting complex regional-scale feedbacks between hydrodynamics and morphological changes associated with marsh erosion.

In this study, we evaluate the fate of the sediments originating from marsh lateral loss and their relative contribution to marsh resilience in comparison to the sediments coming from sub-tidal erosion and offshore by using high-resolution numerical model simulations of Jamaica Bay, a small estuary located in New York City (NYC). Our findings show that the sediments released during marsh edge erosion are redistributed in the tidal flats nearby the eroded areas and contribute to the local sediment budget, albeit only a small fraction get trapped by vegetated marsh platforms. In Jamaica Bay, the majority of sediments deposited on marsh platforms derived from erosional processes and only a small portion of offshore sediments contribute to marsh accretion rates. Our study highlights the relevance of multiple sediment sources for the maintenance of the marsh complex.

Keywords: marsh loss, COAWST, sea-level rise, Jamaica Bay.

Salt marshes occur at the interface of land and sea offering critical ecosystem services to coastal communities [Costanza et al., 1997]. The economic value of the services provided by salt marshes has been estimated up to 5 million USD per km^2 in the United States, and 786 million GBP per year for all UK marshes [Costanza et al., 2008; Foster et al., 2013; U.K. National Ecosystem Assessment, 2011; Leonardi et al., 2017]. Salt marshes are inherently unstable horizontally and they can retreat or expand in response of sediment supply and erosional agents creating a dynamic landscape [Fagherazzi et al. 2013; Tommasini et al., 2019]. Marsh dynamics in the horizontal direction are strongly related to the rate of sea-level rise and to the extension of tidal flats [Mariotti and Fagherazzi, 2013; Fagherazzi et al., 2013]. Indeed waves are locally generated by winds in tidal basins, and large tidal flats increase wave heights and promote higher erosion rates [Fagherazzi and Wiberg, 2009]. Lateral marsh erosion is recognized as the chief mechanism by which salt marshes are being lost in many estuaries and coastal lagoons around the world [e.g., Schwimmer, 2001; Mariotti and Fagherazzi, 2010; Marani et al., 2011]. On the contrary, salt marshes are thought to be more stable in the vertical direction due to positive feedbacks between depth of tidal inundation, vegetation biomass production and sediment trapping efficiency [Morris et al., 2002; Marani et al., 2007; Marani et al., 2010; Pasternack et al., 2000]. Projections of coastal wetlands response to accelerated sea-level rise suggest a 20% to 50% reduction of the present-day marsh area by 2100 [McFadden et al., 2007; Craft et al., 2009]. These catastrophic predictions raise concerns about the adaptive capacity of salt marshes to environmental change; hence a better understanding of the mechanisms

governing salt marsh evolution is imperative in order to predict the future impact of sea-level rise in coastal areas [Orson et al., 1985; Stevenson et al., 1985; Reed, 1995].

Coastal bays must trap sediments in order to adapt to rising sea level [Fagherazzi et al., 2014; Zhang et al., 2019]. Indeed, a positive sediment budget is necessary for the survival of salt marshes and tidal flats [Fagherazzi et al. 2014; Ganju et al. 2015]. Ganju et al. [2017] demonstrate the existence of a relationship between sediment budget and the unvegetated-vegetated marsh ratio, indicating that sediment deficits are linked to the conversion of vegetated marsh portions into open water. Marsh loss might in turn affect the ability of estuarine systems to retain sediments and cause further deterioration of salt marshes through a positive feedback-loop (Chapters 2 and 3). Recent studies indicate that the capacity of salt marshes to keep pace with sea-level rise strongly depends on the local tidal range, and on the suspended sediment concentration in the water that floods the marsh complex during each tidal cycle [Kirwan et al., 2010; Kirwan et al., 2016]. At present, marsh vertical accretion has been rarely analyzed along with horizontal erosional processes [Mariotti and Canestrelli, 2017], although the source of sediments generated by edge erosion has been experimentally demonstrated to further increase threshold rates of sea-level rise in systems with landward corridor [Ganju et al., 2015; Hopkinson et al., 2017]. Simplified marsh-mudflat models have included sediment recycling in salt marsh evolution [e.g. Mariotti and Carr, 2014], but this contribution has been evaluated only in idealized test cases [Mariotti and Canestrelli, 2017] and might neglect complex regional-scale hydrodynamic and geomorphological feedbacks. Herein, we use Jamaica Bay as test case to show how the amount of the sediments derived from marsh deterioration is redistributed

within this highly urbanized estuarine embayment in New York City (USA). For this purpose, we present results of numerical model experiments for the hydrodynamics and sediment transport of Jamaica Bay, using the Coupled-Ocean-Atmosphere-Wave-Sediment Transport (COAWST) modelling system [Warner et al., 2010] and the associated flow vegetation module [Beudin et al., 2017]. A new routine recently implemented in COAWST was used, which explicitly computes marsh lateral erosion based on wave thrust values acting at the marsh boundary [Leonardi et al., 2016].

Jamaica Bay watershed hosts more than 2 million people and its high level of urbanization strongly limits the capacity of this estuary to adapt in response to external disturbances. Hence, many concerns are rising about the resilience of the bay [e.g., Sanderson et al., 2016]. The sediment budget of an estuary is an important resilience indicator because it controls the evolution of intertidal areas and their vulnerability to storms and sea-level rise. Marine-derived sediment has historically been a crucial component of the sediment budget of the bay [Renfro et al., 2016], but human interventions at Rockaway Inlet have drastically reduced the movement of offshore sediments into the back-barrier basin [Englebright, 1975; Harting et al., 2002]. Peteet et al. [2018] demonstrated using two sediment cores taken from marshes located in the Eastern and Western part of the bay that the inorganic fraction is strongly reduced with respect to the past and only the increase in organic matter flux has allowed Jamaica Bay marshes to keep pace with sea-level rise. The lower mineral content due to the reduction in the sediment supply has also caused marsh structural weakness and edge failure [Peteet et al., 2018]. Our study attempts to investigate the fate of the sediments released during marsh edge erosion in shallow estuaries, and provides an

101

excellent opportunity to analyse the mechanisms governing the sediment dynamics in Jamaica Bay.

4.2 Study site

Jamaica Bay is a small and highly urbanized estuary located in Brooklyn, New York City (NYC, Figure 4.1a).
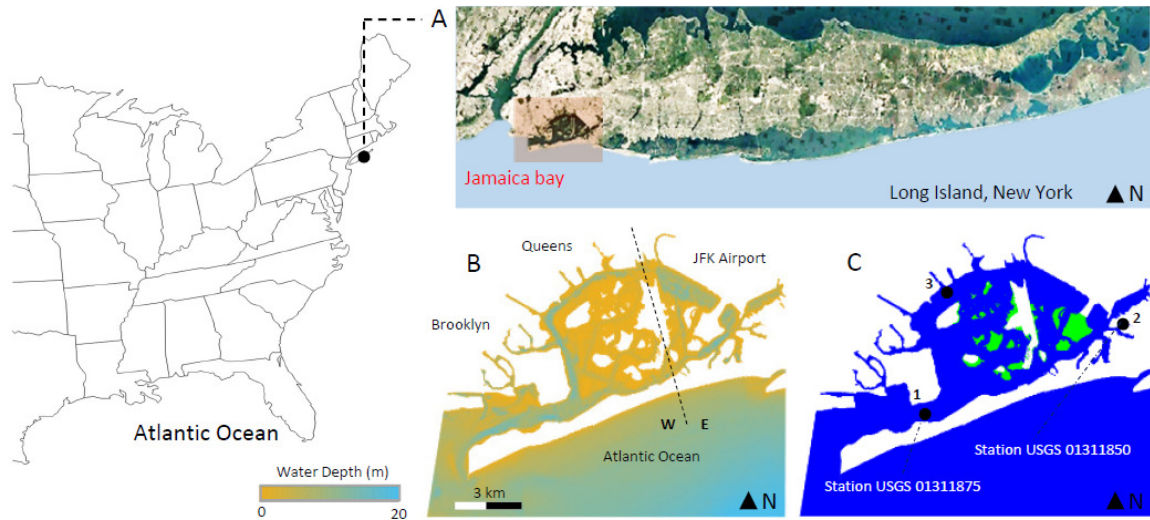
Figure 4.1 Study area. Long Island (New York City, NYC) and Jamaica Bay location (a); bathymetry of Jamaica Bay (b); present-day salt marsh distribution (green areas) and locations of measurements (c). Points 1 and 2 represent the USGS stations (01311875 and 01311850) where water level and SSC data are collected; point 3 represents the location of the flow velocity measurements.

The bay has an area of 50 km^2 with a diameter of approximately 7.5 km and it is connected to the Atlantic Ocean through Rockaway Inlet. The inlet dimensions are limited by the former airport Floyd Bennett Field at the north side and the Rockaway Peninsula at the south side. This barrier peninsula has an average width of 500 meters and is a combination of parks, houses and beaches. Tides are mainly semidiurnal, with a mean tidal range of ~1.6 m, and waves are locally generated. The system is flood-dominated with a net import of sediment from offshore [Renfro et al., 2016]. Deep navigating channels (average depth of 10 m) border the basin, while the central region is shallower and characterized by

extensive salt marshes and mudflats (Figure 4.1b), which provide critical ecosystem services in terms of coastal protection [Marsooli et al., 2017]. Furthermore, these wetlands host 324 species of migratory and resident birds, over 90 fish species and are also deemed important for horseshoe crabs and diamondback terrapins [New York City Department of Environmental Protection, 2007]. As documented by the New York City Department of Environmental Protection [2007], over 75% of salt marshes in Jamaica Bay have been lost since the mid-1800s, and up to a 50% of the marsh deterioration has occurred in the few decades. The main causes of salt marsh decline are related to an elevated wave activity associated with ship wakes [New York City Department of Environmental Protection, 2007; Black, 1981], rising sea level [Gornitz et al., 2001; Hartig et al., 2002], increased tidal range [Swanson & Wilson, 2008] and excess nutrients [Wigand et al., 2014]. Furthermore, human interventions may have exacerbated marsh loss through alteration of the circulation patterns and sediment budget [Renfro et al., 2016]. The present-day salt marsh distribution is depicted in Figure 4.1c.

4.3 Methods

The hydrodynamics of the system has been simulated using the COAWST (Coupled-Ocean-Atmosphere-Wave-Sediment Transport Modeling System) modeling framework [Warner et al., 2010]. In this study, the circulation model ROMS [Shchepetkin and McWilliams, 2005; Warner et al., 2008] and the wave model SWAN [Booij et al., 1999] have been fully coupled on the same computational grid, with data exchange every 600 s. ROMS (Regional Ocean Modeling System) is a three-dimensional, free surface, finite-difference, terrain following model that solves the Reynold-Averaged Navier-Stokes (RANS) equations using the hydrostatic and Boussinesq assumptions [Haidvogel et al., 2008]. SWAN (Simulating WAves Nearshore) is a third-generation spectral wave model based on the action balance equation [Booij et al., 1999]. The model simulates the generation and propagation of wind-waves accounting for shifting in relative frequency due to variations in water depth and currents, depth-induced refraction, wave-wave interactions and dissipation (white-capping, depth-induced breaking and bottom friction). The flow-vegetation interaction is computed employing the new vegetation module implemented by Beudin et al. [2017], which includes plant posture-dependent three-dimensional drag, in-canopy wave-induced streaming, and production and dissipation of turbulent kinetic energy for the vertical mixing parameterization.

The spatially averaged vegetation drag force is calculated using a quadratic law, and the reduction in drag due to plant flexibility is computed following Luhar and Nepf [2011]. The selected turbulence model is the k–ε scheme which accounts for extra dissipation and turbulence kinetic energy production due to vegetation [Uittenbogaard, 2003]. Similarly, wave dissipation due to vegetation is accounted by the model modifying the source term

of the action balance equation following the formulation of Mendez and Losada [2004].

The friction exerted by the bed on the flow is computed using a bottom boundary layer

formulation [Warner et al., 2008], which includes enhanced wave-based apparent

roughness [Madsen, 1994]. Wind data are based on observations collected every six

minutes at the NOAA buoy 40025 and applied uniformly on the numerical domain (Figure

4.4a).

The number of interior cells are 997 x 387, with cell size varying from 25m to 54m in

along-bay and cross-bay directions; 7 layers equally spaced are defined in the vertical

direction. The model is forced at the seaward boundaries with tides, based on observations

from the USGS station (USGS 01311875) located at the Rockaway Inlet (station 1, Figure

4.1c); a reduction factor is applied to the measured water elevations to consider the effects

of convergent topography on the tide [Marsooli et al., 2016]. The results of the model are

compared with water level data collected in two weeks during August 2015 in two USGS

stations (USGS 01311875 and USGS 01311850, Point 1 and 2 in Figure 4.1c) and with

flow velocity data measured at the North Channel (Point 3, Figure 4.1c). The model

performance is evaluated using root-squared-error (RMSE), bias and skill scores

(Appendix 4, Table A.4.1). The sediment model incorporates five sediment classes: two

non-cohesive and three cohesive (Table 4.1).

	Sediment class	Origin	Settling velocity (mm/s)	Critical shear stress (N/m^2)
1	Medium sand	Bed	40	0.5
2	Fine sand	Bed	5	0.1
3	Silt	Bed	1.5	0.05
4	Mud	Marsh boundary	0.1	0.05
5	Mud	Offshore	0.01	0.05

Table 4.1 Sediment characteristics: sediment class, origin, settling velocity (mm/s^{-1}) and critical shear stress for erosion (N m^{-2}).

Sediment deposition and erosion fluxes at the bottom boundary are formulated as in Warner et al. [2008]. One bed layer is implemented with a thickness of 0.25 m and a uniform porosity of 0.5. Three sediment types are initially uniformly distributed over the bed (medium sand, fine sand and medium silt). A simulation with the initial bed sediment distribution is run for 200 days using realistic forcing. A morphological factor is applied to speed up the process [e.g. Van der Wegen et al., 2010] and the sediment bed resulting from the 200 day run (Figure 4.2a, Appendix 4, Figure A.4.1) is used as initial condition for all the simulations carried out in this study [Ralston et al., 2012]. The wave thrust (the integral along the vertical of the dynamic pressure of waves) is explicitly computed by the model following Tonelli et al. [2010] and Leonardi et al. [2016]. When the thrust acts on the marsh boundary, the marsh erosion takes place leading to accretion of sediment bedload on the adjacent cell face that causes the thrust. Two cohesive sediment classes are used to simulate respectively the material eroded from the marsh boundary [Fagherazzi et al., 2013] and the sediments imported from offshore (Table 4.1). The input of sediment coming from the ocean is defined imposing a constant suspended sediment concentration (SSC) at the western boundary of the numerical domain. The sediment parameters (Table 4.1) are chosen comparing the modeled signal with the SSC data collected in the USGS station at the Rockaway inlet (Figure 4.1c, Figure 4.2b). The modeled SSC time series present a good agreement with the measurements (Appendix 4, Table A.4.1, Figure A.4.2).
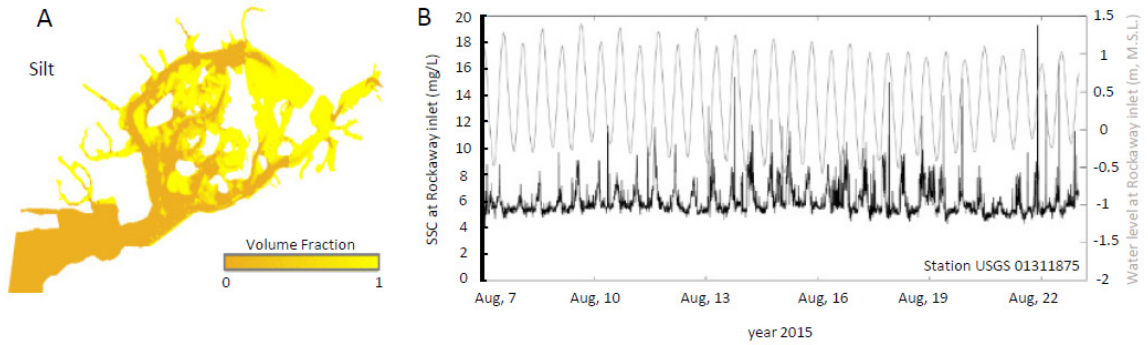
Figure 4.2 Distribution of bed sediment in mud fraction (a); water level (m) and SSC (mg/L) measurements collected at the inlet mouth in August 2015 (b).

Salt marsh coverage data were derived from the CRSSA's (Center for Remote Sensing and Spatial Analysis) geographic information systems (GIS) data base. Vegetation parameters are set as follows: stem height of 0.8 m, diameter of 0.6 cm and density of 120 shoots/m^2 [Marsooli et al., 2016].

4.4 Results

The convergent shape of the inlet increases tides in the bay resulting in water levels greater than the offshore tidal amplitude [Van Rijn, 2011; Aretxabaleta et al., 2016]. The tidal wave experiences a distortion due to the basin morphology, altering its symmetric shape. Asymmetric tides are important for the transport and deposition of sediment in shallow estuaries [Aubrey and Speer, 1985]. The distortion of the tidal wave is evaluated using the Friedrichs and Aubrey [1988] formulation. The amplitude and phase ratios between the fourth-diurnal M_4 constituent and the semidiurnal M_2 were computed within the entire back-barrier basin using T_TIDE [Pawlowicz et al., 2002]. The ratio between the amplitude of the overtide and the M_2 component shows the magnitude of the asymmetry (Appendix 4, Figure A.4.3a), while the relative phase difference ($\varphi = 2 \cdot \vartheta_{M_2} - \vartheta_{M_4}$) reveals the sense of the asymmetry ($0° < \varphi < 180°$: flood dominant, Appendix 4, Figure A.4.3b). An examination of slack durations and maximum velocities is performed following Dronkers [1986]. An asymmetry in the slack water periods may affect the residual transport of fine sediments, while a difference in the peak velocities during ebb and flood may influence the residual transport of coarse sediments. Flood dominant slack period asymmetry occurs when the time derivative of the velocity at high water is smaller of the velocity variation at low water. The water slack period has been defined as the time where the depth-averaged flow velocity is below a critical value defined following Vermeulen [2003]. The average periods of high (HWS) and low (LWS) slack water have been calculated for the entire bay for a spring-neap tidal cycle and used to compute the tidal averaged slack water dominance (ΔWS=HWS-LWS). A positive ΔWS value indicates that fine sediments have longer time to deposit during the slack period after the flood phase than after the ebb phase (Figure

4.3a). Our results show how this asymmetry is pronounced only in shallow tidal flats, while in deeper tidal flats and channels is negligible. Figure 4.3b presents the difference in the depth-averaged peak velocity currents during the flood and ebb phases; this plot is in agreement with the results depicted in Figure A.4.3b (Appendix 4) and shows the flood dominance of the estuary.
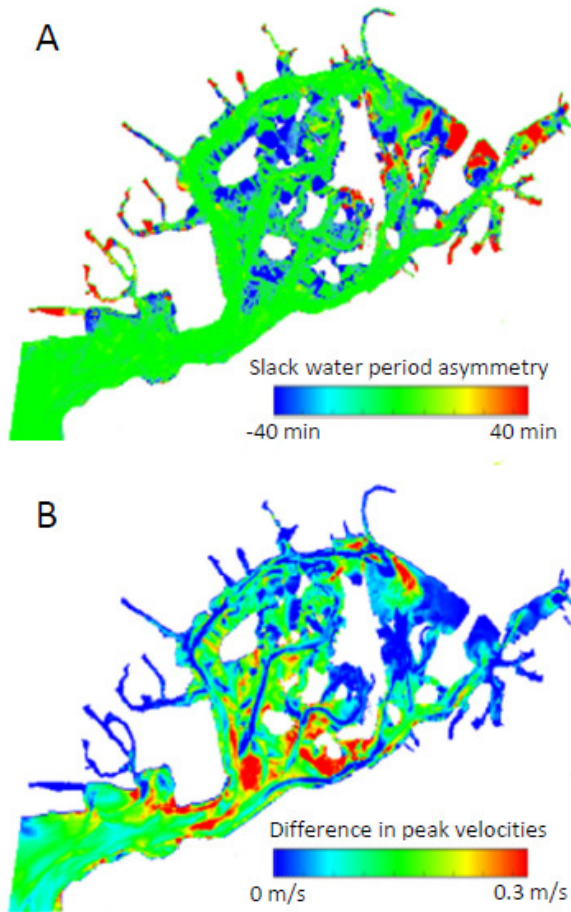
Figure 4.3 Slack water period asymmetry (minutes, a) and difference in peak velocities (m/s, b) in Jamaica Bay.

Figure 4.4b shows the distribution of the mean wave heights in each sub-basin (Basin W= western basin and Basin E= eastern basin, Figure 4.1b). The mean wave height is defined as the mean value throughout the entire simulation computed at each cell.
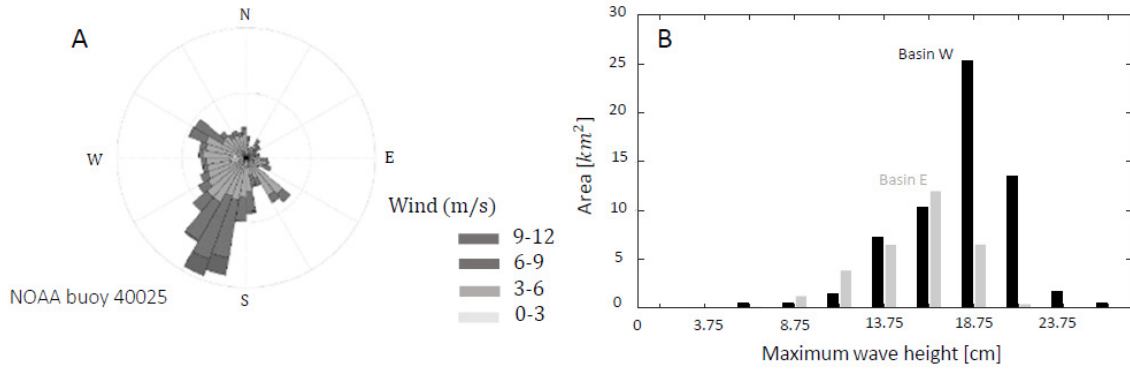
Figure 4.4 Wind rose for the study area in August 2015 (wind station: NOAA buoy 40065, a); distribution of the maximum wave height (cm) for each sub-basin. Wave height data are binned every 2.5 cm.

Figure 4.5 depicts the fate of marine-derived sediments within the estuary and shows that only a small fraction (<2%) of the sediments coming from offshore is deposited over salt marshes, although more than 50% of this mass is in suspension and remains available to be potentially trapped by vegetation at a later time. Furthermore, we evaluated the net sediment mass imported from offshore in 30 days as 5 x 10^6 kg.
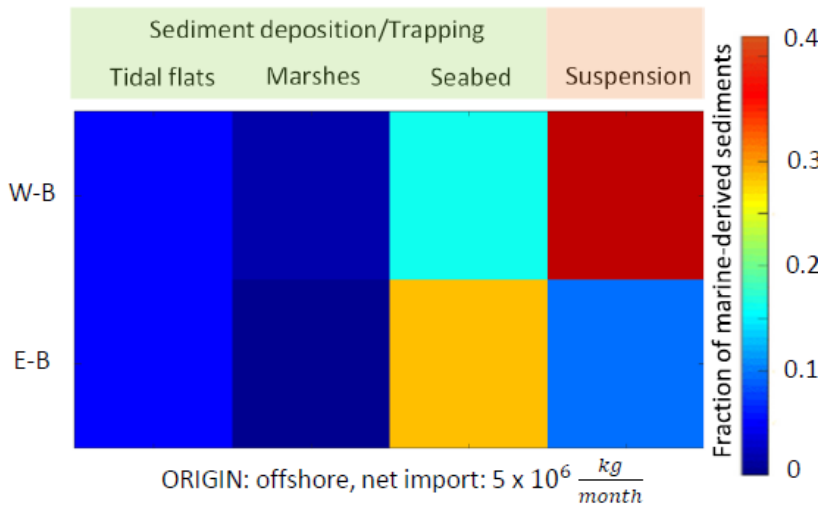
Figure 4.5 Fate of marine-derived sediments within the estuary after 30 days. Values (i,j) in the table indicate the mass fraction of sediments imported into the bay.

The distributions of the mean bottom shear stresses as a function of water depth show that in the Western part of the basin bottom shear stresses increase monotonically with the water depth, while intermediate water depths experience the maximum value in bottom shear stress in the Eastern part of the estuary (Figure 4.6a). Figure 4.6b shows the time of marsh submergence in each sub-basin. Marshes located in the Eastern sub-basin have a shorter time of submergence and lower suspended sediment concentrations in the adjacent mudflats (SSC, Figure 4.6c).
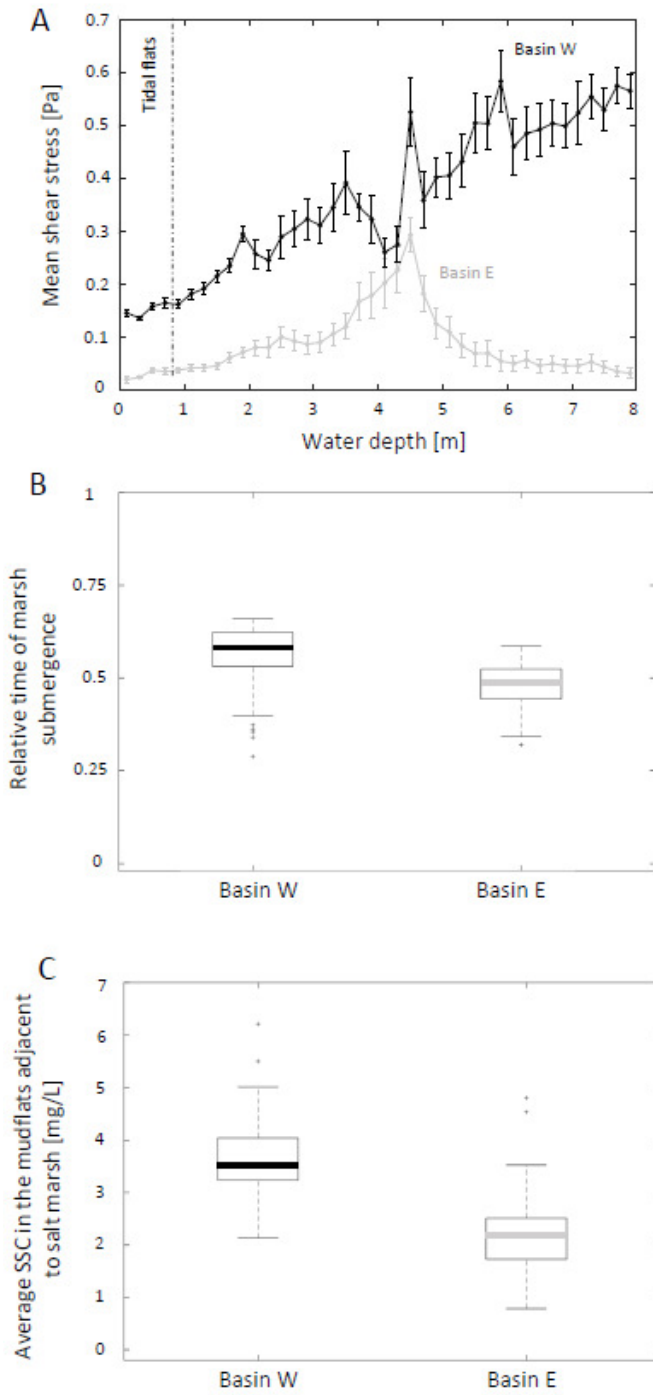
Figure 4.6 Mean shear stress (Pa) distribution as a function of the water depth (m) for each sub-basin (a). Water depth data are binned every 0.2 m. Time of marsh submergence relative to a spring-neap tidal cycle in each sub-basin (b). SSC (mg/L) in the mudflats adjacent to salt marshes in each sub-basin (c).

As presented in Figure 4.7, the sediment delivery to marsh platforms is mainly controlled by the SSC in the nearby tidal flats. On the contrary, a weak correlation relates the marsh inorganic accretion rate and the time of marsh submergence (Figure 4.7b).
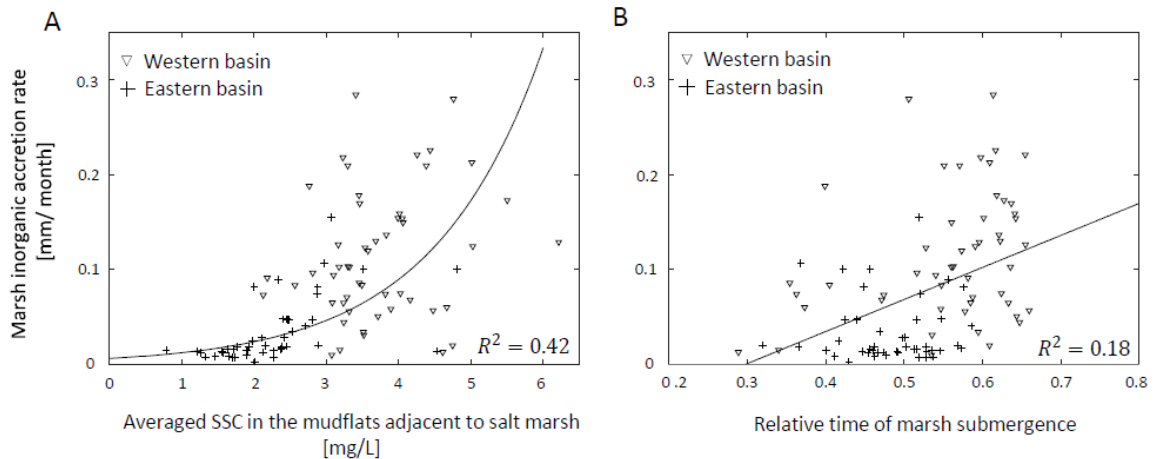
Figure 4.7 Marsh inorganic accretion rate (mm/month) as a function of SSC (mg/L) in the adjacent mudflats (a), and as a function of submergence time relative to a spring-neap tidal cycle (b).

Figure 4.8 depicts the average inorganic accretion rate (mm/month) in Jamaica Bay marshes, and the accretion rate for marshes located in the Western and Eastern sub-basins. The mean accretion rate is consistent with a previous investigation carried out by Kolker [2005]. We further analyzed the provenance of the total amount of sediments stored on marsh platforms. Sediments were divided into two fractions, where each fraction is characterized by a different origin: ocean or subtidal erosion (Figure 4.8b). Our results show that the majority of sediments deposited on marsh platforms derive from the erosion of the basin bottom. Eroded sediments contribute to around 62% to 92% of the deposit on the marsh platform. Offshore sediments contribute up to 38% to the deposit on marsh platform in the Eastern Basin, and less than 8% in the Western basin. These results suggest

that erosional processes might be the main drivers for the Jamaica Bay marshes' accretion (Figure 4.8b).
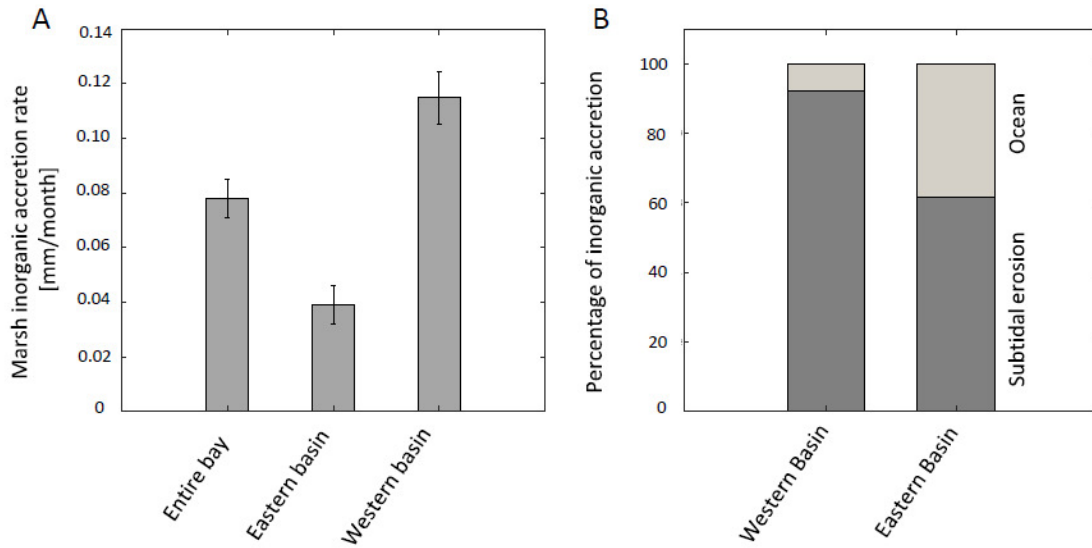
Figure 4.8 Marsh inorganic accretion rate (mm/month) in the entire bay, only in the Western sub-basin and only in the Eastern sub-basin (a). Percentage of marine-derive sediments and sediments coming from subtidal erosion in marsh vertical accretion (b) for each sub-basin.

To better understand the mechanisms governing the sediment dynamics in Jamaica Bay, we ran an idealized simulation to quantitatively evaluate whether fine sediments can accumulate in the deep channels bordering the basin until their removal by dredging, or whether these sediments can be reworked and eventually be deposited on marsh platforms as well. The box plot of shear stresses induced by tides, calculated in a neap-spring tidal cycle, shows that the deep channels in the Eastern sub-basin are more likely to serve as potential sediment sinks for the coarsest fractions given their low shear stress levels (Figure 4.9).
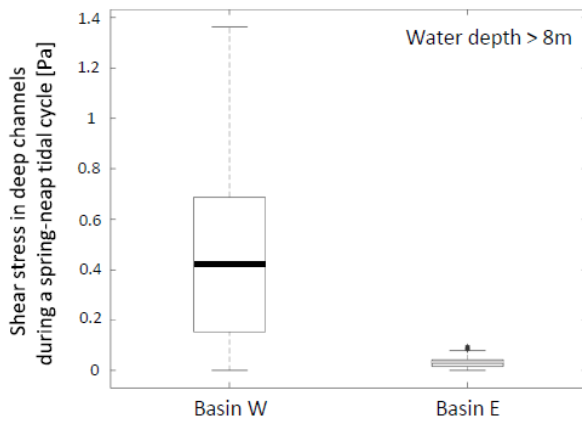
Figure 4.9 Variability of shear stress in deep channels during a spring-neap tidal cycle.

Figure 4.10 demonstrates that shear stresses are higher or equal to 0.05 Pa for the 18% of the spring-neap tidal cycle during which silt and mud can be re-suspended and potentially trapped by salt marshes. To further verify that fine sediments from the deepest channels can be suspended, we defined an initial bed thickness of 0.2 m within the sole channels in the Eastern sub-basin and then computed the sediment mass stored over marshes and the mass still presents in the channels (given the setup, no other sediments can be remobilized except the ones in the channels). Our numerical experiment shows that fine sediments deposited in deep channels can be remobilized during spring tides (Appendix 4 Figure A.4.5).

116
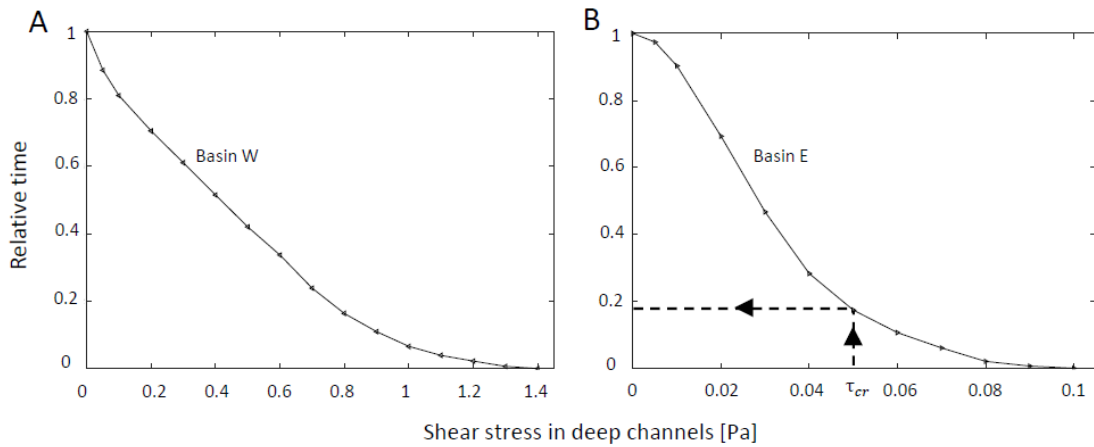
Figure 4.10 Relative time in a spring-neap tidal cycle in which shear stresses are higher of a certain value in the Western (a) and Eastern (b) sub-basins.

The impact of wind-waves along the marsh boundaries is evaluated in terms of wave thrust per unit width, computed as the vertical integral of the dynamic wave pressure. The average wave thrust over the entire simulation time is depicted in Figure 4.11 for marshes located in the western (W-B), central (C-B) and eastern (E-B) part of the bay. The variability of the averaged wave thrust is higher in the Eastern sub-basin, while the mean wave thrust is lower for marshes located in the central part of the bay.
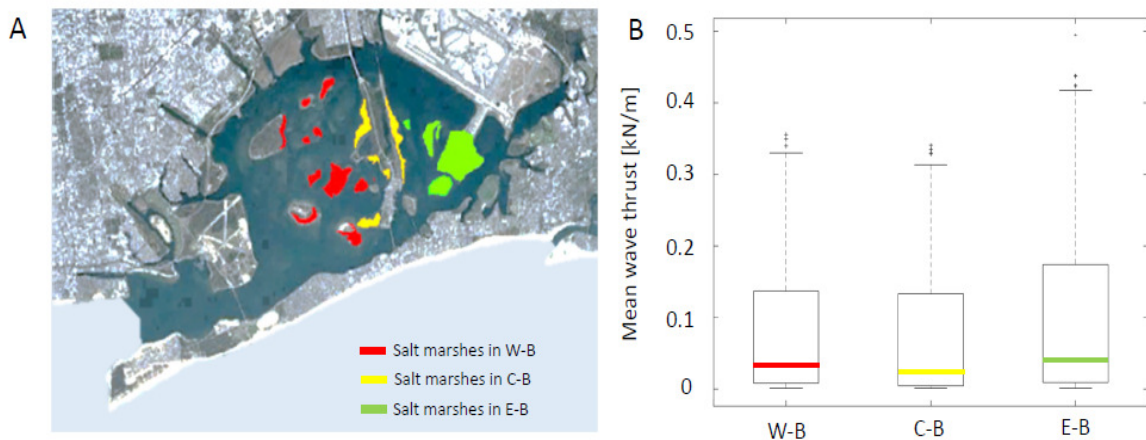
Figure 4.11 Marsh location in the basin (W-B = western sub-basin, C-B = central sub-basin, E-B = eastern sub-basin, a); wave thrust values (kN/m) for each group (b).

Figures 4.12 shows the simulated mass eroded from marshes in one month. These sediments were redistributed across the bay as presented in Figure 4.13.
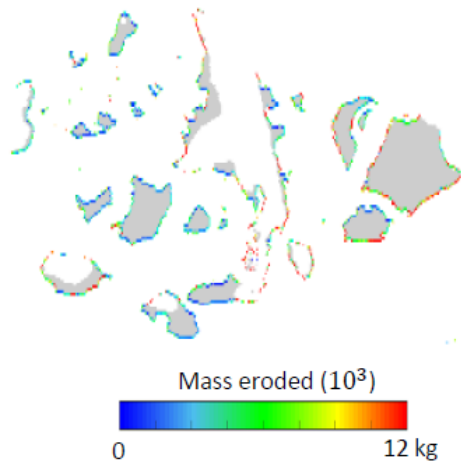
Figure 4.12 Sediment eroded from marsh boundary (kg) after 30 days.
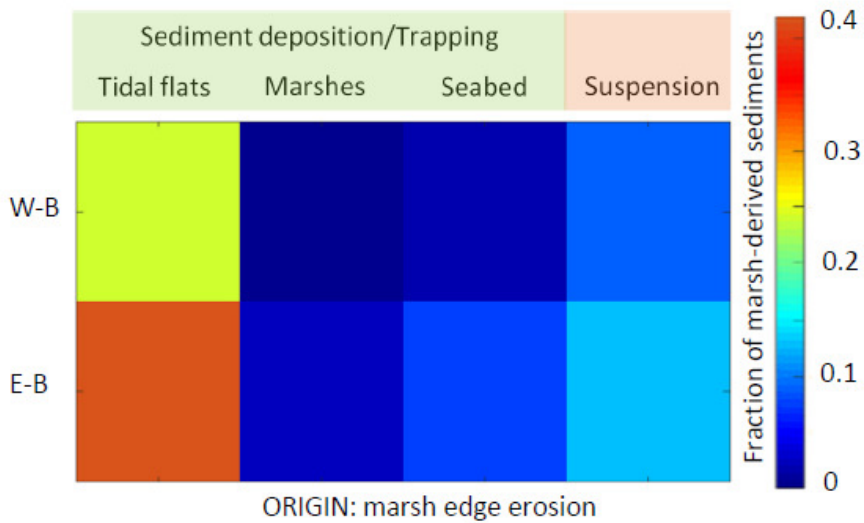
Figure 4.13 Fate of marsh-derived sediments within the estuary after 30 days. Values (i,j) in the table indicate the mass fraction of sediments released by wave-induce lateral erosion.

The 67% of the eroded material deposits in the tidal flats near marshes, while only a small fraction (<0.27%) is trapped by vegetated surfaces. The remaining sediment is kept in

suspension by waves and tides in the water column. After investigating the destination of

the eroded sediments, we have analyzed temporal changes in the deposit. Specifically, the

marsh boundary erosion routine was switched off after 30 days, and the redistribution of

the mass initially eroded from marsh edge was tracked in time. For this last set of analyses,

the model setup was such that only sediments previously eroded form the marsh edge were

tracked. Figure 4.14 reveals how the sediment volume trapped by salt marshes increases in

time after 75, 280 and 563 days. Our findings demonstrate that even after 563 days, only a

small percentage (<6%) of the mass released during marsh erosion has deposited on

vegetated surfaces.
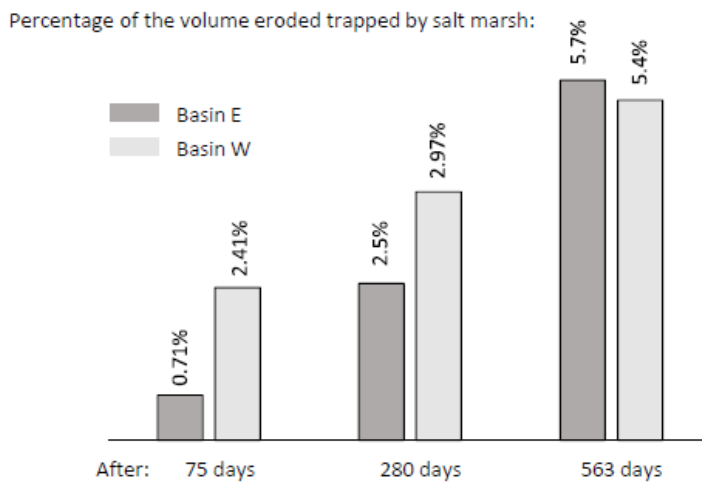
Figure 4.14 Percentage of the sediment volume released during marsh erosion that is trapped by salt marshes after 75, 280 and 563 days.

4.5 Discussion

This research investigates how sediments from different sources (i.e. sediments coming from the ocean or from the erosion of tidal flats and marsh boundaries) redistribute across a lagoon-estuarine system. Jamaica Bay is a small and highly modified embayment located on the Northeastern shore of the United States which has been significantly altered by urbanization and large-scale bathymetric modifications for navigational purposes [Swanson and Wilson, 2008; Ralston et al., 2018]. The salt marshes in Jamaica Bay provide critical ecosystem services to the New York City coastal community, but they have been disappearing at high rates over the last few decades [Peteet et al., 2017]. Here, we aim to highlight the relative contribution of different sediment sources to the accretion rate of salt marshes by also focusing on sediments derived from the wave-induced lateral erosion. Results are based on a fully coupled hydrodynamics and morphological model that accounts for non-linear feedbacks between hydrodynamic and morphological changes. High-resolution modelling results show that the sediment released from marshes during wave-induced lateral erosion deposits on the adjacent tidal flats, and only a small fraction is re-suspended by waves and advected on vegetated surfaces (Figure 4.13, 4.14). We reveal that subtidal erosion represents the major source of sediments for these salt marshes, and that the external sediment input provides a smaller contribute to the sediment stock on marsh platforms (Figure 4.8). The resilience of salt marshes has been linked not only to the sediment budget of the vegetated surfaces, but also of surrounding tidal flats, sea bed and tidal channels [Ganju et al., 2013; Fagherazzi, 2014]. Therefore, even though only a small fraction of sediments deposit on vegetated surfaces, our findings suggest that marsh-derived sediment can increase the resistance of salt marshes and tidal flats to sea-level rise

by contributing to the overall sediment budget within the bay. This is in agreement with the previous works of Ganju et al. [2015] and Hopkinson et al. [2018].

Several insightful studies have investigated the resilience of salt marshes to sea-level rise under different sediment supply conditions. However, many of these use simplified approaches prescribing constant suspended sediment concentration and do not account for the hydro-morphodynamic feedbacks regulating the redistribution of sediments derived from the erosion of marsh boundaries [Morris et al., 2002; Kirwan et al., 2010; Mariotti, 2016]. For example, Kirwan et al. [2010] estimate threshold rates of sea-level rise by imposing various suspended sediment values, ignoring the origin of the sediment, their spatiotemporal variability, and the impact of marsh disappearance on the regional scale hydrodynamics [Ganju et al., 2015; Hopkinson et al., 2018; Donatelli et al., 2018b]. Herein, we have demonstrated that salt marsh resilience to sea-level rise can benefit from edge erosion as the latter can contribute to the local sediment budget, although in this specific test case marsh lateral erosion results in a loss of habitat as salt marshes cannot migrate landward.

Although marsh erosion would positively affect the sediment budget of the marsh complex in the short-term, the increase in the flushing capacity of the system associated with extensive marsh loss might compromise the fate of the estuary, and marshes themselves, over long time scales (Chapters 2 and 3). Indeed, large-scale marsh deterioration increases the sediment storage volume of the estuary, dampen the tidal wave and reduce the sediment trapping capacity of the system. As a consequence, the sediment deposition on marsh platforms decreases non-linearly with marsh decline and this may reduce their ability to

counteract sea-level rise even accounting for sediment recycling [Donatelli et al., 2018b]. In the long-term, changes in the sediment availability associated with marsh loss might also influence erosional processes. More specifically a simplified model proposed by Mariotti and Fagherazzi [2013] demonstrates that the ratio between marsh to open water area in a bay is controlled by the amount of sediment stored within the basin, showing how sea-level rise can speed up marsh lateral erosion by reducing the overall sediment storage. Moreover, lower marsh to open water ratios might trigger a positive feedback-loop with further marsh deteriorations [Tambroni and Seminara, 2012; Mariotti and Carr, 2014], but erosion rates would decrease with the widening of tidal flats [Mariotti and Canetrelli, 2017]. The interplay between marsh lateral erosion and sediment trapping on marsh platforms might be also influenced by the bottom characteristics of the basin. As proposed by the exploratory model of Donatelli et al. [2019] (Chapter 5), submerged aquatic vegetation reduces wave thrust values along marsh boundaries and alters the sediment exchange between tidal flats and marshes, enhancing deposition on vegetated beds rather than resuspension and deposition on marsh platforms [Nardin et al., 2018]. Our research underlines the role of autogenous processes on the stability and evolution of intertidal areas, and shows the fate of the sediments derived from marsh edge erosion in shallow estuaries.

Acknowledgment

References

Aretxabaleta, A. L., Butman, B., and Ganju, N.K., (2014). Water level response in back-barrier bays unchanged following Hurricane Sandy, Geophys. Res. Lett., 41, 3163–3171, doi:10.1002/2014GL059957.

Aubrey, D.G., and Speer, P.E., (1985). A study of non-linear tidal propagation in shallow inlet estuarine systems. Part I. Observations. Estuar. Coast. Shelf Sci. 21, 185-205.

Beudin, A., Kalra, T.S., Ganju, N.K., and Warner, J.C., (2017a). Development of a coupled wave-flow vegetation interaction model. Computers & Geosciences.

Black, F.R., (1981). Jamaica Bay: A History. Cultural Resource Management Study 3 (Natl Park Serv, Washington, DC).

Booij, N., Ris, R.C., and Holthuijsen, L.H., (1999). A third-generation wave model for coastal regions, part I, model description and validation. Journal of Geophysical Research, C4, 7649–7666. https://doi.org/10.1029/98JC02622

Bricker-Urso, S., and Nixon, S.W., (1989). Accretion rates and sediment accumulation in Rhode Island salt marshes, Estuaries, 12, 300–317, doi:10.2307/1351908.

Castagno, K.A., Jiménez-Robles, A.M., Donnelly, J.P., Wiberg, P.L., Fenster, M.S., and Fagherazzi, S., (2018). Intense storms increase the stability of tidal bays. Geophysical Research Letters, 45, 5491– 5500. https://doi.org/10.1029/2018GL078208

Costanza, R., d'Arge, R., de Groot, R.S., Farber, S., Grasso, M., Hannon, B., Limburg, K., Naeem, S., O'Neill, R.V., Paruelo, J., Raskin, R.G., Sutton, P., and van den Belt, M., (1997). The value of the world's ecosystem services and natural capital. Nature, 387, pp. 253-260.

Costanza, R., Perez-Maqueo, O., Martinez, M. L., Sutton, P., Anderson, S. J., and Mulder, K., (2008). The value of coastal wetlands for hurricane protection: Ambio, v. 37, no. 4, p. 241-248.

Craft, C., et al. (2009), Forecasting the effects of accelerated sea-level rise on tidal marsh ecosystem services, Front. Ecol. Environ, 7, 73– 78, doi:10.1890/070219.

Deegan LA, et al., (2012). Coastal eutrophication as a driver of salt marsh loss. Nature 490:388–392.

Donatelli, C., Ganju, N.K., Fagherazzi, S., and Leonardi, N., (2018a). Seagrass impact on sediment exchange between tidal flats and salt marsh, and the sediment budget of shallow bays, Geophysical Research Letters, doi:10.1029/2018GL078056.

Donatelli, C., Ganju, N.K., Zhang, X., Fagherazzi, S., and Leonardi, N., (2018b). Salt marsh loss affects tides and the sediment budget of shallow bays, Journal of Geophysical Research: Earth Surface, doi: 10.1029/2018JF004617.

Donatelli, C., Ganju, N. K., Kalra, T., Fagherazzi, S., Leonardi, N., Changes in hydrodynamics and wave energy as a result of seagrass decline along the shoreline of a microtidal back-barrier estuary, Advances in Water Resources (2019), doi: 10.1016/j.advwatres.2019.04.017

Dronkers, J., (1988). Coastal-offshore ecosystem. Lecture Notes on Coastal and Estuaries Studies, ed Jansson B-O (AGU, Washington, DC), Vol 22, pp 3-39.

Fagherazzi, S., and Wiberg, P.L., (2009). Importance of wind conditions, fetch, and water levels on wave-generated shear stresses in shallow intertidal basins, J. Geophys. Res., 114, F03022, doi:10.1029/2008JF001139.

Fagherazzi, S., (2013). The ephemeral life of a salt marsh. Geology 41, 943–944.

Fagherazzi, S., Mariotti, G., Wiberg, P.L. and McGlathery, K.J. (2013). Marsh collapse does not require sea level rise. Oceanography 26, 70–77.

Fagherazzi, S., (2014). Coastal processes: Storm-proofing with marshes. Nat Geosci 7(10): 701–702.

Friedrichs, C.T., and Aubrey, D.G., (1988). Non-linear tidal distortion in shallow well-mixed estuaries: a synthesis. Estuarine Coastal and Shelf Science, 27(5), 521-545.

Ganju, N. K., M. L. Kirwan, P. J. Dickhudt, G. R. Guntenspergen, D. R. Cahoon, and K. D. Kroeger (2015), Sediment transport-based metrics of wetland stability, Geophys. Res. Lett., 42, 7992–8000, doi:10.1002/2015GL065980.

Ganju, N.K., Defne, Z., Kirwan, M.L., Fagherazzi, S., D'Alpaos, A. and Carniello, L., (2017). Spatially integrative metrics reveal hidden vulnerability of microtidal salt marshes. Nature communications, 8, p.ncomms14156.

Gornitz V., Couch S., Hartig E.K., (2001). Impacts of sea level rise in the New York City metropolitan area. Global Planet Change 32:61–88.

Hartig E.K., Gornitz V., Kolker A., Mushacke F., and Fallon, D., (2002). Anthropogenic and climate-change impacts on salt marshes of Jamaica Bay, New York City. Wetlands 22:71–89.

Hopkinson, C.S., Morris, J.T., Fagherazzi, S., Wollheim, W.M., and Raymond, P.A., (2018). Lateral Marsh Edge Erosion as a Source of Sediments for Vertical Marsh Accretion. Journal of Geophysical Research: Biogeosciences. https://doi.org/10.1029/2017JG004358.

Kirwan, M. L., and Murray, A. B. (2007), A coupled geomorphic and ecological model of tidal marsh evolution, Proc. Natl. Acad. Sci. U.S.A., 104, 6118–6122, doi:10.1073/pnas.0700958104.

Kirwan, M. L., and Guntenspergen, G. R. (2010), The influence of tidal range on the stability of coastal marshland, J. Geophys. Res., 115, F02009, doi:10.1029/2009JF001400.

Kirwan, M. L. and Blum, L. K., (2011). Enhanced decomposition offsets enhanced productivity and soil carbon accumulation in coastal wetlands responding to climate change. Biogeosciences 8, 987–993.

Kirwan, M.L. and Megonigal, J.P., (2013). Tidal wetland stability in the face of human impacts and sea-level rise. Nature 504, 53–60.

Kirwan, M.L., Temmerman, S., Skeehan, E.E., Guntenspergen, G.R. and Fagherazzi, S., (2016). Overestimation of marsh vulnerability to sea level rise. Nat. Clim. Change 6, 253–260.

Lapentina, A., and Sheng, Y.P., (2014). Three-dimensional modeling of storm surge and inundation including the effects of coastal vegetation. Estuaries and Coasts, 37(4), 1028–1040. https://doi.org/10.1007/s12237-013-9730-0

Leonardi, N. and Fagherazzi, S., 2014. How waves shape salt marshes. Geology, 42(10), pp.887-890.

Leonardi, N., Defne, Z., Ganju, N.K. and Fagherazzi, S., (2016a). Salt marsh erosion rates and boundary features in a shallow Bay. Journal of Geophysical Research: Earth Surface, 121(10), pp.1861-1875.

Leonardi, N., Ganju, N.K., and Fagherazzi, S., (2016b). A linear relationship between wave power and erosion determines salt-marsh resilience to violent storms and hurricanes. Proceedings of the National Academy of Sciences, 113(1), pp.64-68.

Leonardi, N., Carnacina, I., Donatelli, C., Ganju, N.K., Plater, A.J., Schuerch, M. and Temmerman, S., (2017). Dynamic interactions between coastal storms and salt marshes: A review. Geomorphology.

Marani, M., D'Alpaos, A., Lanzoni, S., Carniello, L. and Rinaldo, A. (2007). Biologically controlled multiple equilibria of tidal landforms and the fate of the Venice lagoon. Geophys. Res. Lett. 34, L11402.

Marani, M., D'Alpaos, A., Lanzoni, S., Carniello, L., Rinaldo, A., (2010). The importance of being coupled: Stable states and catastrophic shifts in tidal biomorphodynamics. J Geophys Res 115:F04004.

Marani, M., D'Alpaos, A., Lanzoni, S., and Santalucia, M., (2011). Understanding and predicting wave erosion of marsh edges, Geophys. Res. Lett., 38, L21401, doi:10.1029/2011GL048995.

Mariotti, G., and Fagherazzi, S., (2013). Critical width of tidal flats triggers marsh collapse in the absence of sea-level rise. Proceedings of the National Academy of Sciences, 110(14), pp.5353-5356.

Mariotti, G., and Carr, J., (2014), Dual role of salt marsh retreat: Long-term loss and short term resilience, Water Resour. Res., 50, 2963–2974, doi:10.1002/2013WR014676.

Mariotti, G., and Canestrelli, A., (2017). Long-term morphodynamics of muddy backbarrier basins: fill in or empty out? Water Resour. Res, 10.1002/2017WR020461

Marjoribanks, T. I., Hardy, R. J., and Lane, S.N., (2014). The hydraulic description of vegetated river channels: The weaknesses of existing formulations and emerging alternatives. WIREs Water, 1(6), 549–560. https://doi.org/10.1002/wat2.1044

Marsooli, R., Orton, P.M., Mellor, G. (2017). Modeling wave attenuation by salt marshes in Jamaica Bay, New York, using a new rapid wave model. J. Geophys. Res.: Oceans, 122 (7), pp. 5689-5707

Marsooli, R., Orton, P.M., Georgas, N., Blumberg, A.F., (2016). Three-dimensional hydrodynamic modeling of coastal flood mitigation by wetlands. Coast Eng., 111, pp. 83-94

McFadden, L., Spencer, T., and Nicholls, R.J., (2007), Broad-scale modeling of coastal wetlands: What is required? Hydrobiologia, 577, 5– 15, doi:10.1007/s10750-006-0413-8.

Morris, J. T., Sundareshwar, P. V., Nietch, C. T., Kjerfve, B., and Cahoon, D. R., (2002). Responses of coastal wetlands to rising sea level, Ecology, 83, 2869– 2877, doi:10.1890/0012-9658(2002)083[2869:ROCWTR]2.0.CO;2

Nardin, W., Larsen, L., Fagherazzi, S. and Wiberg, P., (2018). Tradeoffs among hydrodynamics, sediment fluxes and vegetation community in the Virginia Coast Reserve, USA. *Estuarine, Coastal and Shelf Science*.

New York City Department of Environmental Protection, (2007). Jamaica Bay Watershed Protection Plan, vol. I, New York.

Orson, R., Panageotou, W., and Leatherman, S.P., (1985), Response of tidal salt marshes of the U.S. Atlantic and Gulf Coasts to rising sea levels, J. Coastal Res., 1, 29–37.

Pasternack, G.B., Hilgartner, W.B., and Brush, G.S., (2000), Biogeomorphology of an upper Chesapeake Bay river-mouth tidal freshwater marsh, Wetlands, 20, 520–537, doi:10.1672/0277-5212(2000)020<0520: BOAUCB>2.0.CO;2.

Pawlowicz, R., Beardsley, B., and Lentz, S., (2002). Classical tidal harmonic analysis including error estimates in MATLAB using T_TIDE, Comput. Geosci., 28, 929–937.

Peteet, DM, Nichols, J, Kenna, T, Chang, C, Browne, J, Reza, M, Kovari, S, Liberman, L, Stern-Protz, SS (2018) Sediment starvation destroys new York City marshes' resistance to sea level rise. Proceedings of the National Academy of Sciences 115: 10281– 10286

Pethick, J. S., (1981), Long-term accretion rates on tidal salt marshes, J. Sediment. Petrol., 51, 571–577.

Priestas, A.M., Mariotti, G., Leonardi, N., and Fagherazzi, S., (2015). Coupled wave energy and erosion dynamics along a salt marsh boundary, Hog Island Bay, Virginia, USA. Journal of Marine Science and Engineering, 3(3), pp.1041-1065.

Reed, D.J., (1995). The response of coastal marshes to sea-level rise: Survival or submergence?, Earth Surf. Processes Landforms, 20, 39–48, doi:10.1002/esp.3290200105.

Renfro, A., Cochran, J., Hirschberg, D., Bokuniewicz, H., Goodbred, S., (2016). The sediment budget of an urban coastal lagoon (Jamaica Bay, NY) determined using 234Th and 210Pb. Estuar Coast Shelf Sci 180:136–149.

Schwimmer, R., (2001). Rates and processes of marsh shoreline erosion in Rehoboth Bay, Delaware, U.S.A., J. Coastal Res., 17(3), 672-683, doi:10.1016/j.csr.2009.08.018.

Stevenson, J. C., M. S. Kearney, and E. C. Pendleton (1985), Sedimentation and erosion in a Chesapeake Bay brackish marsh system, Mar. Geol., 67, 213–235, doi:10.1016/0025-3227(85)90093-3.

Swanson R.L., Wilson, R.E., (2008). Increased tidal ranges contribute to marsh flooding. J Coast Res 24:1565–1569.

Tonelli, M., Fagherazzi, S., and Petti, M., (2010). Modeling wave impact on salt marsh boundaries, J. Geophys. Res., 115, C09028, doi:10.1029/2009JC006026.

Tommasini, L., Carniello, L., Ghinassi, M., Roner, M., and D'Alpaos, A., (2019). Changes in the wind-wave field and related salt-marsh lateral erosion: interferences from the evolution of the Venice Lagoon in the last four centuries. Earth Surf. Process. Landforms (2019), 10.1002/esp.4599

Warner, J.C., Armstrong, B., He, R., and Zambon, J.B., (2010). Development of a coupled ocean-atmosphere-wave-sediment transport (COAWST) modeling system. Ocean Model., 35 (3), pp. 230-244.

Wigand, C., et al., (2014). Below the disappearing marshes of an urban estuary: Historic nitrogen trends and soil structure. Ecol Appl 24:633–649

Zhang, X., Leonardi, N., Donatelli, C., and Fagherazzi, S., (2019). Fate of cohesive sediments in a marsh-dominated estuary. Advances in Water Resources, 125, 32-40.

Seagrass decline has changed hydrodynamics and wave energy along the shoreline of a

microtidal back-barrier estuary

Carmine Donatelli[1] [(*)], Neil K. Ganju[2], Tarandeep Kalra[3], Sergio Fagherazzi[4], Nicoletta Leonardi[1]

*corresponding Author: Carmine@liverpool.ac.uk

(1) Department of Geography and Planning, School of Environmental Sciences, Faculty of Science and Engineering, University of Liverpool, Roxby Building, Chatham St., Liverpool L69 7ZT, UK

(2) U.S. Geological Survey, Woods Hole Coastal and Marine Science Center, MA 02543, USA

(3) Integrated Statistics, Contracted to the U.S. Geological Survey, Woods Hole Coastal and Marine Science Center, MA 02543, USA

(4) Department of Earth and Environment, Boston University, 675 Commonwealth Avenue, Boston, MA 02215, USA

Citation (supplementary material): Donatelli, C., Ganju, N. K., Kalra, T., Fagherazzi, S., Leonardi, N., (2019b). Numerical modelling results of wave thrust acting on salt marsh boundaries with different seagrass coverages in a shallow back-barrier estuary, Data in Brief, doi: 10.1016/j.dib.2019.104197

Supplementary material can be found in doi: 10.1029/2018JF004617

C.D. performed COAWST simulations and carried out the analysis; C.D. wrote the manuscript assisted by N.L., S.F. and N.K.G.; C.D. designed part of the study.

Abstract

Seagrasses are marine flowering plants that provide key ecological services. In recent decades, multiple stressors have caused a worldwide decline in seagrass beds. Changes in bottom friction associated with seagrass loss are expected to influence the ability of estuarine systems to trap sediment inputs through local and regional changes in hydrodynamics. Herein, we document a numerical study using six historical maps of seagrass distribution in Barnegat Bay, USA, to demonstrate that reductions in seagrass coverage destabilize estuarine systems, decreasing flood-dominance in areas affected by seagrass disappearance and increasing bed-shear stress values across the entire back-barrier basin. Furthermore, we reveal how seagrass decline has considerably increased the impact of wind-waves on marsh edges between 1968 and 2009. From a comparison with a numerical experiment without submerged aquatic vegetation, we estimate that up to 40% of the computed wave thrust on marsh boundaries can be reduced by seagrass beds and we find that the location of a seagrass patch in addition to its aerial extent plays a crucial role in this attenuation process. This study highlights the benefits of seagrass meadows in enhancing estuarine resilience and reducing wave energy along marsh edges.

Keywords: seagrass, COAWST, ecosystem services, coastal resilience, tidal asymmetry.

5.1 Introduction

Seagrasses are marine flowering plants that can form dense underwater meadows. They are typically found in shallow depths with sufficient light levels. Seagrasses act as ecological engineers, modifying the physical and ecological environment [e.g. Carniello et al., 2016]. For instance, by reducing sediment resuspension, seagrasses can produce adequate light conditions to stimulate their own biomass production [Dennison et al., 1993; Orth et al., 2006; Carr et al., 2010]. Furthermore by stabilizing sediments, seagrasses enhance their survival rate during extreme storm conditions [Terrados and Duarte, 2000; Madsen et al., 2001; Cardoso et al., 2004]. Seagrasses provide critical ecosystem services such as nutrient cycling, organic carbon production and export, and enhanced biodiversity [Moriarty and Boon, 1989; Koch, 2001; Waycott et al., 2009]. Unfortunately, many studies have documented a large-scale seagrass decline due to global, regional and local stressors [Cambridge et al., 1986; Short and Burdick, 1996; Orth et al., 2006]. Moreover, extreme weather events (e.g. hurricanes, tsunamis) can threaten seagrass communities through meadow uprooting and burial caused by increased sediment loads [Preen et al., 1995; Koch, 1999].

Numerous studies have assessed the role of submerged aquatic vegetation (SAV) on flow and sediment transport at small scales in laboratory conditions [Dijkstra and Uittenbogaard, 2010; Nepf, 2012]. Sediment convergence and divergence, and the ensuing erosional and depositional patterns, are largely influenced by changes in the velocity field as a consequence of flow deflection and increased friction across seagrass meadows [Fonseca et al., 1982; Koch et al., 2006, Peterson et al., 2004]. Large horizontal velocity gradients are generally present between the vegetated and bare beds, and the vertical velocity profile

presents significant discontinuities at the interface between the water column occupied by the canopy and the free flow over it [e.g. Gambi et al., 1990; Koch, 2001; Ghisalberti & Nepf, 2002]. Apart from their capacity to modify tidal currents, seagrasses influence waves [e.g. Fonseca & Cahalan, 1992]. Indeed, their ability to reduce wave energy has been recognized as an important ecosystem service [Madsen et al., 2001]; several field studies and laboratory experiments have investigated the non-linear response of their buffering function to changes in vegetation characteristics [e.g. Bouma et al., 2010; Fonseca and Cahalan, 1992; Paul and Amos, 2011].

Previous numerical modelling studies have investigated the impact of climate change and water quality on seagrass decline [Carr et al., 2010; Carr et al., 2012]. In addition, Van der Heide et al. [2007] have demonstrated how the positive feedbacks between seagrass presence and turbidity in the water column might rapidly shift seagrass habitats from a stable state with clear water and high light levels to a state with strong light attenuation and no seagrass cover [Carr et al., 2010]. However, the role of seagrass has rarely been quantified at a regional scale [Ganthy et al., 2013; Nardin et al., 2018], and there is a paucity of studies investigating the impact of changes in seagrass extent on tidal asymmetry and wave thrust attenuation along marsh boundaries using large-scale historical seagrass distribution maps.

In this study, we use numerical simulations to analyse how variations in seagrass coverage influence the hydrodynamics across an entire back-barrier estuary located in New Jersey, USA. Six historical seagrass coverage maps of the Barnegat Bay Little-Egg Harbor system for the period 1968-2009 have been used. We used the Coupled Ocean Atmosphere-Wave

Sediment Transport (COAWST) modelling system [Warner et al., 2010] and the associated submerged aquatic vegetation model, recently implemented by Beudin et al., [2017a] to determine tidal water level fluctuations and wind-waves within the estuary in different years. Contrary to a simple drag increase parameterization [e.g., Morin et al., 2000], the new vegetation module provides a more physically based approach to simulate the three-dimensional effect of vegetation on the mean and turbulent flow [e.g., Lapentina & Sheng, 2014; Marjoribanks et al., 2014].

In this investigation, we first focus on the separate impact of seagrass on tidal propagation and wave height; we then explore changes in shear stress and wave thrust on marsh boundaries due to the compound wave and tidal actions. Our study suggests that seagrass presence can play a key role in protecting salt marshes against wind-wave attack. We also show that seagrass presence shortens the period of flood and reduces shear stresses on the estuarine seabed, which in turn influences the capacity of estuarine systems to capture and store sediment inputs from rivers and the ocean. These outcomes are relevant for the long-term survival of coastal bays [e.g. Fagherazzi et al., 2014] and suggest that seagrass can provide significant coastal protection [Temmerman et al., 2013].

5.2 Study site

The Barnegat Bay-Little Harbor estuary (BB-LEH) is a shallow lagoon-type estuary located in New Jersey, USA. The back-barrier bay is approximately 70 km long with a width ranging from 2.0 to 6.5 km, and an average water depth of 1.5 m [Hunchak-Kariouk et al., 1999]. The lagoon is composed of three shallow bays (Barnegat Bay, Manahawkin Bay, and Little Egg Harbor) and is connected to the ocean through two inlets (Little Egg Inlet and Barnegat Inlet). Tides are mainly semidiurnal, with the M_2 harmonic being the dominant constituent. Offshore, the tidal amplitude is ~1 m but energy dissipation through the inlets decreases the amplitude within the bay to a minimum of 0.2 m [Aretxabaleta et al., 2014]. Circulation patterns are strongly influenced by winds [Kennish et al., 2001; Defne & Ganju, 2014].

In BB-LEH, the submerged aquatic vegetation (SAV) is characterized by two main species: *Zostera marina* and *Ruppia maritima*. As showed in recent studies [Bologna et al., 2000], seagrass coverage has decreased by 62% over the last several decades; the total loss is estimated as 2000-3000 ha in 30 years (from 1960 to 1990). The main causes of the seagrass decline are related to the shading effect of phytoplankton blooms, increased growth of epiphytic algae, and wasting disease [Bologna et al., 2000; Kennish, 2001; Kennish et al., 2007a].

The bathymetry of the model used in this study is based on the National Ocean Hydrographic Survey data [NOAA-NOS, 2012] updated with field measurements [Miselis et al., 2012]. Since the 1940s there have been negligible bathymetric changes [Defne and Ganju, 2014] and even Hurricane Sandy did not alter the estuary's bathymetry over large spatial scale [Miselis et al., 2015]. The bathymetry of the study area and historical seagrass

coverage are illustrated in Figure 1 of Donatelli et al. [2019] and Figure 5.1 in this manuscript (Figure 5.1g illustrating a potential future scenario with no seagrass).
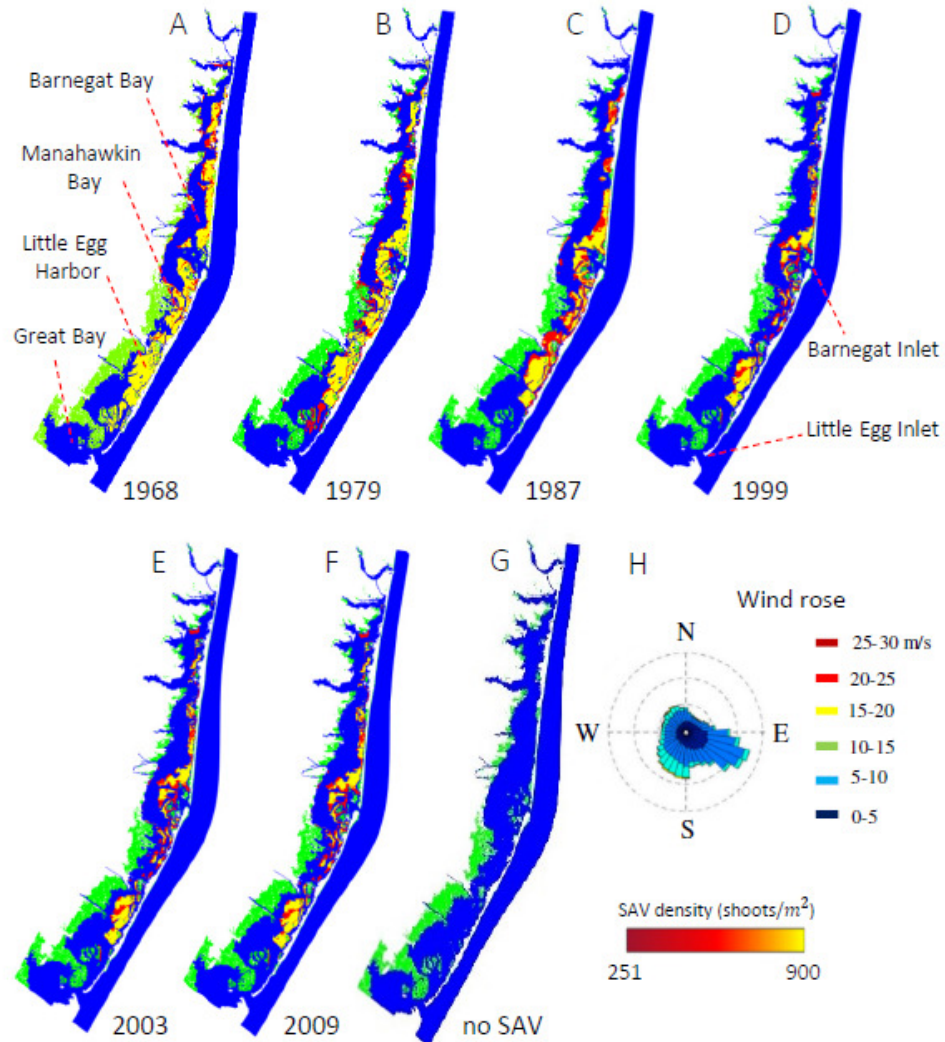
Figure 5.1 Seagrass coverages (a-f) for different years, i.e. 1968, 1979, 1987, 1999, 2003 and 2009; base-case: no-SAV (g); wind rose for the area (wind station, station 44025 (LLNR 830), 40°15'3''N, 73°9'52''W). For panels a-g green areas are locations where salt marshes are present. Yellow to red shading indicates areas were seagrasses are present as sparse (red), moderate (orange) or dense (yellow). Wind rose (h).

5.3 Methods

The hydrodynamics of the system have been simulated using the COAWST (Coupled-Ocean-Atmosphere-Wave-Sediment Transport Modeling System) modeling framework [Warner et al., 2010]. In this study, the circulation model ROMS [Shchepetkin and McWilliams, 2005; Warner et al., 2008] and the wave model SWAN [Booij et al., 1999] have been fully coupled on the same computational grid, with data exchange every 600 s. ROMS (Regional Ocean Modeling System) is a three-dimensional, free surface, finite-difference, terrain following model that solves the Reynold-Averaged Navier-Stokes (RANS) equations using the hydrostatic and Boussinesq assumptions [Haidvogel et al., 2008]. SWAN (Simulating WAves Nearshore) is a third-generation spectral wave model based on the action balance equation [Booij et al., 1999]. The model simulates the generation and propagation of wind-waves accounting for shifting in relative frequency due to variations in water depth and currents, depth-induced refraction, wave-wave interactions and dissipation (white-capping, depth-induced breaking and bottom friction). The number of interior cells is 160 x 800 in cross-bay and along-bay directions with 7 vertical layers equally spaced with cell size varying from 40 to 200 m. The model is forced at the seaward boundaries with tides, using a combination of Flather [1976] and Chapman [1985] boundary conditions; a radiation boundary condition Orlanski [1976] is prescribed on the landward boundary. The tidal constituents (K_1, O_1, Q_1, M_2, S_2, N_2, K_2, M_4 and M_6) are extracted from the ADCIRC tidal database for the North Atlantic Ocean [Mukai et al., 2002]. The model framework has been implemented and calibrated by Defne and Ganju [2014]. The model was calibrated by changing the bottom roughness coefficient to attain the best agreement between model results and water level data and water discharge

measurements collected by the U.S. Geological Survey in March 2012 [Defne & Ganju, 2014]. The calibration did not include SAV-hydrodynamic feedbacks. The friction exerted by the bed on flow is computed using a bottom boundary layer formulation [Warner et al., 2008] that includes enhanced wave based apparent roughness [Madsen, 1994]. The wave thrust (the integral along the vertical of the dynamic pressure of waves) is explicitly computed by the model following Tonelli et al. [2010] and Leonardi et al. [2016]. The flow-vegetation interaction is computed using the vegetation module recently implemented in COAWST [Beudin et al., 2017; Kalra et al., 2017]. The flow-vegetation module includes plant posture-dependent three-dimensional drag, in-canopy wave-induced streaming, and production of turbulent kinetic energy and enstrophy for the vertical mixing parameterization; the spatially averaged vegetation drag force is approximated using a quadratic drag law and the effect of plant flexibility on drag is computed using the approach of Luhar and Nepf [2011]. The selected turbulence model is the k–ε scheme which accounts for extra dissipation and turbulence kinetic energy production due to vegetation [Uittenbogaard, 2003]. Similarly, the wave dissipation due to vegetation is accounted by the model modifying the source term of the action balance equation following the formulation of Mendez and Losada [2004]. The other external contributions to wave energy such as wind, wave breaking, bottom dissipation and nonlinear waves interactions are computed as follows: i) wind energy input according to Cavalieri and Malanotte-Rizzoli [1981] and Komen et al. [1984] formulations for the linear and exponential wind growth respectively; ii) bottom friction following Madsen [1988]; and iii) whitecapping following Komen et al. [1984]. An idealized wind field was used, as these numerical experiments are not intended to quantify the real wave thrust on marsh boundaries but are built with the

139

goal to unravel the effect of seagrass loss on wave energy. Different scenarios were considered for the wind forcing characterized by winds of constant speed (5, 10 and 15 m/s) blowing from south-west and south-east (Figure 5.1h) for the entire simulation period. As wave action on marsh edges is strongly related to tidal level [Tonelli et al., 2010], we ran the simulations for a spring-neap tidal cycle. The temporal evolution of the study site has not been considered and the present-day morphology has been used for each year. Particularly, recent studies [e.g. Leonardi, et al., 2016a, b] show that marshes are eroding at around 0.5-2 m/year, with the highest erosion rate registered in Great Bay. The resolution of the model domain is such that morphological changes due to marsh edge erosion cannot be taken into account at these erosion rates; therefore, we focus solely on the impact of seagrass coverage on waves and tides by adopting an exploratory model approach [Murray, 2007]. Salt marsh and seagrass coverage data were derived from the CRSSA's (Center for Remote Sensing and Spatial Analysis) geographic information systems (GIS) database. Vegetation parameters are listed in Table 5.2 of Donatelli et al. [2019] nominally selected using Kennish et al. [2013] for guidance. Simulations are run implementing different seagrass coverages corresponding to the years 1968, 1979, 1987, 1999, 2003, 2009, and for a test case without seagrasses [1968 map, U.S. Army Corps of Engineers, 1976; 1979 map, Macomber and Allen, 1979; 1987 map, Joseph et al., 1992; 1999 map, McClain and McHale 1996; Bologna et al., 2000; 2003 and 2009 maps, Lathrop and Haag, 2011].

5.4 Results

From 1968 until 2009, the extent of seagrass meadows within the Barnegat Bay-Little Egg

Harbor system largely declined (Figure 5.1, Figure 5.2; Table 1 in Donatelli et al. [2019]).

Figure 5.2 shows the area colonized by seagrass as a function of water depth for each year.
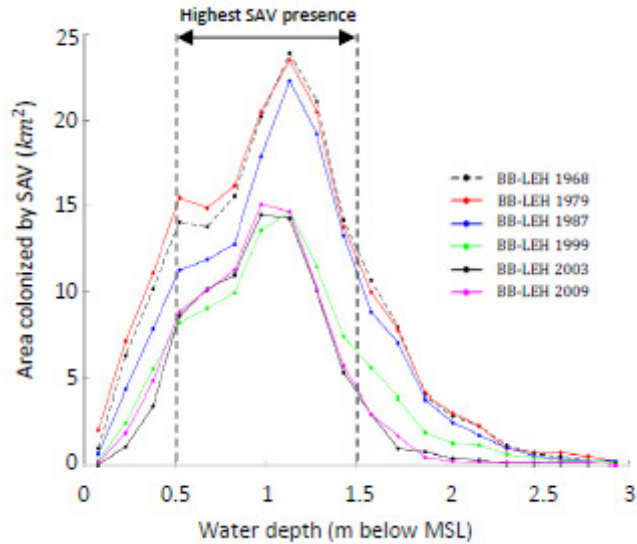
Figure 5.2 Area colonized by seagrass as a function of water depth for each year. Water depth data are binned every 0.15 m.

The impact of seagrass loss on tidal propagation was evaluated following classic harmonic

analysis using T_TIDE [Pawlowicz et al., 2002], and by computing the spatial distribution

of the amplitude and phase lag of the M_2 constituent within the entire back-barrier basin.

For coastal areas with multiple inlets, water levels are controlled by the interaction between

tidal forcing propagating from each inlet, and changes in bottom friction that can alter their

relative phase. A comparison between amplitude and phase lag values for the scenario with

maximum seagrass coverage (year 1979) and a scenario without seagrass reveals that the

phase lag of the tidal wave coming from Great Bay and directed to Barnegat Bay decreased

with seagrass removal. As a consequence, the tidal amplitude within the entire northern part of the estuary increases for the non-seagrass case, because the tidal waves from Barnegat Inlet and from Great Bay have a similar phase and become additive.
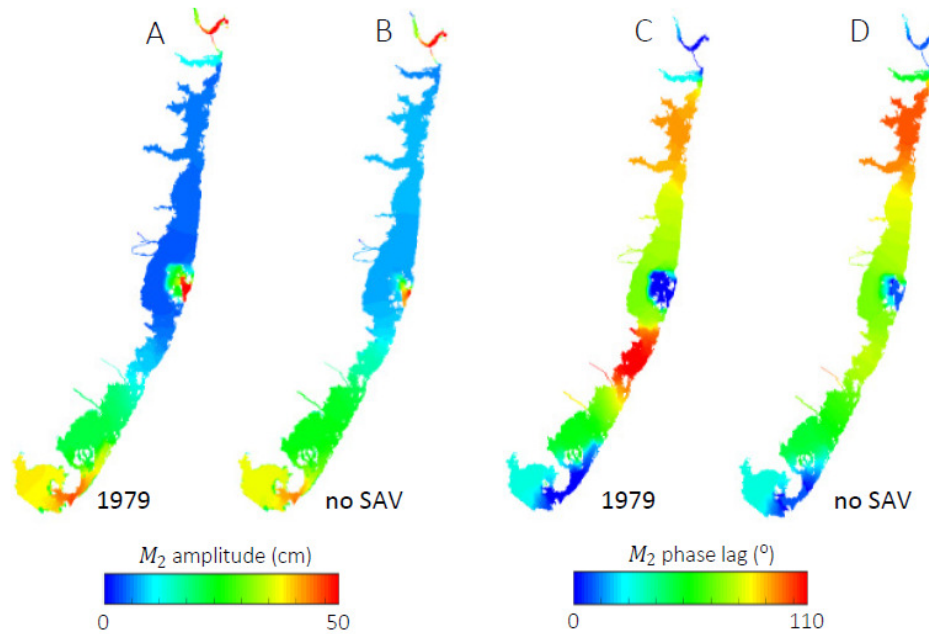
Figure 5.3 M_2 amplitude (cm) and phase lag (°) for year 1979 (a, c) and no SAV case (b, d).

Seagrass loss also influences tidal asymmetry. Asymmetric tides are important for the transport and deposition of sediments in shallow estuaries [Aubrey and Speer, 1985]. Changes in tidal asymmetry were calculated following the formulation of Friedrichs and Aubrey [1988] and are depicted in Figure 5.4. The amplitude and phase ratios between the fourth-diurnal M_4 constituent and the semidiurnal M_2 constituent have been calculated. Our results suggest that seagrass meadows tend to enhance the flood dominance of the system increasing the M_4 to M_2 water level amplitude ratio, as tidal nonlinearities are enhanced.
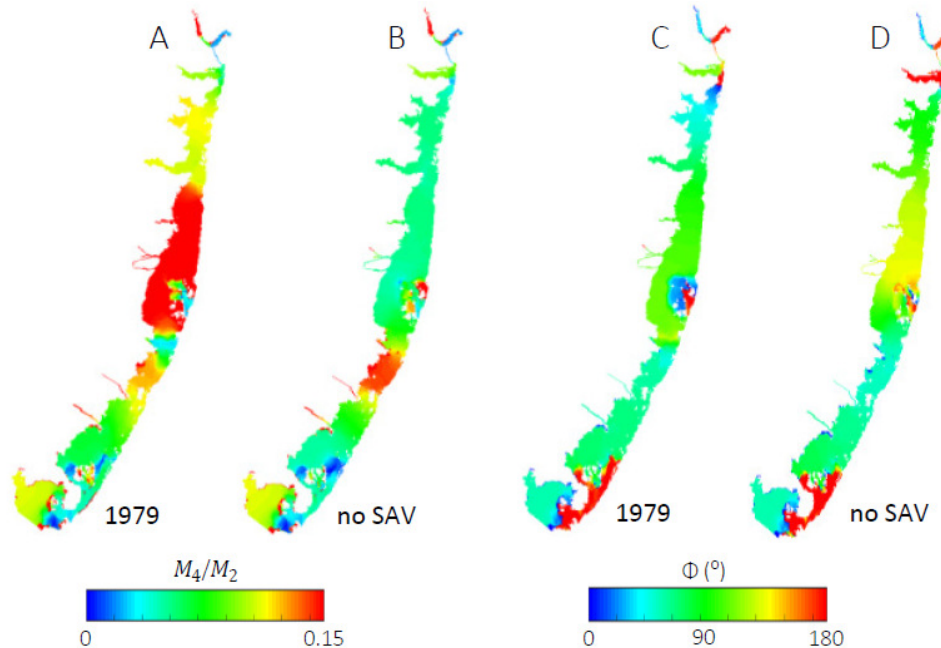
Figure 5.4 Sea-surface amplitude ratio and sea-surface phase of M_4 relative to M_2 for year 1979 (a, c) and no SAV case (b, d).

In this study, we also evaluated the influence of seagrass beds on locally generated wind-waves for winds of 5, 10, and 15 m/s blowing from the southwest and southeast. Wind directions and speeds were chosen based on the most frequent winds (Figure 5.1h), with southwest winds maximizing fetch in the southern half of the estuary. Figure 5.5 presents the distribution of mean wave heights as a function of water depth in the non-seagrass case and for the scenarios with maximum (year 1979) and minimum (year 2009) seagrass coverage. The mean wave height is the mean value throughout the entire simulation computed at each cell. Our results show that the presence of seagrass attenuates waves across the entire bay, although this damping effect is more limited on bare beds (Figure 5.6). Colored areas in Figure 5.5 indicate locations where some seagrass is present, while no seagrass is present in the white areas of the plot. Figure 5.6 distinguishes areas with and without seagrass meadows for every depth. For areas with meadows, the reduction in wave

height peaks where seagrass presence is maximum. In contrast, the reduction in wave height over bare beds is more uniform across all depths with small decreases occurring where seagrass presence is maximum as well as across transitional depth values above which no seagrass are present. Results for all wind speed values are presented in the supplementary material (Figure 3-4 in Donatelli et al. [2019]).
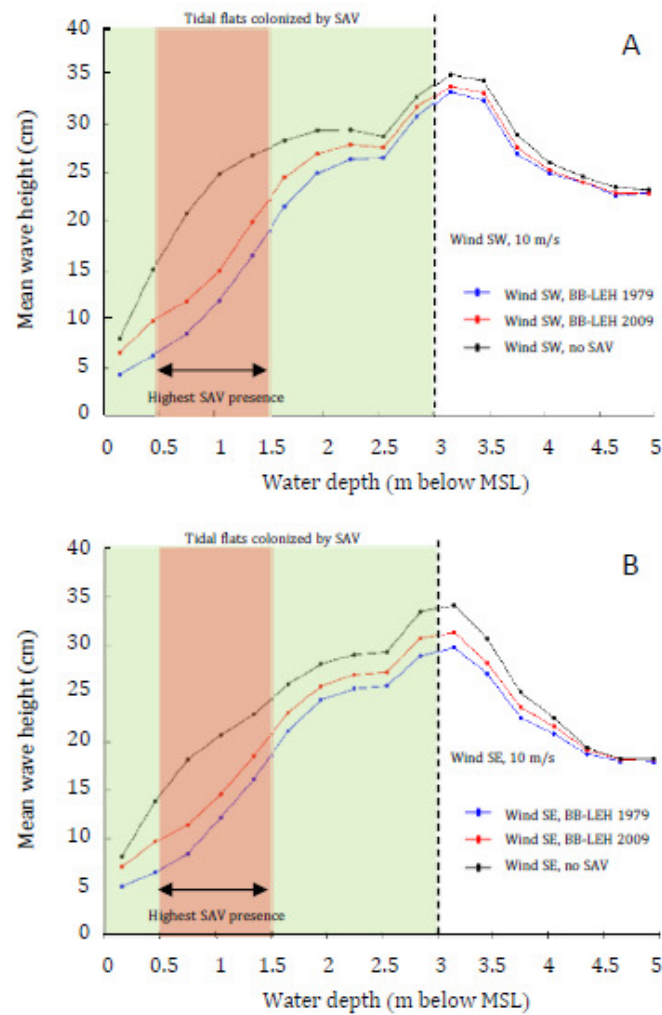
Figure 5.5 Mean wave height (cm) as a function of water depth (m) for a wind blowing from South-West (a) and South-East (b) with a speed of 10 m s-1 for three different scenarios: year 1979, year 2009 and no SAV case. Water depth data are binned every 0.3 m. Red and green areas are water depths where seagrass is present, while no seagrass is present in the white areas of the plot. Red areas are locations where seagrass presence is maximum (see Figure 5.2). Coloured areas do not necessary have 100% seagrass coverage.

144

A

Tidal flats colonized by SAV

Wind SW, 10 m/s

- BB-LEH 1979, bare beds
- No SAV, bare beds
- difference
- BB-LEH 1979, meadows
- No SAV, meadows
- difference

B

Wind SW, 10 m/s

- BB-LEH 2009, bare beds
- No SAV, bare beds
- difference
- BB-LEH 2009, meadows
- No SAV, meadows
- difference

C

Wind SE, 10 m/s

- BB-LEH 1979, bare beds
- No SAV, bare beds
- difference
- BB-LEH 1979, meadows
- No SAV, meadows
- difference

D

Wind SE, 10 m/s

- BB-LEH 2009, bare beds
- No SAV, bare beds
- difference
- BB-LEH 2009, meadows
- No SAV, meadows
- difference

Figure 5.6 Mean wave height (cm) over bare beds (every depth in areas without vegetation) and meadows (every depth where seagrass meadows are present) as a function of water depth (m) for a wind blowing from South-West (a, b) and South-East (c, d) with a speed of 10 m s-1. Panels a, c refer to seagrass distribution of 1979, while panels b, d refer to seagrass distribution of 2009; differences are made with respect to the no seagrass case. Water depth data are binned every 0.3 m.

Seagrass loss increases the action of waves and tides at the basin bottom. The distributions of shear stresses are presented in Figure 5.7.
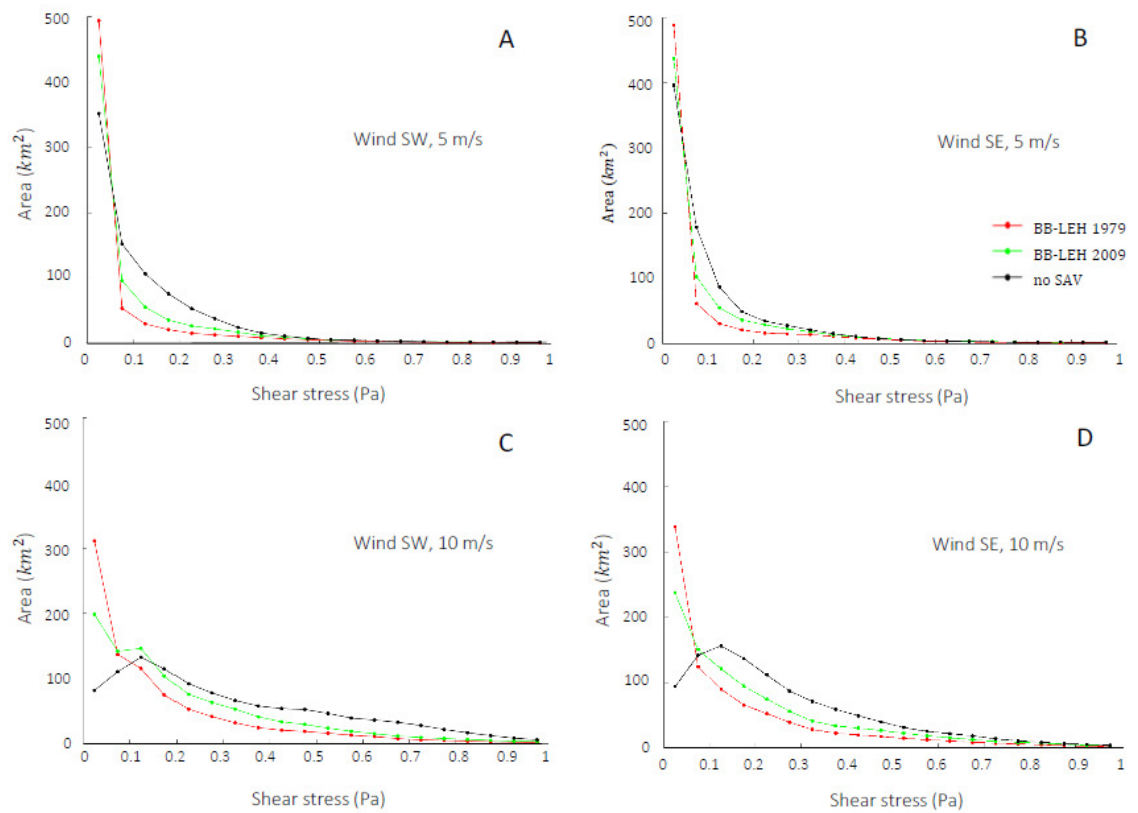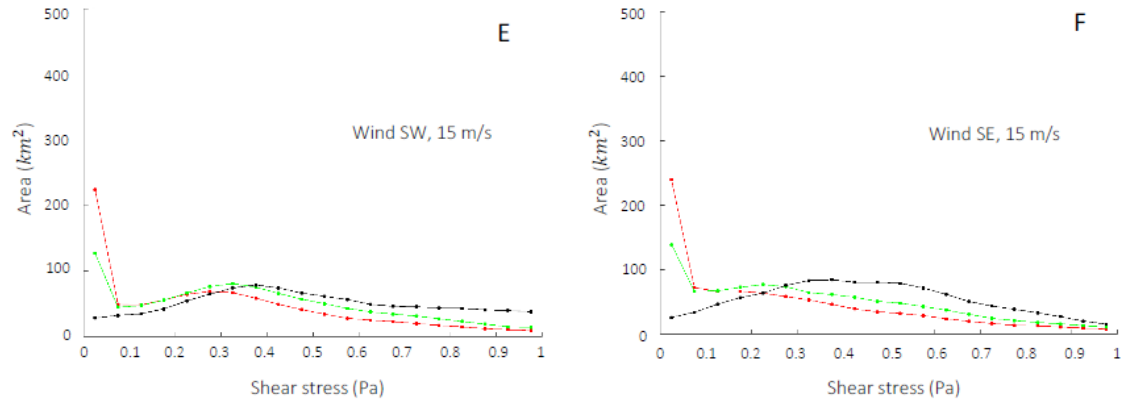
Figure 5.7 Distribution of shear stresses (Pa) produced by a wind of 5, 10 and 15 m s-1 blowing from South-West (a, c, e) and South-East (b, d, f) for three different scenarios: year 1979, year 2009 and no SAV case. Shear stress data are binned every 0.05 Pa.

The presence of seagrass largely increases the extent of basin areas with shear stress values smaller than 0.1 Pa. In addition, seagrass removal raises the lateral wave thrust exerted on marsh boundaries. The spatial distribution of wave thrust averaged throughout a spring-neap tidal cycle is depicted in Figure 5.8 for the non-seagrass case and for the case with maximum seagrass coverage (1979).
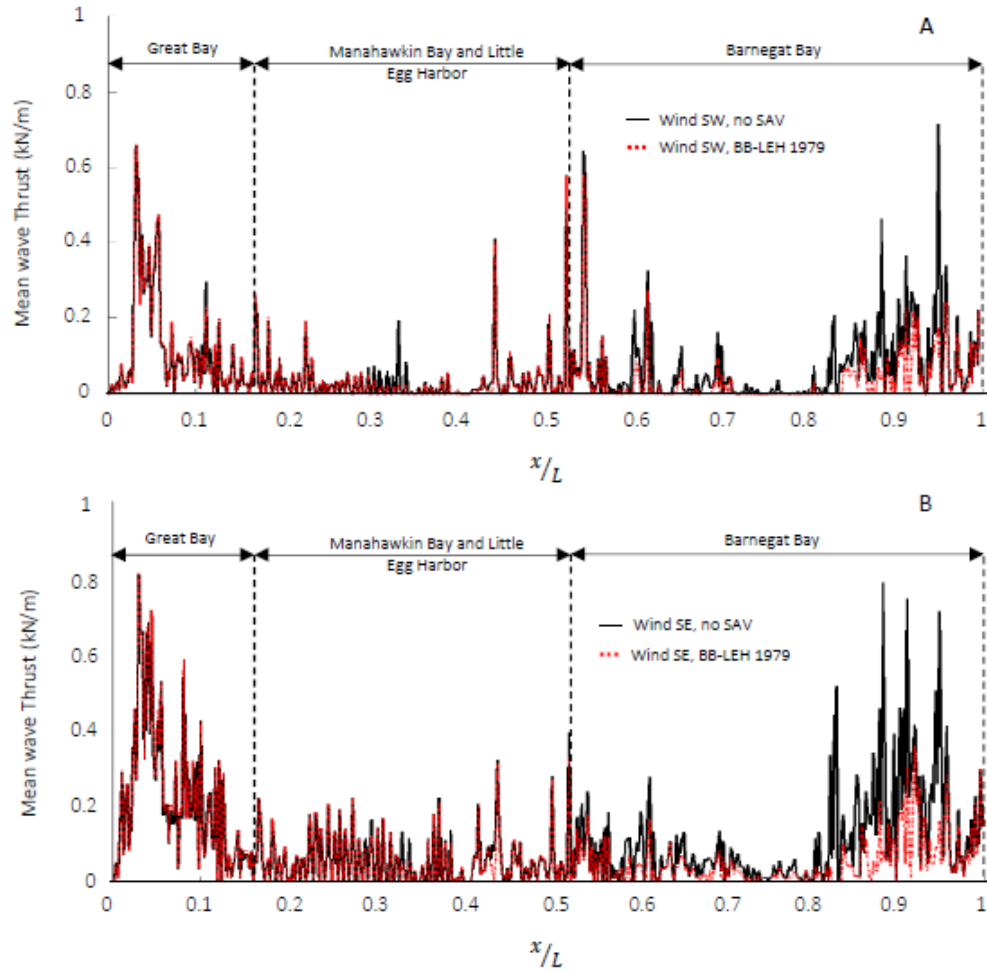
Figure 5.8 Mean wave thrust on marsh boundary during a spring-neap cycle for a wind blowing from South-West (a) and South-East (b) with a speed of 10 m s^{-1} for two different scenarios: year 1979 and no SAV case.

Figure 5.9 shows the decrease in wave action due to seagrass presence with respect to the non-seagrass case over the last 50 years. Average wave thrust reduction in time and across the entire Bay are thus expressed in terms of percentage reduction with respect to the non-seagrass case (Figure 5.9).
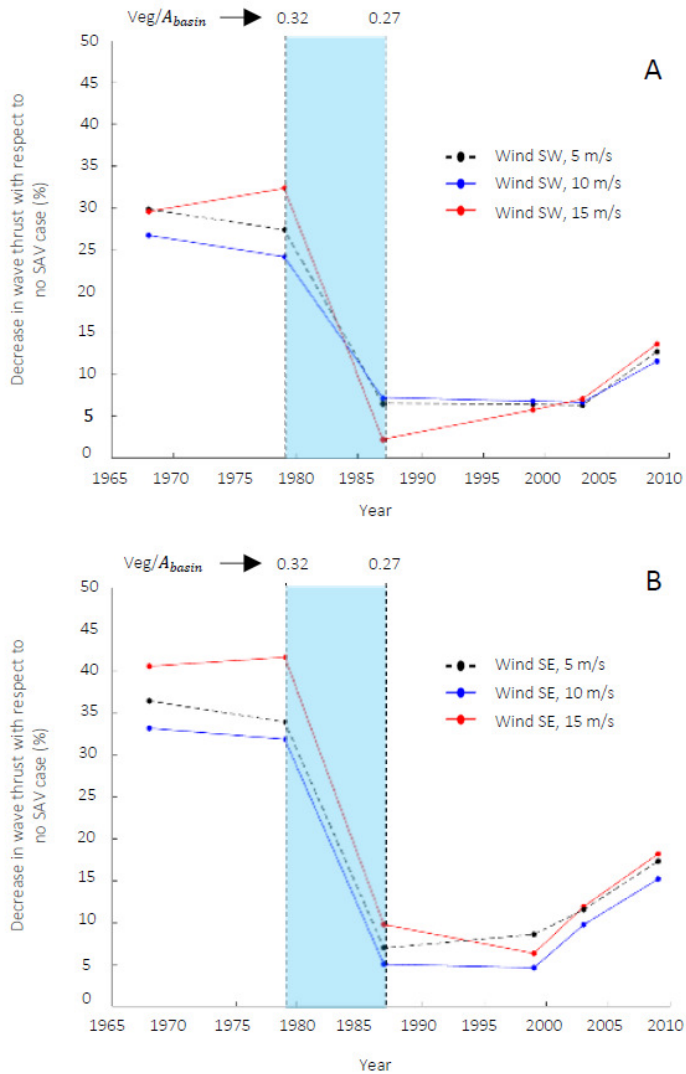
Figure 5.9 Decrease in wave thrust (%) with respect to no SAV case for a wind blowing from South-West (a) and South-East (b) with a speed of 5, 10 and 15 m s^{-1} over the entire bay (Great Bay excluded).

Our numerical findings suggest that in Barnegat Bay, the wave attack on marsh boundaries increased significantly between 1979 and 1987 (light blue areas in Figure 5.10), although, on average, a small reduction in seagrass coverage occurred (Figure 5.10 and Table 1 in Donatelli et al. [2019]). Though the average decrease in seagrass extent was small, seagrass loss was greater in areas sheltering the marsh boundaries (Figure 2c in Donatelli et al.

[2019]). On the contrary, in the last five decades, the wave thrust increased uniformly in Manahawkin Bay (Figure 5.10) as the seagrass removal was uniform.
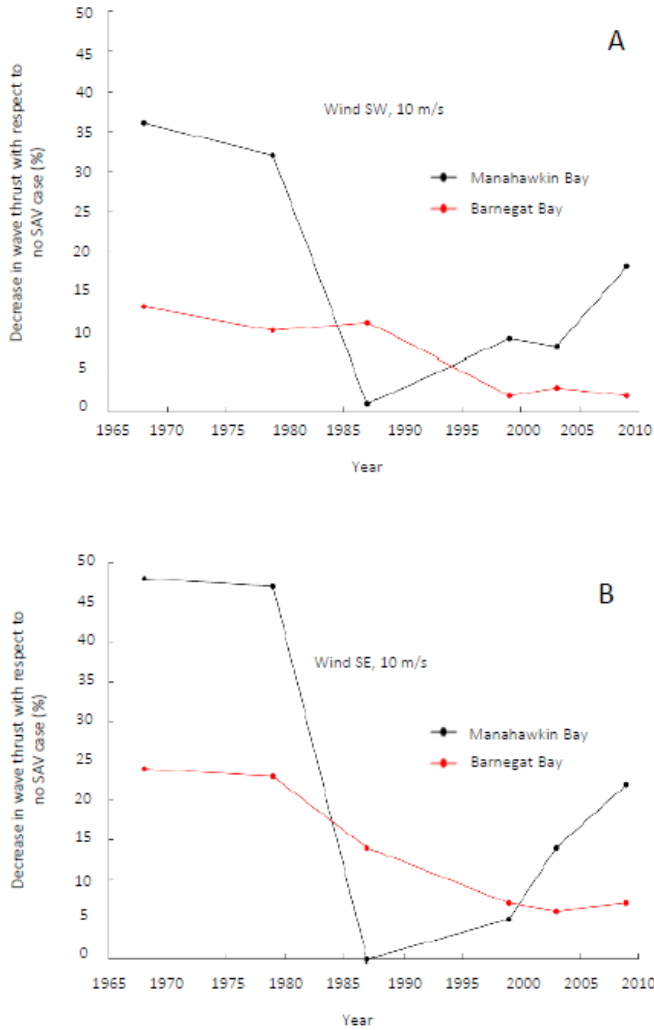
Figure 5.10 Decrease in wave thrust (%) with respect to no SAV case for a wind blowing from South-West (a) and South-East (b) with a speed of 10 m s-1 in Manahawkin Bay and Barnegat Bay.

5.5 Discussion and conclusion

The impact of submerged aquatic vegetation on wind waves and tides within a semi-enclosed shallow lagoon system has been evaluated using the Barnegat Bay-Little

Egg Harbor system as a test case. The analyses are based on historical trends of seagrass distribution from 1968 to 2009; a scenario with no seagrass represents a plausible system configuration in the near future. This study has shown that seagrass decline influences tidal propagation in shallow bays with multiple inlets. Specifically, changes in bottom friction alter the relative phase between the tidal waves coming from each inlet modifying water levels within the entire estuary (Figure 5.3).

Tidal asymmetry in coastal embayments and estuaries is governed by the ratio of tidal amplitude to mean water depth and the ratio of intertidal storage area occupied by tidal flats and salt marshes to that of channels [Speer and Aubrey, 1985]. Previous studies have investigated the impact of tidal flat elevations [e.g. Fortunato & Oliveira, 2005] and salt marsh erosion [Donatelli et al., 2018b] on tidal propagation and asymmetry within shallow estuaries. In this study, we show that seagrass also influences tidal asymmetry. For this test case, the average increase in tidal nonlinearities due to seagrass presence (Figure 4) is higher than the one caused by an increase in intertidal storage volume due to a complete removal of salt marsh areas. The latter was explored in Donatelli et al. [2018b]. Hence, submerged aquatic vegetation might increase the flood dominance of microtidal back-barrier estuaries. Particularly, the friction due to seagrasses slows the propagation of tidal water levels around low tide relative to high tide [Dronkers, 1986], leading to longer ebb and higher velocity currents during the flood phase. Moreover, we show that increased seagrass coverage decreases bed shear stress across the entire basin (Figure 5.7). These findings agree with previous field measurements and numerical studies [Hansen and Reidenbach, 2012; Donatelli et al., 2018a], which demonstrate that seagrasses reduce

bottom shear stresses within and behind patches, and also impact the sediment budget of coastal bays.

Marsh loss associated with edge erosion is a major mechanism of marsh deterioration in estuaries and lagoons worldwide [Schwimmer, 2001; Barbier et al., 2008; Marani et al., 2011; Tommasini et al., 2019]. Wind-waves are recognized as the chief erosional agent and Schwimmer [2001] first suggested the existence of a relationship between wave energy and marsh retreat; subsequent studies further corroborated this finding [e.g., Marani et al., 2011; Leonardi & Fagherazzi, 2014; Leonardi, et al., 2016a,b]. Tidal levels play a key role in wind-wave attack, determining the elevation at which waves attack the marsh edge. Wave action on marsh boundaries increases with tidal elevation and then drops when the marsh is submerged [Tonelli et al., 2010]. In this study we showed, in agreement with previous researches [e.g., Nowacki et al., 2017; Beudin et al., 2017b; Nardin et al. 2018], that submerged aquatic vegetation has a local effect in dampening waves. Indeed, seagrasses strongly reduce wave heights over meadows but have a more limited effect on un-vegetated flats (Figure 5.6). Therefore, given a certain seagrass distribution, marsh boundaries experience a decrease in wave attack and such decrease in wave action is significantly larger for those salt marshes located next to meadows.

Our numerical results show that, over the last five decades, the wave action on salt marshes fringing the mainland in the Barnegat Bay-Little Egg Harbor estuary increased with seagrass loss. Figure 5.10 reveals how seagrass deterioration affected wave attack in the central and north part of the estuary and highlights how the disappearance of small SAV patches next to marsh boundaries (Table 1 and Figure 2 in Donatelli et al., [2019]) increased the wave thrust by 35% in the period 1979-1987. These results highlight that, in

terms of protection of the marsh boundary, the location of disappearing seagrasses is important. Our research underlines how seagrass decline can decrease bay sediment storage capacity and potentially enhance salt marsh lateral erosion. Because salt marsh loss reduces the ability of shallow estuaries to retain sediments [Donatelli et al., 2018b], this might in turn promote further deterioration of salt marshes through a positive feedback loop [e.g., Ganju et al., 2017]. The influence of seagrasses on hydrodynamics should be explored seasonally as aboveground biomass peaks during June-July and declines significantly during fall, when it becomes five times smaller [Kennish et al., 2007b, 2008; Farnsworth, 1998; Koch et al., 2009; Hansen and Reidenbach, 2013]. The capacity of meadows to influence waves changes over the year and a minimum shoot density is necessary to initiate wave attenuation [e.g., Paul & Amos, 2011]. The lack of seasonal data in our study constitutes a significant gap in the understanding of how these ecosystems can affect the stability of coastal embayments over long time scales.

References

Aubrey, D.G., and Speer, P.E., (1985). A study of non-linear tidal propagation in shallow inlet estuarine systems. Part I. Observations. Estuar. Coast. Shelf Sci. 21, 185-205.

Beudin, A., Kalra, T.S., Ganju, N.K., and Warner, J.C., (2017a). Development of a coupled wave-flow vegetation interaction model. Computers & Geosciences.

Beudin, A., Ganju, N.K., Defne, Z., and Aretxabaleta, A.L., (2017b). Physical response of a back-barrier estuary to a post-tropical cyclone. Journal of Geophysical Research: Oceans, 122, 5888–5904. https://doi.org/10.1002/2016JC012344.

Bologna, P., Lathrop, R., Bowers, P., and Able, K., (2000). Assessment of submerged aquatic vegetation in Little Egg Harbor, New Jersey. Technical Report 2000-11, Institute of Marine and Coastal Sciences, Rutgers University, New Brunswick, New Jersey, USA.

Booij, N., Ris, R.C., and Holthuijsen, L.H., (1999). A third-generation wave model for coastal regions, part I, model description and validation. Journal of Geophysical Research, C4, 7649–7666. https://doi.org/10.1029/98JC02622

Cambridge, M.L., Chiffings, A.W., Brittan, C., Moore, L., and McComb, A.J., (1986). The loss of seagrass in Cockburn Sound western Australia II; Possible causes of seagrass decline. Aquatic Botany 24: 269-286.

Cardoso, P.G., Pardal, M.A., Lillebo, A.I., Ferreira, S.M., Raffaelli, D., and Marques, J.C., (2004). Dynamic changes in seagrass assemblages under eutrophication and implications for recovery. Journal of Experimental Marine Biology and Ecology 302: 233-248.

Carr, J., Mariotti, G., Fahgerazzi, S., McGlathery, K., and Wiberg, P., (2018). Exploring the impacts of seagrass on coupled marsh-tidal flat morphodynamics. Frontiers in Environmental Science 6: 92.

Cavaleri, L., Malanotte-Rizzoli, P., (1981). Wind wave prediction in shallow water: Theory and applications, J. Geophys. Res., 86C11, 10,961–10,973.

Chapman, D. C., (1985). Numerical treatment of cross-shelf open boundaries in a barotropic coastal ocean model, J. Phys. Oceanogr., 15, 1060–1075.

Defne, Z., and Ganju, N.K., (2014). Quantifying the residence time and flushing characteristics of a shallow, back-barrier estuary: Application of hydrodynamic and particle tracking models, Estuaries Coasts,1 – 16, doi:10.1007/s12237-014-9885-3.

Dennison, W.C., Orth, R.J., Moore, K.A., Stevenson, J.C., Carter, V., Kollar, S., Bergstrom, P.W., Batiuk, R.A., (1993). Assessing water quality with submersed aquatic vegetation. BioScience 43: 86-94.

Dias, J. M., Lopes, J. F., and Dekeyser, I., (2000). Tidal propagation in Ria de Aveiro Lagoon, Portugal, Phys. Chem. Earth 25(4), 369–374.

Dijkstra, J., and Uittenbogaard, R., (2010). Modeling the interaction between flow and highly flexible aquatic vegetation. Water. Resour. Res. 46: W12547.

Donatelli, C., Ganju, N.K., Fagherazzi, S., and Leonardi, N., (2018a). Seagrass impact on sediment exchange between tidal flats and salt marsh, and the sediment budget of shallow bays, Geophysical Research Letters, doi:10.1029/2018GL078056.

Donatelli, C., Ganju, N.K., Zhang, X., Fagherazzi, S., and Leonardi, N., (2018b). Salt marsh loss affects tides and the sediment budget of shallow bays, Journal of Geophysical Research: Earth Surface, doi: 10.1029/2018JF004617.

Donatelli, C., Ganju, N.K., Kalra, T.S., Fagherazzi, S., and Leonardi, N., (2019). Dataset of numerical modelling results of wave thrust on salt marsh boundaries with different seagrass coverages, Data in Brief (published at the time article, https://www.sciencedirect.com/science/article/pii/S2352340919305517).

Dronkers, J., (1988). Coastal-offshore ecosystem. Lecture Notes on Coastal and Estuaries Studies, ed Jansson B-O (AGU, Washington, DC), Vol 22, pp 3-39.

Fagherazzi, S., (2014). Coastal processes: Storm-proofing with marshes. Nat Geosci 7(10): 701–702.

Farnsworth, E., (1998). Issues of spatial, taxonomic and temporal scale in delineating links between mangrove diversity and ecosystem function. Global Ecol Biogeogr 7 : 15–25.

Flather, R.A., (1976). A tidal model of the northwest European continental shelf, Mem. Soc. R. Sci. Liege, 6, 141–164.

Fonseca, M.S., Fisher, J.S., Zieman, J.C., and Thayer, G.W., (1982). Influence of the seagrass Zostera marina on current flow. Estuarine Coastal and Shelf Science 15: 351-364.

Fonseca, M.S., and Cahalan, J.A., (1992). A preliminary evaluation of wave attenuation by four species of seagrass. Estuarine, Coastal, Shelf Sci., 35: 565–576.

Fortunato, A.B., and Oliveira, A., (2005). Influence of intertidal flats on tidal asymmetry. Journal of Coastal Research 21 (5), 1062-1067.

Friedrichs, C.T., and Aubrey, D.G., (1988). Non-linear tidal distortion in shallow well-mixed estuaries: a synthesis. Estuarine Coastal and Shelf Science, 27(5), 521-545.

Gambi, M.C., Nowell, A.R. M., and Jumars, P.A., (1990). Flume observations on flow dynamics in Zostera marina eelgrass beds. Marine Ecology Progress Series 61: 159-169.

Ganthy, F., Sottolichio, A., Verney, R., (2013). Seasonal modification of tidal flat sediment dynamics by seagrass meadows of Zostera noltii (Bassin d'Arcachon, France). J. Mar. Syst., 109–110, pp. S233-S240.

Ganju, N.K., Defne, Z., Kirwan, M.L., Fagherazzi, S., D'Alpaos, A. and Carniello, L., (2017). Spatially integrative metrics reveal hidden vulnerability of microtidal salt marshes. Nature communications, 8, p.ncomms14156.

Ghisalberti, M., and Nepf, H.M., (2002). Mixing layers and coherent structures in vegetated aquatic flows. J. Geophys. Res. 107: 3011, doi:10.1029/2001JC000871.

Hansen, J.C. and Reidenbach, M.A., (2012). Wave and tidally driven flows in eelgrass beds and their effect on sediment suspension. Marine Ecology Progress Series, 448, pp.271-287.

Harlin, M.M., Thorne Miller, B., and Boothroyd, J.C., (1982). Seagrass sediment dynamics of a flood tidal delta in Rhode Island (USA). Aquatic Botany, 14, 127–138.

Hansen, J.C., and Reidenbach, M.A., (2013). Seasonal growth and senescence of a Zostera marina seagrass meadow alters wave-dominated flow and sediment suspension within a coastal bay. Estuaries and coasts, 36(6), pp.1099-1114.

Hunchak-Kariouk, K., (1999). Relation of water quality to land use in the drainage basins of four tributaries to the Toms River, New Jersey, 1994--1995. No. PB-99-149098/XAB; USGS/WRI--99-4001. Geological Survey, Water Resources Div., West Trenton, NJ (United States); New Jersey Dept. of Environmental Protection, Trenton, NJ (United States).

Joseph, J., Purdy, K., and Figley, B., (1992). The influence of water depth and bottom sediment on the occurrence of eelgrass in Barnegat, Manahawkin and Little Egg Harbor bays. Marine Fisheries Administration, New Jersey Department of Environmental Protection and Energy, Nacote Creek, New Jersey.

Kalra, T.S., Aretxabaleta, A., Seshadri, P., Ganju, N.K. and Beudin, A., (2017). Sensitivity analysis of a coupled hydrodynamic-vegetation model using the effectively subsampled quadratures method (ESQM v5. 2). Geoscientific Model Development, 10, pp.4511-4523.

Kennish, M.J., (2001). State of the estuary and watershed: an overview. Journal of Coastal Research Special Issue 32:243– 273.

Kennish, M.J., Bricker, S.B., Dennison, W.C., Glibert, P.M., Livingston, R.J., Moore, K.A., Noble, R.T., Paerl, H.W., Ramstack, J., Seitzinger, S., Tomasko, D.A., and Valiela, I., (2007a). Barnegat Bay-Little Egg Harbor Estuary: Case Study of a Highly Eutrophic Coastal Bay System. Ecological Applications 17 (Special Issue), S3-S16.

Kennish, M., Haag, S., and Sakowicz, G., (2008). Seagrass demographic and Spatial Habitat Characterization in Little Egg Harbor, New Jersey, Using Fixed Transects. Journal of Coastal Research, Special Issue 55, 148-170.

Koch, E.W., (1999). Sediment resuspension in a shallow Thalassia testudinum banks ex König bed. Aquatic Botany 65: 269-280.

Koch, E.W., (2001). Beyond light: Physical, geological, and geochemical parameters as possible submersed aquatic vegetation habit requirements. Estuaries 24: 1-17.

Koch, E.W., Sanford, L.P., Chen, S.-N., Shafer, D.J., and Smith, J.M., (2006). Waves in seagrass systems: review and technical recommendations. U.S. Army Corps of Engineers, Washington, DC.

Komen, G.J., Hasselmann, S., and Hasselmann, K., (1984). On the existence of a fully developed wind-sea spectrum, J. Phys. Oceanogr., 14, 1271–1285.

Lapentina, A., and Sheng, Y.P., (2014). Three-dimensional modeling of storm surge and inundation including the effects of coastal vegetation. Estuaries and Coasts, 37(4), 1028–1040. https://doi.org/10.1007/s12237-013-9730-0

Lathrop, R.G., Jr., and Bognar, J.A., (2001). Habitat loss and alteration in the Barnegat Bay Region, J. Coastal Res., 212–228, doi:10.2307/25736235.

Lathrop, R.G. and Haag, S., (2011). Assessment of Seagrass Status in the Barnegat Bay-Little Egg Harbor Estuary: 2003 and 2009. CRSSA Technical Report#2011-01. Rutgers University, Grant F. Walton Center for Remote Sensing and Spatial Analysis, New Brunswick, NJ.

Leonardi, N., and Fagherazzi, S., (2014). How waves shape salt marshes. Geology, 42(10), pp.887-890.

Leonardi, N., Defne, Z., Ganju, N.K. and Fagherazzi, S., (2016a). Salt marsh erosion rates and boundary features in a shallow Bay. Journal of Geophysical Research: Earth Surface, 121(10), pp.1861-1875.

Leonardi, N., Ganju, N.K., and Fagherazzi, S., (2016b). A linear relationship between wave power and erosion determines salt-marsh resilience to violent storms and hurricanes. Proceedings of the National Academy of Sciences, 113(1), pp.64-68.

Leonardi, N., Carnacina, I., Donatelli, C., Ganju, N.K., Plater, A.J., Schuerch, M. and Temmerman, S., (2017). Dynamic interactions between coastal storms and salt marshes: A review. Geomorphology.

Macomber, R.T., and Allen, D., (1979). The New Jersey submerged aquatic vegetation distribution atlas final report. Earth Satellite Corporation, Washington, D.C.

Madsen, O.S., Poon, Y.-K., and Graber, H.C., (1988). Spectral wave attenuation by bottom friction: Theory, Proceedings of 21th International Conference on Coastal Engineering, 492–504Am. Soc. of Civ. Eng., New York.

Madsen, J.D., Chambers, P.A., James, W.F., Koch, E.W., and Westlake, D.F., (2001). The interaction between water movement, sediment dynamics and submersed macrophytes. Hydrobiologia 444: 71-84.

Marani, M., D'Alpaos, A., Lanzoni, S., and Santalucia, M., (2011). Understanding and predicting wave erosion of marsh edges, Geophys. Res. Lett., 38, L21401, doi:10.1029/2011GL048995.

Marjoribanks, T. I., Hardy, R. J., and Lane, S.N., (2014). The hydraulic description of vegetated river channels: The weaknesses of existing formulations and emerging alternatives. WIREs Water, 1(6), 549–560. https://doi.org/10.1002/wat2.1044

McCLain, P., and McHale, M., (1996). Barnegat Bay eelgrass investigations 1995–1996, p. 165–172. In G. Flimlin and M. Kennish (eds.), Proceedings of the Barnegat Bay EcosystemWorkshop. Rutgers Cooperative Extension, Toms River, New Jersey.

Mendez, F.M., and Losada, I.J., (2004). An empirical model to estimate the propagation of random breaking and nonbreaking waves over vegetation fields. Coast. Eng. 51, 103-118.

Miselis, J., Andrews, B., Baker, R., Danforth, W., DePaul, V., Defne, Z., Feinson, L., Ganju, N., Gibs, J., Hickman, R.E., Lopez, A., Navoy, A., Nicholson, R., Reilly, T., Reiser,

R., Spitz, F., Watson, A., Wieben, C., and Wilson, T., (2012). Characterizing physical, chemical, and biological conditions and processes in the Barnegat Bay-Little Egg Harbor Estuary, New Jersey. 2012 Barnegat Bay Researchers Workshop, Bordentown Township, NJ.

Miselis, J.L., Andrews, B.D., Nicholson, R.S., Defne, Z., Ganju, N.K., and Navoy, A., (2015). Evolution of mid-Atlantic coastal and back-barrier estuary environments in response to a hurricane: Implications for barrier-estuary connectivity. Estuaries and Coasts. doi: 10.1007/s12237-015-0057-x.

Möller, I., Spencer, T., (2002). Wave dissipation over macro-tidal saltmarshes: Effects of marsh edge typology and vegetation change. Journal of Coastal Research, 36 (Special Issue), pp. 506-521

Moriarty, D.J.W., and Boon, P.I., (1989). Interactions of seagrass with sediment and water. In Larkum, A.W.D. and S.A. Sheppard (eds), Biology of Seagrasses. Elsevier, Amsterdam, 500-535.

Morin, J., Leclerc, M.M., Secretan, Y., and Boudreau, P., (2000). Integrated two-dimensional macrophytes-hydrodynamic modelling. Journal of Hydraulic Research, 38(3), 163–172. https://doi.org/10.1080/00221680009498334

Mukai, A.Y., Westerink, J.J., Luettich, R.A. Jr., and Mark, D., (2002). Eastcoast 2001: A tidal constituent database for the western North Atlantic, Gulf of Mexico and Caribbean Sea. US Army Engineer Research and Development Center, Coastal and Hydraulics Laboratory, Technical Report, ERDC/CHL TR-02-24.

Murray, A.B., (2007). Reducing model complexity for explanation and prediction. Geomorphology, 90 (3-4), 178-191.

Nardin, W., Larsen, L., Fagherazzi, S. and Wiberg, P., (2018). Tradeoffs among hydrodynamics, sediment fluxes and vegetation community in the Virginia Coast Reserve, USA. Estuarine, Coastal and Shelf Science.

Nepf, H., (2012). Flow and transport in regions with aquatic vegetation. Ann. Rev. Fluid Mech., 44: 123–142.

NOAA NOS. (2012). National Ocean Service Hydrographic Survey data, National Oceanic and Atmospheric Administration, http://www.ngdc.noaa.gov/mgg/bathymetry/hydo.html. Accessed 2012.

Nowacki, D.J., Beudin, A., and Ganju, N.K., (2017). Spectral wave dissipation by submerged aquatic vegetation in a back-barrier estuary. Limnol. Oceanogr., 62 (2), pp. 736-753

Orlanski, I., (1976), A simple boundary condition for unbounded hyperbolic flows, J. Comp. Sci., 21(3), 251–269.

Orth, R.J., Luckenbach, M.L., Marion, S.R., Moore, K.A., and Wilcox, D.J., (2006). Seagrass recovery in the Delmarva Coastal Bays, USA. Aquatic Botany 84: 26-36.

Peterson, C.H., Luettich, R.A., Micheli, F., and Skilleter, G.A., (2004). Attenuation of water flow inside seagrass canopies of differing structure. Mar. Ecol. Prog. Ser., 268, pp. 81-92.

Paul, M., and Amos, C.L., (2011). Spatial and seasonal variation in wave attenuation over Zostera noltii. J. Geophysical Research 116, C09019.

Pawlowicz, R., Beardsley, B., and Lentz, S., (2002). Classical tidal harmonic analysis including error estimates in MATLAB using T_TIDE, Comput. Geosci., 28, 929–937.

Picado, A., Dias, J.M., and Fortunato, A.B., (2010). Tidal changes in estuarine systems induced by local geomorphologic modifications. Continental Shelf Research, 30 (17), pp. 1854-1864, 10.1016/j.csr.2010.08.012.

Potouroglou, M., Bull, J.C., Krauss, K.W., Kennedy, H.A., Fusi, M., Daffonchio, D., Mangora, M.M., Githaiga, M.N., Diele, K., and Huxham, M., (2017). Measuring the role of seagrasses in regulating sediment surface elevation. Scientific Report, doi:10 .1038/s41598-017-12354-y.

Preen, A.R., Long, W.-J.L., and Coles, R.G., (1995). Flood and cyclone related loss, and partial recovery, of more than 1000 km2 of seagrass in Hervey Bay. Queens-land, Australia. Aquatic Botany 52: 3-17.

Priestas, A.M., Mariotti, G., Leonardi, N., and Fagherazzi, S., (2015). Coupled wave energy and erosion dynamics along a salt marsh boundary, Hog Island Bay, Virginia, USA. Journal of Marine Science and Engineering, 3(3), pp.1041-1065.

Schwimmer, R., (2001). Rates and processes of marsh shoreline erosion in Rehoboth Bay, Delaware, U.S.A., J. Coastal Res., 17(3), 672-683, doi:10.1016/j.csr.2009.08.018.

Short, F.T and Burdick, D.B., (1996). Quantifying eelgrass habit loss in relation to housing development and nitrogen loading in Waquoit Bay, Massachusetts. Estuaries 19: 730-739.

Suzuki, T., Zijlema, M., Burger, B., Meijer, M.C., and Narayan, S., (2012). Wave dissipation by vegetation with layer schematization in SWAN. Coast. Eng. 59 (1), 64-71.

Temmerman, S., Meire, P., Bouma, T.J., Herman, P.M., Ysebaert, T., and De Vriend, H.J., (2013). Ecosystem-based coastal defence in the face of global change. Nature 504 (7478): 79–83. https://doi.org/10. 1038/nature12859.

Terrados, J. and Duarte, C.M., (2000). Experimental evidence of reduced particle resuspension within a seagrass (Posidonia oceanica L.) meadow. Journal of Experimental Marine Biology and Ecology 243: 45-53.

Tommasini, L., Carniello, L., Ghinassi, M., Roner, M., and D'Alpaos, A., (2019). Changes in the wind-wave field and related salt-marsh lateral erosion: interferences from the evolution of the Venice Lagoon in the last four centuries, Earth Surface Processes and Landforms, doi:10.1002/esp.4599.

Tonelli, M., Fagherazzi, S., and Petti, M., (2010). Modeling wave impact on salt marsh boundaries, J. Geophys. Res., 115, C09028, doi:10.1029/2009JC006026.

U.S. Army Corps of Engineers, (1976). Aquatic Plant Control Project for the State of New Jersey: Design Memorandum No.1. Philadelphia District, Philadelphia, Pennsylvania.

Warner, J.C., Armstrong, B., He, R., and Zambon, J.B., (2010). Development of a coupled ocean-atmosphere-wave-sediment transport (COAWST) modeling system. Ocean Model., 35 (3), pp. 230-244.

Waycott, M., Duarte, C.M., Carruthers, T.J.B., Orth, R.J., Dennison, W.C., et al. (2009). Accelerating loss of seagrasses across the globe threatens coastal ecosystems. Proc. Natl. Acad. Sci. USA 106:12377-81.

Seagrasses impact sediment exchange between tidal flats and salt marsh, and the sediment budget of shallow bays

Carmine Donatelli[1] [(*)], Neil K. Ganju[2], Sergio Fagherazzi[3], Nicoletta Leonardi[1]

*corresponding Author: Carmine@liverpool.ac.uk

(1) Department of Geography and Planning, School of Environmental Sciences, Faculty of Science and Engineering, University of Liverpool, Roxby Building, Chatham St., Liverpool L69 7ZT, UK

(2) U.S. Geological Survey, Woods Hole Coastal and Marine Science Center, MA 02543, USA

(3) Department of Earth and Environment, Boston University, 675 Commonwealth Avenue, Boston, MA 02215, USA

Supplementary material can be found in Appendix 6

C.D. performed COAWST simulations and carried out the analysis; C.D. wrote the manuscript assisted by N.L., S.F. and N.K.G.

Abstract

Seagrasses are marine flowering plants that strongly impact their physical and biological surroundings and are therefore frequently referred to as ecological engineers. The effect of seagrasses on coastal bays resilience and sediment transport dynamics is understudied. Here we use six historical maps of seagrass distribution in Barnegat Bay, USA, to investigate the role of these vegetated surfaces on the sediment storage capacity of shallow bays. Analyses are carried out by means of the Coupled-Ocean-Atmosphere-Wave-Sediment Transport (COAWST) numerical modelling framework. Results show that a decline in the extent of seagrass meadows reduces the sediment mass potentially stored within bay systems. The presence of seagrass reduces shear stress values across the entire bay, including un-vegetated areas, and promotes sediment deposition on tidal flats. On the other hand, the presence of seagrasses decreases suspended sediment concentrations, which in turn reduces the delivery of sediment to marsh platforms. Results highlight the relevance of seagrasses for the long-term survival of coastal ecosystems, and the complex dynamics regulating the interaction between subtidal and intertidal landscapes.

Keywords: seagrass, sediment transport, COAWST, salt marsh, ecosystems.

Seagrasses are marine flowering plants that provide important ecosystem services such as sediment stabilization, nutrient cycling, organic carbon production and export, and enhanced biodiversity [Moriarty and Boon, 1989; Koch, 2001; Waycott et al., 2009]. Seagrasses act as ecological engineers, modifying the physical and ecological environment to promote their growth and reduce mortality. For instance, by reducing bed shear stress and sediment resuspension, seagrasses increase light penetration, and indirectly stimulate their own biomass production. By stabilizing sediments, seagrasses enhance their survival rate during extreme storm conditions [Terrados and Duarte, 2000; Madsen et al., 2001; Cardoso et al., 2004]. The influence of seagrasses on suspended sediment concentrations can significantly vary during the year and can be maximum during summer; in fall and spring, SSC values over vegetated beds are similar, while during the winter suspended sediment concentrations within the less dense meadows can be higher as the finer particles settled during summer get easily re-suspended [Hansen and Reidenbach, 2013].

Seagrasses are sensitive to external agents and can decline as a consequence of multiple stressors including eutrophication, overfishing, overgrazing, and temperature stress. Many studies have documented a decline in the extent of seagrasses for many areas worldwide [Cambridge et al., 1986; Short and Burdick, 1996; Daby, 2003; Campbell and McKenzie, 2004; Cardoso et al., 2004; Hughes et al., 2004; Morris and Viknstein, 2004; Gonzalez et al., 2005; Polte et al;, 2005; Waycott et al., 2005; Orth et al., 2006]. Seagrasses also impact systems morphology due to their capacity to hold sediments and favor deposition [Ganthy et al., 2013; Harlin et al., 1982; Potouroglou et al., 2017]. For instance, Ganthy et al. [2013] studied sediment transport dynamics in tidal flats in the Arcachon lagoon, measured

165

centimeter scale accretion rates over seagrass meadow, and found that these were correlated with seasonal growth rates. They found that during growth periods, particle trapping dominates, leading to accretion, while during senescence periods erosion occurs, but less than in un-vegetated areas. Massive seagrass losses have also been documented after storms and cyclones as a consequence of meadow uprooting, and burial caused by increased sediment loads [Preen et al., 1995; Koch, 1999].

Sediment convergence and divergence, and the ensuing erosional and depositional patterns, are largely influenced by changes in the velocity field as a consequence of flow deflection, and increased friction across seagrass meadows [Fonseca et al., 1982; Koch et al., 2006, Peterson et al., 2004]. Large horizontal velocity gradients are generally present between the un-vegetated seabed and vegetated meadows, and the vertical velocity profile presents significant discontinuities at the interface between the water column occupied by the meadow and the free flow over it [e.g. Gambi et al., 1990; Koch, 2001]. The impact of submerged canopies on the hydrodynamic of surrounding bare beds has been documented in previous studies; for instance, within the context of patchy vegetation, it has been shown that a decrease in shear stress is observable before and after vegetation patches, and that the areal extent of the bare beds affected by vegetation depends on stem density [e.g. Souliotis et al., 2011]. Numerous studies have investigated the role of submerged vegetation on hydrodynamics and sediment transport; however, many of these studies solely focus on vegetation-flow interactions at small scales and in uniform field and laboratory conditions [Dijkstra and Uittenbogaard, 2010; Nepf, 2012].

The role of seagrasses has rarely been quantified at the basin-scale, nor in terms of the estuary-wide sediment budget [Ward et al., 1984; Ganthy et al., 2013]. In this

manuscript we use a numerical model to investigate how variations in seagrass meadow coverage and density influence sediment trapping across an entire back-barrier estuary, and the exchange of sediments between marsh platforms and tidal flats. Six historical seagrass coverage maps of Barnegat Bay Little-Egg Harbor Estuary for the period 1968-2009 have been used in combination with the Coupled-Ocean-Atmosphere-Wave-Sediment Transport (COAWST) modelling system [Warner et al., 2010], and associated flow-vegetation module [Beudin et al., 2016]. To the best of our knowledge there is a lack of studies presenting results about the impact of seagrasses on sediment transport dynamics at a decadal time scale and through the combined use of numerical models and multiple years' seagrass maps. Results demonstrate that seagrasses can significantly impact the sediment budget of coastal environments, and also influence the dynamics between salt marshes and tidal flats.

6.2 Study site

The Barnegat Bay-Little Harbor Estuary (BBLEH) is a shallow lagoon-type estuary located along the east coast of New Jersey, USA, between 39º41' N and 39º56' N latitude and 74º04' W and 74º12' W longitude. The system is a long and narrow water body extending approximately 70 km in the north-south direction. The lagoon is composed by three shallow bays (Barnegat Bay, Manahawkin Bay and Little Egg Harbor) and is connected to the ocean through two inlets (Little Egg Inlet and Barnegat Inlet) and the Point Pleasant Canal. The total basin area is around 280 km^2 with a maximum depth of 5 m, mean depth of 1.5 m, and width ranging from 2.0 to 6.5 km [Hunchak-Kariouk et al., 1999]. The composition of the seabed is a mixture of sand, silt, shells and organic matter [Rogers et al., 1990]. Tides are mainly semidiurnal, with the M_2 harmonic being the dominant constituent. The tidal range in the ocean is over 1 m, but the tidal signal within the Bay is damped through the inlets and the range within the bay reduces to a minimum of 15-20 cm [Aretxabaleta et al., 2014]. In Barnegat Bay-Little Harbor Estuary, the submerged aquatic vegetation (SAV) is characterized by two main species: *Zostera marina* and *Ruppia maritima*. As showed by recent studies [Bologna et al., 2000], the seagrass coverage has decreased by 62% over the last several decades; the central and northern part of the bay have been the most affected by this decline [Lathrop et al., 2001]. The total loss can be estimated as 2000-3000 ha in 30 years (from 1960 to 1990). The main causes of the seagrass decline are related to the shading effect of phytoplankton blooms, increased growth of epiphytic algae and wasting disease [Bologna et al., 2000; Kennish, 2001; Kennish et al., 2007a].

The bathymetry of the model used in this study is based on the National Ocean Hydrographic Survey data [NOAA NOS 2012] updated with field measurements [Miselis et al., 2012]. Bathymetric data were collected by using a SWATHplus-H interferometric sonar, operating at a frequency of 468 kilohertz (kHz), with +/- 1 cm accuracy [Andrews et al., 2016]. Since the 1940s there have been negligible bathymetric changes, with exception of areas near the jetty [Defne and Ganjiu, 2014], and even Hurricane Sandy did not alter the estuary's bathymetry [Miselis et al., 2015]. The bathymetry of the study area and historical seagrass coverages are illustrated in Figure 6.1, with Figure 6.1h illustrating an idealized test case with no seagrass.

169
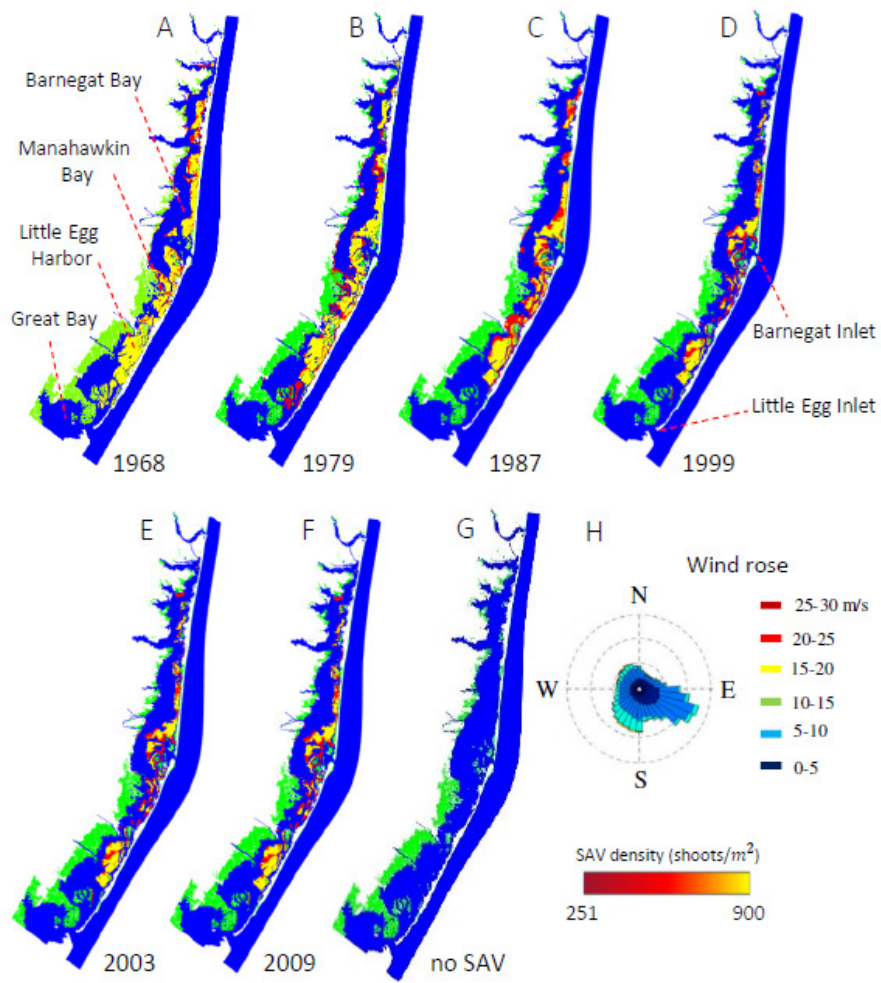
Figure 6.1 Seagrass coverages (a-f) for different years, i.e. 1968, 1979, 1987, 1999, 2003 and 2009; base-case: no-SAV (g); wind rose for the area (wind station, station 44025 (LLNR 830), 40°15'3''N, 73°9'52''W). For panels a-g green areas are locations where salt marshes are present. Yellow to red shading indicates areas were seagrasses are present as sparse (red), moderate (orange) or dense (yellow). Wind rose (h).

6.3 Methods

The hydrodynamics and sediment transport of the system have been simulated using the COAWST (Coupled-Ocean-Atmosphere-Wave-Sediment Transport Modeling System) modeling framework [Warner et al., 2010]. The ocean model used in COAWST is ROMS (Regional Ocean Modeling System), which currently incorporates a sediment transport module based on CSTMS (the Community Sediment Transport Modeling System) [Shchepetkin and McWilliams, 2005; Warner et al., 2008].

The numerical domain is defined by a grid having 160x800 cells, with cells resolution ranging from 40 m to 200 m with refinement at the inlets and areas with detailed coastal features. The water column is divided vertically into 7 equally spaced layers. The model boundary is forced by tides defined using the ADCIRC tidal constituents' database (http://adcirc.org/products/adcirc-tidal-databases/) for the North Atlantic Ocean. The ROMS barotropic and baroclinic time steps are 0.1 s and 2 s, respectively. The model has been implemented and calibrated by Defne and Ganju [2014]. The calibration of the model was made by changing the bottom roughness coefficient in order to obtain the best accordance with measurements from seven water level stations and three tidal discharge stations within the Barnegat Bay-Little Egg Harbor estuary. The Brier-Skill-Score [Murphy and Epstein, 1989] was used to evaluate the model performance. Skill assessment of the model varies from very good to excellent.

As shown by Lathrop and Bognar [2001], natural and human drivers have drastically reduced the salt marsh area from around 14,850 ha to 9940 ha in Barnegat Bay-Little Harbor Estuary over the last century. Around half of the interior shoreline is eroding less than 0.5 m/yr, or is not eroding at all; the other half is eroding at around 0.5-2 m/yr and 2% of the marsh had erosion rates exceeding 2 m/yr. The highest erosion rate is found in the marshes surrounding Great Bay [Leonardi et al., 2016]. The impact of marsh erosion has not been taken into account. This is in line with the goal of our manuscript which aims to evaluate the sole impact of seagrass and for which is thus convenient to maintain all other variables constant.

The suspended sediment transport is calculated by solving the advection diffusion equation, and by accounting for source/sink terms induced by downward settling or upward flux of eroded material. Sediment sources from the bed are computed following Arulanandan [1978], and sink terms are proportional to settling velocity values; the bed stress is calculated following a logarithmic bottom stress formulation [Warner et al., 2008]. For this study, one class of sediments is defined having a mass density of 2650 kg/m^3, settling velocity of 0.5 mm/s, erodibility and critical shear stress equal to 0.0005 kg m^{-2}s^{-1} and 0.05 N/m^{-2} respectively; values were chosen based on sediment characteristics typical of a coastal embayment [Fagherazzi et al., 2013]. The seabed is defined as one layer having an initial thickness of zero. The time frame of the analysis is 30 days. As the initial condition, a uniform suspended sediment concentration is imposed for each water cell inside the bay; specifically, the sediment injection occurs at mean sea level, and during the first flood period. Three different initial suspended sediment concentrations have been tested, i.e. 50, 100, and 200 mg/l. As the initial sediment thickness at the bottom is zero,

sediment transport, as well as erosive or depositional fluxes, are solely related to the concentration imposed at the beginning of the simulation.

The flow-vegetation interaction is computed using the vegetation module recently implemented in COAWST [Beudin et al., 2016]. The flow-vegetation module includes plant posture-dependent three-dimensional drag, in-canopy wave-induced streaming, and production of turbulent kinetic energy and enstrophy for the vertical mixing parametrization; the spatially averaged vegetation drag force is approximated using a quadratic drag law and the effect of plant flexibility on drag is computed using the approach of Luhar and Nepf [2011]. Apart from the mean flow velocity, vegetation also significantly impacts turbulence intensity and mixing. The selected turbulence model is the k–ε scheme which accounts for extra dissipation and turbulence kinetic energy production due to vegetation [Uittenbogaard, 2003]. The vertical discontinuity of the drag across the canopy interface generates turbulent shear stress which peaks near the top of the seagrass [Ghisalberti and Nepf 2002, 2006; Nepf et al., 2007] and provides efficient exchange between the canopy and the overlying flow. This effect is explicitly accounted for in the k–ε model by expressing eddy viscosity and Reynolds stresses as a function of velocity variations along the vertical; the model calculates the velocity profile assuming extraction of momentum by the canopy, which is then fed into the turbulence model [Beudin et al., 2016].

Seagrass meadows in the model are defined as sparse (251 shoots/m^2), moderate (600 shoots/m^2) or dense (900 shoots/m^2), nominally selected using Kennish et al. [2013] for guidance. Seagrass canopy height is set equal to 20 cm. For salt marshes, canopy height is 50 cm, and stem density is equal to 248 stems/m^2 [U.S. Department of Agriculture, 2008].

The typical mass density and Young's modulus of the seagrass *Zostera marina* vary in the range 700-900 kg/m^3 [Abdwlrhman, 2007; Fonseca, 1998; Fonseca et al., 2007] and 0.4-2.4 GPa [Brandley and Houser, 2009] respectively. These values can be also used for *Spartina alerniflora* [Feagin et al., 2011]. Therefore, mass density and elastic modulus are set equal to 700 kg/m^3 and 1 KN/mm^2, respectively. The dynamic frontal area is set equal to 1cm, and the drag coefficient is set to 1. Salt marsh and seagrass coverage data came from the CRSSA's (Center for Remote Sensing and Spatial Analysis) geographic information systems (GIS) data base. Simulations are run implementing different seagrass distributions corresponding to the years 1968, 1979, 1987, 1999, 2003, 2009, and for a test case where the meadow is completely removed [1968 map, U.S. Army Corps of Engineers, 1976; 1979, Macomber and Allen, 1979; 1987, Joseph et al., 1992; 1999, McClain and McHale 1996; Bologna et al., 2000; 2003 and 2009, Lathrop and Haag, 2011].

From 1968 until 2009, the extent of seagrass meadows within the Barnegat Bay-
Little Egg Harbor system largely declined (Figure 6.1, Figure S1). The presence of
seagrass decreases bed shear stress (Figure 6.2a, b), and suspended sediment
concentrations (Figure 6.2c, d) across the entire bay, as demonstrated by the comparison
between the 1968 and no-seagrass model results. In the presence of seagrass (Figure 6.2a,
b), flow velocity decreases over the meadows, which in turn leads to lower suspended
sediment concentrations in the water column and limited resuspension (Figure 6.2c, d).
Changes in suspended sediment concentrations are observed across the entire bay.
Numerical results show that seagrasses affect suspended sediment concentrations across
52% of the bare beds (Figure 6.2c, 6.2d), even if changes are more dramatic for
previously vegetated beds (which for the 1968, constitute 31% of the entire estuary area)
and nearby areas.
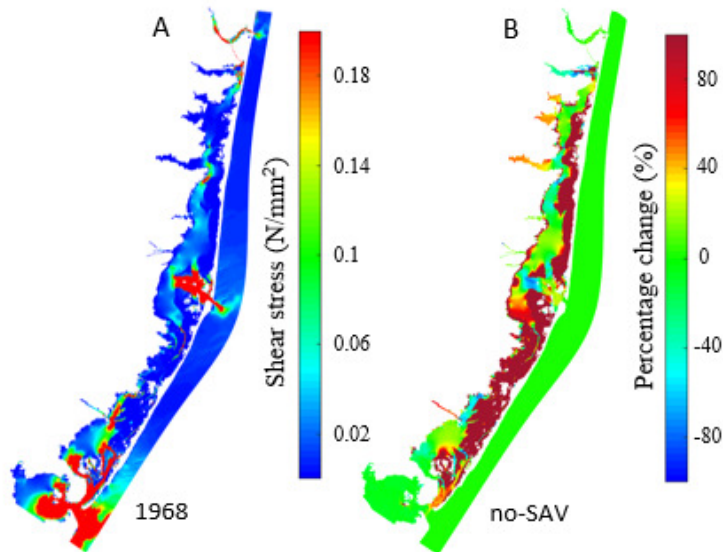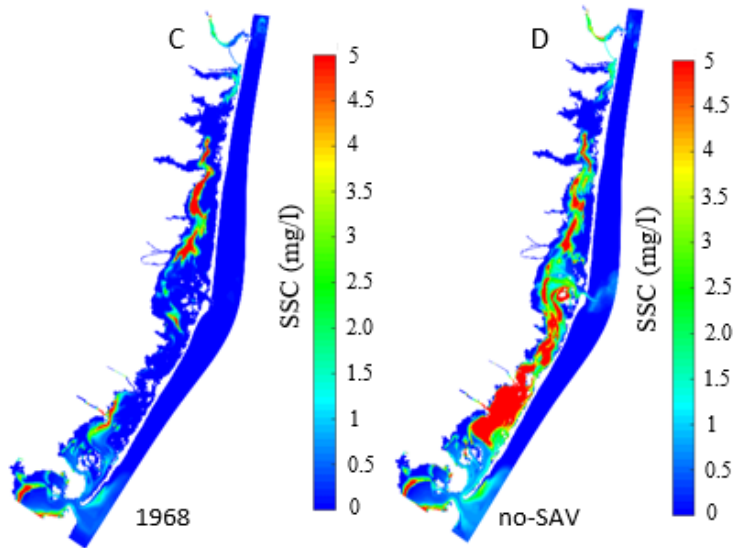
Figure 6.2 Average shear stresses [Pa] at spring tide for the 1968 seagrass distribution case (a), and percentage change in shear stress after removal of the seagrass (no-SAV test case) (b); average suspended sediment concentration [SSC; mg/l] during spring tide and after 27 simulated days for the 1968 seagrass distribution case (c), and for the no-SAV test case (d).

Differences in the probability density function of bed shear stresses between the 1968 and the no-seagrass test case further highlight this trend (Figure 6.3). Specifically, as the seagrass is removed the mean shear stress increases for both un-vegetated (Figure 6.3a) and vegetated areas (Figure 6.3b), even if differences in previously vegetated areas are more evident (Figure 6.3b).
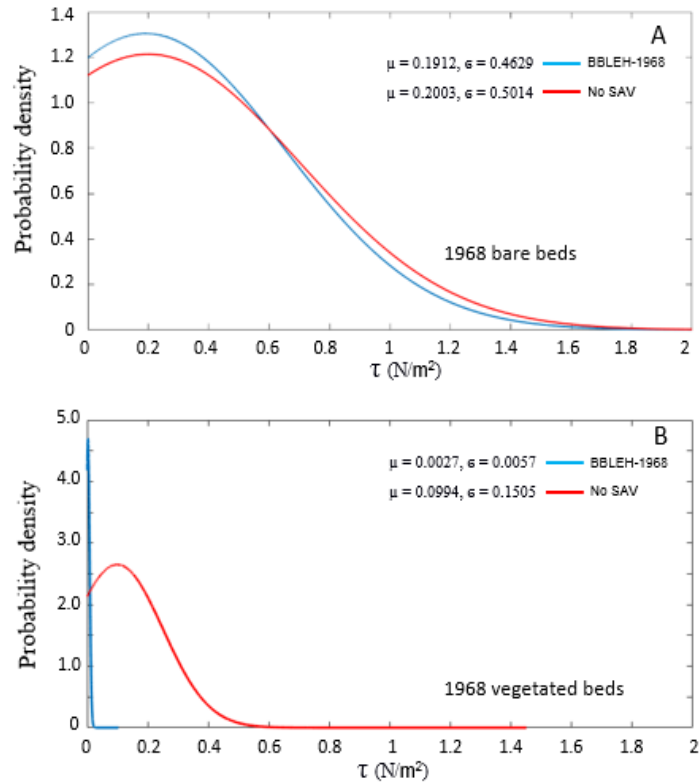
Figure 6.3 Probability density functions of average shear stress values [Pa] during spring tide given the 1968 seagrass distribution (blue lines), and for the test case with no seagrasses (red lines); the probability density functions refer to areas with no seagrass in 1968 (a) and areas with seagrass in 1968 (b).

The probability distribution functions of shear stress within bare beds are slightly shifted, as the friction exerted by vegetation reduces the flow velocity next to the meadows as well. This effect also depends on plants density and tends to decrease for less dense meadows (Figure S4). To quantitatively evaluate the impact of seagrasses on the sediment budget, a series of simulations were conducted to relate changes in the extent of meadows with the amount of sediment stored within the bay after 30 days, given the same input concentration and sediment distribution. A uniformly distributed input sediment concentration represents potential riverine inputs during flood conditions, or large resuspension events during storms; such situations are the major contributors of

inorganic sediments to salt marsh systems [e.g. Fagherazzi and Priestas 2010; Falcini et al 2012; Leonardi et al., 2017]. The total sediment mass can be stored within the estuary in one of the following reservoirs: i) suspended sediment in the water column, ii) deposits on the bay seafloor, and iii) deposits on the marsh platform. Suspended sediments are considered as a contribution to the sediment budget of the system because, even if not yet deposited, they remain available for the potential storage on the seafloor and on the marsh platforms. Results are presented as a function of the ratio between vegetated seabed and basin area following the seagrass maps for the 1968-2009 period (Figure 6.4, 6.5). Given the same sediment input, the total sediment mass stored within the bay increases as the area occupied by seagrasses increases (Figure 6.4, Figure S5).
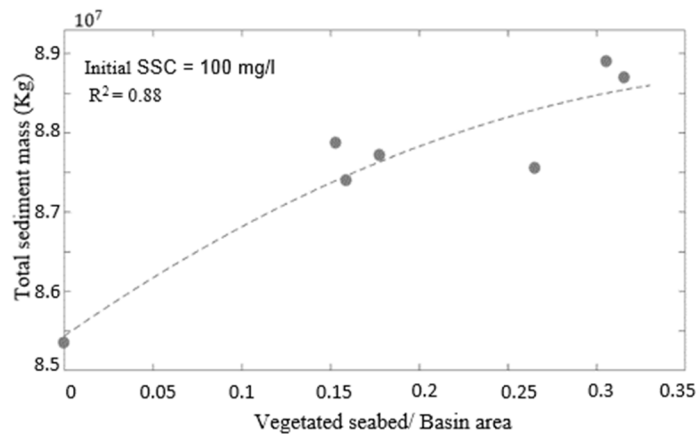
Figure 6.4 Total sediment mass within the lagoon as a function of vegetated bed/basin area ratios, after 30 simulated days. The vegetated bed/basin area ratios are calculated based on seagrasses extent presented in Figure 6.1.

A time series of the decline in the total amount of suspended sediment within the bay system is provided in Figure S2, which also shows that 30 simulations days are sufficient to reach equilibrium conditions. Going into more detail, seagrasses mostly influence the deposition of sediment on the seafloor (Figure 6.5a, Figure S6a, S7a);

however, the presence of seagrasses also reduces the sediment mass in suspension
(Figure 6.5b, Figure S6b, S7b), and deposited on the marsh platform (Figure 6.5c, Figure
S6c, S7c).
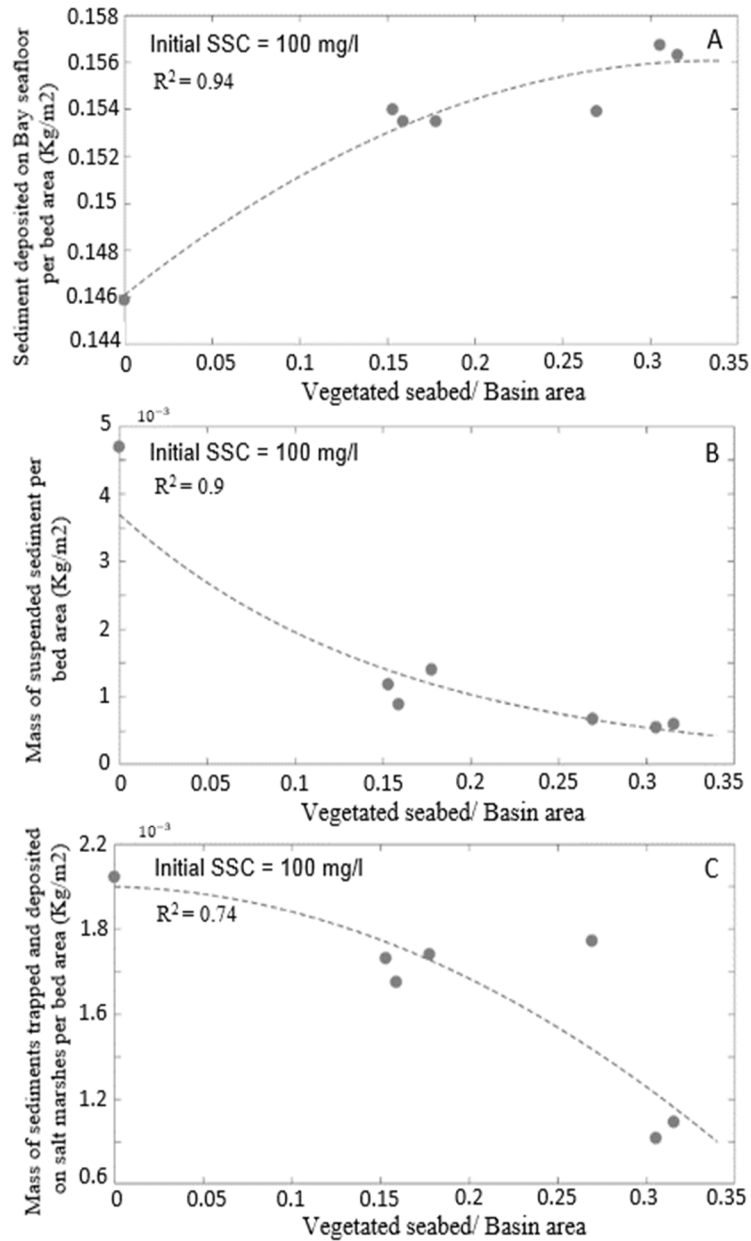
Figure 6.5 Mass of sediments per unit area: deposited on the seafloor within the bay (a); in suspension (b); deposited on salt marsh platforms (c). Data are presented after 30 simulated days, and as a function of the vegetated bed/basin area ratios obtained from the maps of figure 1 and corresponding to different years.

6.5 Discussion and conclusion

Numerous studies have investigated the role of seagrasses as ecosystem engineers, and their contribution to the dissipation of flow energy [e.g. Duarte et al., 2013; Koch et al., 2006; Ondiviela et al., 2013]. However, there is limited insight about the importance of seagrasses from a sediment storage point of view, and within the context of large-scale bay systems comprising salt marshes and un-vegetated intertidal flats. The impact of submerged aquatic vegetation (SAV) on the storage of sediments within enclosed bay systems is evaluated using the Barnegat Bay-Little Egg Harbor system as test case. The analyses are based on historical trends of seagrass distribution from 1968 to 2009; a scenario with no SAV is also included as a plausible system configuration in the near future (Figure S3).

In tidal landscapes, flow velocities are influenced by vegetation as plants exert a frictional effect and obstruct the flow [Temmerman et al., 2007]. Our results also indicate that seagrasses are reducing flow velocity and bottom shear stresses within the canopy, in agreement with the field measurements of Hansen and Reidenbach [2012]. While the presence of vegetation is generally associated with a decrease in flow velocity, in case of patchy emergent canopies, the deviation of the flow from vegetated to un-vegetated areas can increase the shear stress, and erode the latter bare zones [Temmerman et al., 2007]. Differently than for emergent canopies, our findings show that the presence of submerged aquatic vegetation lowers bottom shear stresses (Figure 6.2a, b) everywhere in the system, including un-vegetated beds (Figure 6.3b), although flow concentrations are registered in small areas between meadows (Figure 6.2b). A comparison in terms of probability density function of the bed shear stress in bare beds shows that a reduction of the mean (from

179

0.2003 to 0.1912 N/m^2) and standard deviation (from 0.5014 to 0.4629 N/m^2) occurs when seagrasses are added to the model. Differences in shear stress across the bay between cases with and without seagrasses (e.g. 1968 compared to no-SAV test case) are significantly higher for areas that have transitioned from vegetated to un-vegetated conditions (Figure 6.3 and Figure S4). Given an initial input of sediment, the presence of seagrasses promotes sediment storage within the bay, especially on the seabed. However, seagrasses also reduce the sediment mass in suspension, and the likelihood for sediments to be transported on marsh platforms during high tide. An increase in the areal extent of meadows reduces the deposited sediment mass on marsh platforms (Figure 6.5c). The areas experiencing the highest reduction in terms of deposition are salt marshes located in the proximity of seagrasses. Seagrasses also decrease the time that sediments remain in suspension (Figure S2), promoting a faster clearing of the water column and increasing the period of light availability for seagrass growth over the year [Carr et al., 2010]. Conversely, as highlighted by our findings the decline of seagrass meadows increases bay-wide sediment concentrations and, therefore, reduces light levels at the lagoon bottom. This causes a change from a state of favorable conditions for seagrass proliferation to a configuration with high water turbidity and light attenuation.

The influence of seagrasses on sediment trapping and on the erosive force of flowing water should be explored seasonally as seagrass aboveground biomass peaks during June-July and declines significantly during fall, when it becomes five times smaller [Kennish et al., 2007b, 2008; Farnsworth, 1998; Koch et al., 2009; Hansen and Reidenbach, 2013]. The lack of seasonal data in our study constitutes a significant gap in the understanding of how these ecosystems can affect erosion and sediment retention on a

long-term basis. Furthermore, by using current salt marsh configurations, we are evaluating the impact of SAV under the worst case scenario in terms of sediment budget. Indeed, as salt marshes migrate landward, the basin area and tidal prism increase, causing higher water exchanges with the ocean and higher sediment losses throughout a tidal cycle. Given that in Barnegat Bay salt marshes have been eroding, the decline in trapping capacity of the bay over the last decades could have been higher than the one predicted by our model due to the compound action of salt marsh erosion and seagrass decline. These considerations are important considering that the survival of coastal wetlands depends on a delicate balance and interaction between processes regulating vertical and horizontal dynamics of the intertidal landscape. The survival of coastal wetlands has been interpreted as a sediment budget problem [e.g. Fagherazzi et al., 2013; Ganju et al., 2017]; for instance Ganju et al. [2017] synthesized the sediment budget of eight micro-tidal salt marsh complexes, demonstrating the link between sediment deficits and the conversion of salt marshes to open water. Apart from sediment availability, the ability of salt marshes to withstand different sea-level rise values has been also related to the likelihood of sediments to be delivered on marsh surfaces during normal tidal conditions, as well as during storms [Schuerch et al., 2012; Kirwan et al., 2016]. The mutual interaction between vegetated seagrass beds and salt marshes is thus complex, and incorporates processes promoting, or possibly obstructing, the maintenance of salt marsh areas, i.e. reduced delivery of sediments on the marsh surface under normal weather conditions. However, the increased deposition in front of marsh platforms in the presence of segrasses could: i) decrease tidal flats depth, which in turn decreases wind and current induced shear stresses at the land interface; ii) directly shelter marsh boundaries from erosive forces; and iii) constitute an

additional source of sediments that, while not being resuspended during normal weather conditions, could be available for resuspension during storms, when surge occurrence can efficiently distribute sediments landward.

Acknowledgment

References

Abdelrhman, M.A., (2007). Modeling coupling between eelgrass Zostera marina and water flow. Mar. Ecol. Prog. Ser. 338: 81–96, doi:10.3354/meps338081.

Andrews, B.D., Miselis, J.L., Danforth, W.W., Irwin, B.J., Worley, C.R., Bergeron, E.M. and Blackwood, D.S., (2016). *Marine geophysical data collected in a shallow back-barrier estuary, Barnegat Bay, New Jersey* (No. 937). US Geological Survey.

Aretxabaleta, A. L.*,* B. Butman, and N. K. Ganju *(*2014*),* Water level response in back-barrier bays unchanged following Hurricane Sandy*,* Geophys. Res. Lett.*,* 41*,* 3163–3171*, doi:*10.1002/2014GL059957*.*

Beudin, A., Kalra, T. S., Ganju, N. K., and Warner, J.C., (2016). Development of a coupled wave-flow vegetation interaction model. Computers & Geosciences.

Bologna, P., Lathrop, R., Bowers, P., and Able, K., (2000). Assessment of submerged aquatic vegetation in Little Egg Harbor, New Jersey. Technical Report 2000-11, Institute of Marine and Coastal Sciences, Rutgers University, New Brunswick, New Jersey, USA.

Bradley, K., and Houser, C., (2009). Relative velocity of seagrass blades: Implications for wave attenuation in low-energy environments. J. Geophys. Res. Earth Surf. 114: F01004, doi:10.1029/2007JF000951.

Cambridge, M.L., Chiffings, A.W., Brittan, C., Moore, L., and McComb, A.J., (1986). The loss of seagrass in Cockburn Sound western Australia II; Possible causes of seagrass decline. Aquatic Botany 24: 269-286.

Campbell, S.J. and McKenzie, L.J., (2004). Flood related loss and recovery of intertidal seagrass meadows in southern Queensland, Australia. Estuarine Coastal and Shelf Science 60: 477-490.

Cardoso, P.G., Pardal, M.A., Lillebo, A.I., Ferreira, S.M., Raffaelli, D., and Marques, J.C., (2004). Dynamic changes in seagrass assemblages under eutrophication and implications for recovery. Journal of Experimental Marine Biology and Ecology 302: 233-248.

Carr, J., D'Odorico, P.D., McGlathery K., Wiberg, P., (2010). Stability and bistability of seagrass ecosystems in shallow coastal lagoons: role of feedbacks with sediment resuspension and light attenuation. J Geophys Res 115, doi: 10.1029/2009JG001103.

Daby, D., (2003). Effects of seagrass bed removal for tourism purposes in a Mauritian bay. Environmental Pollution 125: 313-324.

Defne, Z., and Ganju, N., (2014), Quantifying the residence time and flushing characteristics of a shallow, back-barrier estuary: Application of hydrodynamic and particle tracking models, Estuaries Coasts,1 – 16, doi:10.1007/s12237-014-9885-3.

Dijkstra, J., Uittenbogaard, R., (2010). Modeling the interaction between flow and highly flexible aquatic vegetation. Water. Resour. Res. 46: W12547.

Donatelli Carmine. (2018a-u). bblehveg_c50. http://doi.org/10.5281/zenodo.1172994.

Duarte, C.M., Losada, I.J., Hendriks, I.E., Mazarrasa, I., Marbà, N., (2013). The role of coastal plant communities for climate change mitigation and adaptation. Rev. Nat. Clim. Change 3, 961-968.

Fagherazzi, S., Wiberg, P.L., Temmerman, S., Struyf, E., Zhao, Y. and Raymond, P.A., (2013). 522 Fluxes of water, sediments, and biogeochemical compounds in salt marshes. Ecological Processes, 523 2(1), p.3.

Fagherazzi, S. and Priestas, A.M., (2010). Sediments and water fluxes in a muddy coastline: interplay between waves and tidal channel hydrodynamics. Earth Surface Processes and Landforms, 35(3), pp.284-293.

Falcini, F., Khan, N.S., Macelloni, L., Horton, B.P., Lutken, C.B., McKee, K.L., Santoleri, R., Colella, S., Li, C., Volpe, G. and D'Emidio, M., (2012). Linking the historic 2011 Mississippi River flood to coastal wetland sedimentation. Nature Geoscience, 5(11), pp.803-807.

Farnsworth E. (1998). Issues of spatial, taxonomic and temporal scale in delineating links between mangrove diversity and ecosystem function. Global Ecol Biogeogr 7 : 15–25.

Feagin, R. A., et al. (2011). Engineering properties of wetland plants with application to wave attenuation. Coastal Engineering 58.3: 251-255.

Fonseca, M.S., Fisher, J.S., Zieman, J.C., and Thayer, G.W., (1982). Influence of the seagrass *Zostera marina* on current flow. Estuarine Coastal and Shelf Science 15: 351-364.

Fonseca, M. S. and Kenworthy, W.J., (1987). Effects of current on photosynthesis and distribution of seagrasses. Aquatic Botany 27: 59–78.

Fonseca, M.S., (1998). Exploring the basis of pattern expression in seagrass landscapes. Ph.D. thesis. Univ. of California, Berkeley.

Fonseca, M.S., Koehl, M.A.R., and Kopp, B.S., (2007). Biomechanical factors contributing to self-organization in seagrass landscapes. J. Exp. Mar. Biol. Ecol. 340: 227–246, doi:10.1016/j.jembe.2006.09.015.

Gambi, M.C., Nowell, A.R.M., and Jumars, P.A., (1990). Flume observations on flow dynamics in Zostera marina eelgrass beds. Marine Ecology Progress Series 61: 159-169.

Ganthy, F., Sottolichio, A., Verney, R., (2013). Seasonal modification of tidal flat sediment dynamics by seagrass meadows of Zostera noltii (Bassin d'Arcachon, France). J. Mar. Syst., 109–110, pp. S233-S240.

Ganju, N.K., Defne, Z., Kirwan, M.L., Fagherazzi, S., D'Alpaos, A. and Carniello, L., (2017). Spatially integrative metrics reveal hidden vulnerability of microtidal salt marshes. Nature communications, 8, p.ncomms14156.

Ghisalberti, M., and Nepf, H.M., (2002). Mixing layers and coherent structures in vegetated aquatic flows. J. Geophys. Res. 107: 3011, doi:10.1029/2001JC000871.

Ghisalberti, M., and Nepf, H.M., (2006). The structure of shear layers in flows over rigid and flexible canopies. Environ. Fluid Mech. 6: 277–301, doi:10.1007/s10652-006-0002-4.

Gonzalez, C.J.M., Bayle, J.T., Sanchez-Lizaso, J.L., Valle, C., Sanchez-Jerez, P., and Ruiz, J.M., (2005). Recovery of deep *Posidonia oceanica* meadows degraded by trawling. Journal of Experimental Marine Biology and Ecology 320: 65-76.

Hansen, J.C. and Reidenbach, M.A., (2012). Wave and tidally driven flows in eelgrass beds and their effect on sediment suspension. Marine Ecology Progress Series, 448, pp.271-287.

Harlin, M.M., Thorne-Miller, B., and Boothroyd, J.C., (1982). Seagrass sediment dynamics of a flood-tidal delta in Rhode Island (USA). Aquat. Bot. 14: 127–138.

Hansen, J.C. and Reidenbach, M.A., (2013). Seasonal growth and senescence of a Zostera marina seagrass meadow alters wave-dominated flow and sediment suspension within a coastal bay. Estuaries and coasts, 36(6), pp.1099-1114.

Hughes, A.R., Bando, K.J., Rodriguez, L.F., and Williams, S.L., (2004). Relative effects of grazers and nutrients on seagrasses: A meta-analysis approach. Marine Ecology Progress Series 282: 87-99.

Hunchak-Kariouk, K. (1999). Relation of water quality to land use in the drainage basins of four tributaries to the Toms River, New Jersey, 1994--1995. No. PB-99-149098/XAB; USGS/WRI--99-4001. Geological Survey, Water Resources Div., West Trenton, NJ (United States); New Jersey Dept. of Environmental Protection, Trenton, NJ (United States).

Leonardi, N., Carnacina, I., Donatelli, C., Ganju, N.K., Plater, A.J., Schuerch, M. and Temmerman, S., (2017). Dynamic interactions between coastal storms and salt marshes: A review. *Geomorphology*.

Joseph, J., Purdy, K., and Figley, B, (1992). The influence of water depth and bottom sediment on the occurrence of eelgrass in Barnegat, Manahawkin and Little Egg Harbor bays. Marine Fisheries Administration, New Jersey Department of Environmental Protection and Energy, Nacote Creek, New Jersey.

Kennish, M. J., (2001). State of the estuary and watershed: an overview. Journal of Coastal Research Special Issue 32:243– 273.

Kennish, M.J., Bricker, S.B., Dennison, W.C., Glibert, P.M., Livingston, R.J., Moore, K.A., Noble, R.T., Paerl, H.W., Ramstack, J., Seitzinger, S., Tomasko, D.A., Valiela, I., (2007a). Barnegat Bay-Little Egg Harbor Estuary: Case Study of a Highly Eutrophic Coastal Bay System. Ecological Applications 17 (Special Issue), S3-S16.

Kennish, M. J., Haag, S., and Sakowicz, G., (2007b). Demographic investigation of SAV in the Barnegat Bay-Little Egg Harbor Estuary with assessment of potential impacts of benthic macroalgae and brown tides. Technical Report 107-15, 47 Institutes of Marine and Coastal Sciences, Rutgers University, New Brunswick, New Jersey. 366 pp.

Kennish, M., Haag, S., and Sakowicz, G. (2008). Seagrass demographic and Spatial Habitat Characterization in Little Egg Harbor, New Jersey, Using Fixed Transects. Journal of Coastal Research, Special Issue 55, 148-170.

Kennish, M.J., Fertig, B.M. and Sakowicz, G.P., (2013). In situ Surveys of Seagrass Habitat in the Northern Segment of the Barnegat Bay-Little Egg Harbor Estuary: Eutrophication Assessment, Final report to the Barnegat Bay Partnership (bbp.ocean.edu/Reports/2011Northernseagrasssurvey. Pdf)

Koch, E.W., (1999). Sediment resuspension in a shallow Thalassia testudinum banks ex König bed. Aquatic Botany 65: 269-280.

Koch, E.W., (2001). Beyond light: Physical, geological, and geochemical parameters as possible submersed aquatic vegetation habit requirements. Estuaries 24: 1-17.

Koch, E.W., Sanford, L.P., Chen, S.-N., Shafer, D.J., Smith, J.M., (2006). Waves in seagrass systems: review and technical recommendations. U.S. Army Corps of Engineers, Washington, DC.

Koch, E.W., Barbier, E.B., Silliman, B.R., Reed, D.J., Perillo, G.M.E., Hacker, S.D., Granek, E.F., Primavera, J.H., Muthiga, N., Polasky, S., Halpern, B.S., Kennedy, C.J., Kappel, C.V., Wolanski, E., (2009). Non-linearity in ecosystem services: temporal and spatial variability in coastal protection. Frontiers. Ecol. Env. 7(1), 29–37.

Lathrop, R. G., Jr., and Bognar, J. A., (2001), Habitat loss and alteration in the Barnegat Bay Region, J. Coastal Res., 212–228, doi:10.2307/25736235.

Lathrop, R.G. and Haag, S., (2011). Assessment of Seagrass Status in the Barnegat Bay-Little Egg Harbor Estuary: 2003 and 2009. CRSSA Technical Report#2011-01. Rutgers University, Grant F. Walton Center for Remote Sensing and Spatial Analysis, New Brunswick, NJ.

Luhar, M., Nepf, H.M., (2011). Flow-induced reconfiguration of buoyant and flexible aquatic vegetation drag. Adv. Water Res. 51, 305-316.

Macomber, R.T. and Allen, D., (1979). The New Jersey submerged aquatic vegetation distribution atlas final report. Earth Satellite Corporation, Washington, D.C.

Madsen, J.D., Chambers, P.A., James, W.F., Koch, E.W., and Westlake, D.F., (2001). The interaction between water movement, sediment dynamics and submersed macrophytes. Hydrobiologia 444: 71-84.

McCLain, P. and McHale, M., (1996). Barnegat Bay eelgrass investigations 1995–1996, p. 165–172. In G. Flimlin and M. Kennish (eds.), Proceedings of the Barnegat Bay EcosystemWorkshop. Rutgers Cooperative Extension, Toms River, New Jersey.

Miselis J., Andrews., B., Baker, R., Danforth, W., DePaul, V., Defne, Z., Feinson, L., Ganju, N., Gibs, J., Hickman, R.E., Lopez, A., Navoy, A., Nicholson, R., Reilly, T., Reiser, R., Spitz, F., Watson, A., Wieben, C., and Wilson, T., (2012). Characterizing physical, chemical, and biological conditions and processes in the Barnegat Bay-Little Egg Harbor Estuary, New Jersey. 2012 Barnegat Bay Researchers Workshop, Bordentown Township, NJ.

Miselis, J.L., Andrews, B.D., Nicholson, R.S., Defne, Z., Ganju, N.K., and Navoy, A., (2015). Evolution of mid-Atlantic coastal and back-barrier estuary environments in response to a hurricane: Implications for barrier-estuary connectivity. Estuaries and Coasts. doi: 10.1007/s12237-015-0057-x.

Moriarty, D.J.W., and Boon, P.I., (1989). Interactions of seagrass with sediment and water. In Larkum, A.W.D. and S.A. Sheppard (eds), Biology of Seagrasses. Elsevier, Amsterdam, 500-535.

Morris, L.J. and Viknstein, R.W., (2004). The demise and recovery of seagrass in the northern Indian River Lagoon, Florida. Estuaries 27: 915-922.

Nepf, H.M., Ghisalberti, M., White, B., and Murphy, E., (2007). Retention time and dispersion associated with submerged aquatic canopies. Water Resour. Res. 43: W04422, doi:10 .1029/2006WR005362.

Nepf, H., (2012). Flow and transport in regions with aquatic vegetation. *Ann. Rev. Fluid Mech.*, 44: 123–142.

NOAA NOS. (2012). National Ocean Service Hydrographic Survey data, National Oceanic and Atmospheric Administration, http://www.ngdc.noaa.gov/mgg/bathymetry/hydo.html. Accessed 2012.

Ondiviela, B., Losada, I.J., Lara, J.L., Maza, M., Galván, C., Bouma, T. J., van Belzen, J., (2014). The role of seagrasses in coastal protection in a changing climate. Coast. Eng. 87, 158–168.

Orth, R.J., Luckenbach, M.L., Marion, S.R., Moore, K.A., and Wilcox, D.J., (2006). Seagrass recovery in the Delmarva Coastal Bays, USA. Aquatic Botany 84: 26-36.

Peterson, C.H., Luettich, R.A., Micheli, F., Skilleter, G.A., (2004). Attenuation of water flow inside seagrass canopies of differing structure. Mar. Ecol. Prog. Ser., 268, pp. 81-92.

Polte, P., Schanz, A., and Asmus, H., (2005). The contribution of seagrass beds (Zostera noltii) to the function of tidal flats as a juvenile habit for dominant, mobile epibenthos in the Wadden Sea. Marine Biology 147: 813-822.

Potouroglou, M., Bull, J.C., Krauss, K.W., Kennedy, H.A., Fusi, M., Daffonchio, D., Mangora, M.M., Githaiga, M.N., Diele, K., and Huxham, M., (2017). Measuring the role of seagrasses in regulating sediment surface elevation. Scientific Report, doi:10 .1038/s41598-017-12354-y.

Preen, A.R., Long, W.-J.L., and Coles, R.G., (1995). Flood and cyclone related loss, and partial recovery, of more than 1000 km^2 of seagrass in Hervey Bay. Queens-land, Australia. Aquatic Botany 52: 3-17.

Schuerch, M., Rapaglia, J., Liebetrau, V., Vafeidis, A., Reise, K., (2012). Salt marsh accretion and storm tide variation: an example from a Barrier Island in the North Sea. Estuay. Coasts 35 (2), 486 – 500.

Shchepetkin, A.F., and McWilliams, J.C., (2005). The Regional Ocean Modeling System: a split-explicit, free-surface, topography following coordinates ocean model. Ocean Modelling 9: 347–404.

Short, F.T, and Burdick, D.B., (1996). Quantifying eelgrass habit loss in relation to housing development and nitrogen loading in Waquoit Bay, Massachusetts. Estuaries 19: 730-739.

Temmerman, S., Bouma, T. J., Van de Koppel, J., Van der Wal, D., De Vries, M.B., and Herman, P. M. J. , (2007), Vegetation causes channel erosion in a tidal landscape, Geology, 35(7), 631–634, doi:10.1130/G23502A.1.

Terrados, J., and Duarte, C.M., (2000). Experimental evidence of reduced particle resuspension within a seagrass (*Posidonia oceanica* L.) meadow. Journal of Experimental Marine Biology and Ecology 243: 45-53.

Uittenbogaard, R., (2003). Modelling turbulence in vegetated aquatic flows. International workshop on Riparian Forest vegetated channels: hydraulic, morphological and ecological aspects, Trento, Italy, 20-22 February 2003.

U.S. Army Corps of Engineers, (1976). Aquatic Plant Control Project for the State of New Jersey: Design Memorandum No.1. Philadelphia District, Philadelphia, Pennsylvania.

U.S. Department of Agriculture, (2008). Plants database. Natural Resources Conservation Service. http://plants.usda.gov.

Ward, L., Kemp, W., Boyton, W., (1984), The influence of waves and seagrass communities on suspended particulates in an estuarine embayment, Mar. Geol., 59, 85–103.

Warner, J.C., Sherwood, C.R., Signell, R.P., Harris, C., Arango, H.G., (2008). Development of a three-dimensional, regional, coupled wave, current, and sediment-transport model, Computers and Geosciences, 34, pp. 1284–1306.

Warner, J.C., Armstrong, B., He, R., Zambon, J.B., (2010). Development of a coupled ocean-atmosphere-wave-sediment transport (COAWST) modeling system. Ocean Model., 35 (3), pp. 230-244.

Waycott, M., Longstaff, B.J., and Mellors, J., (2005). Seagrass population dynamics and water quality in the Great Barrier Reef region: A review and future research directions. Marine Pollution Bulletin 51: 343-350.

Waycott, M., Duarte, C.M., Carruthers, T.J.B., Orth, R.J., Dennison, W.C., et al. (2009). Accelerating loss of seagrasses across the globe threatens coastal ecosystems. Proc. Natl. Acad. Sci. USA 106:12377-81.

Chapter 7.

Summary

7.1 General findings

The results presented in this manuscript show how seagrass and salt marsh deterioration reduces the capacity of shallow estuaries to retain sediment inputs from the watershed and marine end-members. Special focus has been given to a positive feedback mechanism between vegetation loss, altered tidal propagation and decreased sediment deposition within the entire back-barrier basin. High-resolution numerical model simulations have been used to explore how hydrodynamics and sediment storage capacity of shallow estuaries change with progressive reductions in subtidal vegetated area and salt marsh extent. Six tidal inlet/estuaries along the U.S. Atlantic Coast characterized by different morphological features and tidal ranges were employed to address these research objectives.

In this thesis, the link between reductions in vegetated area, tidal propagation characteristics and sediment dynamics has been analysed in detail, by pointing out the physical mechanisms responsible for changes in tidal prism values and hydrodynamics, and by specifically taking into account the impact of marsh and seagrass disappearance on tidal asymmetry, which gives an indication for the importing or exporting nature of a tidal channel or estuary. This thesis has documented systematic sediment-budget variations

related to reductions in vegetated surfaces which negatively affect the resilience of shallow estuaries to natural threats. We have demonstrated that vegetation loss enhances the export of sediments, and decreases the sediment stored in the entire system. This finding is important for the long-term survival of salt marshes, because a decrease in the amount of sediment trapped by the estuary compromises marsh stability. Indeed, Ganju et al. [2017] revealed, using eight micro-tidal sites along the Atlantic and Pacific coasts of United States, that marsh conversion into open-water is connected to deficits in the sediment budget of the entire marsh complex.

Previous studies have related the sediment trapping capacity of salt marshes to marsh elevation, local tidal range, sediment supply, vegetation characteristics, and exposure to disturbances [e.g., Fagherazzi et al., 2012]. In this dissertation, it is suggested that the ability of salt marshes to build-up vertically depends also on their size compared to the area of the back-barrier basin. The existence of a feedback between salt marsh extent and the stability of the entire ecosystem has been corroborated by numerical results and we showed that small salt marshes are more sensitive to the deleterious effects of sea-level rise. More specifically, the sediment deposition per unit area on marsh platforms decreases exponentially reducing the ratio marsh/basin area. Furthermore, this research has documented the importance to use high-resolution numerical model simulations when evaluating the response of salt marshes to sea-level rise. Indeed, global assessments employ simplified hydrodynamic conditions and do not consider that marsh retreat associated with edge erosion reduces the sediment stock in estuarine systems, affecting the fate of the remaining salt marshes under future sea-level rise scenarios.

192

This thesis also investiagated seagrass beds, analyzing the influence of this aquatic ecosystem on marsh dynamics in the vertical and horizontal directions, and on the sediment budget in shallow bays. On one hand, this work highlights the benefit of seagrass meadows in reducing marsh-edge retreat by wind-wave attack, which is recognized as a chief agent in lateral marsh loss, and on the other hand it has been found that the sediment stock on marsh platforms is reduced when seagrasses are present. Indeed, it has been demonstrated that seagrass meadows lower bed shear stresses within the entire embayment and decrease the sediment suspended in the water column, depleting the sediments which could be potentially trapped by salt marshes in each tidal cycle.

7.2 Extreme events and human disturbances

This manuscript has investigated the influence of salt marsh and seagrass loss on the sediment trapping capacity of shallow tidal lagoons under the effect of tides and wind-waves. Extreme events are important sediment drivers in back-barrier basins [Castagno et al., 2018]. As presented in Figure 1.5, changes in morphology have a negligible effect on low-frequency actions propagating into shallow tidal lagoons, and therefore the import of sediment during extreme conditions may be unaffected by the marsh/basin area ratio. Furthermore, storms increase bed shear stresses and can alter the sediment exchange between vegetated beds and salt marshes. More specifically, sediments trapped by seagrass meadows in summer can be resuspended and stored over vegetated marsh platforms during winter, when the frequency of intense storms increases and the friction exerted by seagrasses is reduced.

Human disturbances can have an important impact on the sediment stock and hydrodynamics in shallow lagoons. For example, channel deepening for navigational purposes can reduce the friction at the inlet and increase water levels in the system. Similarly, the conversion of intertidal areas into land modifies the ratio between the inlet cross-sectional area and the basin planform area increasing tidal water levels in the back-barrier basin [Orton et al., 2015]. In Chapters 2 and 3, I demonstrated that salt marsh lateral erosion enlarges the intertidal storage volume of the basin, enhancing its ebb dominance. On the contrary, loss of intertidal areas associated with reclamation projects reduces the intertidal storage volume of the lagoon, increasing its flood-dominance. These considerations are in agreement with Fortunato and Oliveira [2005], who showed the influence of intertidal flat elevation on tidal asymmetry.

7.3 Development of research

This research has explored the large-scale effects associated with seagrass and salt marsh loss in shallow tidal lagoons using high resolution numerical modelling simulations. The findings presented in this manuscript have been verified for six lagoon type estuaries. A shortcoming of this research is related to the fact that for Chapter 2 and 3 all the sediment deriving from marsh edge erosion have been removed from the system, overstimating marsh vulnerability to sea-level rise. Marsh lateral loss generates a source of sediments, which can be trapped by the remaining salt marshes and tidal flats, affecting the geomorphological evolution of the system over long time-scales. A more focused approach similar to what is proposed in Chapter 4 would contribute a better understanding of the way in which salt marsh retreat influences the sediment budget in a particular system. This point could be also improved by studying in detail the feedback between marsh deterioration and tidal flat stability. Following the paradigm introduced by Marani et al. [2007] and elaborated by Mariotti and Fagherazzi [2010; 2013], the depth of tidal flats will tend toward an equilibrium, which is defined by a balance between erosion from wave-generated shear stress and deposition proportional to sediment concentration, modulated by sea-level rise. As marshes erode laterally, expanding the fetch and tending to increase wave strength, the equilibrium depth (as a function of sea-level rise rate) tends to increase. In the experiments presented in this thesis, this effect would translate to a tendency for the tidal flat bed to erode (i.e. sediment trapping efficiency decreases), which would be stronger as more of the marsh is removed. On the other hand, the sediment generated by marsh edge erosion would contribute to marsh and tidal flat vertical accretion, as

demonstrated in Chapter 4. However, the time frame of the analysis carried out for Jamaica Bay could be increased in order to have a more realistic result of the long-term sediment patterns of the bay. More specifically, long-term numerical simulations would provide a comprehensive view of how marsh-derived sediments are redistributed within the system under a wider range of forcings. Indeed, interseasonal and interannual variability in the wind field could drive large changes in the sediment transport in back-barrier estuaries [e.g., Duran-Matute, 2016]. Equally, this methodology may be extended to other lagoon-bay-estuary settings to broaden the parameter space of my investigation and make the results even more relevant to back-barrier estuaries not only throughout the US but worldwide. Furthermore, a comparison between the effects associated with salt marsh loss in lagoon-type estuaries and in open coast would provide a clearer picture of the role played by these vegetated ecosystems in increasing coastal resilience.

Another important point is to determine how seagrass coastal protection functions change with seasons. Indeed, the mean aboveground biomass can strongly increase in June-July and decrease dramatically during fall, as documented by Kennish et al. [2008] in Barnegat Bay. The lack of seasonal aspect in my study constitutes a significant gap in the understanding of how subtidal vegetation can reduce tidal flat erosion and marsh retreat on a long-term basis, as illustrated in the preliminary considerations illustrated below.

The aboveground biomass measurements available in Kennish et al. [2008] (Figure 7.1) could be employed to obtain canopy height and stem density using the empirical formulations presented in Krause-Jensen et al. [2000]. The shear stress distributions could be compared in vegetated and un-vegetated beds with the maximum and minimum

aboveground biomass, investigating whether the sediment deposited over vegetated tidal flats in summer and spring can be resuspended and trapped by marsh platforms during fall and winter. Moreover, the ability of seagrass patches to reduce wave energy along the shoreline can be analyzed as a function of the distance marsh-seagrass edge (Figure 7.2), highlighting the non-linearty of the ecosystem service provided by seagrass meadows in reducing marsh edge erosion (Figure 7.3).
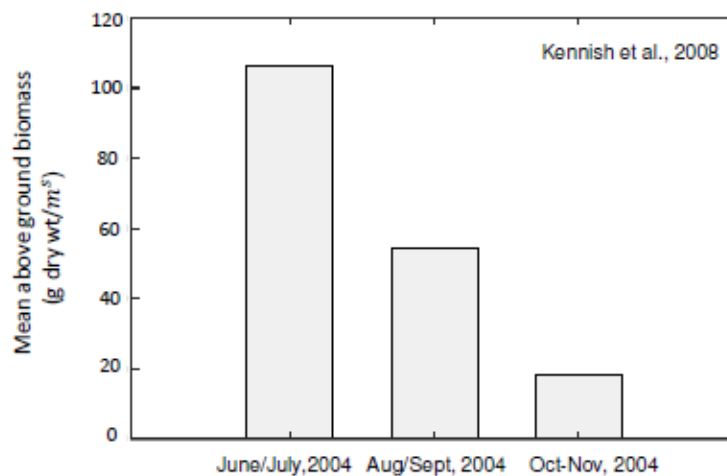

Figure 7.1 Mean above ground biomass of seagrass canopy from Kennish et al. [2008].
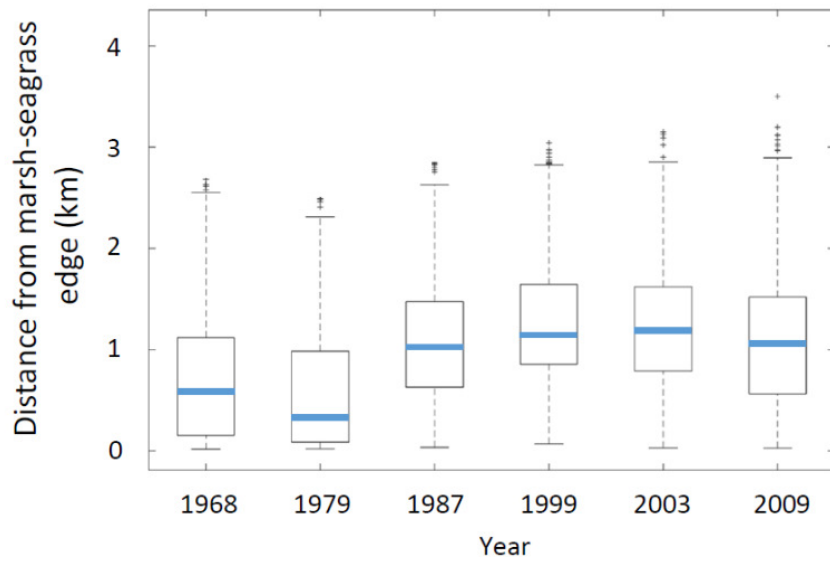
Figure 7.2 Distance between marsh and seagrass edge as a function of the year.
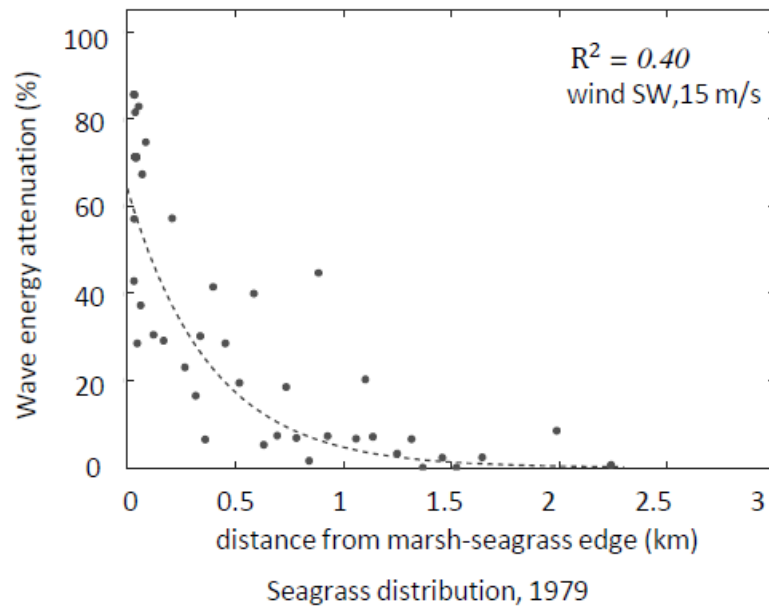

Figure 7.3 Reduction in wave energy along marsh boundary as a function of marsh-seagrass edge distance.

By using the current salt marsh configuration, this work has evaluated only the impact of seagrass loss on bay sediment budget, neglecting the influence of the changes in estuarine

morphology occurred over the last 50 years on the sediment trapping capacity of the system. The next step might be to consider the changes in estuarine morphology and in bottom friction associated with salt marsh and seagrass decline, evaluating how the estuarine sediment budget has been influenced by vegetation loss in the last decades.

7.4 Implications of research

Salt marshes and seagrass beds influence the resilience of shallow estuaries to sea-level rise, by altering the regional scale hydrodynamics and consequently their ability to trap sediments. In many areas worldwide vegetated habitats are declining. This thesis has revealed how subtidal and intertidal vegetation loss depletes the sediment budget in shallow bays employing a numerical modelling approach. I have found that vegetation is important for the stock of sediments within both vegetated and un-vegetated areas in coastal embayments, and when salt marshes and seagrasses are present less sediment is lost in the ocean. These findings are relevant for the long-term survival of estuaries, as an abundance of sediments generally corresponds to more resilient systems to natural threats. Thus, this thesis has emphatized the pivotal role played by these vegetated ecosystems in increasing coastal resilience, and are relevant for coastal communities and coastal managers worldwide.

The study of the interactions between estuaries, vegetated surfaces, and sediment budget is timely. The importance of salt marshes and seagrass beds within estuaries is an active area of research with scientists trying to unravel the potential for these vegetated ecosystems to increase the resilience of coastal bays to sea-level rise. This research project has showed that the sediment availability in the back-barrier basin decreases with salt marsh and seagrass loss, and has demonstrated that the stability of the entire estuary is strongly linked to the areal extent of these vegetated ecosystems. Thus, the results of this research are at forefront of both current science and policy directions in our understanding of coastal resilience in the face of climate change.

References

Castagno, K.A., Jiménez-Robles, A.M., Donnelly, J.P., Wiberg, P.L., Fenster, M.S., and Fagherazzi, S., (2018). Intense storms increase the stability of tidal bays. Geophysical Research Letters, 45, 5491– 5500. https://doi.org/10.1029/2018GL078208

de Jonge, V.N., Schuttelaars, H.M., van Beusekom, J.E.E., Talke, S.A., de Swart, H.E., (2014). The influence of channel deepening on estuarine turbidity levels and dynamics, as exemplified by the Ems estuary, Estuar, Coast. Shelf Sci., 10.1016/j.ecss.2013.12.030

Duran-Matute, M., Gerkema, T., Sassi, M., (2016). Quantifying the residual volume transport through a multiple-inlet system in response to wind forcing: the case of the western Dutch Wadden Sea. J Geophys Res Oceans 121(12):8888–8903

Fagherazzi, S., et al. (2012), Numerical models of salt marsh evolution: Ecological, geomorphic, and climatic factors, Rev. Geophys., 50, RG1002, doi:10.1029/2011RG000359.

Fortunato, A.B., Oliveira, A., (2005). Influence of intertidal flats on tidal asymmetry. Journal of Coastal Research 21 (5), 1062-1067.

Ganju, N.K., Defne, Z., Kirwan, M.L., Fagherazzi, S., D'Alpaos, A. and Carniello, L., (2017). Spatially integrative metrics reveal hidden vulnerability of microtidal salt marshes. Nature communications, 8, p.ncomms14156.

Kentish, M., Haag, S., and Sakowicz, G. (2008). Seagrass demographic and Spatial Habitat Characterization in Little Egg Harbor, New Jersey, Using Fixed Transects. Journal of Coastal Research, Special Issue 55, 148-170.

Krause-Jensen, D., Middelboe, A.L., Sand-Jensen K, Christensen, P.B., (2000). Eelgrass, Zostera marina, growth along depth gradients: upper boundaries of the variation as a powerful predictive tool. Oikos, 91, 233-244.

Mariotti, G., and Fagherazzi, S., (2010). A numerical model for the coupled long-term evolution of salt marshes and tidal flats. J Geophys Res 115:F01004.

Mariotti, G., and Fagherazzi, S., (2013). Critical width of tidal flats triggers marsh collapse in the absence of sea-level rise. Proceedings of the National Academy of Sciences, 110(14), pp.5353-5356.

Marani, M., D'Alpaos, A., Lanzoni, S., Carniello, L. and Rinaldo, A., (2007). Biologically☐controlled multiple equilibria of tidal landforms and the fate of the Venice lagoon. Geophysical Research Letters, 34(11).

Model validation

The systems analysed in this manuscript have been the object of several studies carried out by the United States Geological Survey (USGS) and by the Long Term Ecological Research Network (LTER) over the last few years. Several investigations have used COAWST and Delft3D as numerical tools in these systems. The numerical models used in this work had been extensively calibrated and tested in such studies (Table A.1.1). Herein, we adopted a cumulative research approach which builds on existing methodologies and tools to develop a new and generalized understanding on the global response of bay systems to marsh loss. For our ensemble modelling approach, we decided to add bays using models already used in those systems, leveraging on the effort of several researchers in the past years. Our goal is to add more bays in the near future by inviting more researchers to collaborate within this framework. Table A.1.1 lists the studies which have first dealt with the calibration of some of the investigated systems and the associated modelling frameworks.

Model validation

The validation of the models and the adopted parameterizations can be found in the following papers:

Estuarine system	Relevant reference from literature	Numerical model
Plum Island	Zhang et al., 2019	Delft3D
Great South Bay	This study	COAWST
Jamaica Bay	This study	COAWST

Barnegat Bay	Defne and Ganju, 2014	COAWST
Chincoteague Bay	Beudin et al., 2017	COAWST
Virginia Coast Reserve	Wiberg et al., 2015	Delft3D

Table A.1.1: literature studies dealing with calibration and validation of the numerical models used in this study.

Great South Bay and Jamaica Bay have been calibrated in this study. The validation has been carried out for the period with the maximum amount of measurements. Model performance is evaluated using root-squared-error (RMSE), bias and skill scores. The performance levels are categorized as follows: skill>0.65 excellent, 0.5-0.65 very good, and 0.2-0.5 good; if skill <0.2, poor fit.

$$RMSE = \left[\frac{1}{N} \sum_{n=1}^{N} (X_{modeled} - X_{observed})^2 \right]^{1/2}$$

$$Bias = \frac{1}{N} \sum_{n=1}^{N} (X_{modeled} - X_{observed})$$

$$skill = 1 - \frac{\sum_{n=1}^{N} (X_{modeled} - X_{observed})^2}{\sum_{n=1}^{N} (X_{modeled} - <X>_{observed})^2}$$

The models are forced at the seaward boundaries with tides, using a combination of Flather [1976] and Chapman [1985] boundary conditions; a radiation boundary condition Orlanski [1976] is prescribed on the landward boundary. Bottom shear-stresses are calculated using a quadratic drag law and assuming a logarithmic velocity profile in the bottom grid cell [Warner et al., 2008].

- The tidal levels at the boundaries are based on observations from the USGS 01311145 station in Great South Bay. The model was calibrated by careful adjustments of the

boundary conditions to attain the best agreement between the first 2 weeks post-spin-up model results and water level data measured within the estuary. The water level data are collected in seven USGS stations between the 29th July and the 12th August 2018. The model presents excellent agreement with the data.

	Site	RMSE	Bias	Skill
Water elevation (m)	USGS 01311145	0.05	-0.03	0.99
Water elevation (m)	USGS 01311143	0.09	-0.08	0.97
Water elevation (m)	USGS 01310521	0.09	-0.07	0.96
Water elevation (m)	USGS 01310740	0.25	0.01	0.75
Water elevation (m)	USGS 01309225	0.06	0.02	0.79
Water elevation (m)	USGS 01304920	0.17	0.03	0.99
Water elevation (m)	USGS 01304746	0.11	0.01	0.92

Table A.1.2: model performance and skill score for Great South Bay.

- The tidal levels at the boundaries are based on observations from the USGS station (USGS 01311875) located at the Rockaway Inlet; a factor of 0.97 is applied to the measured water elevations to consider the effects of convergent topography on the tide [Marsooli et al., 2016]. The results of the model are compared with water level data collected in two USGS stations (USGS 01311875 and USGS 01311850) and with flow velocities data measured at the North Channel. During the first two weeks of August 2015. The model presents excellent/very good agreement with the data.

	Site	RMSE	Bias	Skill
Water elevation (m)	USGS 01311875	0.04	-0.02	0.99
Water elevation (m)	USGS 01311850	0.14	0	0.99
U_{bar} (m/s)	North Channel	0.09	0.04	0.93
V_{bar} (m/s)	North Channel	0.16	-0.1	0.76
SSC (mg/L)	USGS 01311875	1.6	0.96	0.55

Table A.1.3: model performance and skill score for Jamaica Bay.

References

Beudin, A., Ganju, N. K., Defne, Z., and Aretxabaleta, A. L., (2017). Physical response of a back‑barrier estuary to a post‑tropical cyclone. Journal of Geophysical Research: Oceans, 122, 5888–5904. https://doi.org/10.1002/2016JC012344.

Chapman, D. C., (1985). Numerical treatment of cross‑shelf open boundaries in a barotropic coastal ocean model, J. Phys. Oceanogr., 15, 1060–1075.

Defne, Z., and Ganju, N., (2014). Quantifying the residence time and flushing characteristics of a shallow, back-barrier estuary: Application of hydrodynamic and particle tracking models, Estuaries Coasts,1 – 16, doi:10.1007/s12237-014-9885-3.

Flather, R. A., (1976). A tidal model of the northwest European continental shelf, Mem. Soc. R. Sci. Liege, 6, 141–164.

Marsooli, R., Orton, P.M., Georgas, N., Blumberg, A.F, (2016). Three-dimensional hydrodynamic modeling of coastal flood mitigation by wetlands. Coast. Eng., 111, pp. 83-94

Orlanski, I., (1976). A simple boundary condition for unbounded hyperbolic flows, J. Comp. Sci., 21(3), 251–269.

Wiberg, P. L., Carr, J. A., Safak, I., and Anutaliya, A., (2015). Quantifying the distribution and influence of non‑uniform bed properties in shallow coastal bays. Limnology and Oceanography: Methods, 13(12), 746–762. https://doi.org/10.1002/lom3.10063

Warner, J. C., Sherwood, C. R., Signell, R. P., Harris, C. K., and Arango, H.G., (2008). Development of a three‑dimensional, regional, coupled wave, current, and sediment‑ transport model, Comput. Geosci., 34(10), 1284–1306.

Zhang, X., Leonardi, N., Donatelli, C., and Fagherazzi, S. (2019). Fate of cohesive sediments in a marsh-dominated estuary. Advances in Water Resources, 125, 32-40.

The wave thrust (the integral along the vertical of the dynamic pressure of waves) acting on marsh boundaries is explicitly computed by the model following Tonelli et al. [2010] and Leonardi et al. [2016]. The COAWST modelling framework is built to allow the user to select any combination of the main three models (ROMS, SWAN and WRF). The user needs to list C-prepocessing options in a header file to select the models, to couple them and to activate any specific individual option available for each model. Specifically, the new wave thrust routine is activated by the following flags:

```
# define MARSH_WAVE_EROSION
# define MARSH_WAVE_THRUST
```

and activating the new vegetation module recently implemented in COAWST by Beudin et al. [2017]:

```
# define  VEGETATION
# ifdef VEGETATION
# undef ANA_VEGETATION
# define VEG_DRAG
# ifdef VEG_DRAG
#  define VEG_FLEX
#  define VEG_TURB
# endif
# define  VEG_SWAN_COUPLING
# ifdef VEG_SWAN_COUPLING
#  define VEG_STREAMING
```

endif

The presence of marsh is felt by the wave thrust routine through the variable marsh_mask, which is specified in the initial condition file. The variable marsh_mask is defined by a matrix with 0 and 1, where marsh pixels have a value of 1.

Finally, the user needs to create a vegetation input file where mass density, number of vegetation types and mechanical properties of plants are listed:

```
NVEG  == 1          ! Number of submerged aquatic vegetation types
CD_VEG == 1.0d0    ! Drag coefficient for each vegetation type
E_VEG == 1.0d9      ! Young's Modulus for each vegetation type
VEG_MASSDENS  == 700.0d0    ! Mass density for each vegetation type
```

! Logical switches (TRUE/FALSE) to activate writing of vegetation fields

! into HISTORY output file: [1:NVEG,Ngrids].

Hout(ipdens)   == F   ! Plant_density   Density of the plant for each vegetation

Hout(iphght)   == F   ! Plant_height   Height of the plant for each vegetation

Hout(ipdiam)   == F   ! Plant_diameter   Diameter of the plant for each vegetation

Hout(ipthck)   == F   ! Plant_thickness   Thickness of the plant for each vegetation

Hout(ipagbm)   == F   ! Plant_agb   Above ground plant biomass

Hout(ipbgbm)   == F   ! Plant_bgb   Below ground plant biomass

Hout(idWdvg)   == F   ! Dissip_veg   Wave dissipation due to vegetation

Hout(idTims)   == T   ! marsh_mask   masking for getting thrust due to waves

```
Hout(idTtot)  == T     ! Thrust_total     Total thrust due to waves

Hout(idTmfo)  == F     ! marsh_flux_out    Marsh flux out

Hout(idTmmr)  == F     ! marsh_retreat     Amount of marsh retreat from all four directions

Hout(idTmsc)  == F     ! marsh_scrp_height    Amount of marsh retreat from all four directions
```

References

Beudin, A., Ganju, N.K., Defne, Z., and Aretxabaleta, A.L., (2017b). Physical response of a back-barrier estuary to a post-tropical cyclone. Journal of Geophysical Research: Oceans, 122, 5888–5904. https://doi.org/10.1002/2016JC012344.

Leonardi, N., Defne, Z., Ganju, N.K. and Fagherazzi, S., (2016). Salt marsh erosion rates and boundary features in a shallow Bay. Journal of Geophysical Research: Earth Surface, 121(10), pp.1861-1875.

Tonelli, M., Fagherazzi, S., and Petti, M., (2010). Modeling wave impact on salt marsh boundaries, J. Geophys. Res., 115, C09028, doi:10.1029/2009JC006026.
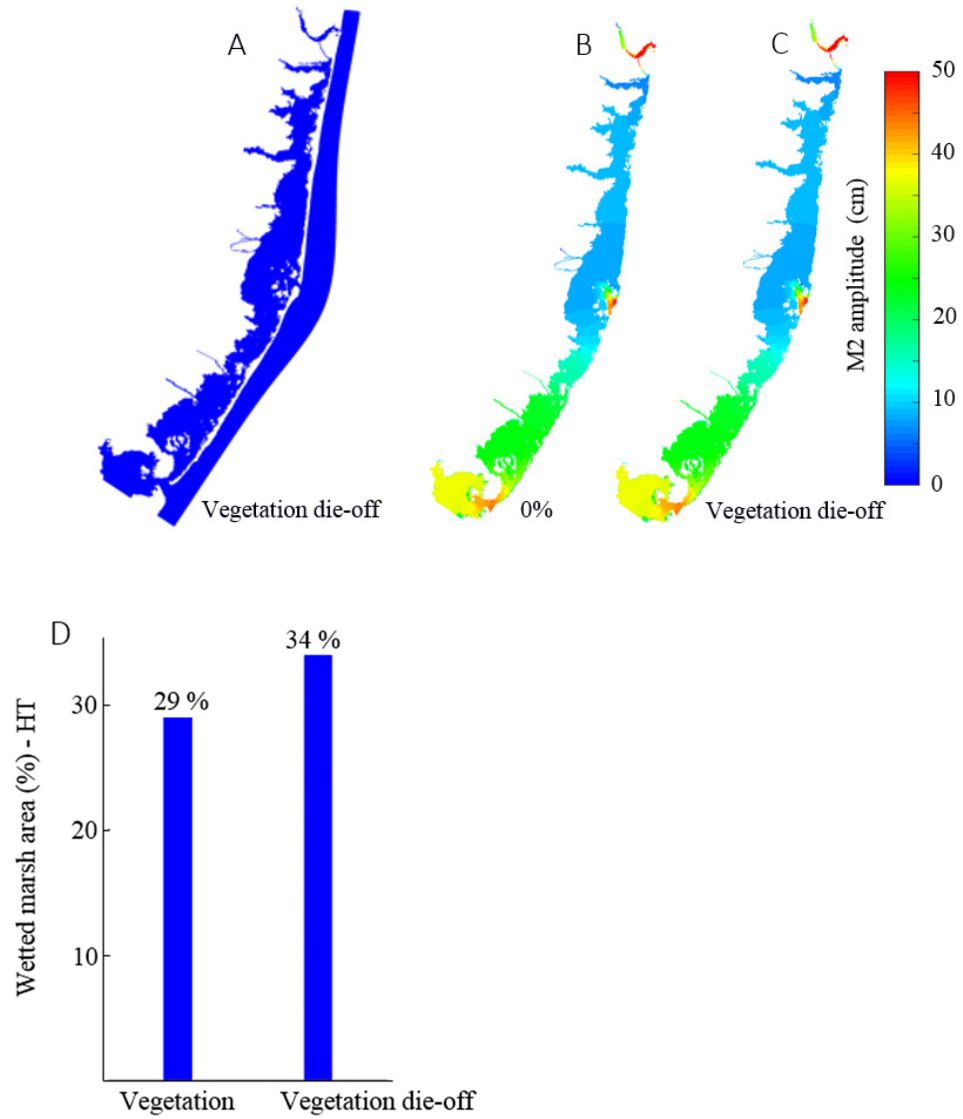
Figure A.3.1: Model domain for the scenario with vegetation die-off (a); M$_2$ amplitude (cm) in BB-LEH (b); M$_2$ amplitude (cm) after the vegetation removal from marsh platforms (c); wetted area in BB-LEH and in vegetation die-off scenarios (d).
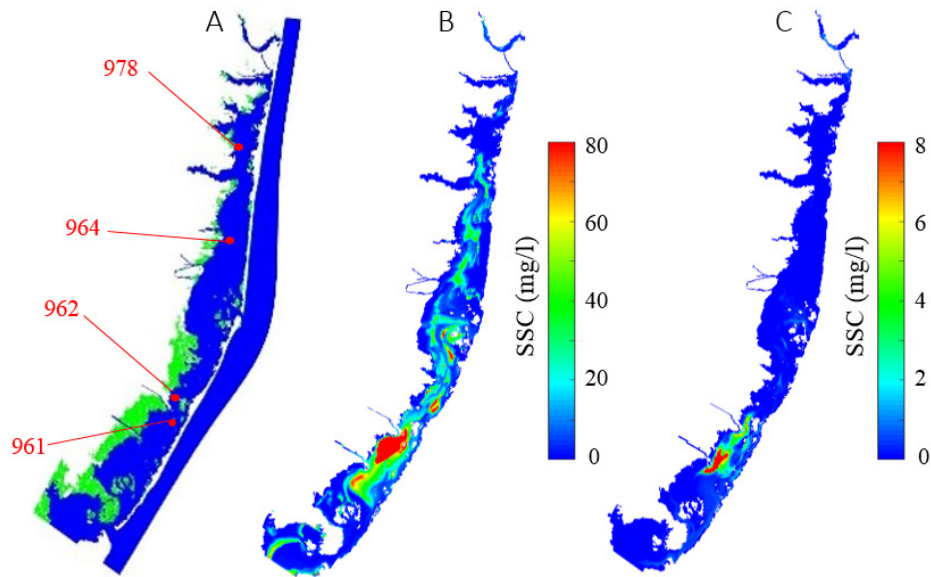
Figure A.3.2: Sites of field measuring (a); maximum (b) and minimum (c) suspended sediment concetration (mg/L) over the last tidal cycle for the current marsh configuration.
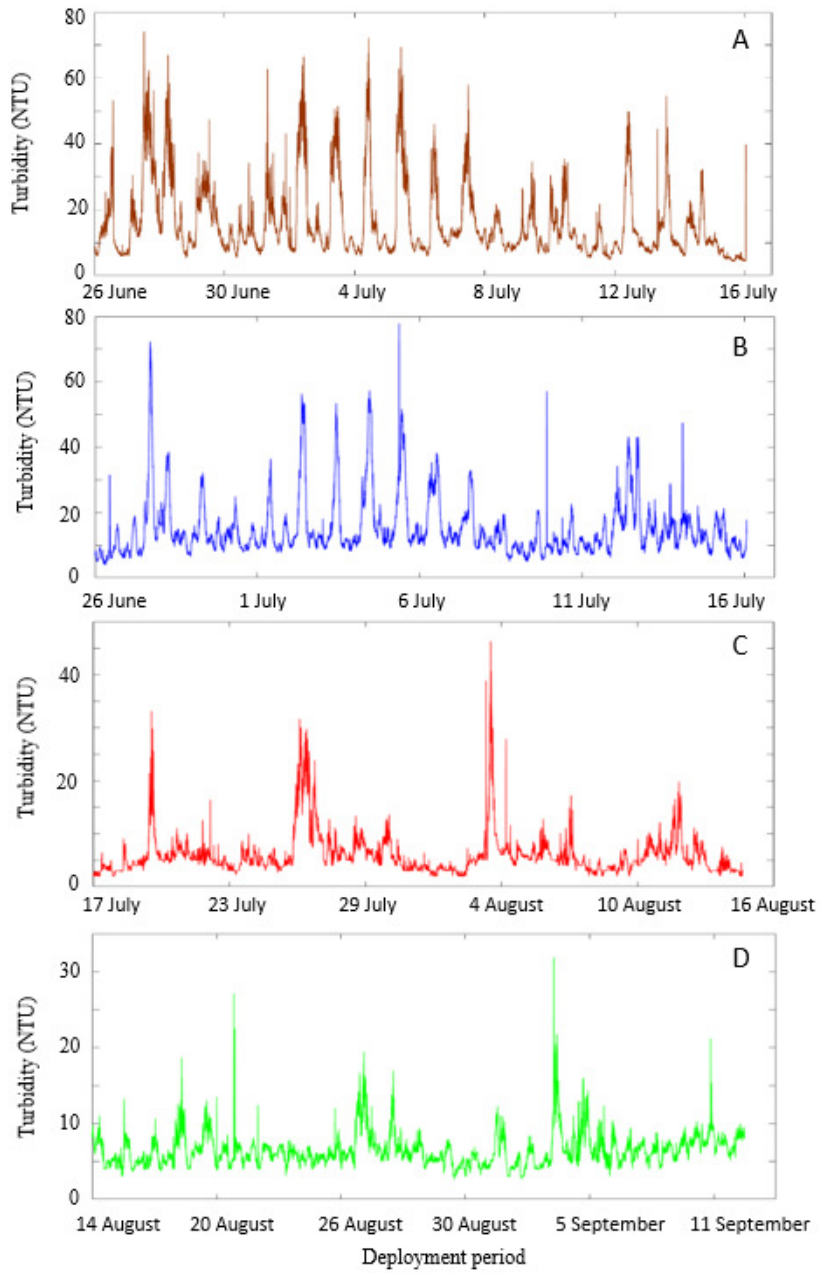
Figure A.3.3: Turbidity time-series data in four different locations: 961 location (a), 962 location (b); 964 location (c); 978 location (d).
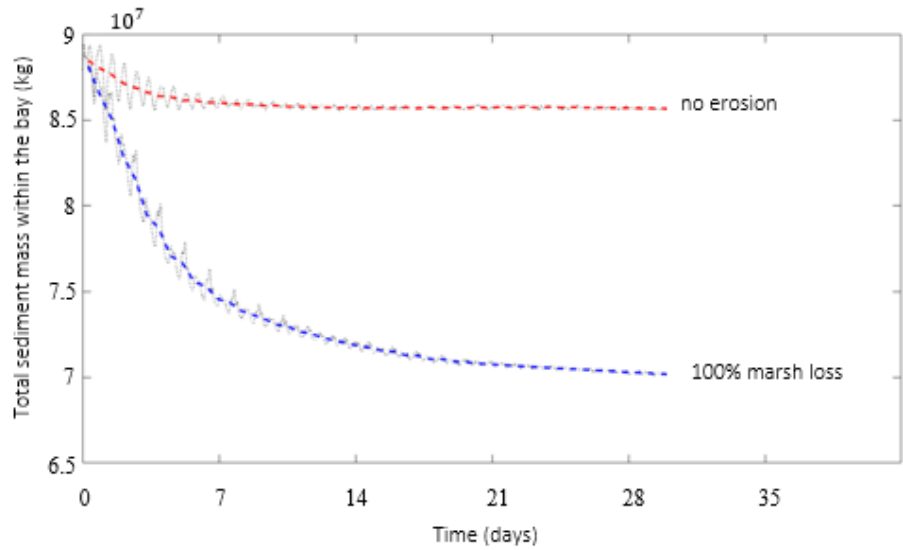
Figure A.3.4: Time series of the total mass of sediments stored within the bay in the case of 0% marsh erosion and for 100% marsh erosion.
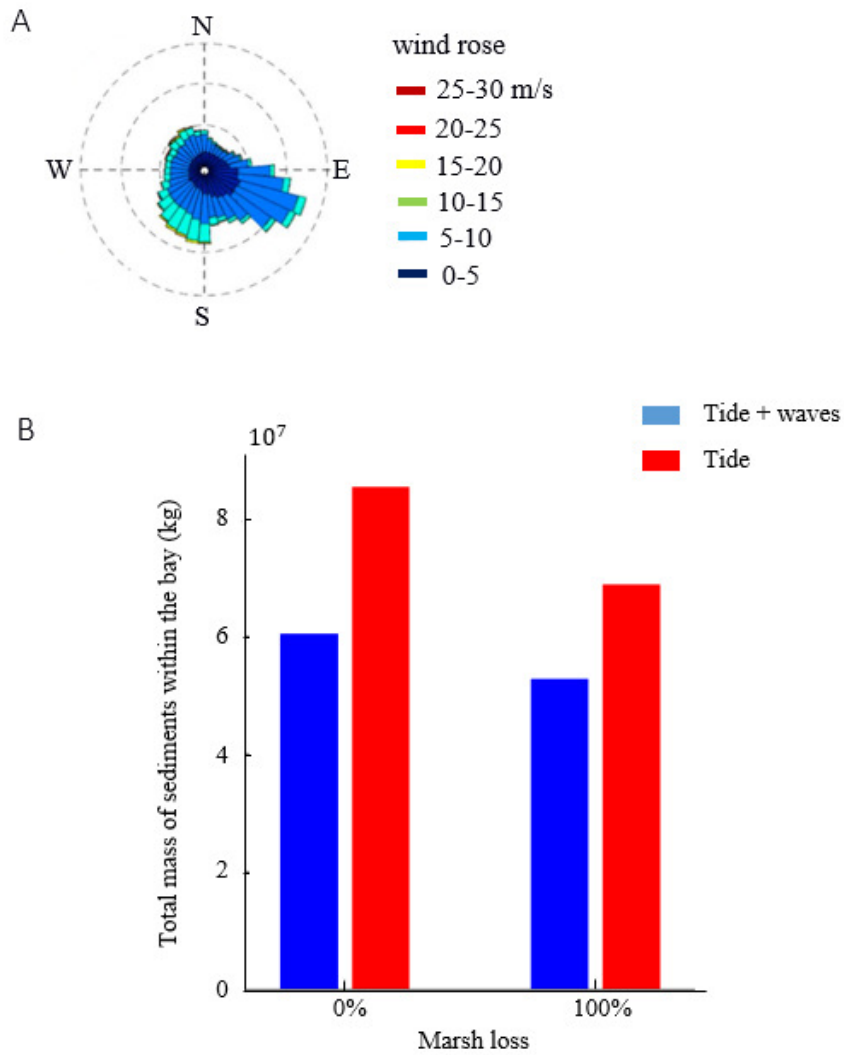
Figure A.3.5: Wind rose of the system (a); total sediment mass stored in the bay for the current scenario (BB-LEH) and for the scenario with salt marshes completely eroded (BB-LEH-100%) (b). The sediment budget after 30 days is evaluated under tides and including wind-waves in the model.
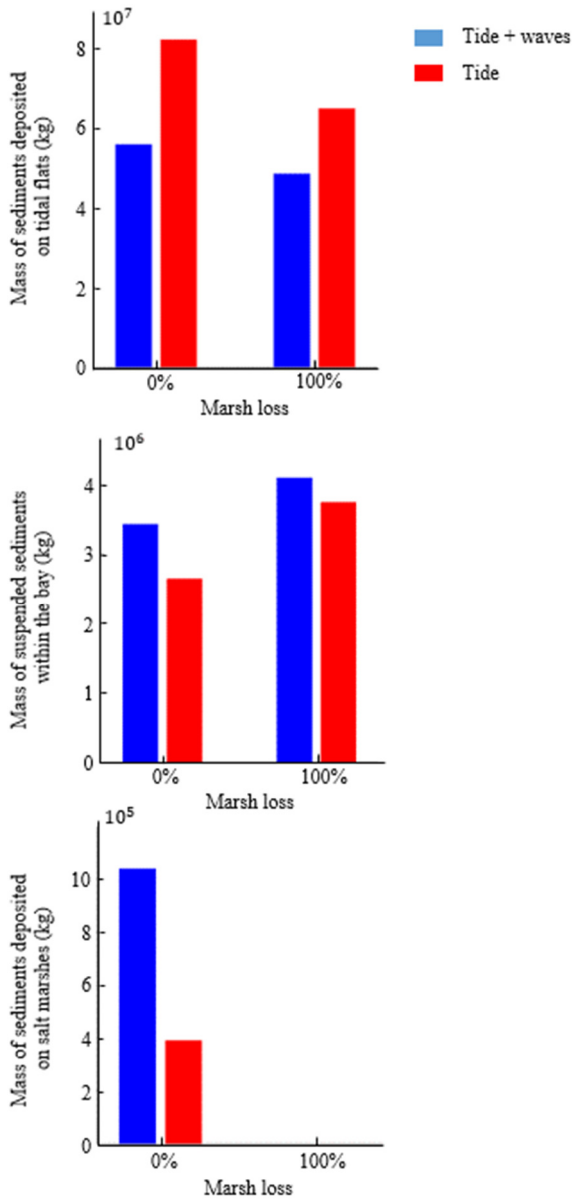
Figure A.3.6: Same as Figure A.3.5 but the total amount of sediments is divided into the three classes mentioned in Chapter 2.
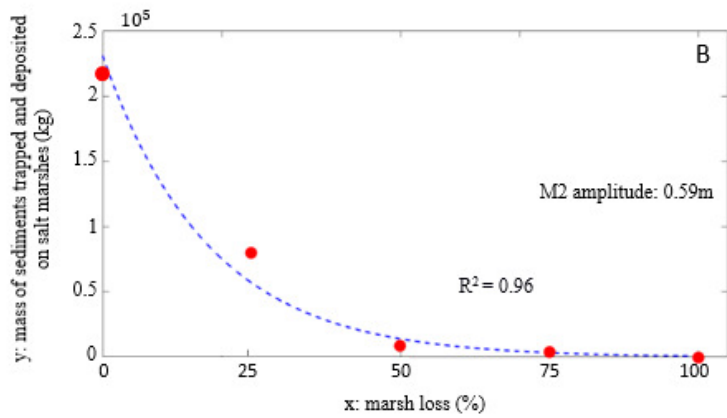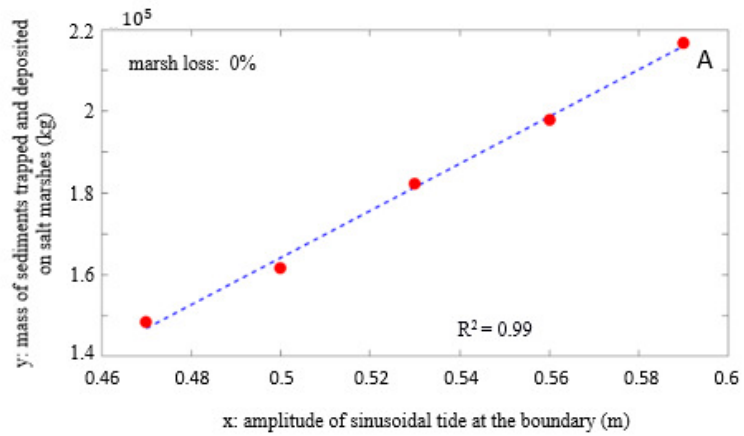
Figure A.3.7: Mass of sediments trapped by salt marshes, as a function of the tidal amplitude (a), and as a function of different percentages of marsh loss (b).

Moring ID	Site name	Latitude	Longitude	Depth (m)	Deployment period
961	Little Egg Island Shoal	39.6316	-74.2186	0.8	June 26, 2013-July 16, 2013
962	State Route 72 bridge	39.84426	74.09628	2	June 26, 2013-July 16, 2013
964	Red channel marker #40	39.86173	74.122253	2.5	July 17, 2013-August 13, 2013
978	Red channel marker #28	39.96017	74.10470	2.5	August 14, 2013-September 12, 2013

Moring ID	Instrument	Serial no.	Sensor elevation (meters above bottom)	Data file
9615	YSI EXO2	13E103375	0.15	9615exo-a.nc
9622	Wet Labs ECO-NTUSB	508	1.22	9622ecn-a.nc
9642	Wet Labs ECO-NTUSB	508	1.72	9642ecn-a.nc
9782	Wet Labs ECO-NTUSB	508	1.72	9782ecn-a.nc

Moring ID	Numerical model - maximum SSC over the last tidal cycle (mg/l)	Numerical model - minimum SSC over the last tidal cycle (mg/l)	Measurements-SSC range (mg/l)
961	80	5	9.37-136
962	80	5	9.37 -146
964	25	1	3.5-87
978	25	1	3.5-87

Table A.3.1: Dickhudt et al. [2015] sensor deployment and location information for mooring deployed in the Barnegat Bay-Little Egg Harbor estuary, New Jersey (a). Site identification number, instrument type, instrument serial number, instrument elevation, and links to the associated data files for platforms deployed in the Barnegat Bay-Little Egg Harbor estuary, New Jersey (b). Comparison between the ranges of SSC obtained by time-series data and the model maximum and minimum SSC values over the last tidal cycle i.e., when plateau values in terms of total mass of sediments have been reached (Figure A.1.3b). We converted NTU values of Figure S3 to SSC values using the following regression: SSC = 1.954*Turbidity – 0.4 (c).
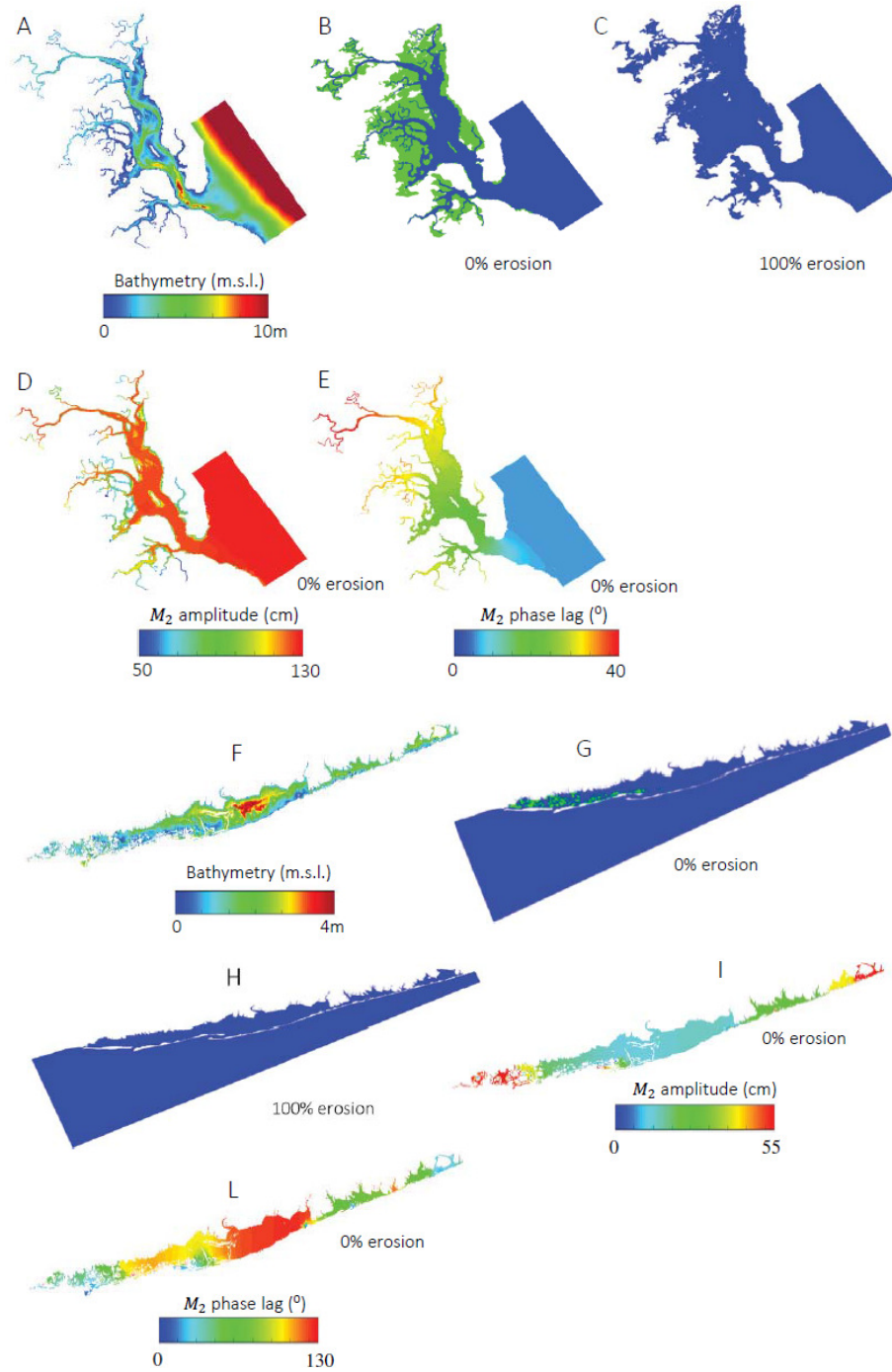
Figure A.4.1: bathymetry of Plum Island Sound and Great South Bay (a, f); model domains: current salt marsh distribution (b, g) and marsh completely eroded (c, h); M₂ amplitude

(cm) and phase lag (°) for the 0% erosion case (d-e, i-l). Missing plots are to be found in Figures 2 and 3.

Figure A.4.2: bathymetry of Jamaica Bay and Barnegat Bay-Little Egg Harbor (a, h); model domains: current salt marsh distribution (b, i) and marsh completely eroded (c, l); M₂ amplitude (cm) and phase lag (°) for the 0% erosion case (d-e, m-n); reduction in M₂

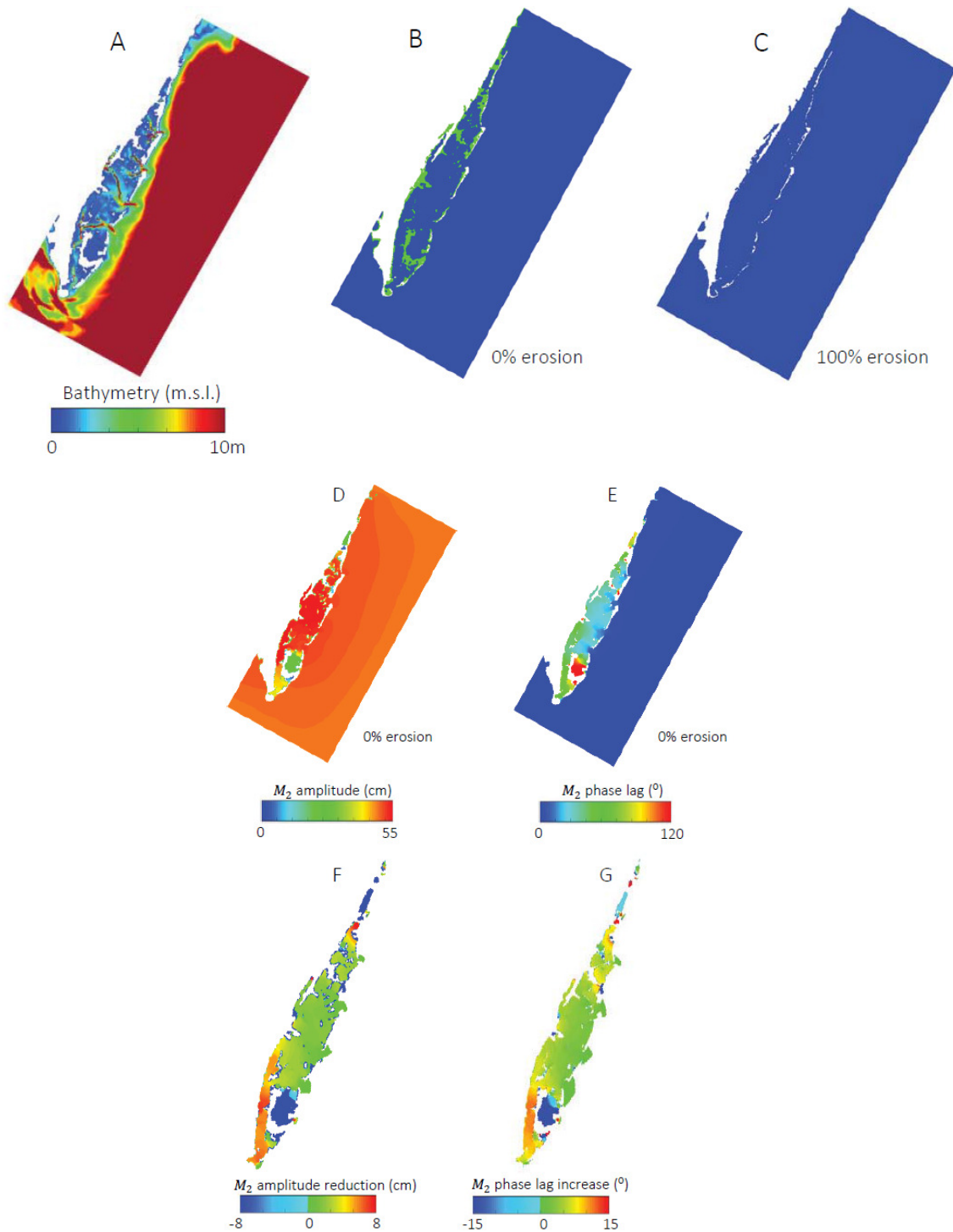amplitude (cm) and increase in phase lag (º) after the removal of the entire marsh surface (f-g, o-p).

Figure A.4.3: bathymetry of Chincoteague Bay (a); model domains: current salt marsh distribution (b) and marsh completely eroded (c); M_2 amplitude (cm) and phase lag (º) for the 0% erosion case (d-e); reduction in M_2 amplitude (cm) and increase in phase lag (º) after the removal of the entire marsh surface (f-g).

222

Figure A.4.4: bathymetry of Virginia Coast Reserve (a); model domains: current salt marsh distribution (b) and marsh completely eroded (c); M_2 amplitude (cm) and phase lag (°) for the 0% erosion case (d-e); reduction in M_2 amplitude (cm) and increase in phase lag (°) after the removal of the entire marsh surface (f-g).
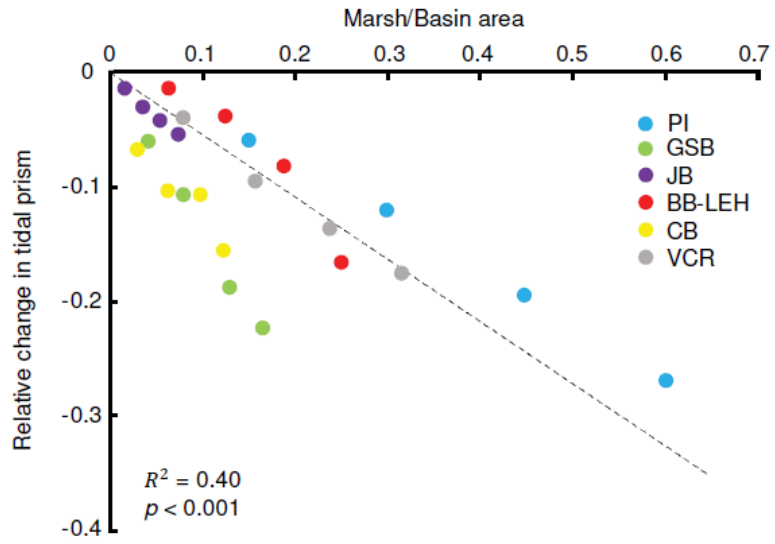
Figure A.4.5: relative change in tidal prism as a function of normalized marsh area. The four values for each location are the four quartiles tested (0, 25, 50 and 75%).
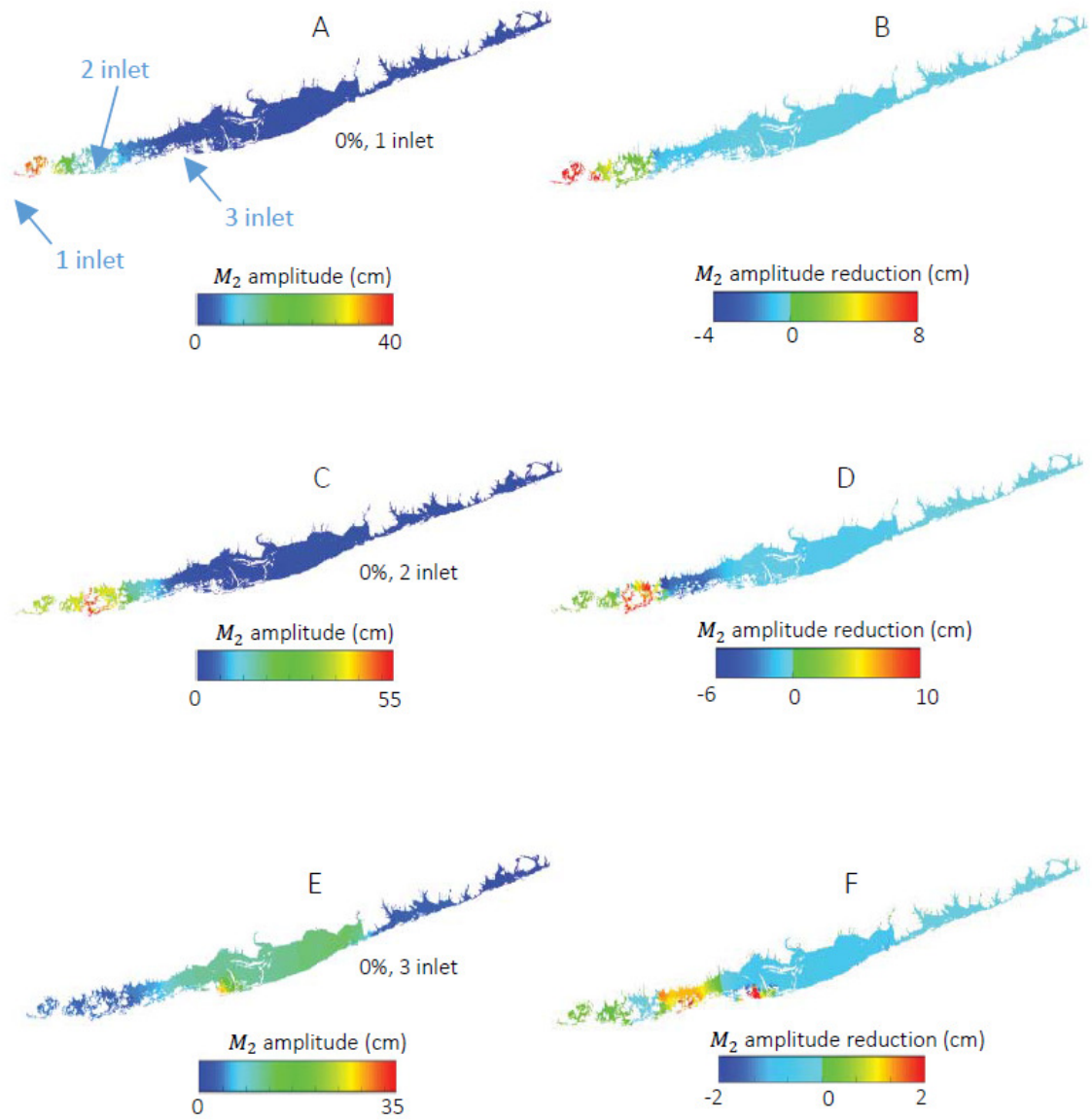
Figure A.4.6: M$_2$ amplitude (cm) for the 0% erosion case with closed inlet 2 and 3 (a), closed inlet 1 and 3 (c), closed inlet 1 and 2 (e); difference in M$_2$ amplitude (cm) between the case with the current salt marsh extent and with salt marshes completely eroded with closed inlet 2 and 3 (b), closed inlet 1 and 3 (d), closed inlet 1 and 2 (f) in Great South Bay.
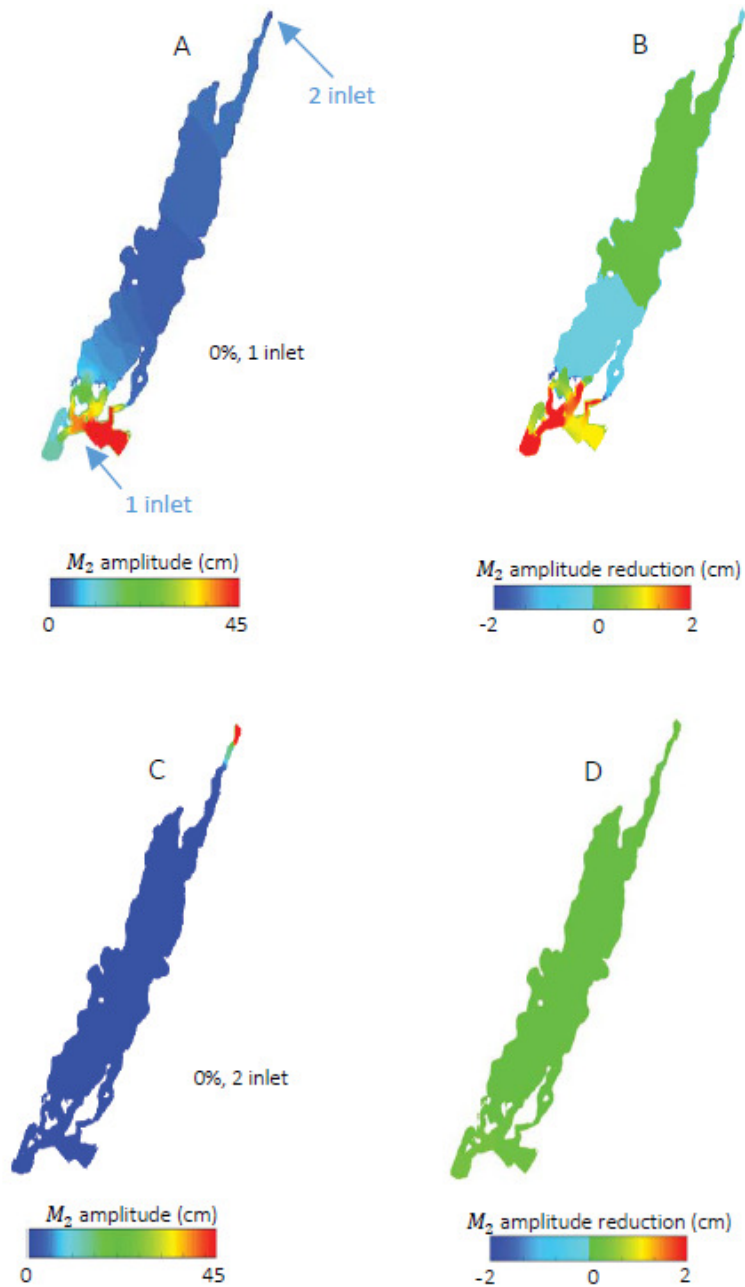
Figure A.4.7: M$_2$ amplitude (cm) for the 0% erosion case with closed inlet 1 (a) and closed inlet 2 (c); difference in M$_2$ amplitude (cm) between the case with the current salt marsh extent and with salt marshes completely eroded with closed inlet 1 (b) and closed inlet 2 (d), in Chincoteague Bay.
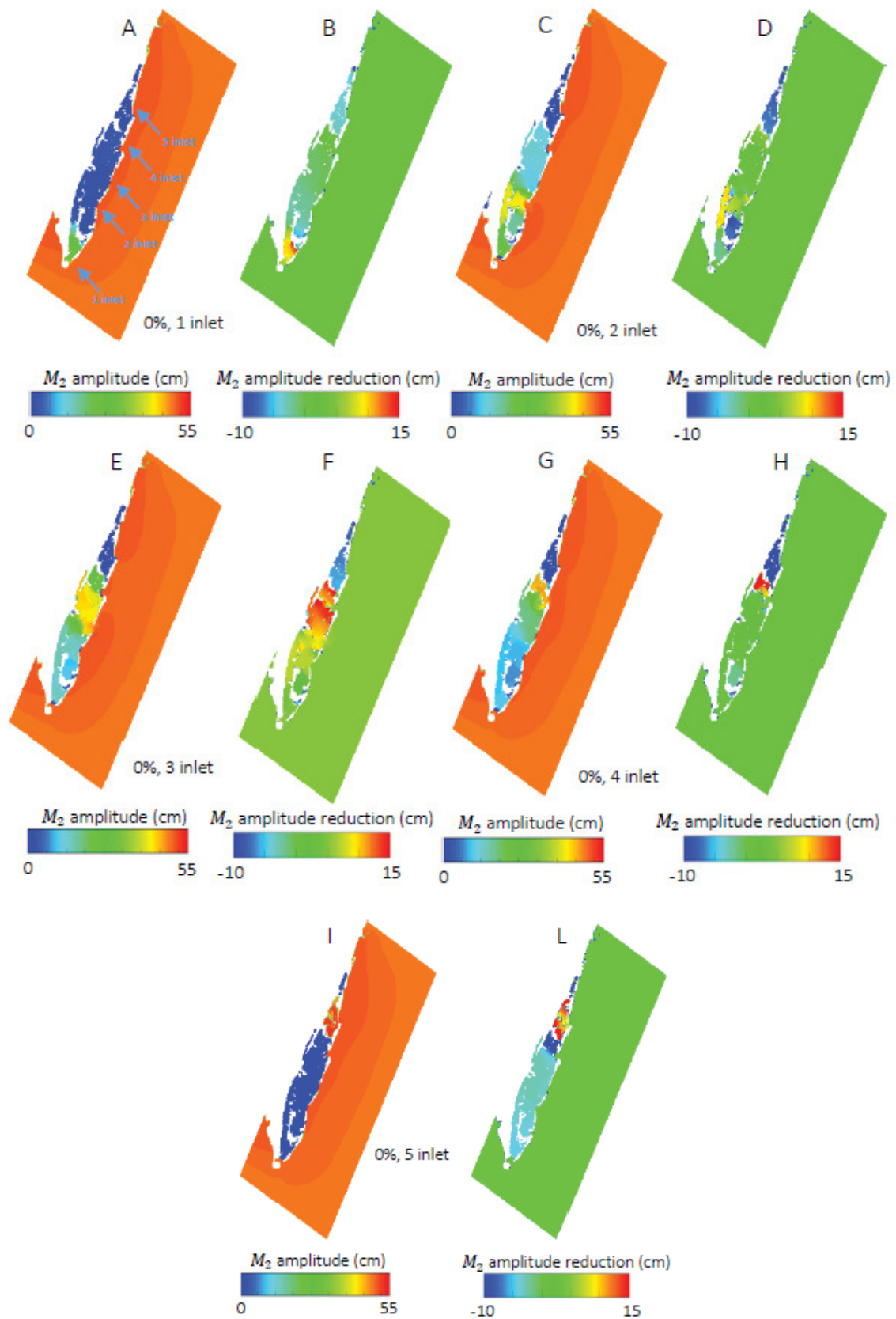
A

5 inlet
4 inlet
3 inlet
2 inlet
1 inlet

0%, 1 inlet

B

C

0%, 2 inlet

D

M_2 amplitude (cm)

0   55

M_2 amplitude reduction (cm)

-10   15

M_2 amplitude (cm)

0   55

M_2 amplitude reduction (cm)

-10   15

E

0%, 3 inlet

F

G

0%, 4 inlet

H

M_2 amplitude (cm)

0   55

M_2 amplitude reduction (cm)

-10   15

M_2 amplitude (cm)

0   55

M_2 amplitude reduction (cm)

-10   15

I

0%, 5 inlet

L

M_2 amplitude (cm)

0   55

M_2 amplitude reduction (cm)

-10   15

227

Figure A.4.8: M_2 amplitude (cm) for the 0% erosion case with inlet 1 opened (a), inlet 2 opened (c), inlet 3 opened (e), inlet 4 opened (g), inlet 5 opened (i); difference in M_2 amplitude (cm) between the case with the current salt marsh extent and with salt marshes completely eroded with inlet 1 opened (b), inlet 2 opened (d), inlet 3 opened (f), inlet 4 opened (h) and inlet 5 opened (l) in Virginia Coast Reserve.
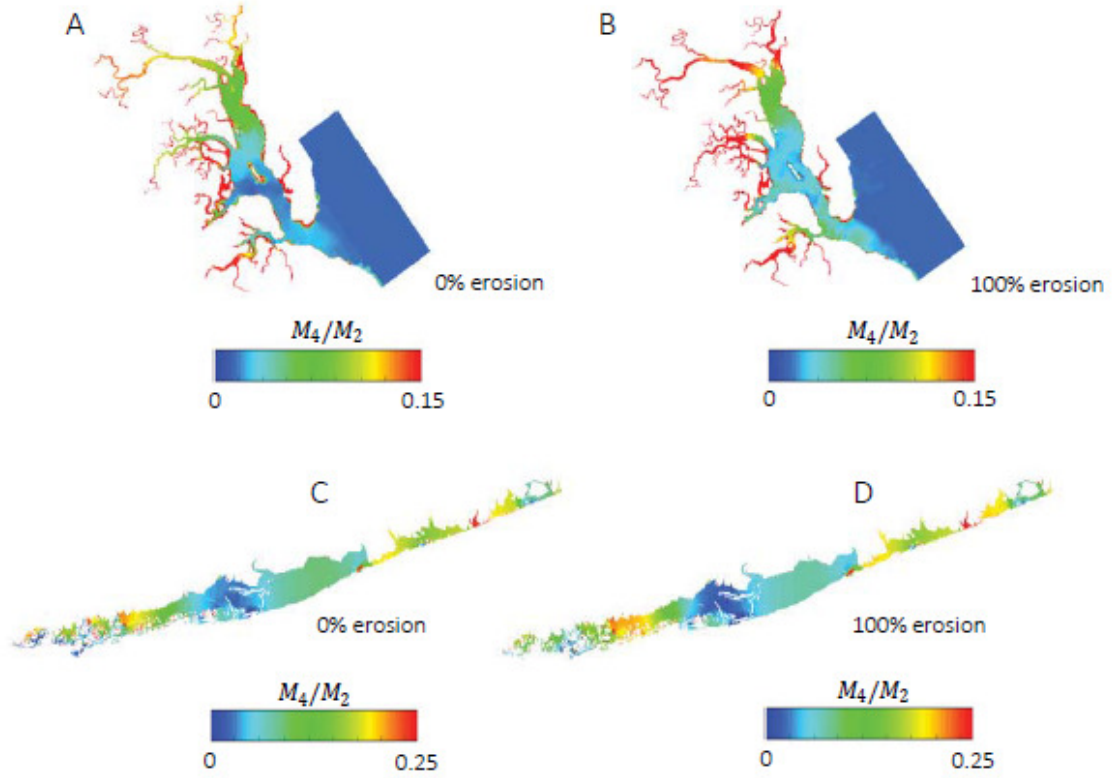
Figure A.4.9: sea-surface M_4/M_2 amplitude ratio for the current marsh distribution (a, c) and marsh completely eroded (b, d) in Plum Island Sound and Great South Bay respectively. Missing plots are to be found in Figures 2 and 3.
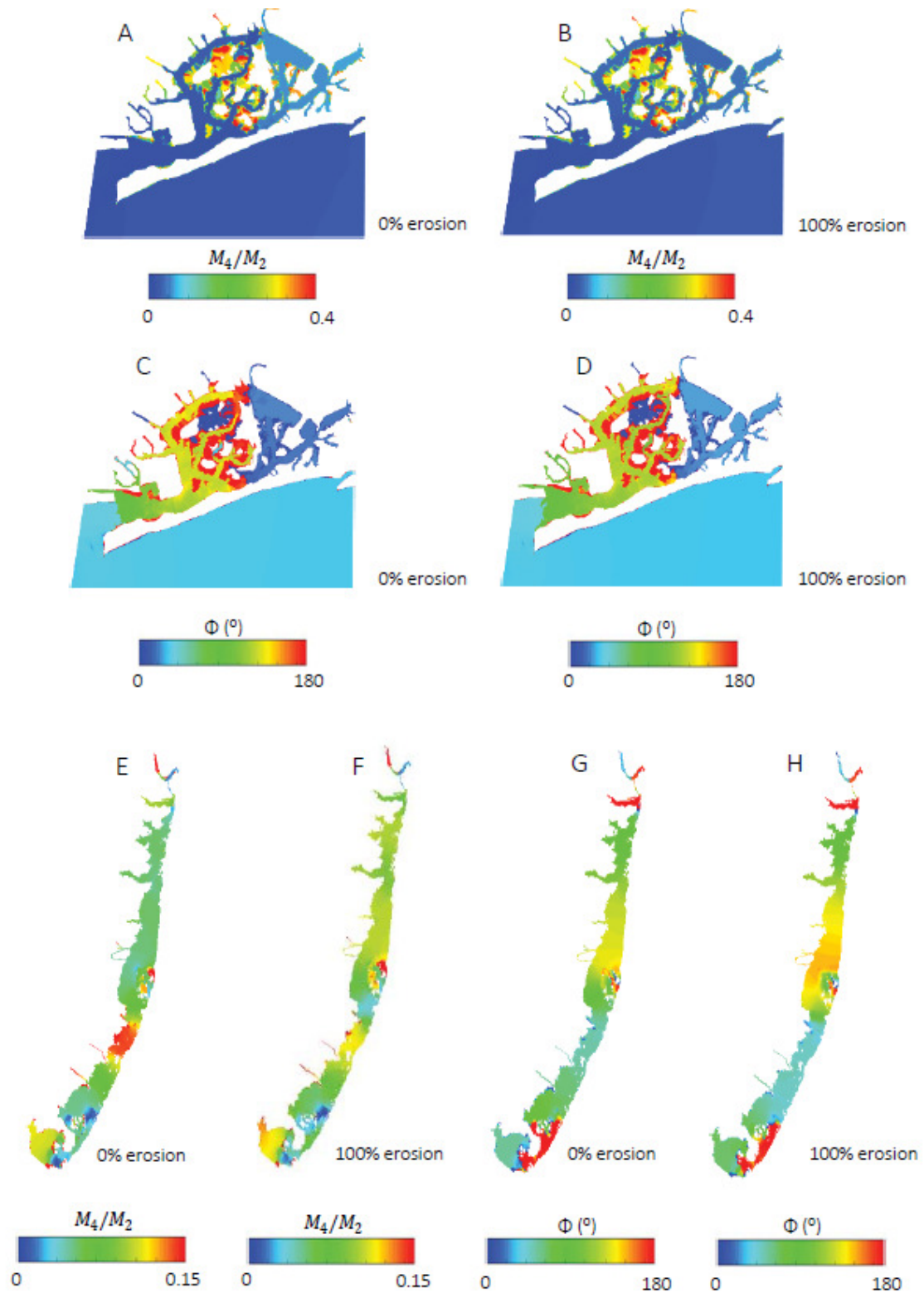
Figure A.4.10: sea-surface amplitude ratio for the current marsh distribution (a, e) and marsh completely eroded (b, f); sea-surface phase of M_4 relative to M_2 for the current marsh

distribution (c, g) and marsh completely eroded (d, h) in Jamaica Bay and Barnegat Bay-Little Egg Harbor respectively.
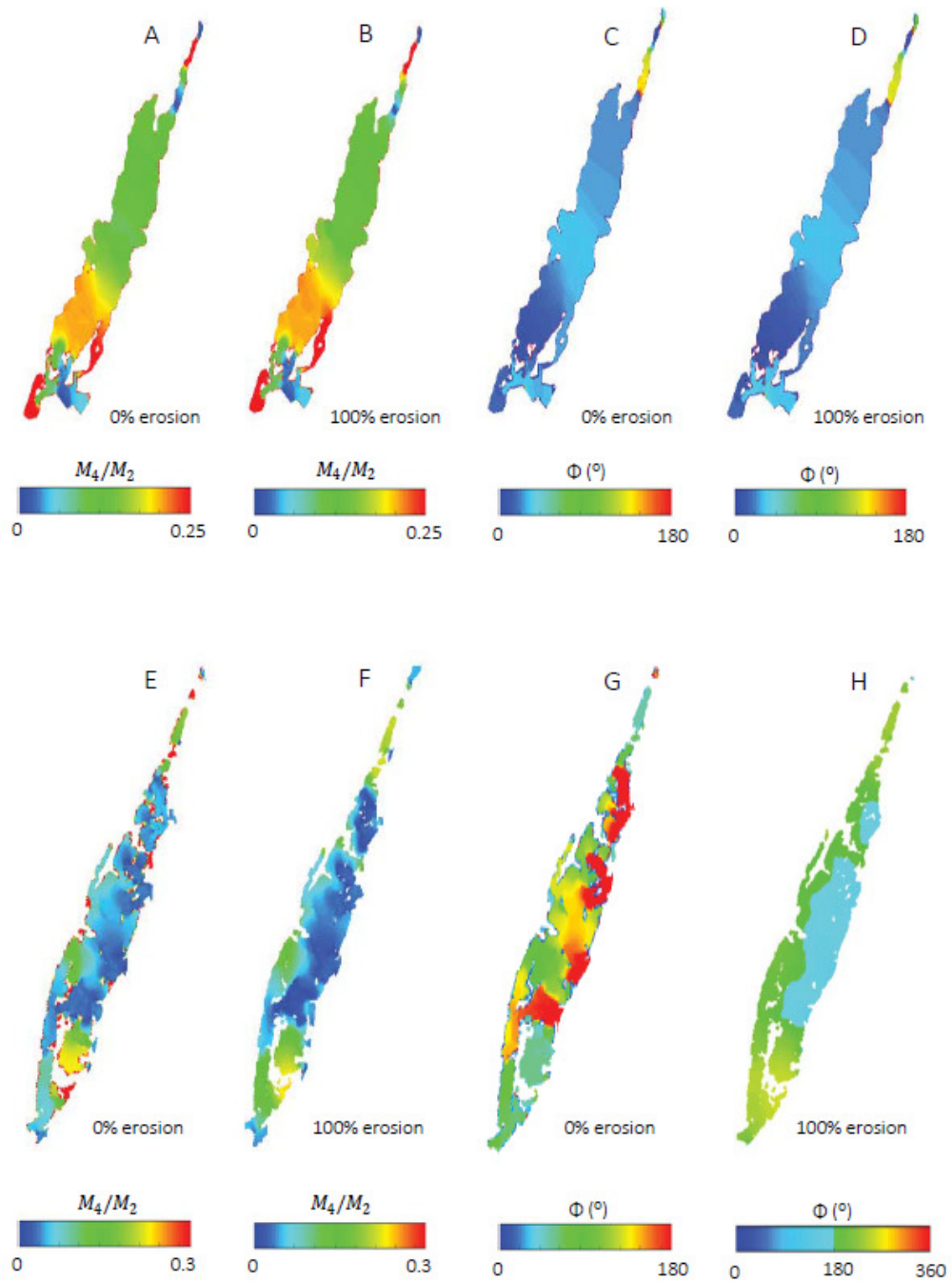
Figure A.4.11: sea-surface amplitude ratio for the current marsh distribution (a, e) and marsh completely eroded (b, f); sea-surface phase of M_4 relative to M_2 for the current marsh distribution (c, g) and marsh completely eroded (d, h) in Chincoteague Bay and Virginia Coast Reserve.
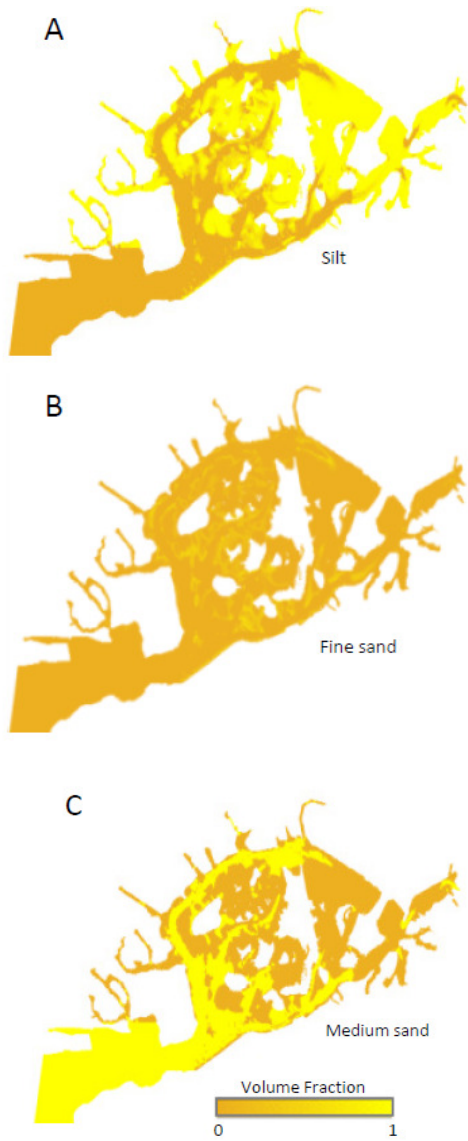
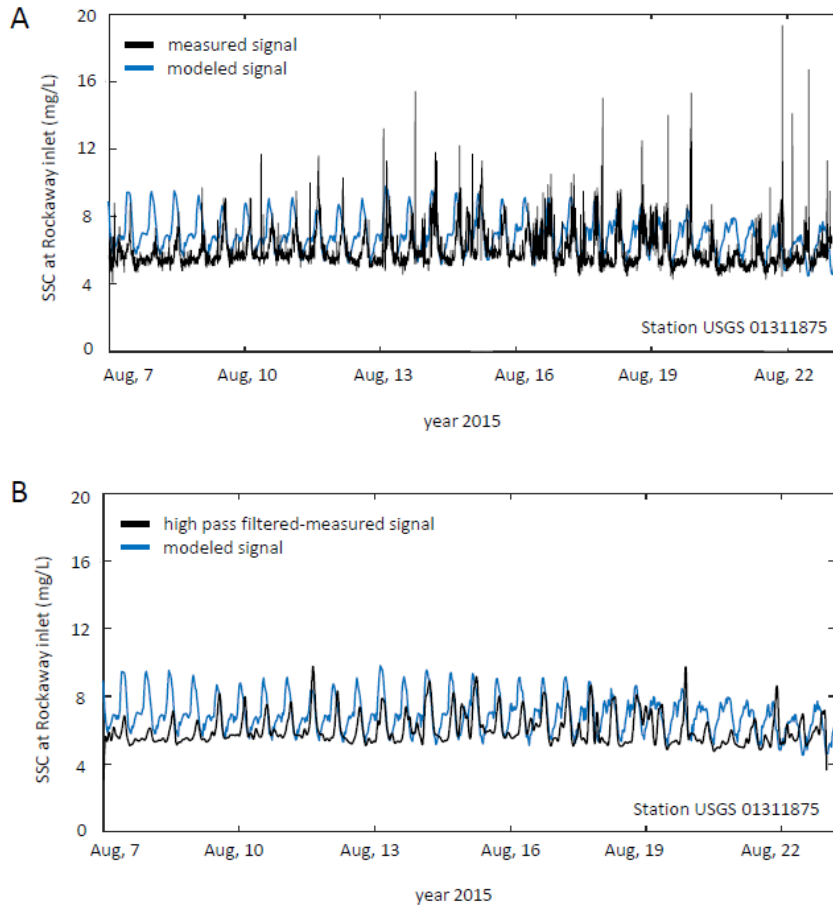Figure A.5.1: Volume fractions of silt, fine sand and medium sand initially distributed on the seabed.

Figure A.5.2: Comparison between the measured and the modeled SSC signal (mg/L) at the mouth of the inlet (a); comparison between the filtered measured signal and the modeled SSC signal (mg/L) at the mouth of the inlet (b).
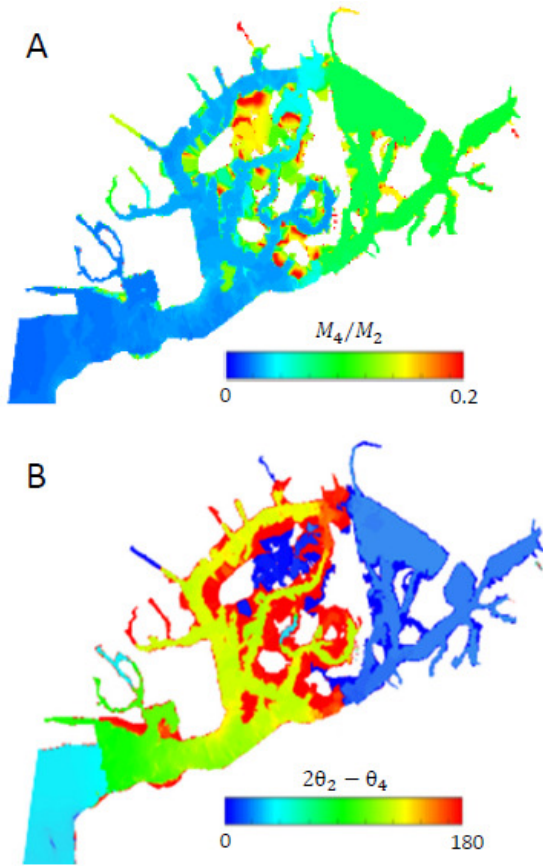
234

Figure A.5.3: Sea-surface amplitude ratio and sea-surface phase of M_4 relative to M_2 for the present-day bay morphology.
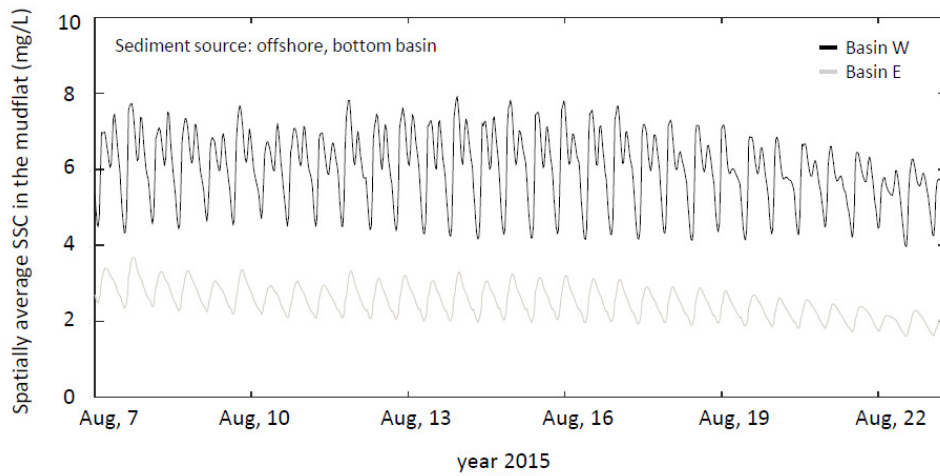
Figure A.5.4: Time series of the spatially average SSC in the mudflat (sediment source: bottom basin and offshore).
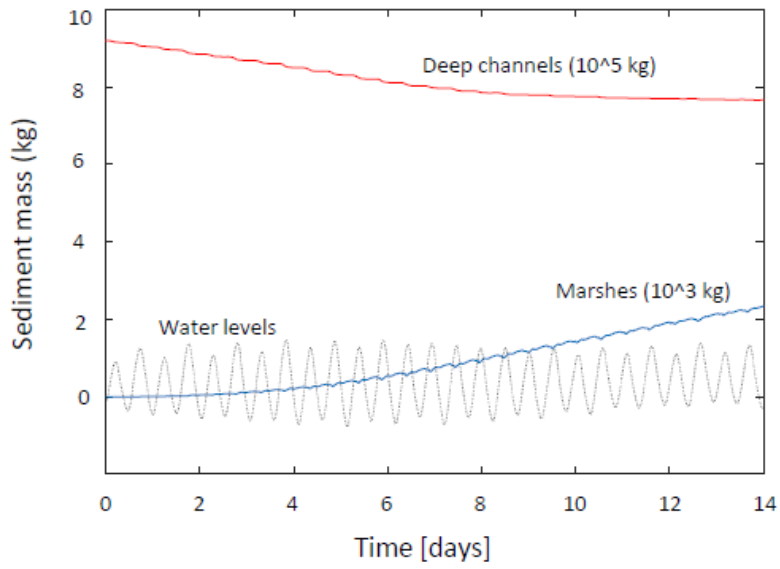
Figure A.5.5: Time-series of the sediment mass deposited in deep channels within the Eastern sub-basin (a) and time-series of the sediment mass trapped by salt marshes (b).

	Site	RMSE	Bias	Skill
Water elevation (m)	1	0.04	-0.02	0.99
Water elevation (m)	2	0.14	0	0.99
U_{bar} (m/s)	3	0.09	0.04	0.93
V_{bar} (m/s)	3	0.16	-0.1	0.76
SSC (mg/L)	1	1.6	0.96	0.55

Table A.5.1: Statistical assessment of the hydrodynamic model for the period 7th-23th August 2015.
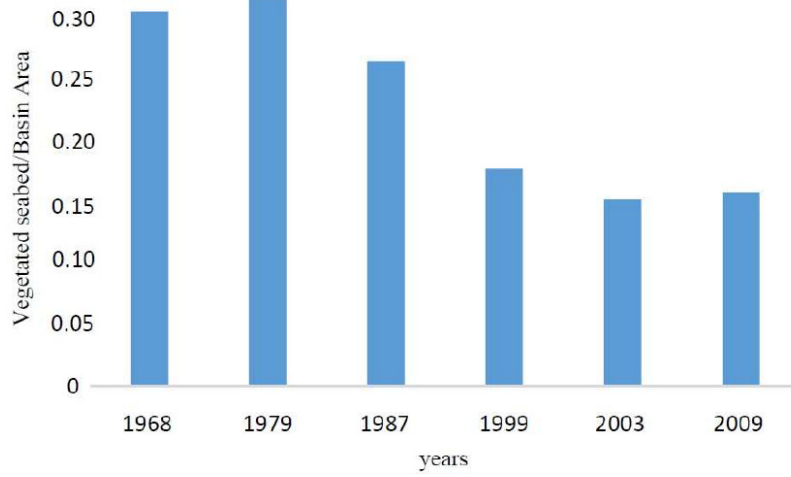
Figure A.6.1: Changes in the ratio between vegetated seabed and basin area for the years from 1968-2009.
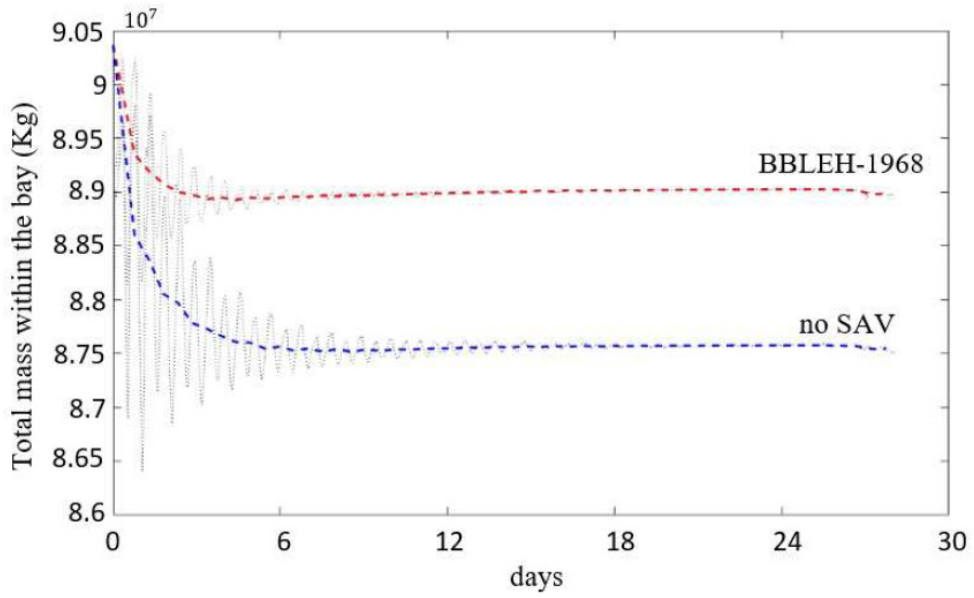
Figure A.6.2: Time series of total sediment mass [kg] in time for the 1968 seagrass extent, and the no-SAV test case.
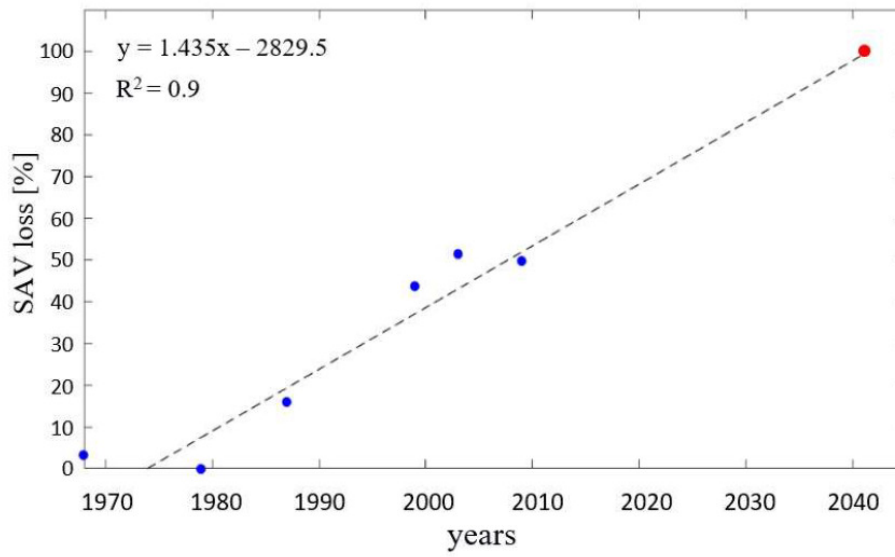
Figure A.6.3: SAV loss [%] through time [years].
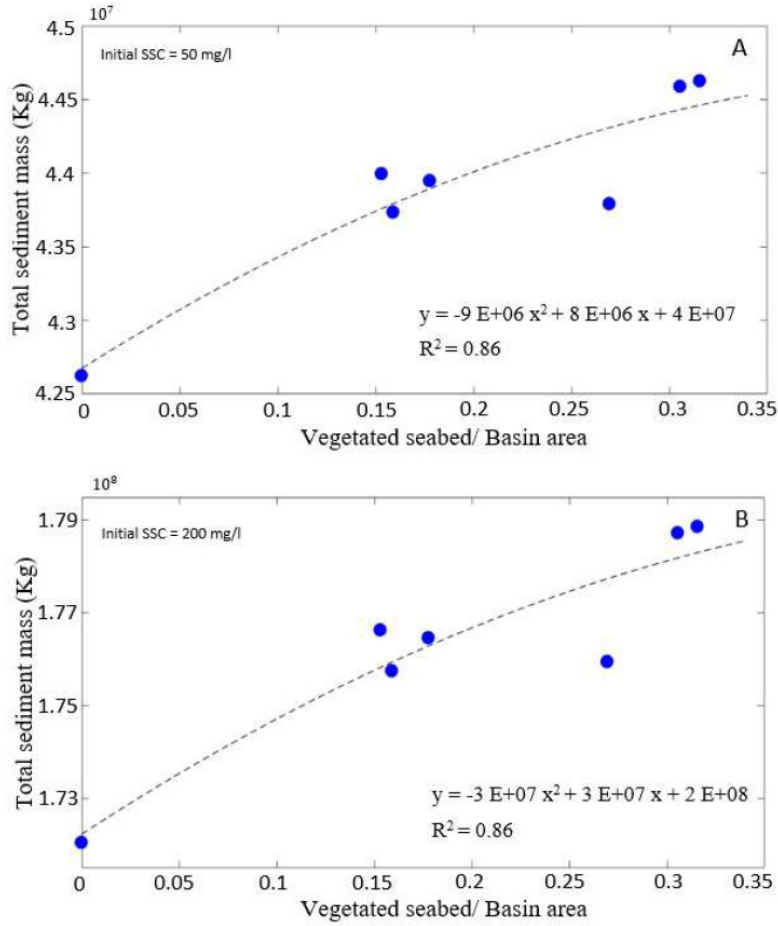
Figure A.6.4: Total sediment mass within the lagoon as a function of vegetated bed/basin area ratios, after 30 simulated days: initial SSC = 50 mg/l (a); initial SSC = 200 mg/l. The vegetated bed/basin area ratios are calculated based on the seagrass areas presented in Figure 6.1.

Figure A.6.5: Mass of sediments (initial SSC = 50 mg/l) per bed area: deposited on the seafloor within the bay (a); in suspension (b); deposited on salt marsh platforms (c). Data are presented after 30 simulated days, and as a function of vegetated bed/basin area ratios obtained from the maps of Figure 6.1 and corresponding to different years.

Figure A.6.6: Mass of sediments (initial SSC = 200 mg/L) per bed area: deposited on the seafloor within the bay (a); in suspension (b); deposited on salt marsh platforms (c). Data are presented after 30 simulated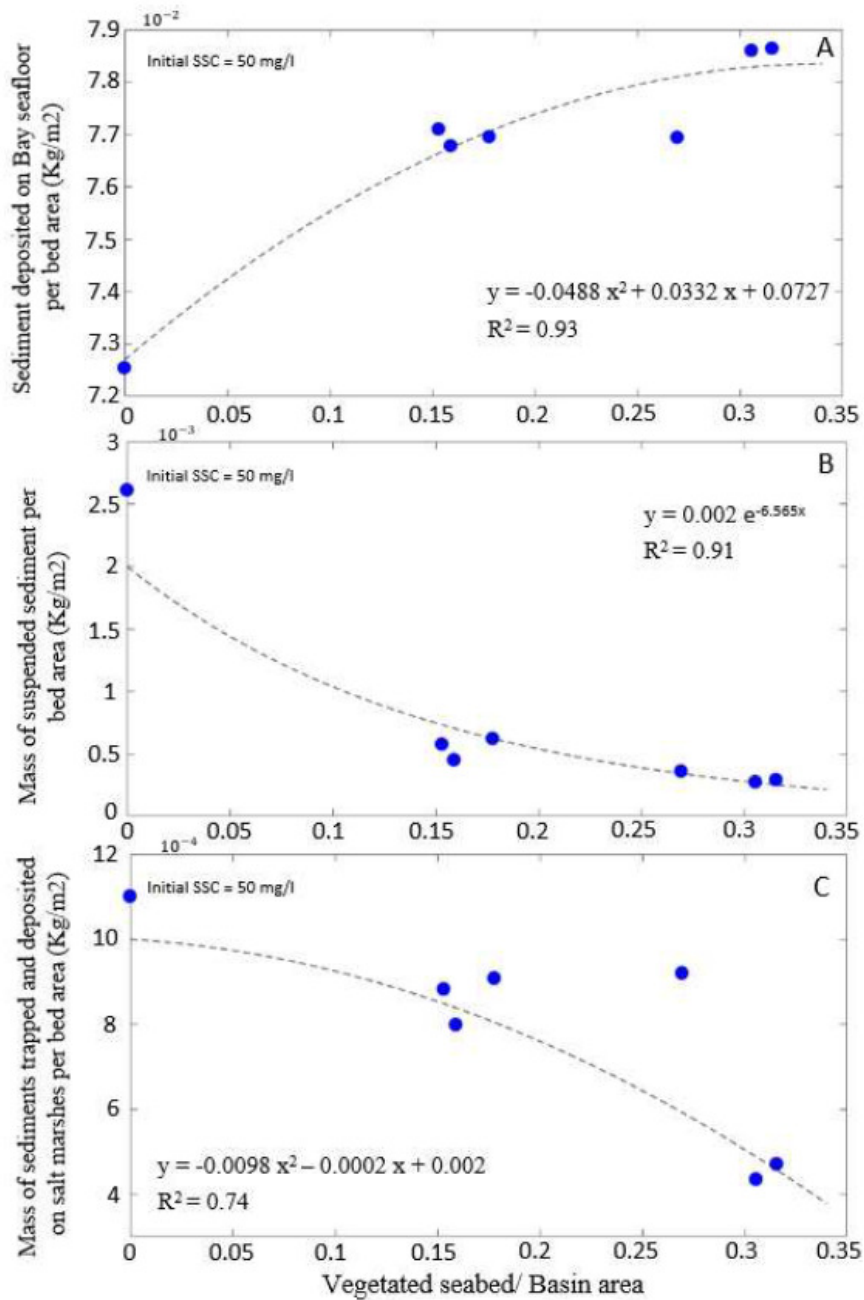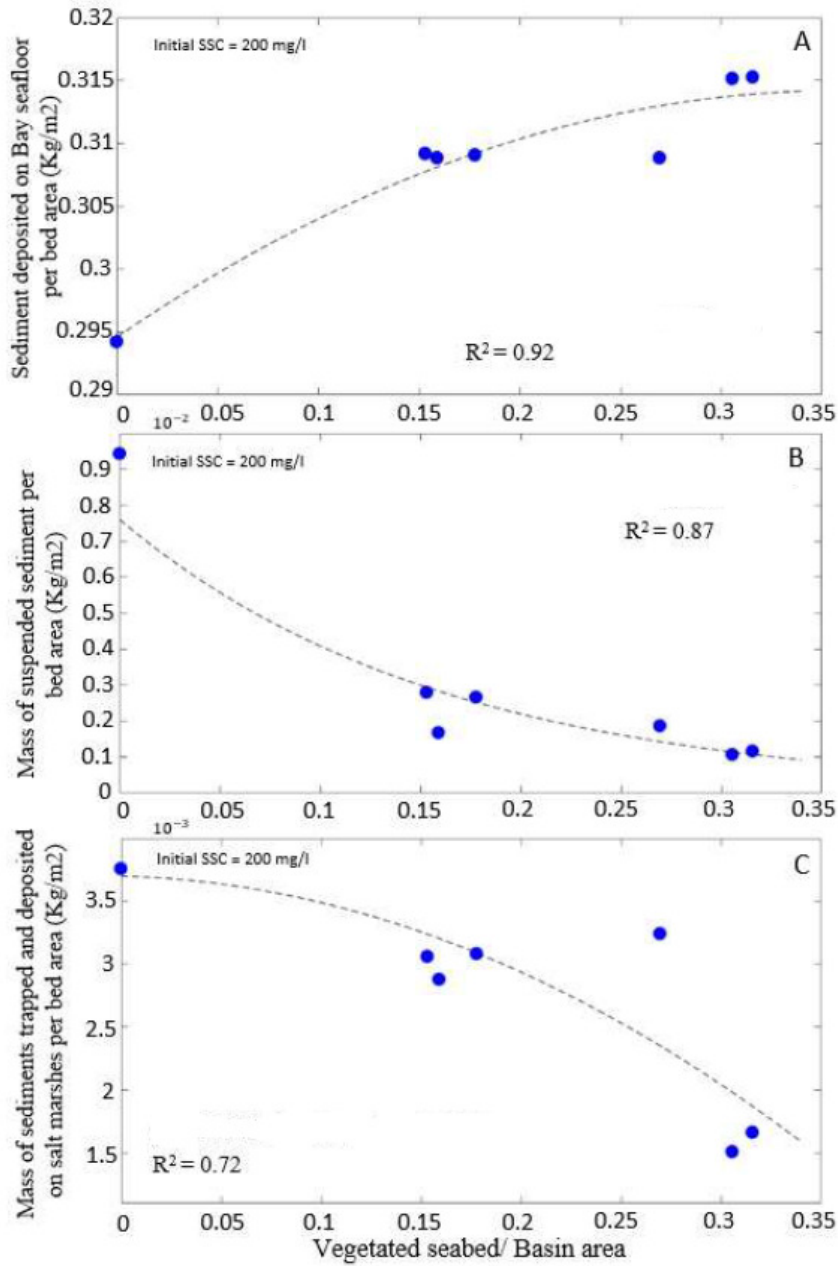 days, and as a function of vegetated bed/basin area ratios obtained from the maps of figure 6.1 and corresponding to different years.

	Model scenario	Plant density (shoot/m2)	μ (bare beds)	σ (bare beds)	μ (vegetated beds)	σ (vegetated beds)
	No-SAV		0.2003	0.5014	0.0994	0.1505
	BBLEH-1968	251,600,900	0.1912	0.4629	0.0027	0.0057
	BBLEH-1968-run1	251	0.1939	0.4690	0.0078	0.0150
	BBLEH-1968-run2	600	0.1920	0.4642	0.0038	0.0077
	BBLEH-1968-run3	900	0.1913	0.4630	0.0025	0.0054

Table A.6.1: Mean and standard deviation of shear stress [Pa] during spring tide within bare beds and meadows for: no-SAV case (a); BBLEH-1968 (b); 1968 seagrass distribution with a uniform plant density of 251 shoots/m^2 (c); 1968 seagrass distribution with a uniform plant density of 600 shoots/m^2 (d); 1968 seagrass distribution with a uniform plant density of 900 shoots/m^2 (e).

Curriculum vitae

Education

Ph.D. Physical geography, *University of Liverpool*, January 2017- May 2020

M.Sc. Civil Engineering, *University of Pisa*, *Summa cum Laude*, 2015

B.Sc. Civil and Environmental Engineering, *University of Pisa*, 2012

Academic Appointments

Postdoctoral Researcher, NOW-NIOZ *Royal Netherlands Institute for Sea Research*, 2020-2023. Department of Estuarine & Delta systems, and *Utrecht University*, Yerseke, NL.

Visiting positions

Visiting PhD student (October-November 2017, November-December 2018), *Department of Earth and Environment*, *Boston University* (MA), USA

Visiting scholar (March-September 2015), *Technical University of Civil Engineering of Bucharest*, Bucharest, Romania

Publications

<div align="center">Works in progress</div>

[12] Zhang, X., **Donatelli, C.**, Ganju, N. K., Fagherazzi, S., Leonardi, N., Sea-level effects in back-barrier estuaries

[11] **Donatelli, C.**, Ganju, N. K., Fagherazzi, S., Leonardi, N., Rapid changes in the efficiency of seagrass beds to protect coastal lagoons

<div align="center">Works under review</div>

[10] Leonardi, N., **Donatelli, C.**, Zhang, X., Ganju, N. K., Fagherazzi, S., Salt marsh erosion triggers large-scale changes in the sediment budget of estuaries, *Earth Surface Processes and Landforms Special Issue*, (2019)

[9] **Donatelli, C.**, Ganju, N. K., Kalra, T., Zhang, X., Fagherazzi, S., Leonardi, N., Marsh-derived sediments affect the resilience of intertidal areas to sea-level rise, *Journal of Geophysical Research: Earth Surface* (2019)

Peer-Reviewed Journal Publications

[8] **Donatelli, C.**, Zhang, X., Ganju, N. K., Aretxabaleta, A.L., Fagherazzi, S., Leonardi, N., A non-linear relationship between marsh size and sediment trapping capacity compromises salt marshes' stability, *Geology* (2020)

[7] Zhang, X., Leonardi, N., **Donatelli, C.**, Fagherazzi, S., Divergence of sediment fluxes triggered by sea level rise will reshape coastal bays, *Geophysical Research Letters* (2019)

[6] **Donatelli, C.**, Ganju, N. K., Kalra, T., Fagherazzi, S., Leonardi, N., Numerical modelling results of wave thrust acting on salt marsh boundaries with different seagrass coverages in a shallow back-barrier estuary, *Data in Brief* (2019), doi: 10.1016/j.dib.2019.104197

[5] **Donatelli, C.**, Ganju, N. K., Kalra, T., Fagherazzi, S., Leonardi, N., Changes in hydrodynamics and wave energy as a result of seagrass decline along the shoreline of a microtidal back-barrier estuary, *Advances in Water Resources* (2019), doi: 10.1016/j.advwatres.2019.04.017

[4] Zhang, X., Leonardi, N., **Donatelli, C.**, Fagherazzi, S., Fate of cohesive sediments in a marsh dominated estuary, *Advances in Water Resources* (2019), DOI: 10.1016/j.advwatres.2019.01.003

[3] **Donatelli, C.**, Ganju, Zhang, X., N. K., Fagherazzi, S., Leonardi, N., Salt marsh loss affects tides and the sediment budget in shallow bays, *Journal of Geophysical Research: Earth Surface* (2018), doi: 10.1029/2018JF004617

[2] **Donatelli, C.**, Ganju, N. K., Fagherazzi, S., Leonardi, N., Seagrasses impact sediment exchange between tidal flats and salt marsh, and the sediment budget of shallow bays, *Geophysical Research Letters* (2018), doi:10.1029/2018GL078056

[1] Leonardi, N., Carnacina, I., **Donatelli, C.**, et al, Dynamic interactions between coastal storms and salt marshes: A review, *Geomorphology* (2017), doi:10.1016/j.geomorph.2017.11.00

Awards, Funding, and Other Support

- *NOW/ENW* (*The Netherlands Organization of Scientific Research*), 2020-2022. Project: 'The Dutch Wadden Sea as an event-driven system: transport and exchange flows'. Institutes: *Royal NIOZ, Department of Applied Physics at TU/e* and *Leibniz Institute for Baltic Sea Research (IOW).*
- Ph.D. funded by US Geological Survey, 2016-2020. Project: Impact of Hurricane Sandy on the salt marshes of Chincoteague Bay, Virginia, and Barnegat Bay, New Jersey. Institutes: *University of Liverpool, BU* and *USGS*
- Fellowship for studies and Research abroad, (March 2015-September 2015), University of Pisa, Italy.
- *Summa cum Laude* distinction University of Pisa, Italy, 2015.
- High school 100/100, Liceo Scientifico G. Moscati, Grottaglie, Italy.

Professional services

Ad-hoc Reviewer

Reviewer for: 'Maryland Sea Grant Competitive Graduate Research Fellowship', 2020

- *Science Advances*
- *Geophysical Research Letters*
- *Science of the Total Environment*
- *Global and Planetary Change*
- *Earth Surface Processes and Landforms*
- *Journal of Geophysical Research*
- *Aquatic Sciences*
- *Estuarine, Coastal and Shelf Science*
- *Frontiers of Earth Science*
- *Estuaries and Coasts*
- *Ocean Dynamics*
- *Natural Hazards and Earth System Sciences*
- *Water*
- *Journal of Hydraulic Research*
- *Data in Brief*

Presentations at Conferences, Symposia, and Workshops

- Leonardi, N., **Donatelli, C.**, Ganju, N.K., Fagherazzi, S., (2020). Impact of salt marshes and seagrass beds on the sediment budget and resilience of coastal areas. Oral presentation at European Geosciences Union General Assembly, Vienna, 8th-13th April.
- **Donatelli, C.**, Ganju, N.K., Fagherazzi, S., Leonardi, N., (2019). A non-linear relationship between marsh size and sediment trapping capacity compromises salt

marshes' resilience to sea level rise. Oral presentation at Postgraduate Conference, Liverpool, 15th May.

- Leonardi, N., **Donatelli, C.**, Li, X., Lyddon, C.E., (2018). Dynamic coastal systems under changing environment. AGU 2018 Fall Meeting, Washington, D.C, 10th-14th December 2018.
- Fagherazzi, S., **Donatelli, C.**, Ganju, N.K., Leonardi, N., (2018). Seagrasses impact sediment exchange between tidal flats and salt marsh, and the sediment budget of shallow bays. AGU 2018 Fall Meeting, Washington, D.C, 10th-14th December 2018.
- **Donatelli, C.**, Ganju, N.K., Fagherazzi, S., Leonardi, N., (2018). How seagrass beds protect coastal lagoons. Oral presentation at Woods Hole Coastal and Marine Science Center (USGS), 3th December.
- Leonardi, N., Li, X., and **Donatelli, C.**, (2018). Impact of waves on coastal areas, lessons from UK and USA case studies. Conference paper at 5th IAHR Europe Congress New challenges in hydraulic research and engineering, Trento, 12th-14th June 2018.
- **Donatelli, C.**, Ganju, N.K., Fagherazzi, S., Leonardi, N., (2018). How seagrass beds protect coastal lagoons. Oral presentation at Postgraduate Conference, Liverpool, 12th May.
- **Donatelli, C.**, Ganju, N.K., Fagherazzi, S., Leonardi, N., (2018). How salt marshes and seagrasses impact the sediment budget in shallow bays. Poster presentation at European Geosciences Union General Assembly, Vienna, 8th-13th April.
- **Donatelli, C.**, Ganju, N.K., Fagherazzi, S., Leonardi, N., (2017). Salt marsh erosion influences tides and sediment dynamics in estuarine systems. Oral presentation at Woods Hole Coastal and Marine Science Center (USGS), 3th November.
- **Donatelli, C.**, Ganju, N.K., Fagherazzi, S., Leonardi, N., (2017). Salt marsh erosion influences tides and sediment dynamics in estuarine systems. Oral presentation at Postgraduate Conference, Liverpool, 10th May.
- Leonardi, N., Li, X., and **Donatelli, C.**, (2017). Coastal recovery: a numerical investigation. Conference paper at 10th Symposium on River, Coastal and Estuarine Morphodynamics, Trento-Padova, 15th-22th September 2017.

Professional Activities

Civil Engineer in Società Italiana per Condotte d'Acqua S.p.A, Italy, 2016

Teaching experience

Course Title	Dates	Institution
ENVS163, Changes in Earth Surface Processes (undergraduate)	Lake District, UK, 2018	University of Liverpool
ENVS376/576, Coastal Environments Spatial and Temporal changes (undergraduate and master)	New Brighton, UK, 2017-18	University of Liverpool
ENVS252, Geomorphology: Ice, Sea & Air (undergraduate)	Formby, UK, 2018, 2017-18	University of Liverpool